INFORMATION TO USERS

This manuscript has been reproduced from the microfilm master. UMI films the text directly from the original or copy submitted. Thus, some thesis and dissertation copies are in typewriter face, while others may be from any type of computer printer.

The quality of this reproduction is dependent upon the quality of the copy submitted. Broken or indistinct print, colored or poor quality illustrations and photographs, print bleedthrough, substandard margins, and improper alignment can adversely affect reproduction.

In the unlikely event that the author did not send UMI a complete manuscript and there are missing pages, these will be noted. Also, if unauthorized copyright material had to be removed, a note will indicate the deletion.

Oversize materials (e.g., maps, drawings, charts) are reproduced by sectioning the original, beginning at the upper left-hand corner and continuing from left to right in equal sections with small overlaps. Each original is also photographed in one exposure and is included in reduced form at the back of the book.

Photographs included in the original manuscript have been reproduced xerographically in this copy. Higher quality 6" x 9" black and white photographic prints are available for any photographs or illustrations appearing in this copy for an additional charge. Contact UMI directly to order.

UMI

A Bell & Howell Information Company
300 North Zeeb Road, Ann Arbor MI 48106-1346 USA
313/761-4700 800/521-0600

MULTI-DIMENSIONAL MODELING OF NATURAL GAS IGNITION, COMBUSTION AND POLLUTANT FORMATION IN DIRECT INJECTION ENGINES

by

Apoorva Agarwal

A dissertation submitted in partial fulfillment
of the requirements for the degree of
Doctor of Philosophy
(Mechanical Engineering)
in The University of Michigan
1998

Doctoral Committee:

Professor Dennis N. Assanis, Chair
Professor Arvind Atreya
Assistant Professor David R. Dowling
Professor James F. Driscoll

To my family
without whose love and support all this would be meaningless

ACKNOWLEDGMENTS

I did not undertake this journey alone and so thanks are due to the people who have helped me along the way. The person I would like to acknowledge first is my thesis advisor Prof. Dennis Assanis. He made a lot of what I was able to do possible. From my early days with him at the University of Illinois to the last few years at Michigan, I have never ceased to be amazed by his ability to think about how best to do a study that is meaningful, clean and presented in the best possible way. Our interactions during the many hours spent writing and polishing technical papers have been a good learning experience for me.

Throughout my student life, I have been fortunate to have come in contact with some exceptional teachers who have had a great impact on me. One person I would like to specifically mention is Professor Vedat Arpaci of the University of Michigan who not only taught me an extremely interesting subject but also left a deep impression on my mind through the quality of his character and intellect.

My graduate experience would have been very incomplete without the love and support of my wife, Preeti, and so I thank her especially for helping me through the not so enjoyable days of graduate life. I would also like to thank my friends and officemates, especially Dr. George Papageorgakis for making the long hours spent working on this dissertation seem not so long. A special word of thanks to my family back home in India for all the love and affection they have given me during the long years I have spent away from them. In the end, I hope, all this has been worthwhile.

This research project was supported by the US Department of Energy under NASA grant NAG3-1552, through the University of Illinois. It was also supported by the Gas Research Institute and Sandia National Laboratories.

TABLE OF CONTENTS

LIST OF FIGURES

Figure

LIST OF TABLES

Table

LIST OF APPENDICES

Appendix

CHAPTER I

INTRODUCTION

Background

Growing concerns about global warming and health related hazards of conventional fossil fuel emissions are prompting administrators and legislators to mandate stricter emission standards for newly manufactured automobiles. In response to these concerns, there is renewed interest in developing alternative concepts that are not only clean but also viable. Although the ultimate objective of producing a zero emission vehicle (ZEV) may one day be realized, it is far from being a reality at the present time. Until a new technology is perfected, the internal combustion (IC) engine will continue to be used as the work horse of the transportation industry.

As prime-movers for automobiles, IC engines powered by gasoline and diesel have been in use for more than a century. The energy conversion process in an IC engine has been made more and more efficient over the years through intensive research efforts. Although modern engines produce significantly lower levels of harmful pollutants than their counterparts manufactured a decade ago, ever increasing demands to further lower or even eliminate emissions of ozone-forming hydrocarbons and diesel particulate matter are prompting researchers to investigate the possibility of substituting cleaner burning alternative fuels for gasoline and diesel fuel. This interest in alternative sources of energy is however not new. Development of the technology required to operate transportation vehicles on alternative sources of energy began in direct response to the energy crisis of the 1970s, and acknowledgment of the fact that the world's crude oil reserves were limited, and depleting fast.

Alternative fuel research worldwide has shown the promise of fuels like natural gas, propane or LPG (liquefied petroleum gas) in improving air quality compared to conventional fuels. Although these fuels may not be the answer to all the air quality problems, they have a significant role to play, both in near and long-terms, in improving the quality of the air we breathe and in substantially reducing the political and economic costs of the dependence of many nations on crude oil as their primary source of energy.

Natural gas is one of the most promising alternative fuel candidates at the present time. It is one of the most environmentally benign fuels, with the most potential for ozone reduction (Nichols, 1994). A comprehensive review of the advantages of natural gas as an environmentally friendly, clean burning (very low propensity to soot), economical and efficient fuel has been reported by Weaver (1989). According to this paper, some of the technical advantages of natural gas in engine applications include extremely low photochemical reactivity, zero evaporative emissions, reduced cold-start and low-temperature emissions due to elimination of cold enrichment, and compatibility with fuel-efficient lean-burn technology. On top of these advantages, the use of natural gas as a fuel is economical as it is readily available at low cost from abundant domestic supplies. Existing transportation and distribution systems also make it readily available in different parts of the country.

In heavy duty applications, natural gas engines have shown much less NOx and particulate emissions than corresponding diesel engines (Hupperich and Dürnholz, 1996; Aesoy, 1996). Even for spark ignition (SI) engines, emissions of natural gas engines are currently slightly lower than the average of gasoline fueled vehicles (Hupperich and Dürnholz, 1996). Efforts have been made to further reduce NOx emissions of natural gas fueled SI engines by operating them under lean conditions (Kim *et al.*, 1996). The high octane quality of methane, the primary constituent of natural gas, estimated at 130 RON, and its consequent good anti-knock properties enable the operation of a lean burn, natural gas fueled SI engine at compression ratios up to 13.2, thereby significantly improving the

fuel conversion efficiency. With slight EGR at part-load (5 to 10%), NOx emissions can be drastically reduced while operating the engine at high compression ratios.

Although most of the applications of natural gas as an engine fuel have been in premixed, spark ignited engines, there are several drawbacks with using natural gas in such a configuration. Even though compression ratios higher than conventional SI engines can be used, knock problems exclude use of compression ratios typical of diesel engines. This, coupled with high intake air pumping losses due to throttling the intake air pressure at part load conditions, results in 15 to 25% lower thermal efficiencies than the diesel-fueled engine (Willi and Richards, 1994). SI engines also have more than 30% higher heat rejection than a diesel engine. This requires a larger, more expensive cooling system, which may be prohibitive in terms of space requirements in a mobile application.

A direct injected natural gas (DING) engine has the potential to match diesel engine performance while maintaining the smoke-free operating characteristics of a spark ignited engine. High thermal efficiencies (greater than 40%) and power densities typical of diesel engines can be potentially achieved by this concept. Furthermore, it has been seen that fuel metering changes as a result of compositional changes in natural gas are not a significant factor in direct injection (DI) applications, as long as condensation as a result of high injection pressures does not occur in the fuel system (Naber *et al.*, 1994). This is a big advantage over carburated, premixed SI engines where natural gas composition changes can lead to significant equivalence ratio changes resulting in engine performance changes (King, 1992). Direct injection of natural gas into the cylinder can also be used to obtain benefits associated with mixture stratification that occurs when the gas is injected very close to the start of combustion (Jennings and Jeske, 1994).

Gas Research Institute (GRI) and Caterpillar Research are developing direct injection natural gas technology on a Caterpillar 3500 series locomotive engine (four-stroke cycle). The technical objectives to match the power density and thermal efficiency of current diesel engines while maintaining the low emissions characteristics of premixed spark ignited natural gas engines have been demonstrated successfully on a single cylinder,

glow plug ignited, DING engine based on the 3500 series engines (Willi and Richards, 1994). A full-load performance and emissions summary of the DING engine and its parent diesel engine is shown in Table 1.1. The DING engine seems to be much more efficient, however, the reported value does not include the work required to compress natural gas to the injection pressure of 2800 psi, which could be 4 to 10% of the engine's output power (Rubas, 1997). The higher thermal efficiency is due to leaner mixture in the DING engine compared to the Diesel engine. Smoke (particulate), NOx and CO emissions are all reduced compared to the baseline engine, though unburned hydrocarbon emissions are higher. A 3516 engine (16 cylinder engine) has been built and is being field tested in a Morrison Knudsen switching locomotive (O' Conner, 1994).

Table 1.1
Comparison of DING engine performance and emissions with a Diesel engine.

	Thermal Efficiency	A/F Ratio	Smoke (Cat)	NOx (g/kW-hr)	CO (g/kW-hr)	HC (g/kW-hr)
DING	46.0 %	31.4	nil	13.14	1.96	0.71
Diesel	40.3 %	25.3	0.08	13.53	3.31	0.21

While liquid injection is a well developed technology, high pressure, supersonic, transient gas injection is not. In diesel injection, the liquid droplets that comprise the bulk of the fuel spray penetrate deep into the combustion chamber before evaporating. The fuel vapor is mixed with air that is located in a region relatively far from the injector nozzle. This method of mixing is fundamentally different from gaseous injection which is characterized by the mixing of the fuel-rich plume core controlled by the turbulence generated in the shear layer.

In a direct injection engine, ignition occurs due to high temperatures that the injected fuel encounters in the cylinder. However, compression ignition of natural gas is not a trivial task. Experiments in a combustion bomb have shown that autoignition of natural

gas under diesel-like conditions requires temperatures as high as 1100-1200 K (Naber *et al.*, 1994). This high temperature requirement mandates that either a high compression ratio (about 23:1) or a high intake air temperature be used, both of which have negative effects on engine performance and durability. Obviously, knowing at what conditions of temperatures, pressures and compositions a methane-air mixture can autoignite, or whether ignition assist in the form of a glow plug (Willi and Richards, 1994) or pilot fuel injection (Gebert *et al.*, 1996) is required is very important.

Since the direct injection gas technology is new, very little understanding of the direct injection gas ignition and combustion processes currently exists. Such an understanding is necessary to help guide further research into issues such as reduced NOx emissions to meet future emission standards, improved combustion stability, and reduced dependence on glow plugs or pilot fuel for ignition. Such understanding would also lead to the development of analytical models that could be used to facilitate technology transfer to other engines and applications.

Present Work

The present doctoral dissertation was part of a broader effort, initially sponsored by GRI and Department of Energy and conducted jointly by Caterpillar Research, University of Illinois at Urbana-Champaign and the University of Michigan. The general objective of this effort was to develop an understanding of fuel/air mixing in a direct injection natural gas engine and its impact on ignition, combustion and emissions.

Specifically, the present work was aimed at multi-dimensional modeling of ignition, combustion and pollutant formation in DING engines. Throughout the work, the emphasis was on gaining a fundamental understanding of the ignition and combustion processes as related to a DING engine. Modified versions of the Los Alamos KIVA-3 and KIVA-3V codes (Amsden, 1993; Amsden, 1997) were used to model these processes along with fuel injection and pollutant formation. Keeping in mind the complexity of the processes involved, the study was carried out in five distinct phases:

1. A comprehensive review of the literature was carried out to understand fully the issues involved with using natural gas as a compression ignition fuel. The ignition properties of natural gas were studied and ignition process parameters identified.
2. Detailed multi-step kinetic mechanisms for natural gas autoignition were used to model ignition in a constant volume chamber *without* modeling the flow. By comparison of predicted trends with measurements under typical end of compression conditions in diesel engines, a multi-step kinetic scheme was identified that was best able to account for the effect of thermodynamic conditions (temperature and pressure) and natural gas composition on ignition delay.
3. The detailed multi-step kinetic scheme identified in phase two was coupled with KIVA-3 and used to simulate natural gas injection and ignition in a constant volume chamber. The experimental work of Naber *et al.* (1994), who measured ignition delay of three different blends of natural gas injected in a pre-heated and pressurized combustion bomb at densities that were representative of end of compression conditions in production diesel engines, was used to compare with the theoretical predictions. Along with validation of the coupled model, a suitable criterion to determine the onset of ignition was identified and the influence of additives in reducing ignition delay was studied.
4. Once ignition occurs, the interactions between chemistry and flow need to be described in the form of a turbulent combustion model. In this phase of the work, different turbulent combustion models like the flamelet model, the eddy dissipation concept (EDC) and the eddy-breakup model (EBU) were studied to investigate their suitability for direct injection engine studies. Also, kinetic mechanisms for nitric oxide (NO) formation were studied to understand the influence of temperature and species concentrations on NO formation rates.
5. Multi-dimensional ignition and combustion models were coupled to investigate the heat release and pollutant formation processes in a typical medium-size direct injection natural gas engine. The emphasis was on studying the impact of operating

conditions of speed and load on engine performance and emissions. Different injection strategies were used to study the performance-emissions trade-off.

The rest of the thesis is organized as follows: In Chapter II, phases one and two are described in detail. The issues involved with natural gas as a compression ignition fuel are presented along with kinetic modeling of its ignition. Chapter III deals with phase three of the work and describes the coupling between detailed chemistry and multi-dimensional flow simulation to study autoignition in a combustion bomb. Chapter IV describes phase four and looks at various combustion models that were investigated during the course of this work. Their feasibility for direct injection engine studies is studied and a kinetic mechanism for NO formation is also described. Chapter V describes phase five and presents results of ignition, combustion and pollutant formation in a typical DING engine under various conditions of speed and load. Finally, Chapter VI provides conclusions of this study along with recommendations for future work.

CHAPTER II

IGNITION PROPERTIES OF NATURAL GAS AND KINETIC MODELING OF ITS AUTOIGNITION

Background

In the direct injection natural gas (DING) concept, fuel is injected late into compression, just like a diesel engine. Due to their nature of operation, ignition becomes the key process in DING engines as it controls the advent of combustion. Simply defined, ignition is a process of starting with reactants and evolving towards a steadily burning flame. More formally, ignition can be defined as a transition from a non-reactive to a reactive state in which external stimuli lead to thermochemical runaway followed by rapid transition to self-sustained combustion (Kuo, 1986). Obviously, knowing the answer to the question as to what temperatures, pressures, and compositions a mixture can be ignited within a desirable time-frame, is very important.

Ignition processes are usually very complex and involve many intricate physical and chemical steps. These steps take a finite amount of time and the period between the start of injection and the start of combustion is referred to as *ignition delay* or *induction time* (Heywood, 1988). For the DING concept, the physical delay is due to the finite rates of fuel injection and mixing of injected fuel with air. The chemical delay is due to pre-combustion reactions of the fuel, air and residual gas mixture that lead to autoignition. These processes are affected by engine design and operating variables, and the characteristics of the fuel. One of the primary objectives of this work is to quantify the ignition delay period under typical conditions that natural gas injected in a DING engine would encounter.

Since ignition delay in direct-injection engines controls the start of combustion, for optimum engine performance and emissions, the ignition delay period should range from 0.5 to 2 milliseconds under most operating conditions (Heywood, 1988). A long and variable ignition delay is undesirable as it leads to spiky heat release due to an increase in the premixed part of combustion. The secondary effects of a long and variable delay are reduced engine efficiency, increased exhaust emissions, noise production and damage to mechanical parts such as piston rings and bearings. Ignition must also be accurately repeated for each engine cycle. Making sure whether ignition would occur is almost as important is knowing how soon it will occur. At an engine speed of 1500 RPM, a difference in ignition delay of 0.5-0.7 ms represents a 4-6 crank angle shift in the start of combustion. So, a delay of even a few milliseconds may have a significant impact on subsequent combustion, peak pressures and hence performance and emissions.

In a diesel engine, ignition occurs due to high temperatures that the injected fuel encounters in the cylinder. However, compression ignition of natural gas is not a trivial task due to the low ignitabiliy of methane, its primary constituent. The properties of natural gas as a compression ignition fuel are discussed in the next section.

Natural Gas as a Compression Ignition Engine Fuel

Natural gas is the common name of mixtures of lower hydrocarbon gases consisting mainly of methane with small percentages of higher alkanes such as ethane, propane, butane and pentane, and possible small fractions of incombustible components like nitrogen, carbon dioxide and helium. The six areas in the United States in which natural gas is found are divided into fields, roughly, as follows (Shnidman, 1954):

1) Appalachian	3) Mid-continent	5) Rocky Mountain
2) Indiana	4) Texas	6) California

A major problem with the use of natural gas as an engine fuel is the wide variation in its composition. Table 2.1 shows some examples of typical natural gas blends to illustrate this variation. These values were taken from a British Petroleum Corporation

report, so they refer to European natural gas blends, but the variation in composition is as wide in the United States too. The characteristic fuel properties in Table 2.2 show that these gaseous fuels represent a wide variety of physical and chemical properties.

Table 2.1
Some examples of natural gas composition by volume (%).
Values taken from Rose and Cooper (1977), and Aesoy (1996)

Component	North Sea NG	Arzew NG	Groningen NG	LNG[1]
Methane	94.4	86.5	81.8	96.6
Ethane	3.0	9.4	2.7	2.3
Propane	0.5	2.6	0.4	1.0
Butane	0.2	1.1	0.1	-
Pentane	0.1	0.1	0.1	-
Nitrogen	1.5	0.3	14.0	0.1
Carbon dioxide	0.2	-	0.9	-

Table 2.2
Characteristic fuel properties of some individual gases.
Values taken from Naber *et al.* (1994)

Gaseous Fuel	Mol. Wt. [gm/mol]	P_{sat} (20 °C) [MPa]	Specific heat ratio (γ)	LHV [MJ/kg]	Laminar Flame Speed [cm/s]	Density at STP [kg/m^3]
Methane	16.04	-	1.23	50.00	38.3	0.7168
Ethane	30.07	4.4	1.13	47.44	40.6	1.3566
Propane	44.09	0.99	1.09	46.35	42.3	2.0096
Butane	58.12	0.26	1.06	45.72	42.6	2.7320

[1] Liquefied Natural Gas - Natural gas in liquid state at atmospheric pressure and temperature below 110 K.

Compared to traditional diesel engine fuels, gaseous fuels require special arrangements to handle the high pressure gaseous fuel supply for injection, variable energy content per unit volume and variable ignition and combustion properties due to compositional changes. However, it has been seen that fuel metering changes as a result of compositional changes in natural gas are not a significant factor in DI applications, as long as condensation as a result of high injection pressures does not occur in the fuel system (Naber *et al.*, 1994). This is a major advantage over carburated, premixed SI engines where natural gas composition changes can lead to equivalence ratio changes resulting in significant engine performance changes (King, 1992).

Ignition Properties of Natural Gas

As already pointed out, ignition is a complex process that is influenced by numerous parameters such as fuel properties, oxidizer, pressure, temperature, flow rates, mixing rates, heat transfer, combustion chamber geometry, material etc. (Aesoy, 1996). Since, fuel quality is only one of many parameters in the ignition process, a precise measure of the ignition quality of a fuel-air mixture becomes a difficult task. Some of the parameters that can be used to characterize the ignition quality of a fuel are:

1. Ignition delay period or induction time: In the literature, it is difficult to find a unique definition of ignition delay. There are variable definitions depending on when combustion or explosion occurs based on different indicators like temperature rise, pressure rise, heat release, luminosity, appearance of certain radicals etc. In fact, sixteen different criteria to determine the onset of ignition were analytically evaluated by Zhou and Karim (1994). One of the objectives of the present work was to address this controversy and to propose a universal indicator of the start of combustion.

Ignition delay properties are usually provided for specific experimental setups and criteria, and are therefore only valid within a limited range. Available data on ignition of gaseous mixtures mainly focus on explosion and fire hazard under atmospheric pressure and hardly any data is available for high pressure ignition conditions that are typical of

compression ignition engines. Recently, Naber *et al.* (1994) conducted experiments in a combustion bomb to measure ignition delay of typical natural gas blends under diesel conditions (ambient pressures ranging from 16-150 atmospheres). They defined ignition delay as the time it took for pressure in the bomb to rise by 14 kPa from the start of injection. The value of 14 kPa corresponded to heat release by burning 2.5% of the total mass of fuel injected. It was found that pure methane had the longest pressure delay and the delay decreased with increasing concentrations of ethane, propane and *n*-butane for temperatures below 1300 K. At typical engine densities (20.5 kg/m^3), the ambient temperature required to produce a 2.0 ms pressure delay for natural gas was found to be 1100-1200 K for the blends examined. Increasing the density (pressure) of the ambient gas in the combustion chamber decreased the ignition delay for the range of densities examined (6.4 to 32.9 kg/m^3). However, the sensitivity of ignition to ambient density was much less compared to temperature . The ignition delay had an Arrehenius dependence on temperature, whereas it had a first order inverse dependence on density or pressure.

2. Minimum autoignition temperature: It is defined as the lowest initial temperature at which a fuel-air mixture can ignite within a defined time period (ignition delay). For explosion or fire safety purposes, this period can be specified in the range of seconds, minutes or hours, while in an I C engine it is typically about one to two milliseconds. Table 2.3 shows some ignition temperature data from experiments by Mullins (1955) at atmospheric pressure and high pressure shock initiated ignition experiments by Burcat *et al.* (1971). The ignition delay period was not defined for these values. Some typical diesel engine fuels tested under the same conditions are also included for comparison. Since autoignition temperatures are not absolute constants but depend markedly on the experimental conditions under which they are determined, these values should only be taken as an approximate guide. The temperatures shown in Table 2.3 are not relevant for compression ignition in a direct injection engine, but are important for observing relative differences between these fuels.

Table 2.3
Ignition properties of some gaseous and typical diesel engine fuels.

Fuel	Minimum Ignition Temp.* [K]	Ignition Temp.** (1 ms delay) [K]	Lean Flammability limit*** [% vol.] (ϕ)	Rich Flammability limit*** [% vol.] (ϕ)
Methane	905	1420	5.0 (0.53)	15.0 (1.6)
Ethane	745	1160	3.0 (0.53)	12.4 (2.2)
Propane	766	1205	2.1 (0.52)	9.5 (2.4)
n-Butane	681	1190	1.8 (0.58)	8.4 (2.7)
Ethylene	755	-	2.7	36
Diesel	543	-	-	-
Kerosene	568	-	-	-

*: Spontaneous ignition in air at atmospheric pressure, Mullins (1955)
**: Shock-tube ignition experiments, Burcat *et al.* (1971)
***: Atmospheric condition data, Zabetakis (1965)

It can be clearly seen that the minimum ignition temperature of methane and other lower hydrocarbons is much higher than diesel and kerosene. This means that they require much more thermal energy to ignite and hence their use in compression ignition engines usually requires some kind of ignition assist.

3. Flammability (or Explosion) Limits: There are under given physical conditions both 'lower' or 'lean' and 'upper' or 'rich' limits of flammability. Within, but not outside, these limits self-propagation of flame can occur once ignition has been achieved. Although, the question of whether measured flammability limits are fundamental properties of combustion systems, independent of the apparatus and method of measurement, or whether absolute flammability limits in fact exist, is not yet fully resolved. However, as long as the experimentally determined limits are obtained under conditions similar to those found in practice, they may be used to assess potential explosion hazards.

Within flammability limits, ignition can be achieved by using minimum temperature or energy input to the mixture. The flammability limits shown in Table 2.3 are at atmospheric pressure and an ambient temperature of 25 °C. Figure 2.1 shows how these limits change with pressure for natural gas and air at an ambient temperature of 28 °C (Zabetakis, 1965). Though the lean flammability limits does not change very much, the rich limit increases considerably at elevated pressures. The variability of the effect of pressure arises from the combined influences of physical factors (heat losses) and chemical factors (reaction rates) which may act in opposing directions. For DING engines, injection occurs when the pressure is typically between 50 and 100 atmospheres.

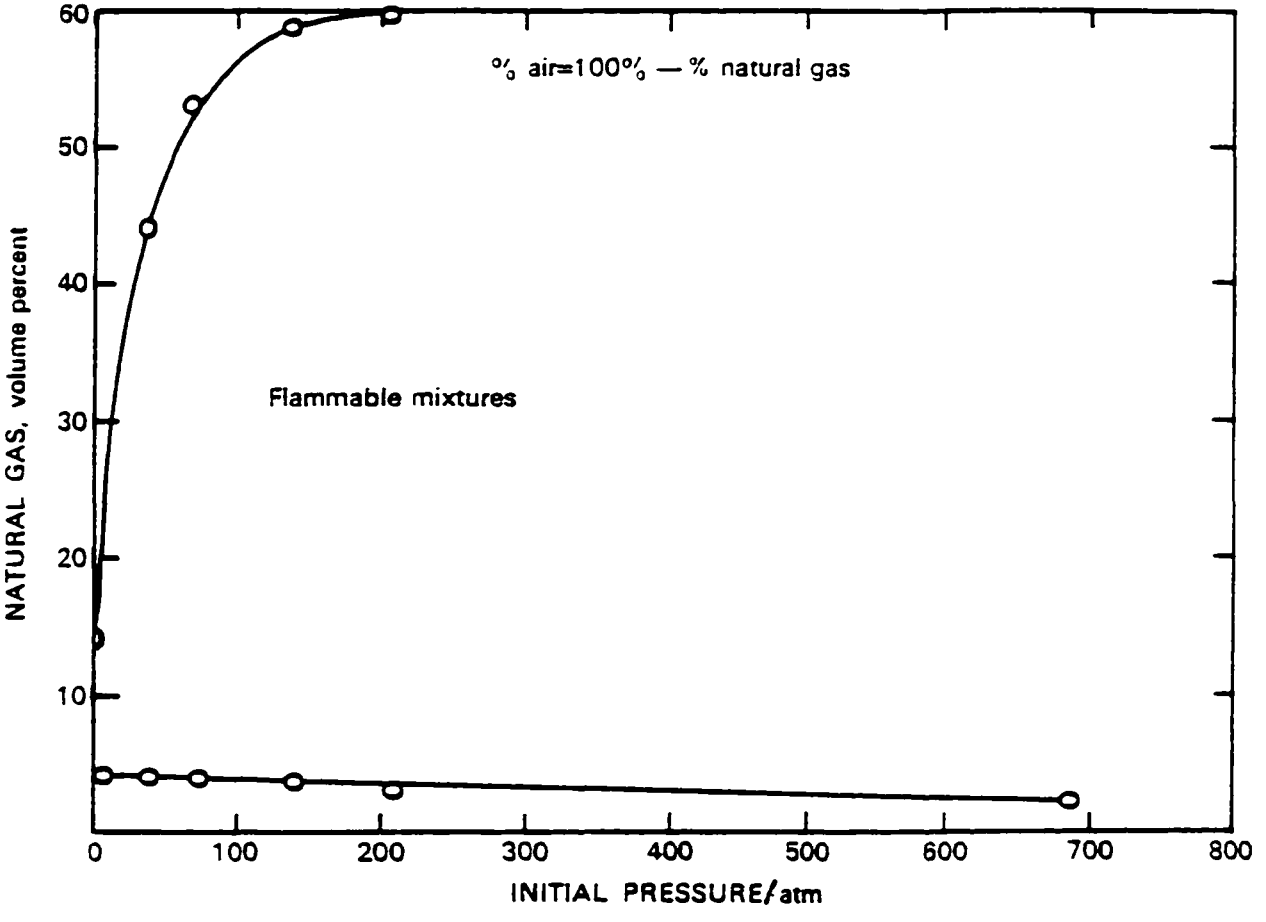

Figure 2.1: Effect of elevated pressures on limits of flammability of natural gas in air at 28 °C (from Zabetakis, 1965).

The reason why methane requires much higher temperatures to autoignite compared to diesel fuels is its simple molecular structure. Since there are no C-C bonds, the initiation reaction for oxidation has to occur by breaking a C-H bonds, requiring more energy than a C-C bond. The methyl radical produced during methane oxidation does not decompose thermally to any extent, while virtually all higher alkyl radicals produce two or smaller hydrocarbon fragments. As a result, the methyl radical must either be oxidized directly through reactions with radicals like O, OH, and HO_2, processes which are quite slow due to the low concentrations of radicals in most cases, or the methyl radicals combine to form ethane, whose formation tends to retard the overall rate of combustion (Westbrook and Pitz, 1987).

Compression Ignition Assistance for DING Engines

It is clear from the previous section that natural gas will require special assistance to ignite within a reasonable delay time under normal engine operating conditions. Some alternatives that are used to alleviate this problem are:

1. Dual Fuel: It is the most commonly used concept, where a pilot fuel is injected to initiate ignition before the gaseous fuel is injected (Gebert *et al.*, 1996). The main problem with this concept is the requirement of a complex fuel injection system that has to cater to two separate fuels.

2. Spark Ignition: Assist in the form of a spark discharge is known to be a problem at high pressures in lean mixtures. It has been shown (Aesoy, 1996) that spark ignition is also very sensitive to variable fuel/air ratio and turbulence intensity, which are both present in a gas jet.

3. Hot Surface Ignition: This is the oldest concept used to assist compression ignition at low temperatures (Willi and Richards, 1994). It uses local heating by a hot surface to

start ignition. It is based on a fairly mature technology, but the main problems of this concept are durability issues due to the high temperatures required from the hot surface (glow plug) over sustained periods of time.

Hot Surface Ignition Process Parameters In a DING Engine

A detailed experimental study of the hot surface ignition assist of natural gas in a direct injection engine was performed by Aesoy (1996). This study reports that the main parameters governing the hot surface ignition process are: surface temperature of the hot surface, combustion chamber conditions (temperature and pressure) at the time of injection, jet flow, geometry and location of the hot surface. These are summarized in Table 2.4.

Table 2.4

Influence of various parameters on the hot surface ignition process (Aesoy, 1996). '+' indicates effect, '++' indicates strong effect and '0' indicates no effect

Parameters	Jet Flow	Fuel / air Mixing	Heat Transfer	Chemical Reaction Rate
Engine Geometry				
• Hot surface location and geometry	++	++	++	+
• Injection nozzle dimensions	++	++	++	+
• Compression Ratio	(+)	(+)	(+)	++
• In-cylinder flow (turbulence, swirl)	+	+	+	+
Engine Operating Conditions				
• Load	+	+	+	+
• Speed (RPM)	+	+	+	0
• Intake air temperature	(0+)	(0+)	(0+)	++
• Intake air pressure	+	+	+	+
• Fuel injection pressure	++	++	++	0
Fuel Composition	(0+)	(0+)	(0+)	++

In this work emphasis was placed on understanding the autoignition and subsequent combustion of natural gas-air mixtures in DING engines. The rest of this chapter deals with kinetic modeling of natural gas autoignition and the effect of parameters like fuel composition, temperature, and pressure on ignition delay under constant volume conditions.

Kinetic Modeling of Natural Gas Ignition

A fundamental understanding of the thermodynamic and fuel composition related factors influencing ignition delay in DING engines can only be obtained by an analysis of the processes leading up to autoignition. However, the inherent transient nature of these processes makes its theoretical treatment difficult. Recourse must almost always be made to numerical techniques involving the solution of time-dependent equations of mass, momentum and energy that include the effect of chemical reactions. Although a qualitative understanding of the ignition phenomena can be obtained from analytical studies, e. g. the pioneering work of Semenov and Frank-Kamenetskii (described in detail in any good combustion text book, e. g. Kuo, 1986 or Warnatz *et al.*, 1996), the complex nature of the physico-chemical processes leading to ignition makes the numerical solution of detailed chemical kinetics coupled with the flow essential for any kind of accurate quantitative prediction.

The first task in modeling of ignition phenomena is to identify a suitable reaction scheme that is capable of accounting for the thermodynamic and fuel composition related conditions of interest. In this initial step, it is best to ignore the details of the flow, so that the analysis can be done within a reasonable time span and also the complexities involved with the coupling of flow and chemistry can be avoided. This also helps in focusing attention on the chemistry of autoignition.

While the importance of detailed chemistry in homogeneous studies of ignition and flame propagation is well documented in the literature (e.g. Agarwal and Assanis, 1997; Sloane and Ronney, 1992; Mulholland *et al.*, 1992; di Blasi *et al.*, 1991; Westbrook, 1979;

Warnatz, 1984), one-step global kinetic mechanisms continue to be used to model ignition (Westbrook and Dryer, 1981; Champion *et al.*, 1986; Tromans and Furzeland, 1988; Frendi and Sibulkin, 1990) due to their computational simplicity. However it has been shown (Sloane and Ronney, 1992) that although properly-calibrated one-step models are able to predict flame speed for planar flame propagation reasonably well, they are very inadequate in accurately predicting minimum ignition energy and induction time. In fact, the induction times for homogeneous ignition of methane-air mixtures predicted by the one-step models were about 60 to 1500 times lower than those predicted by a detailed kinetic mechanism over a range of temperatures (1500 K to 2222 K). This was due to the lack of initiation and chain-branching steps in the overall models that was needed to bring about the onset of heat release in the detailed mechanism. Also, the use of overall reactions to model combustion in novel situations is of very little value as these models are usually tailored to a very specific situation.

The literature abounds with multi-step kinetic mechanisms for methane-air combustion. The relative simplicity of the methane molecule has made it one of the most intensively researched fuels from a kinetic perspective. Some detailed multi-step kinetic mechanisms for methane-air oxidation are due to Westbrook and Pitz, 1987, Frenklach and Bornside, 1984, Tan *et al.*, 1994 and Hunter *et al.*, 1994. Such mechanisms divide the ignition process into a large number of elementary reactions, accounting for chain initiation, propagation, branching and termination. In between single-step and detailed multi-step mechanisms, reduced mechanisms at various levels of detail have also been proposed (e.g. Nicol and Malte, 1994; Peters and Kee, 1987; Bilger *et al.*, 1990). While most of the multi-step mechanisms are based on experimental work involving fundamental species and radicals, they have generally been verified only under low pressure conditions. Hence the present work focuses on exploring the ability of several of the proposed multi-step mechanisms to predict ignition delay under high pressure and high temperature conditions.

Perhaps the most comprehensive mechanism for natural gas ignition presently is the GRI-Mech 1.2 (Frenklach *et al.*, 1995a and b). It consists of 30 species (plus nitrogen and argon) and 177 elementary reactions to describe oxidation of mixtures of methane and ethane. This mechanism was primarily developed for shock-tube ignition and laminar premixed flame speed propagation, although it has been shown to work well in other cases also. However, most of the validation studies for this mechanism have been done at low temperatures and pressures.

Another mechanism that has been proposed is the reduced set DRM22 of Kazakov and Frenklach (1996), derived from the GRI-Mech 1.2 mechanism. The reduction technique is based on systematic elimination of less important reactions. The reduced set consists of 22 species (plus nitrogen and argon) and 104 elementary reactions. Validation studies have compared DRM22 predictions of ignition delays and adiabatic flame velocities with those of the full GRI-Mech 1.2 mechanism. While those studies were limited to pure methane-air mixtures and pressures up to 20 atm, they found that deviations from the GRI-Mech 1.2 mechanism can be relatively small (below 4%). A skeletal methane-air reaction mechanism, consisting of only 15 species (plus nitrogen) and 25 elementary reactions has also been reported (Smooke, 1991); however, its predictiveness of ignition delay under high pressure conditions has not been assessed.

Table 2.5 summarizes the species involved in each of these three mechanisms. Note that the skeletal mechanism does not consist of any species containing two carbon atoms. This is a drawback since it has been shown that even for oxidation of pure methane, methyl radicals combine to form ethane (Westbrook and Pitz, 1987). Nevertheless, a systematic evaluation of the skeletal and the more detailed multi-step mechanisms (GRI-Mech 1.2 and DRM22) was conducted in this study. The evaluation was based on comparison of ignition delay predictions with measurements in a combustion bomb under controlled conditions. Before proceeding, the experimental set-up and the numerical model that incorporates the alternative kinetic models is described.

Table 2.5

Species and radicals involved in each of the three mechanisms studied.

Species	GRI-Mech 1.2	DRM22	Skeletal Mechanism
H_2	X	X	X
H	X	X	X
O	X	X	X
O_2	X	X	X
OH	X	X	X
H_2O	X	X	X
HO_2	X	X	X
H_2O_2	X	X	X
C	X		
CH	X		
CH_2	X	X	
CH_2 (s)	X	X	
CH_3	X	X	X
CH_4	X	X	X
CO	X	X	X
CO_2	X	X	X
HCO	X	X	X
CH_2O	X	X	X
CH_2OH	X		
CH_3O	X	X	X
CH_3OH	X		
C_2H	X		
C_2H_2	X	X	
C_2H_3	X	X	
C_2H_4	X	X	
C_2H_5	X	X	
C_2H_6	X	X	
HCCO	X		
CH_2CO	X		
HCCOH	X		
Inert (N_2)	X	X	X
Inert (Ar)	X	X	

Predicting Ignition Delay in a Combustion Bomb

Experimental set-up for validation of kinetic models

The experimental work of Naber *et al.* (1994) which focused on ignition delay measurements under high pressures and temperatures was used for validation of the kinetic models. Ignition delay was measured in a constant volume chamber at different temperatures for three different ambient densities (6.4, 20.4 and 32.6 kg/m^3) in the chamber. For the range of temperatures investigated, these ambient densities corresponded to pressures ranging from 16 atm to 150 atm. Three different blends of natural gas were investigated. These are summarized in Table 2.6. Since the three kinetic mechanisms outlined above are not able to predict effects of propane and higher hydrocarbons, the non-methane hydrocarbons were lumped together as "ethane" for the simulations. Hence, it was assumed that mean natural gas consisted of 4.30% "ethane" and high ethane natural gas consisted of 10.25% "ethane".

Table 2.6

Natural gas mixtures studied in the experimental and theoretical investigations.

Constituent	Methane	Mean Natural Gas	High Ethane NG
Nitrogen	-	1.37	7.76
Carbon dioxide	-	1.21	1.43
Methane	100.00	93.12	80.56
Ethane	-	3.20	8.99
Propane	-	0.70	1.00
Butane	-	0.40	0.26

The experimental apparatus consisted of a constant-volume combustion vessel and an electronically controlled gaseous fuel injector. The vessel had a disk shaped combustion chamber with a 114 mm diameter and a 28.6 mm width. The chamber walls were kept at a constant temperature of 450 K. The injector had a single orifice, 0.25 mm in diameter, that was oriented to inject fuel through the center of the chamber. The injection pressure was kept fixed at 20.7 MPa and the injection duration was 11-13 ms.

The injector temperature (i.e. fuel temperature) was held constant at 450 K. A piezoelectric pressure transducer, controlled by a high-speed data acquisition system, was used to record pressure data at 24 μs intervals during the diesel burn period. The mass flow rate had a "top-hat" profile and the injector pressure and ambient pressures at injection were such that the flow through the orifice of the injector remained choked throughout combustion except for ambient temperatures above 1250 K for the highest ambient density condition (32.6 kg/m^3).

A two-step combustion process was used to simulate quiescent compression ignition top-dead-center (TDC) combustion processes in the constant-volume combustion vessel. Combustion of lean premixed combustible gases in the first stage yielded products of combustion at high temperature and pressure at a composition very similar to that of air. In their paper, Naber *et al.* pointed out that the composition of the premixed combustible mixture had no significant effect on the subsequent diesel combustion process in stage two.

Ignition delay was defined as the time it took for the pressure in the bomb to rise 14 kPa from the start of injection. This value of 14 kPa corresponded to heat release by burning 0.33 mg of fuel or 2.5% of the total mass of fuel injected. The measured pressure delay data was fitted to the following ignition delay correlation :

$$\tau_{pd} = \left\{ C^2 + \left[A\left(p/p_o\right)^{-r} exp\left(E_a/\tilde{R}T\right) \right]^2 \right\}^{1/2} \qquad (2.1)$$

where C is the constant representing physical delays, A is the Arrhenius constant (fuel dependent), p is the ambient pressure, p_o is a reference pressure (6.2 MPa), r is a pressure correlation exponent (fuel dependent), E_a is the Arrhenius apparent activation energy (fuel dependent), $\tilde{R}$ is the universal gas constant and T is the core temperature of the ambient gas. The core temperature refers to the uniform temperature of almost 90% of the volume of the bomb and is slightly higher than the thermodynamic temperature of the constant volume vessel due to lower temperature of the rest 10% of the volume (made up of 1-2 mm thick wall boundary layers with steep temperature gradients). The value

chosen for C is the minimum observable delay in the bomb and is the sum of two physical delays associated with the finite rate of injection and finite sound speed. This value is equal to 0.41 ms. Values for r, A and E_a for each natural gas fuel were obtained from a linear regression analysis to fit the dependent variable $\ln\left[\left(\tau_{pd}\right)^2 - C^2\right]$ to the independent variables $1/T$ and $\ln(p/p_o)$.

Model description

To compute ignition delays of mixtures of natural gas and air using the alternative multi-step kinetic mechanisms under consideration, unsteady energy and species equations were solved using the Sandia kinetic code CHEMKIN-II (Kee *et al.*, 1991). Pressure and temperature rise in a constant volume bomb due to autoignition at given ambient densities and a range of temperatures from 900 K to 1600 K was studied. To simplify the computations, spatial variation of temperature and species concentrations was ignored. This can be justified by the fact that the temperature in the bomb was kept uniform before injection by a high speed fan. The core temperature used in the correlation was used as the input temperature in the simulation.

Ignoring spatial variation, the governing energy and species equations for this system can be written as (see Appendix A for detailed derivation)

$$\frac{dT}{dt} = -\frac{1}{\rho \overline{C}_v} \sum_{m=1}^{M} u_m \dot{\omega}_m W_m \tag{2.2}$$

$$\frac{dY_m}{dt} = \frac{\dot{\omega}_m W_m}{\rho}, \qquad m = 1, \ldots, M \tag{2.3}$$

where T is the temperature and Y_m are the mass fractions of the M species involved in a kinetic mechanism. The independent variable is the time t. Other variables are the mass density, ρ; the mean specific heat at constant volume, $\overline{C}_v$; the specific internal energies of the species, u_m; the molar production rates of the species, $\dot{\omega}_m$; and the molecular weights of the species, W_m.

The governing system of ordinary differential equations and the accompanying initial conditions form an initial value problem. These equations have been solved using the code LSODE (Hindmarsh, 1983). This code has been found to be highly reliable for the solution of a wide range of "stiff" initial-value problems (Kee *et al.*, 1991). It should be noted that both the computer storage requirements and the CPU time needed increase roughly as $(M+1)^2$. When transport effects are included, the same (M+1) equations need to be solved for each spatial zone, in addition to the equations of conservation of mass and momentum. Furthermore, these equations must be solved at each time step in the numerical solution of the combustion problem. So, judicious choice of a kinetic mechanism for multi-dimensional simulations is quite critical.

The initial conditions were prescribed by calculating the ambient pressure for a given density, temperature and a stoichiometric mixture of the natural gas blend and air. Though the initial concentrations of different species in the experiments at the time of fuel injection were different (due to a two step combustion process involving acetylene), it was found that the difference in ignition delay was within experimental error limits when the primary fuel was changed to ethylene. So, the use of unreacted mixture of fuel and air as the initial condition for the calculation is justified for the comparison.

Since it is not possible to compute physical delays using the method just described, the comparison between experiments and computations was based on "chemical" delays abstracted from the pressure delay measurements. This was done by subtracting the limiting physical delay value of 0.41 ms from the total delay. Although these delays are not additive, the "chemical" delay so calculated gives a better representation of the ignition process, especially at higher temperatures.

Results

Comparison of different mechanisms with measurements

Figure 2.2 (a) shows the variation of ignition delay with temperature for pure methane at an ambient density of 20.4 kg/m^3. For the range of temperatures examined (900-1600 K), the ambient pressure varies from 54 to 97 atm. The experimental pressure delay shown in the figure has been plotted using the fit to the experimental data of Naber *et al.* (1994) (see Eq. 2.1). In the Arrhenius coordinates of the plot (logarithm of time versus inverse of temperature), the straight line variation of ignition delay at temperatures below 1200K shows the Arrhenius dependence of delay on temperature. At higher temperatures, the experimental pressure delay asymptotes to a value close to the physical delay of 0.41 ms. As already pointed out, meaningful comparisons with experiments can only be made by subtracting this limiting value from the pressure delay to get some measure of the chemical delay. It can be seen that values of ignition delay predicted by GRI-Mech 1.2 and DRM22 are almost identical to each other but those predicted by the skeletal mechanism are higher by one-three orders of magnitude. The GRI-Mech 1.2 and DRM22 predict ignition delay that is of the same order as the chemical delay over the whole range of temperatures. These calculations were done assuming a stoichiometric fuel-air mixture. Although a precise agreement with the experimental values is not expected due to the simplifications made in the modeling work, the trends predicted are consistent with experiments. The reduction in ignition delay over the range of temperatures is the same order as the chemical delay. This shows that the two mechanisms are able to predict the effect of changing temperature and pressure.

Figures 2.2 (b) and (c) show the variation of ignition delay with temperature for mean natural gas and high ethane natural gas respectively. The trends in delay are the same as those for methane. The predictions are made using the GRI-Mech 1.2 and DRM22 mechanisms as the skeletal mechanism is valid only for pure methane. Again, we see that the values of delay predicted by the two mechanisms are almost identical to each and are consistent with the experiments. We may thus conclude that both the GRI-Mech

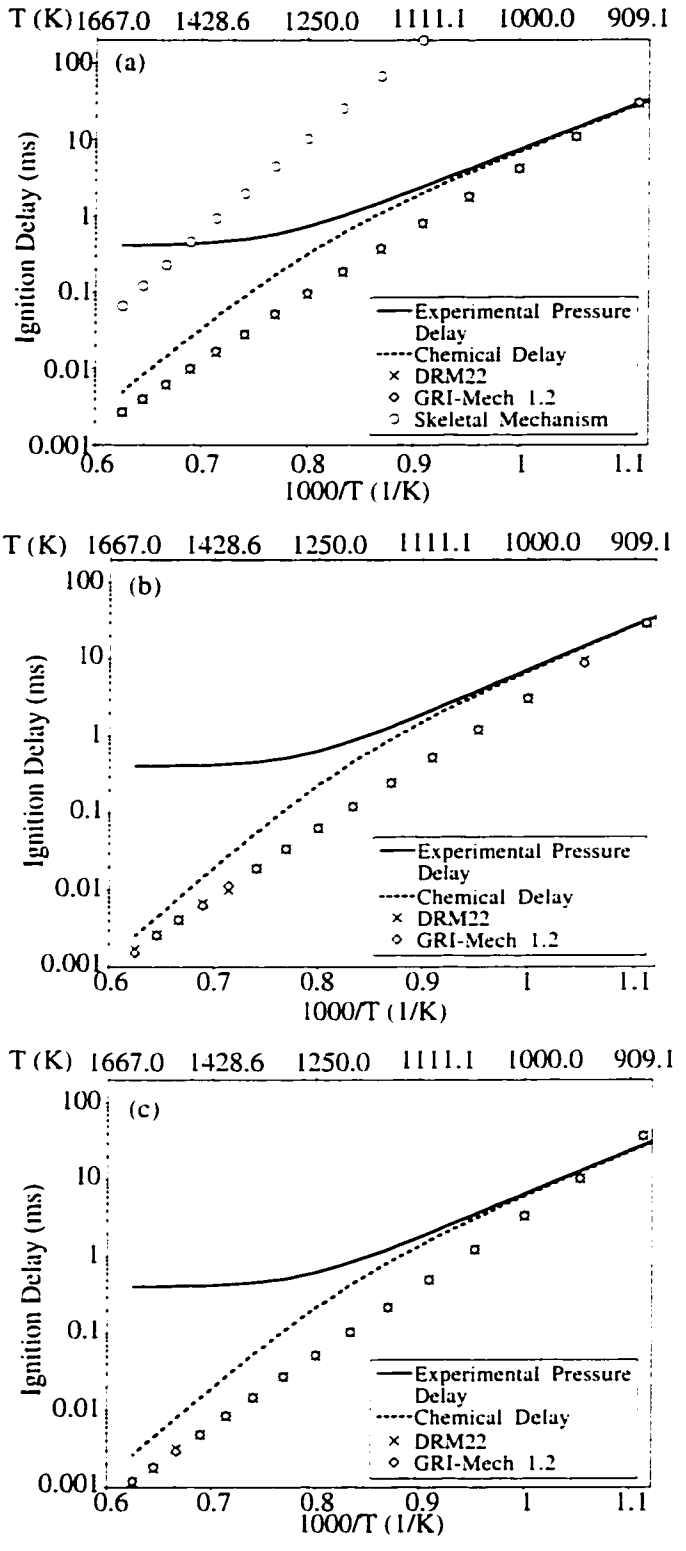

Figure 2.2: Variation of ignition delay with temperature for (a) methane; (b) mean natural gas; and (c) high ethane natural gas. Ambient density is 20.4 kg/m^3 and ambient pressure ranges from 54 atm to 96 atm.

1.2 and DRM22 mechanisms can predict ignition delay in reasonable agreement with experiments at high pressures and temperatures.

The choice of a suitable detailed mechanism for studies using a multi-dimensional flow simulation has to be a judicious mix of complexity and expediency. The mechanism has to be detailed enough to be able to capture the variation in thermodynamic parameters and composition, and at the same time it should be reduced enough to be able to run on typical engineering workstations within a reasonable time frame. Since both the GRI-Mech 1.2 and the reduced set DRM22 mechanisms produce almost identical results, further studies were continued with DRM22, primarily because of its reduced computational requirements and better potential for incorporation in multi-dimensional simulations.

Parametric studies using DRM22

In this section, parametric studies are conducted using the DRM22 mechanism to investigate the effects of fuel composition, ambient density, equivalence ratio, and compression ratio on ignition delay.

1. Effect of Fuel Composition: Figure 2.3 shows the variation of chamber pressure with time for the three different fuels investigated in the study. The initial temperature is 1100 K and the chamber consists of a stoichiometric fuel-air mixture at an ambient density of 20.4 kg/m^3. The DRM22 mechanism is used for the calculations. The chamber pressure stays constant in the pre-ignition phase, since heat transfer through the cold walls is not modeled. In the real bomb, the pressure decreases initially due to heat loss. Ignition is characterized by a rapid increase in pressure after the pre-flame reactions are completed. The time for autoignition is maximum for methane, followed by mean natural gas and high ethane natural gas. This corroborates with previous experimental observations (Naber *et al.*, 1994; Aesoy, 1996; Fraser *et al.*, 1991).

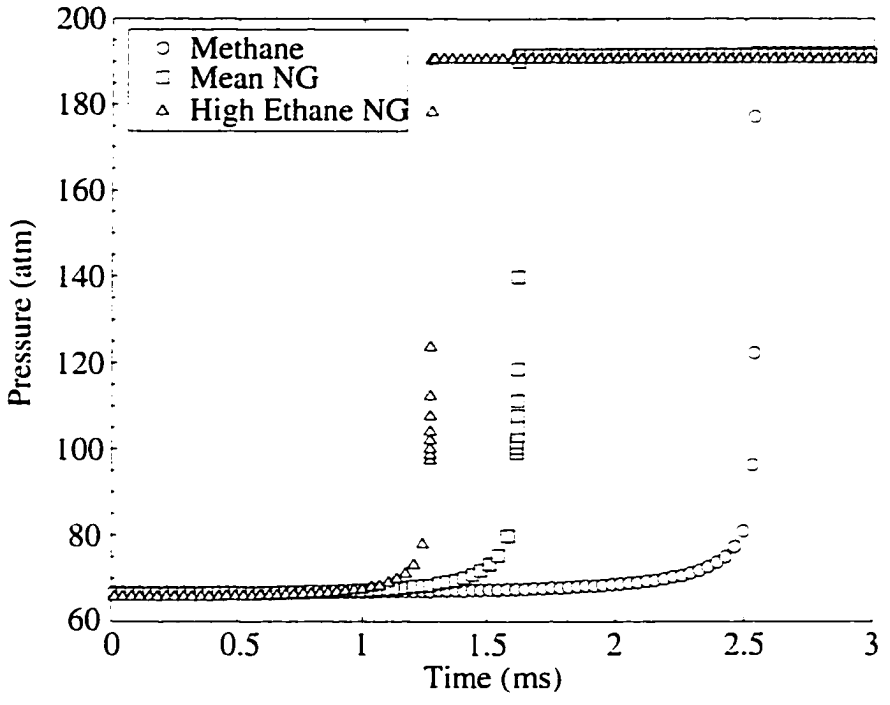

Figure 2.3: Variation of chamber pressure with time for three different fuel blends. The initial temperature is 1100 K, ambient density is 20.4 kg/m^3 and ϕ is 1.0.

The effect of fuel composition on ignition delay is seen in Fig. 2.4. Pure methane has a distinctly higher chemical delay at higher temperatures as compared to mean and high ethane natural gases. The same trends can be seen in the predicted values using DRM22. The chemical delays of the two blends with ethane are not very distinguishable from each other, especially at high initial temperatures. This shows that the experimental values of ignition delay for the two blends obtained from the correlation provided with the experiments (Eq. 2.1) are almost indistinguishable at higher temperatures. This is due to the fact that though high ethane natural gas has a significantly higher percentage of higher hydrocarbons (10.25%) compared to mean natural gas (4.3%), it also has a much higher percentage of inerts (nitrogen and carbon dioxide), thereby neutralizing some of the effect of increased reactivity due to higher hydrocarbons. The computed ignition delays show a distinct drop in ignition delay in going from pure methane to the blends with increased percentage of higher hydrocarbons.

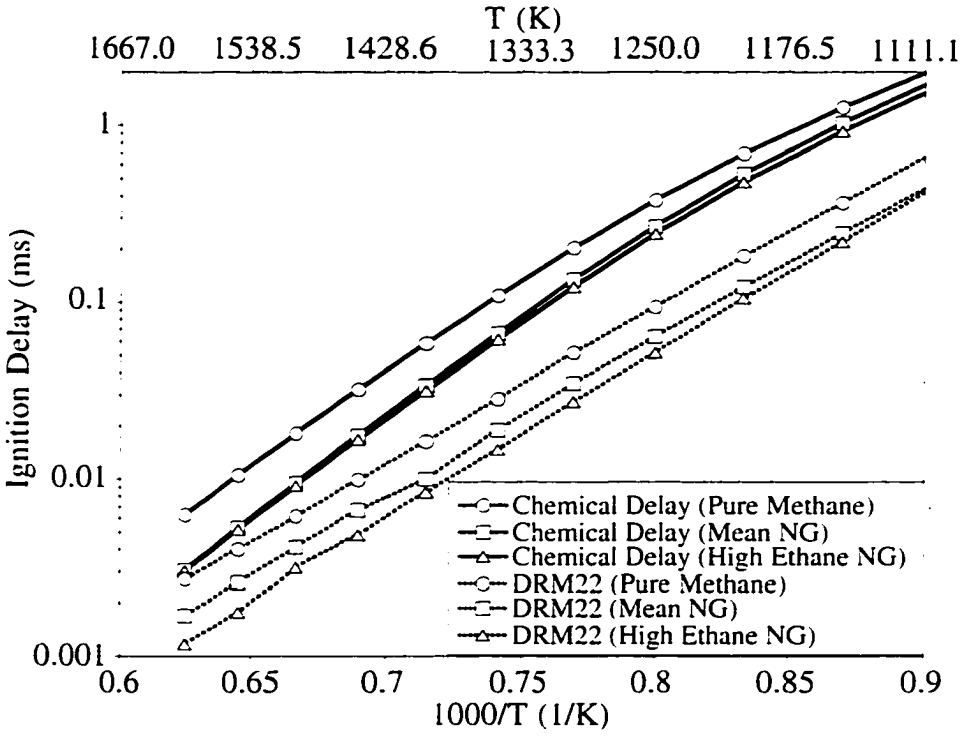

Figure 2.4: Variation of ignition delay for different fuels. Ambient density is 20.4 kg/m^3 for each case.

2. Effect of Ambient Density: Figure 2.5 shows the effect of ambient density on ignition delay of mean natural gas at an initial temperature of 1100 K. As the ambient density (and hence initial pressure) increases, the ignition delay decreases. This trend has also been reported in experimental investigations with an almost first order decrease in ignition delay with increasing pressure.

Figure 2.6 shows the effect of ambient density on ignition delay of mean natural gas over a range of temperatures. The bold lines joining the white circles, squares and triangles represent the chemical delay for ambient densities of 6.4, 20.4 and 32.6 kg/m^3 respectively. The dotted lines represent the calculated delay using the DRM22 mechanism for stoichiometric mixtures. It can be seen that DRM22 is able to capture the effect of ambient density on ignition delay over the range of temperatures that are typical of chamber temperatures in diesel applications.

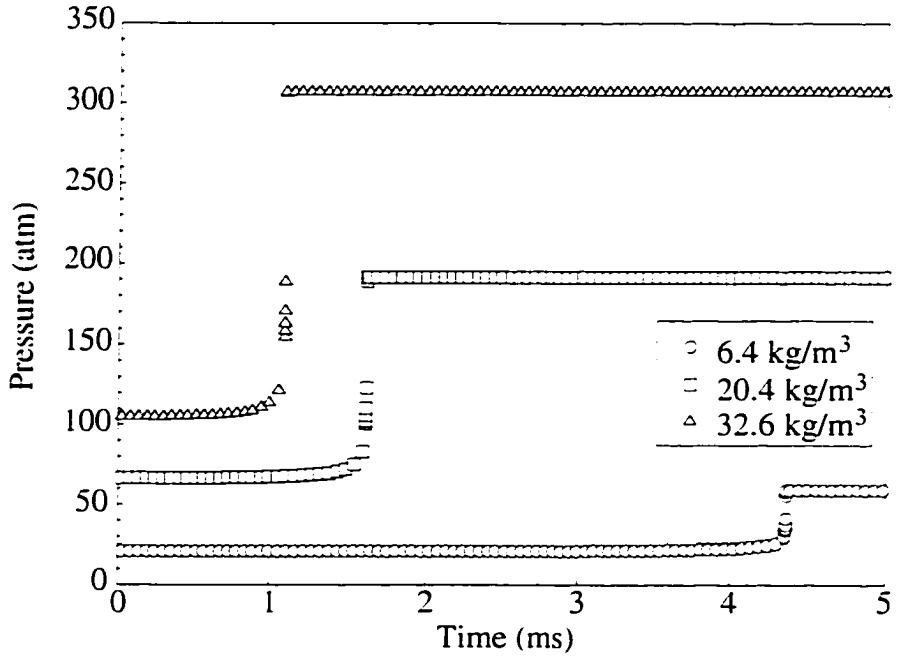

Figure 2.5: Variation of chamber pressure with time for three different ambient densities. Fuel used is mean natural gas and initial temperature is 1100 K.

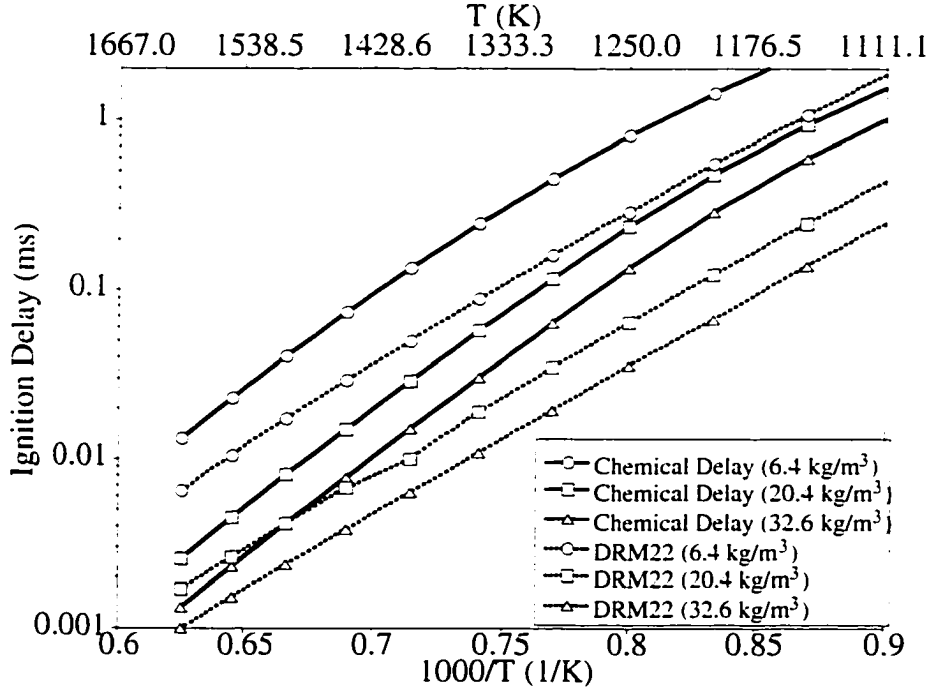

Figure 2.6: Variation of ignition delay with ambient density for mean natural gas. Ambient pressure ranges from 17 atm to 154 atm.

3. Effect of Equivalence Ratio: Figure 2.7 shows the effect of the equivalence ratio on the predicted ignition delay for mean natural gas using the DRM22 mechanism. It can be seen that the predicted delay decreases with increasing fuel-air ratio. Since the calculations are made at the same temperature for each fuel-air ratio, the difference in computed delay is due to chemical kinetic effects associated with fuel and oxidizer concentrations. As the fuel concentration increases, there are more radicals available for reaction, and hence the delay decreases. In a direct injection engine, chemical reactions would of course occur over a broad range of equivalence ratios. The trends of ignition delay with equivalence ratio are similar for high ethane natural gas, though ignition delay of pure methane is not as sensitive to equivalence ratio changes. These trends compare well with the simulations of Naber *et al.* (1994).

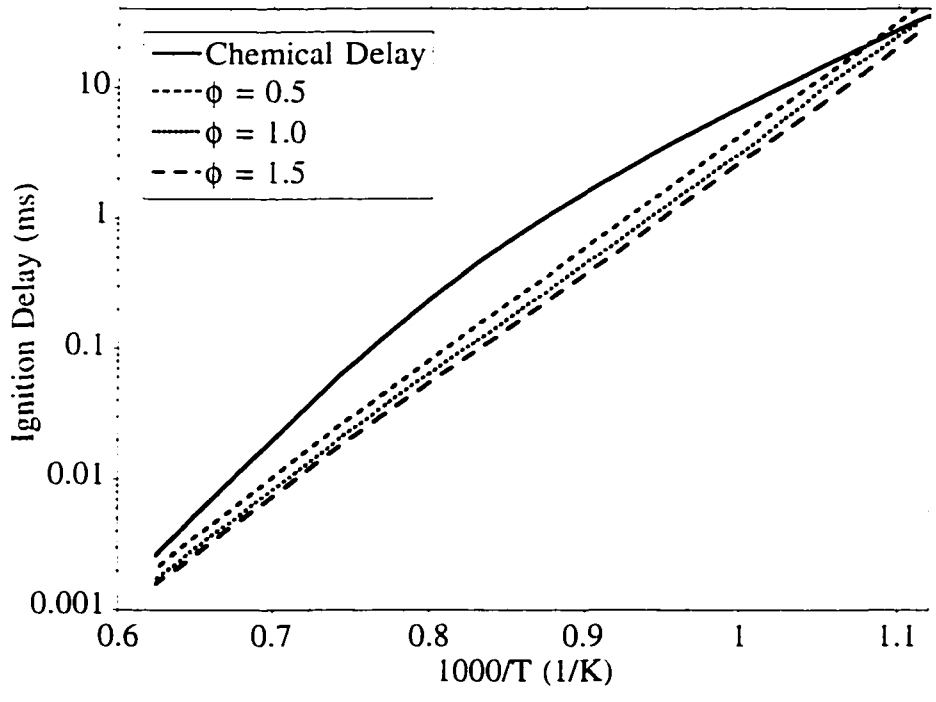

Figure 2.7: Variation of ignition delay with equivalence ratio for mean natural gas at a density of 20.4 kg/m^3.

4. Effect of Compression Ratio: It was pointed out earlier that compression ignition of natural gas occurs at high chamber temperatures (1100-1200 K). As a consequence, either high inlet air temperatures or high compression ratios would be required in an engine. Figure 2.8 shows the variation of ignition delay of mean natural gas with compression ratio for different intake air temperatures.ssures and temperatures for each compression ratio, based on different intake temperatures and an intake pressure of 1 atm. The definition of ignition delay was the same as that in the previous studies, i.e. the time taken for pressure to rise by 14 kPa in a constant volume chamber.

Typical values of ignition delay in diesel engines have been shown to be below 2 ms (Heywood, 1988). This delay time includes both physical and chemical delays. Since most of the factors involving physical delay in diesel engines (atomization, evaporation etc.) are absent in DING engines, the chemical delay could be an approximate indicator of the total delay. Figure 2.8 clearly shows that at low compression ratios (less than 9), even very high intake air temperatures (up to 450 K) are not able to ignite the natural gas-air mixture within 2 ms. No ignition was observed at compression ratios less than 12 for initial temperatures of 300 and 325 K for even up to 1 sec. As the compression ratio increases, the delay decreases owing to an increase in both pressure and temperature. It is seen that for a reasonable intake air temperature (300 K), a compression ratio of approximately 21 is needed for the delay to be within 2 ms.

Figure 2.8 can provide useful guidelines to an engine designer in selecting the optimum combination of intake air temperature and compression ratio. Note that high intake air temperatures would tend to reduce volumetric efficiency, while increased compression ratio results in high cylinder pressures, and hence higher mechanical stresses. From the computational and experimental studies conducted in a combustion bomb, it is also evident that to achieve reasonable ignition delay of natural gas under compression ignition conditions requires some sort of ignition assist.

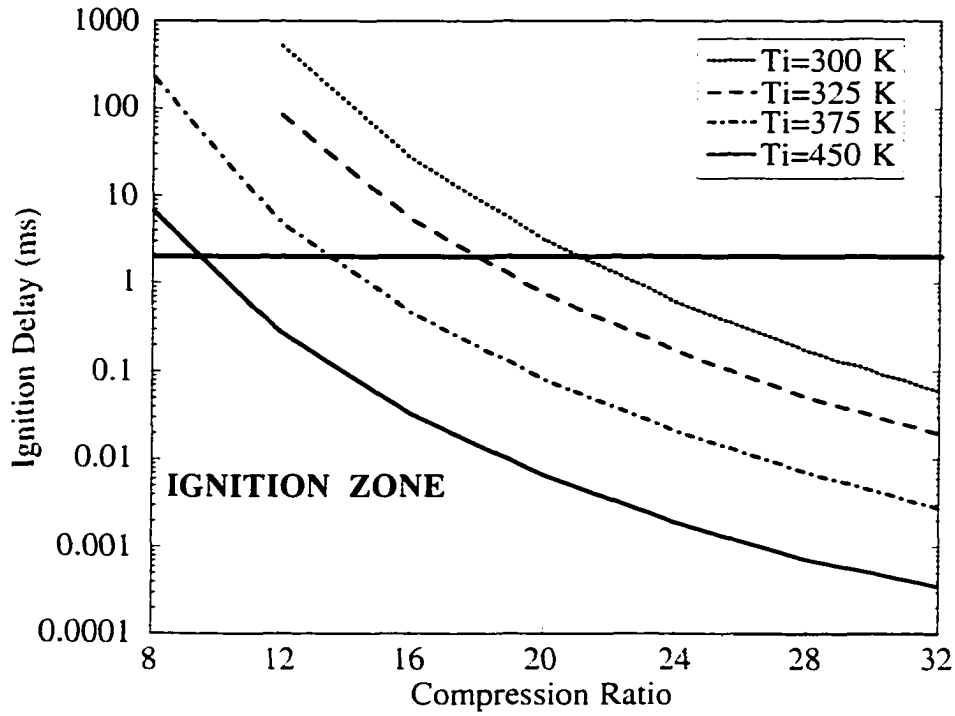

Figure 2.8: Variation of ignition delay with compression ratio for mean natural gas.

Closure

The effect of natural gas composition on ignition delay under compression ignition conditions was investigated numerically by using detailed and reduced chemical kinetic mechanisms. It was shown that the skeletal mechanism was inadequate to predict ignition delay even for pure methane mixtures under high pressure conditions. On the other hand, the potential of more detailed multi-step kinetic mechanisms, GRI-Mech 1.2 and DRM22 to predict ignition delay of natural gas under a range of temperatures, pressures, and compositions was revealed. Since both mechanisms showed excellent agreement with experimental trends under a variety of in-cylinder conditions, DRM22 was chosen to continue further studies, primarily because of its reduced computational costs.

The computational studies performed in a combustion bomb demonstrated the importance of natural gas composition on ignition delay, especially at high temperatures.

Adding traces of higher hydrocarbons (ethane, propane etc.) can reduce the ignition delay period considerably. This could be used to offset the high temperature and pressure requirements for the autoignition of pure methane.

The computations also showed that increasing ambient density decreases ignition delay for all the fuel blends examined here. Higher ambient density means higher compression ratio or higher intake air pressure. Hence, super-charged operation of a direct injection engine could be a feasible way to reduce ignition delay while operating at reasonable compression ratios and intake air temperatures.

Kinetic modeling was shown to be able to account for the effect of changing fuel-air ratio. This is important because autoignition in a direct injection engine occurs over a wide range of equivalence ratios. This effect will be further investigated in the next chapter in a multi-dimensional setting which will involve an interface between KIVA-3 and CHEMKIN-II.

Overall, it was shown that prediction of ignition delay of natural gas under compression ignition conditions can be accomplished by the choice of an appropriate kinetic scheme. The mechanism chosen for predictions should be fundamental enough to account for thermodynamic and compositional difference. At the same time, though, the scheme should be appropriately reduced to run efficiently in conjunction with multi-dimensional simulations on engineering workstations.

CHAPTER III

MULTI-DIMENSIONAL MODELING OF NATURAL GAS IGNITION USING DETAILED CHEMISTRY

Background

In the previous chapter, systematic analysis of a detailed chemical kinetic mechanism was conducted to investigate its predictive capabilities under typical thermodynamic and fuel composition related conditions that natural gas injected in a compression ignition engine would encounter. Although, this study focused only on the chemical aspects of ignition delay, it underscored the importance of using a mechanism that has adequate level of detail to describe the oxidation of mixtures of methane and ethane under conditions suitable for DI engines.

To get accurate quantitative predictions of the ignition delay period, it is essential to combine both flow and chemical kinetics modeling. Studies that simulate flow with very simplified chemistry, using one to two step kinetic mechanisms to describe the conversion of fuel and oxidizer to products of combustion, are only appropriate for predicting properties like laminar flame speeds that depend on aggregate heat release. The constants in the Arrhenius reaction rates for these mechanisms could be calibrated under certain very specific conditions to yield the aggregate heat release accurately. However, these reduced mechanisms are not at all suitable for modeling ignition phenomena as they lack the initiation and chain-branching steps that are needed to describe the ignition process. Also, reduced mechanisms often do not have adequate pressure dependency built into them, so their predictions are usually only valid at a constant pressure.

Studies that use detailed chemistry without simulating the flow are often restricted to a very simplified, homogeneous system in which fuel and air are assumed to be perfectly mixed. Such studies only provide an idea of the chemical delay associated with the kinetic reactions rather than the total ignition delay in which physical delay due to finite rate of fuel injection and fuel-air mixing is also included. As will be shown later in this chapter, the chemical delay thus predicted could be orders of magnitude smaller than the total delay, especially at high ambient temperatures. Studies that include spatial variation, often restrict it to only one dimension (Sloan and Ronney, 1992; di Blasi *et al.*, 1991; Tang *et al.*, 1991; Choi *et al.*, 1991). Such studies cannot be used in practical combustion systems like direct injection engines, as the evolution of injection, mixing and ignition are essentially three-dimensional and transient.

Papers that combine detailed chemistry with multi-dimensional flow simulation are rarely found in the literature because of concerns about the enormous computational costs involved in combining these two computationally intensive fields. However, with rapid advancements in computer speed and memory with each passing year, their coupling can be accomplished within reasonable time-frames. So, the objectives of the next phase of the ignition modeling effort were (i) to couple a detailed chemical kinetic mechanism for natural gas ignition with the multi-dimensional reactive flow code KIVA-3, and (ii) to explore the predictive ability of the coupled model in simulating autoignition of natural gas injected in a quiescent chamber under typical top-dead-center conditions in diesel engines. The experimental work of Naber *et al.* (1994), who measured ignition delay of three different blends of natural gas injected in a pre-heated and pressurized combustion bomb at densities that were representative of end of compression conditions in production diesel engines, was used to benchmark the theoretical predictions. Although the ultimate goal was to study ignition in a direct injection engine, ignition in a combustion bomb was used for validation studies as it provides the full physics of direct injection engine combustion in a simplified geometry.

Another objective of this work was to investigate a suitable criterion for the onset of ignition. Autoignition occurs when sufficient self-heating by chemical reactions takes place to accelerate the rates of reactions to produce full-scale combustion. Although ignition phenomena have been the focus of intensive studies over the years, the choice of a criterion to detect the onset of ignition has been rather arbitrary. Different investigators use different sets of definitions; some of the more popular ones being a specified pressure rise, a specified temperature rise, time when the net heat release rate becomes positive, chemiluminiscence, appearance of certain radicals like OH, depletion of the oxidizer, etc. The lack of agreement over a universal indicator for the onset of ignition can lead to significant controversy over the values obtained when evaluating different ignition systems. In this chapter, two different criteria for identifying the onset of ignition have been studied: pressure rise and mass of fuel burned. Although pressure and temperature rise seem to be the criteria of choice (Zhou and Karim, 1994), their values depend on thermodynamic parameters like heat capacities, which vary with mixture composition and temperature. To evaluate the ignition process itself, it is necessary to monitor a phenomenon that is a direct consequence of ignition.

Lastly, the influence of additives, either stable species like higher hydrocarbon fuels or gas catalysts like hydrogen peroxide, was examined in reducing the ignition delay time of pure methane. Addition of increasing amounts of ethane and hydrogen peroxide separately to methane has been shown to substantially decrease its ignition delay. These additives can be used in assisting ignition of methane-air mixtures without having to rely on expensive and complex alternatives like pilot fuel injection, glow plugs or spark plugs.

The methodology developed to couple a detailed multi-step kinetic mechanism with a multi-dimensional flow simulation is described in the next section. Next, details of the modeling approach used to simulate the experiments are given and the predicted ignition delay values are compared with the measurements. The details of the experimental work (Naber *et al.*, 1994) were given in Chapter II and will not be repeated here. Calculations are done for three blends of natural gas and two different criteria to detect the onset of

ignition are compared. Temporal variation of volume-averaged pressure and mass of fuel burned is used to understand the differences in predicted delays at different ambient temperatures and pressures. After confidence in the model is established, parametric studies are performed to investigate the influence of additives, fuel injection rate and fuel temperature on ignition delay of pure methane in the same geometry as the experiments. It is shown that apart from accurate predictions of ignition delay, the coupling between multi-dimensional flow and multi-step chemistry is essential to reveal detailed features of the ignition process.

Multi-Dimensional Flow Modeling With Detailed Chemistry

The detailed chemical kinetic mechanism chosen is the reduced set DRM22 of Kazakov and Frenklach (1996), derived from the full GRI-Mech 1.2 mechanism (Frenklach *et al.*, 1995a and b) by systematically eliminating less important reactions. This reaction set consists of 22 species (plus nitrogen and argon which are inert) and 104 elementary reactions, as compared to 30 species and 177 elementary reactions in the full GRI-Mech 1.2 mechanism. The flow was simulated using a version of the Los Alamos code KIVA-3 (Amsden, 1993), modified at the University of Michigan to simulate gaseous fuel injection (Papageorgakis, 1997). KIVA-3 is a computer program for the numerical calculation of transient, two and three dimensional chemically reactive flows with sprays. It uses a time-marching, finite-volume scheme which solves the equations of mass, momentum, energy and turbulence using a combined Lagrangian and Eulerian technique in three solution phases. Spatial differences are formed with respect to a generalized mesh of arbitrary hexahedrons whose location are specified functions of time. The finite volume procedure is second order accurate in space and first order accurate in time. The standard k-ε model is used for modeling turbulence.

To model ignition, source terms in the energy and species equations due to chemical reactions need to be calculated. The arbitrary Lagrangian-Eulerian (ALE) method used in KIVA-3 for temporal differencing allows for the calculation of the chemical source terms

in phase A, the Lagrangian phase. This decouples their solution from the calculation of the diffusion, acoustic, and convection terms. Hence, at each time-step, each computational cell can be treated as a homogeneously mixed volume of fuel and air with given species concentration, temperature and pressure. The chemical kinetic algorithm can then provide values for the updated species densities and heat release rate due to chemical reactions for each computational cell, at each time-step. Since the energy equation is not solved completely in phase A, the computational cell is assumed to be isothermal during the kinetic calculations at a given time-step. The cell temperature and species concentrations are updated at the end of each solution phase.

The rate of change of species densities, for each computational cell , at each time-step is given by

$$\dot{\rho}_m = \dot{\omega}_m W_m, \qquad m = 1,\ldots, M \tag{3.1}$$

where ρ_m is the density (gm/cm^3) of the M species involved in the reaction mechanism, and $\dot{\omega}_m$ and W_m are the molar production rate (mole/(cm^3-sec)) and molecular weight (gm/mole) of the species, respectively. The molar production rate for any species can be written as the difference of the molar creation rate and the molar destruction rate of that species, i.e.

$$\dot{\omega}_m = \dot{C}_m - \dot{D}_m \tag{3.2}$$

If N elementary reversible (or irreversible) reactions involving M chemical species are represented in the general form,

$$\sum_{m=1}^{M} \nu'_{mn} \chi_m \Leftrightarrow \sum_{m=1}^{M} \nu''_{mn} \chi_m, \qquad n = 1,\ldots, N \tag{3.3}$$

the molar creation and destruction rates are respectively given by,

$$\dot{C}_m = \sum_{n=1}^{N} \nu'_{mn} k_{r_n} \prod_{m=1}^{M} \left[X_m\right]^{\nu''_{mn}} + \sum_{n=1}^{N} \nu''_{mn} k_{f_n} \prod_{m=1}^{M} \left[X_m\right]^{\nu'_{mn}} \tag{3.4}$$

and

$$\dot{D}_m = \sum_{n=1}^{N} \nu'_{mn} k_{f_n} \prod_{m=1}^{M} \left[X_m\right]^{\nu'_{mn}} + \sum_{n=1}^{N} \nu''_{mn} k_{r_n} \prod_{m=1}^{M} \left[X_m\right]^{\nu''_{mn}} \tag{3.5}$$

where ν_{mn} are the stoichiometric coefficients, χ_m is the chemical symbol for the mth species, k_{f_n} and k_{r_n} are the forward and reverse rate constants for the reaction n and $[X_m]$ is the molar concentration of the species m. The forward (or reverse) rate constants for N reactions are assumed to have the following Arrhenius temperature dependence,

$$k_{f_n}\left(\text{or } k_{r_n}\right) = A_n T^{\beta_n} \exp\left(-\frac{E_n}{RT}\right) \tag{3.6}$$

where the pre-exponential factor A_n, the temperature exponent β_n, and the activation energy E_n are specified for each reaction by the kinetic mechanism used, and R is the gas constant with units compatible with activation energy such that the ratio E_n/RT is dimensionless.

The chemical heat release term in the energy equation is given by

$$\dot{Q}_c = \sum_{n=1}^{N} Q_n \dot{q}_n \tag{3.7}$$

where Q_n is the negative of the heat of reaction at a reference temperature, given by

$$Q_n = \sum_{m=1}^{M} \left(\nu'_{mn} - \nu''_{mn}\right)\left(\Delta h_f^o\right)_m W_m \tag{3.8}$$

$\left(\Delta h_f^o\right)_m$ being the heat of formation of species m per unit mass at the reference temperature, and $\dot{q}_n$ the rate of progress of reaction n, given by

$$\dot{q}_n = k_{f_n} \prod_{m=1}^{M} [X_m]^{\nu'_{mn}} - k_{r_n} \prod_{m=1}^{M} [X_m]^{\nu''_{mn}} \tag{3.9}$$

By combining, Eqs. 3.7 and 3.8,

$$\dot{Q}_c = \sum_{n=1}^{N} \left[\sum_{m=1}^{M} \left(\nu'_{mn} - \nu''_{mn}\right)\left(\Delta h_f^o\right)_m W_m \right]_n \dot{q}_n \tag{3.10}$$

and from the definitions of $\dot{q}_n$ (Eq. 3.9) and $\dot{\omega}_m$ (Eqs. 3.2, 3.4 and 3.5), one obtains

$$\dot{Q}_c = -\sum_{m=1}^{M} \dot{\omega}_m \left(\Delta h_f^o\right)_m W_m \tag{3.11}$$

The Sandia chemical kinetics code CHEMKIN-II (Kee *et al.*, 1991) was used to read the reaction mechanism and calculate the chemical source terms in Eqs. 3.1 and 3.11. A new subroutine was written to replace the original subroutine *chem* used to calculate chemical kinetic reactions in KIVA-3. This subroutine is called for each computational cell in the domain at each time-step and calculates the terms on the right-hand side of Eq. 3.1. After initializing CHEMKIN, this subroutine reads the values of species densities, temperature and pressure for that cell. It then repeatedly calls an ordinary differential equation integrator, LSODE (Hindmarsh, 1981) to obtain the updated species densities at the next time-step (from the solution of the M differential equations in Eq. 3.1), the increment in time having been already decided at the beginning of that particular time-step in subroutine *timstp*. Since chemical kinetic equations are usually "stiff" (meaning they have a multitude of time-scales), their integration needs a special numerical scheme, and LSODE has been shown to be highly reliable for the solution of a wide range of "stiff" initial-value problems (Kee *et al.*, 1991). It should be noted that within a time-step, LSODE may be called a number of times till the time for the next time-step $(t + \Delta t)$ is reached. The right-hand side of Eq. 3.1 is updated every time LSODE is called within a time-step. This procedure ensures accuracy and also avoids the risk of any particular species reaching a negative density at the final time, $t + \Delta t$.

Once the updated species densities are obtained, the chemical heat release term (Eq. 3.11) is calculated using the *updated* values. The change in internal energy is then obtained by multiplying $\dot{Q}_c$ by the time increment and dividing by the cell density (for consistency of units). It is a moot point whether $\dot{Q}_c$ should be calculated at *both* the present and next time-steps and an average value used, or the present method is accurate enough. Since the time increment in the calculations done was very small (less than 2 μs), it was thought unnecessary to calculate the value of $\dot{Q}_c$ two times. For stability purposes, the time-step increment is limited so that the ratio of maximum increase in internal energy to the internal energy, over all the cells is less than 0.25. This is a

standard procedure used in KIVA-3 to avoid stability problems due to potentially very high heat release in a particular computational cell.

For the kind of problems being studied by this method, the flow field is usually turbulent. The use of *mean* values of species concentration and temperature in the Arrhenius expressions for reaction rates (in other words, assuming that the flow is laminar) can lead to rates that are two-three orders of magnitude slower than a turbulent situation in which the fluctuations occur on the time-scales of the chemical reactions (Jones and Whitelaw, 1982). However, if the chemistry is slow, as is the case in the ignition process, and the chemical reactions occur at a rate that is much slower than the rate of decay of fluctuations of temperature and concentration, the mean term in the reaction rate dominates. The distinction between "slow" and "fast" chemistry is determined by the Damköhler number, defined as the ratio of the mixing time-scale to the time-scale at which the chemical reactions take place. For turbulent flows, the mixing time-scale is proportional to the time of decay of the turbulent fluctuations. During the ignition delay period, the Damköhler number is small and the autoignition process depends mainly on the chemistry of fuel oxidation. After the initial stages of combustion and subsequent temperature rise, the chemical reaction rate increases and the Damköhler number becomes much larger than unity. In such a situation, the use of mean quantities to evaluate the reaction rates is not justified and a turbulent combustion model is needed. Since this chapter is primarily concerned with the ignition process, the interaction between turbulence and chemistry has not been described. However, a turbulent combustion model based on the interaction between flow and chemical time-scales will be described in the next chapter and used to study the entire energy conversion process, from fuel injection to ignition, turbulent combustion and pollutant formation.

Comparison of Model Predictions with Measurements

As noted before, the experimental work of Naber *et al.* (1994), which focused on ignition delay measurements of natural gas injected in a combustion bomb at high ambient pressures and temperatures was used for the validation of the flow-detailed chemistry model developed in this work. A Cartesian three-dimensional computational grid ($11.4 \times 11.4 \times 2.86$ cm^3) was used for the calculations. Top and side views of this grid are shown in Fig. 3.1. Since the injector orifice was much smaller than the chamber dimensions, a non-uniform grid was created by patching 75 blocks together. The use of a Cartesian geometry allowed for easy control of the cell dimensions. Fine grid resolution was used close to the injector and for the regions where the injected fuel spray was expected to be present. A total of 7569 cells comprised the fluid domain after all the blocks were patched together. To verify that the results obtained using this grid were independent of the mesh size, the number of grid points in the regions close to the injector was doubled in all the three directions. The fine grid so obtained gave almost identical values of ignition delay as compared to the original grid, and so grid independence is assumed in the results described in the next sub-section.

Injection of natural gas was simulated by specifying time-varying mass flow, velocity and internal energy in the cell that corresponded to the injector location. Further details of the gaseous injection model can be found in Papageorgakis (1997). The injector cell was located in the center of the computational domain and had a cross-section of 0.3 mm × 0.3 mm. It is the cell at the intersection of the thick cross in the center of the side view in Fig. 3.1. Based on the stagnation values of intake pressure and temperature (P_o=20.7 MPa and T_o=450 K), and assuming a specific heat ratio, γ of 1.237 (for pure methane at 450 K), the critical pressure and temperature at the exit of the orifice were found to be 11.54 MPa and 402 K respectively. Since the flow was choked, the isentropic injection velocity could simply be calculated as the speed of sound at the critical temperature at the exit and was found to be 508.5 m/sec. To account for real affects, the isentropic injection velocity was multiplied by a discharge coefficient

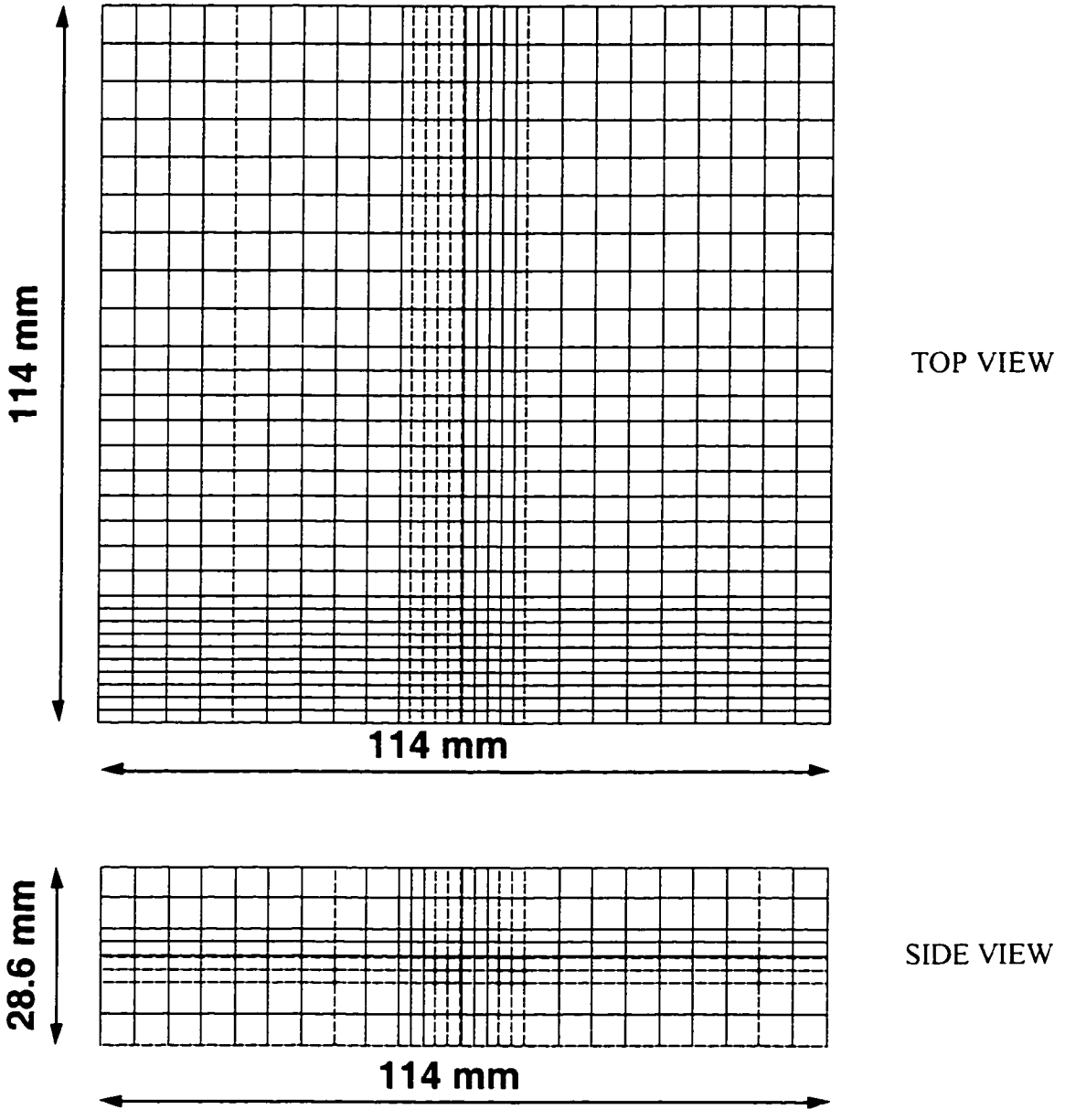

Figure 3.1: Top and side views of the computational grid used in the simulations.

(C_D=0.87), found in the experiments. So the actual injection velocity used in the calculations was 442.4 m/sec. The mass flow rate based on the injection velocity, cross-sectional area of the orifice and the critical pressure and temperature was found to be 1.2 gm/sec. This corresponded exactly to the injection rate during the steady state portion of injection as 14 mg of fuel was injected over a period of 11-13 ms, leading to a mass flow rate between 1.1 gm/sec and 1.27 gm/sec. An independent verification of the injection velocity was also provided by comparing the theoretical value of 442.4 m/sec to the gas jet velocity at the orifice of about 400 m/sec reported by Naber *et al.*

Internal energy corresponding to fuel at a temperature of 400 K was specified in the injector cell to simulate the cold fuel injected in the domain. This value of internal energy was found directly from the internal energy tables for each species in KIVA-3. The thermodynamic properties of extra species were obtained from the JANAF tables. To account for turbulence coming in with the fuel, a value of turbulent kinetic energy corresponding to 1% of injection velocity squared was added to the turbulent kinetic energy in the injection cell. Injection was assumed to start from the beginning of the computation and was terminated after 12 ms. A range of ambient temperatures from 1150 K to 1500 K was simulated at an ambient density of 20.4 kg/m^3. This corresponded to ambient pressures from 65 to 85 atm. The constituents of the chamber at the beginning of the calculation were assumed to be atmospheric air in the proportion 79% nitrogen and 21% oxygen. Although, in the experiments, the fuel was injected in a slightly different environment due to the two stage combustion process used, the effect of ambient air concentration on measured ignition delay was found to be insignificant by the experimentalists. The first stage combustion process yielded products that had slightly higher concentration of carbon-dioxide and water than normal air. In an independent study, Yossefi *et al.* (1995) found that only *substantial* proportions of CO_2 could have a significant impact on the ignition delay period of methane and ethane. This fact was also confirmed independently by performing a few calculations of ignition of fuel-air mixtures with varying proportions of CO_2 and H_2O in a homogeneous configuration. No

appreciable differences in ignition delay were observed for concentrations of CO_2 and H_2O as high as 10% in the air.

At each time-step, volume averaged pressure in the computational domain was monitored and the calculation terminated when the pressure rise exceeded a value of 11 kPa from the start of the calculation. This value of 11 kPa is $\pi/4$ times the value of 14 kPa used in the experiments. Since the computations were performed on a grid whose volume was $4/\pi$ times the experimental chamber volume, for the same heat release, first law dictates that the average computational pressure rise should be $\pi/4$ times the experimental value. Also, pressure rise is only a secondary effect of the ignition process; consumption of the fuel being the primary one. For a certain amount of heat release, the value of pressure rise would depend on the specific heats of the mixture, which vary with ambient temperature and mixture composition. So, to get a more direct measure of the ignition delay at different ambient temperatures, and also to compare the ignition delays of different fuels, the mass of fuel burned was also monitored at each time-step. It should be noted that due to the multi-step nature of the kinetic mechanism used in this study, at each time-step, fuel is consumed as well as formed (see Eq. 3.2). In order to avoid confusion between "original" and "formed" fuel from various reacting species, the fuel destruction rate, $\dot{D}_{fuel}$ given by Eq. 3.5, was calculated and integrated over time to get a value of mass of fuel burned.

Comparison with experiments

Figure 3.2 shows the variation of ignition delay of pure methane with temperature at an ambient density of 20.4 kg/m^3. The experimental delay is obtained from the ignition delay correlation (Eq. 2.1) and two criteria are used for the theoretical delay: pressure rise of 11 kPa and 0.33 mg of methane burned. It is seen that both criteria give values that are close to experimental ignition delay over the range of temperatures studied. Figure 3.2 also shows the variation of "chemical" delay with temperature. This delay is obtained by simulating the autoignition of a homogeneous methane-air mixture by ignoring spatial

variation (see Chapter II for details). It can be clearly seen that ignoring the injection and flow processes can lead to predicted values of delay that are lower by more than an order of magnitude compared to the experimental values.

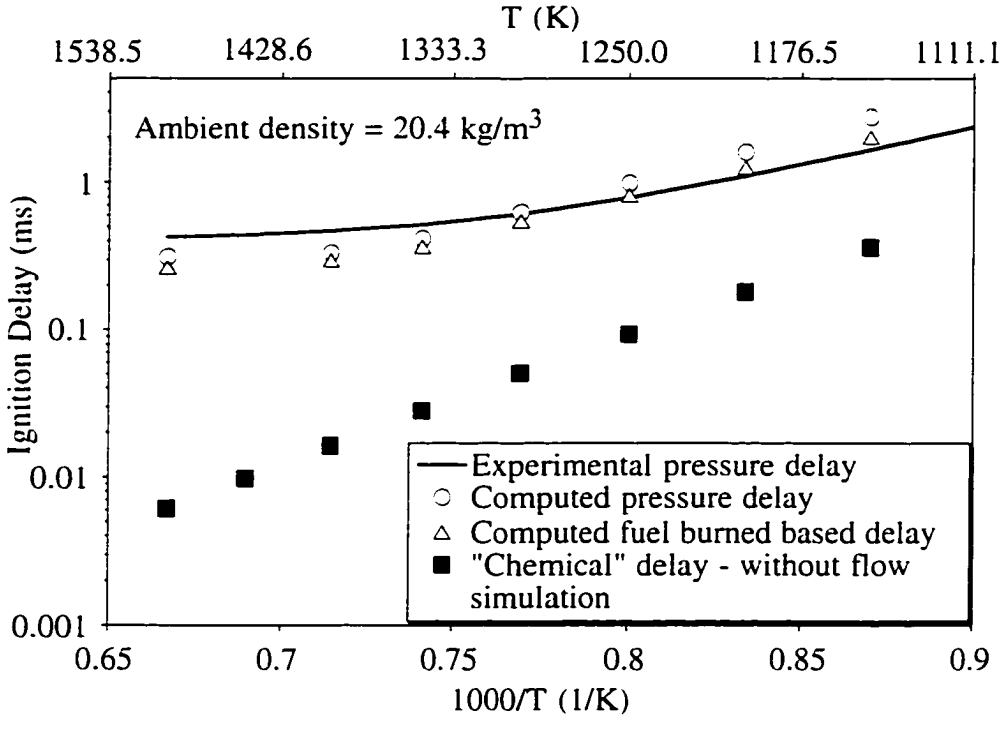

Figure 3.2: Variation of ignition delay of pure methane with temperature in Arrhenius coordinates.

Figure 3.2 has been drawn in Arrhenius coordinates, following the usual practice to show the Arrhenius dependence of ignition delay on temperature. The variation of log(delay) with inverse temperature (T^{-1}) is not a straight line due to the effect of ambient pressure, which is different at each temperature, as the density is kept fixed. Figure 3.2 clearly shows that the coupled chemistry-flow model is able to capture the effect of temperature and pressure on ignition delay of pure methane. The numerical values agree almost perfectly in the range of initial temperatures from 1200 K to 1300 K. This is the range that is most useful for direct injection engine studies as it leads to delays that are between 1 ms to 2 ms, the range for normal engine operation. The discrepancy at higher initial temperatures is due to the fact that the ignition delay correlation (Eq. 2.1) was

designed to asymptote to a value of 0.41 ms at high temperatures. This value of 0.41 ms represents the shortest pressure delay that could be measured in the experiments accurately. The actual experimental ignition delay values varied between 0.35 and 0.6 ms for ambient temperatures greater than 1400 K. Based on the scatter in the data and the confidence levels reported by Naber *et al.* (1994) for the various parameters in Eq. 2.1, the agreement with experimental data is very good. All the computations reported here were done on a SUN Ultra2 workstation and took between 20 hours and 7 days of CPU time depending on the time of the simulation (ranging between 0.3 ms to 2.8 ms).

Figure 3.3 shows the temporal variation of volume-averaged pressure rise of pure methane at different ambient temperatures. It can be seen that at all temperatures a distinct drop in pressure is observed during the pre-ignition phase. This drop is due to heat transfer through the cold walls and the mixing of the cold fuel (at 400 K) with the hot air inside the chamber and the endothermic formation of radicals before ignition. Pre-ignition reactions have been shown to appreciably decrease the temperature in the initial period of ignition lag (di Blasi *et al.*, 1991). Also, this drop in pressure can be used to explain the increasing difference between the two computed delays in Fig. 3.2 at lower ambient temperatures. As the temperature decreases, the pre-ignition phase becomes longer and more cold fuel is injected into the domain. This results in a higher pressure drop and thus more time is taken for pressure to rise by 11 kPa from the *start* of injection. However, the delay based on a specified mass of fuel burned is independent of this "cooling" effect and is thus a more consistent criterion when comparing ignition delays over a range of temperatures.

As the ambient temperature increases, the ignition delay decreases not only because of thermal effects but also due to increasing ambient pressure. Other studies have shown a first order inverse (p^{-1}) dependence of ignition delay on pressure (Naber *et al.*, 1994; Agarwal and Assanis, 1997; Westbrook and Pitz, 1987). It is interesting to note that at initial temperatures greater than 1300 K, pressure increases rapidly initially and then the rate of pressure rise starts decreasing. This is due to a change in fuel consumption rate, a

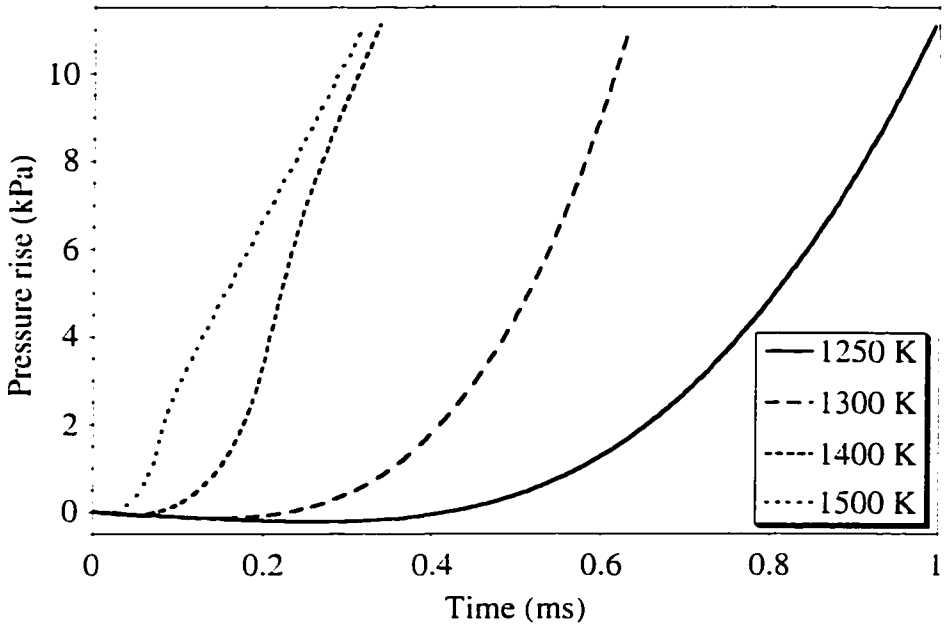

Figure 3.3: Variation of volume-averaged pressure rise of methane with time at different ambient temperatures.

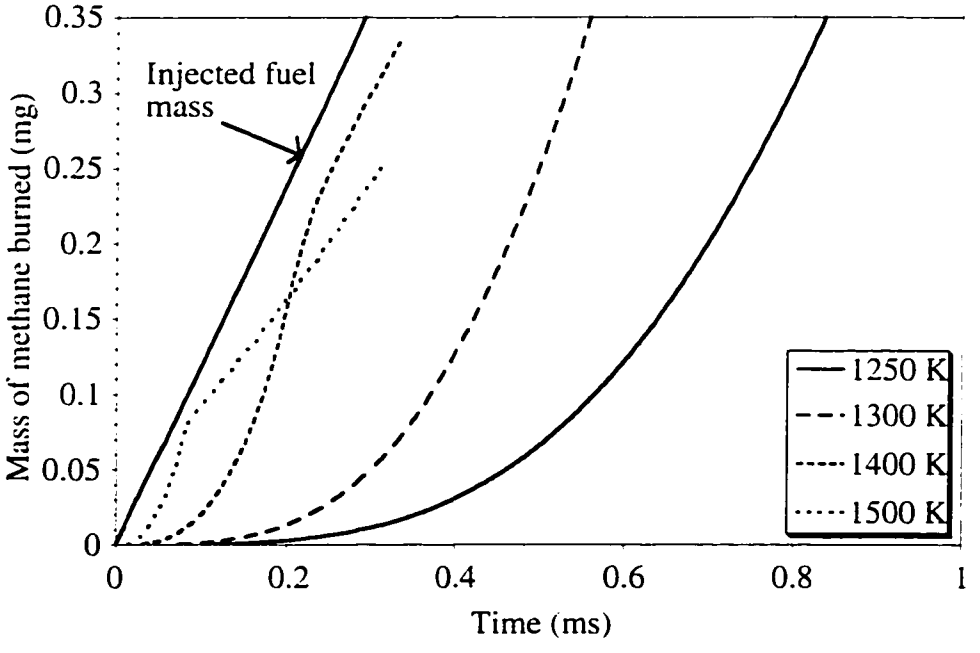

Figure 3.4: Variation of mass of methane burned with time at different ambient temperatures.

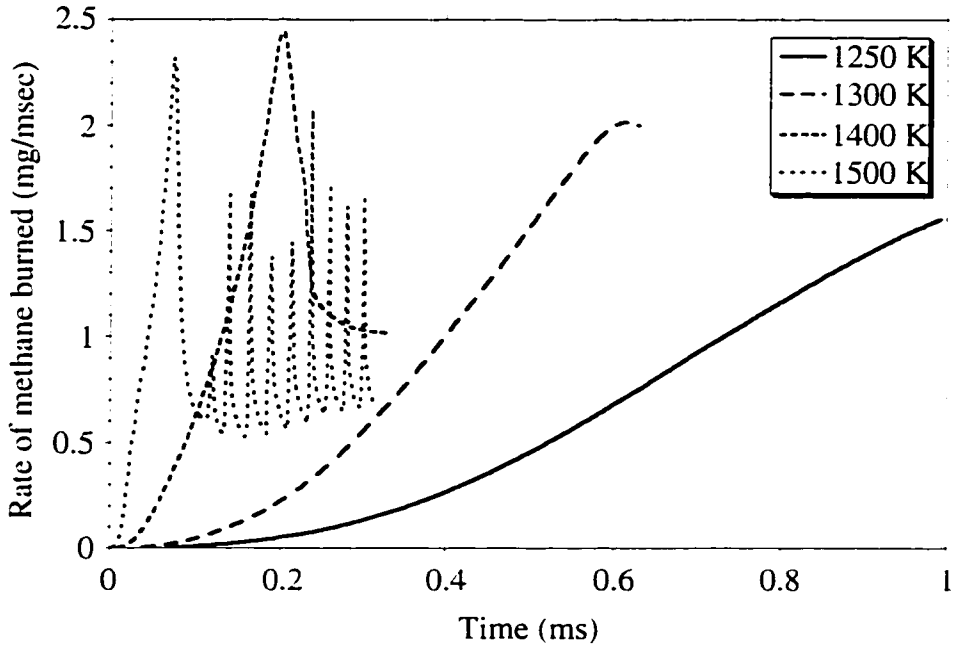

Figure 3.5: Variation of rate of methane burned with time at different ambient temperatures.

fact that becomes clear in Fig. 3.4. This figure also shows that it takes a distinct time-delay (e.g. about 0.2 ms for an ambient temperature of 1250 K) for the fuel to start getting consumed. It is only after this delay phase is over that the pressure starts rising.

Figure 3.4 shows the variation of mass of methane burned with time for four different initial temperatures. The straight line shows the mass of methane injected in the domain as a function of time. At ambient temperatures below 1300 K, chemistry is slow and, over the time scale examined in this problem, fuel gets burned at a rate that is much lower than the injection rate. However, at an ambient temperature of 1400 K, there is a rapid increase in mass burn rate at 0.2 ms due to kinetic reactions. Since the fuel is being injected at a finite rate, and not much of it has accumulated in the chamber over such a short period of time, almost all the fuel in the chamber is consumed leading to a decrease in mass burn rate. The fuel that remains is too rich to burn. The same process is repeated at 1500 K, but sooner, and the mass burn rate quickly becomes injection and mixing limited. It should be noted that due to the extremely rapid rate of burning and consequent

fast pressure rise in the early stages, much less fuel needs to be burned to get a rise of 11 kPa as compared to lower ambient temperatures. Investigation of the flow field temperatures for the two highest ambient temperatures reveals that the temperature in the computational cells where ignition occurs quickly increases by more than 400 K, whereas for the lower ambient temperatures, it does not increase by more than 50 K for the duration of the simulations (terminated when a pressure rise of 11 kPa is detected). This situation of rapid temperature rise is akin to a thermal explosion.

Figure 3.5 shows the rate of fuel mass burned for the four initial temperatures studied. It can be seen that for the two highest temperatures investigated, the burn rate quickly increases above the injection rate of 1.2 mg/ms. This leads to rapid depletion of the fuel that has mixed with air within flammability limits and soon the ignition process becomes limited by the rate at which the fuel is being injected. Oscillations are seen in the burn rate due to the dependence of burning on injection and mixing. When the burning rate becomes very high, the ignition model loses its validity. The assumption that the Damköhler number is small can no longer be valid, and some kind of a turbulent combustion model is needed to describe flame propagation after the pre-mixed fuel has been consumed and a diffusion flame has been initiated. Since turbulent combustion modeling was not part of the study at this stage, attention has been focused on lower initial temperatures (below 1300 K) for the rest of the cases shown in this chapter.

Two more blends of natural gas were examined by Naber *et al.* over the same range of thermodynamic conditions as methane. The compositions of each of these blends were summarized in Table 2.6. As pointed out before, due to the inability of the selected reaction scheme to simulate hydrocarbons having more than two carbon atoms, the concentrations of propane and butane were lumped with those of ethane. So the computational mean natural gas consisted of 4.3% "ethane" and the computational high ethane natural gas consisted of 10.25% "ethane". Table 3.1 compares experimental and computed ignition delays for the three blends at initial temperatures of 1250 K and 1300 K. The experiments clearly show that ignition delay decreases, as the concentration of

Table 3.1
Comparison of ignition delay for three different blends of natural gas at initial temperatures of 1250 K and 1300 K and an ambient density of 20.4 kg/m^3.

Fuel	Experimental pressure delay (ms)	Computational pressure delay (ms)	Computational fuel burned delay (ms)
	Ambient Temperature of 1250 K		
Methane	0.85	0.99	0.82
Mean Natural Gas	0.71	0.96	0.75
High Ethane NG	0.67	0.98	0.74
	Ambient Temperature of 1300 K		
Methane	0.61	0.63	0.55
Mean Natural Gas	0.54	0.61	0.50
High Ethane NG	0.53	0.63	0.49

ethane in the mixture is increased. This is due to an increase in the radical concentration pool due to the addition of more reactive ethane (Agarwal and Assanis, 1997; Westbrook, 1979; Westbrook and Pitz, 1987; Zamansky and Borisov, 1992). Not much difference can be noticed between mean and high ethane natural gas. In general, values of ignition delays computed using the two criteria outlined before are close to the experimental values at both initial temperatures. However, computed delay based on a specified pressure rise does not consistently decrease with increasing concentration of ethane in the mixture. On the other hand, computed delay based on a specified mass of fuel burned shows a monotonic decrease in going from pure methane to high ethane natural gas. This is because the pressure delay also includes the effects of heat capacity of the mixture, whereas a delay based on mass of fuel burned depends only on kinetics, and hence is a better indicator of the reactivity of a fuel-air mixture. Furthermore, decrease in pressure during the pre-ignition period, as a result of the mixing of cold injected fuel with the hot air inside the chamber, could influence the values of computed pressure delays. This

pressure drop would not be a factor if a delay based on the mass of fuel burned is used as a criterion for the onset of ignition.

Parametric Studies

The coupling of detailed chemistry and flow has provided results that compare very well with the experimental data. In this section, a series of parametric studies will be performed to gain a better understanding of the physico-chemical processes occurring when parameters like fuel composition, injection rate and fuel temperature are changed.

Influence of additives on ignition delay of pure methane

Since methane is the least reactive among hydrocarbon fuels, selection of efficient promoters for its oxidation is of practical interest. Due to the requirement of very high ambient temperatures (1100-1200 K) for reasonable ignition delay times, complex, external ignition systems like glow plugs, spark plugs or pilot fuel injection are needed. In response to these concerns, recent studies (Zamansky and Borisov, 1992; Karim *et al.*, 1991; Wong and Karim, 1996; Glovitchev *et al.*, 1996), have examined the effects of additives in promoting autoignition of methane at high temperatures. Systematic data on the effect of stable additives, higher hydrocarbon fuels, and free radicals on methane autoignition are summarized by Zamansky and Borisov (1992). According to their findings, the best promoters are additives which are able to increase the radical concentration without disappearing during the induction period. Although a number of studies involving promoters like ethane, propane, nitrogen-dioxide etc. were referenced, none of them were done under the conditions of the present investigation. The use of formaldehyde as an additive in reducing ignition delay of dual fuel engines running on methane was investigated analytically by Karim *et al.* (1991). Wong and Karim (1996) analyzed the effects of exhaust gas recirculation (EGR) on the autoignition of engines running with gaseous fuels. They found that controlled EGR could enhance the

autoignition processes in gas-fueled compression ignition engines by suitably seeding the intake charge with the chemical species found in the exhaust of the previous cycle.

Glovitchev *et al.* (1996) investigated the efficiency of hydrogen peroxide (H_2O_2) in promoting the autoignition of methane. Using a time dependent model, with no spatial variation, they found that replacing 5-10% (volumetric) of the fuel with H_2O_2 shortens the ignition delay by over *one order of magnitude* for all the conditions examined in their work. The effect of promotion was particularly pronounced at temperatures below 1500 K. Since the effectiveness of H_2O_2 was shown to be so dramatic, its effect on the ignition delay of pure methane was studied in the present investigation under the same conditions as the experiments. Two mixtures were studied: 95% CH_4 plus 5% H_2O_2 and 90% CH_4 plus 10% H_2O_2 (by volume). The calculations were done at an initial ambient temperature of 1250 K.

Figures 3.6 (a) and (b) show the variation of pressure rise and fuel burned as a function of time for pure methane and the two mixtures with added H_2O_2. It can be clearly seen that addition of just 5% of H_2O_2 to pure methane reduces the ignition delay substantially. Note that due to the action of H_2O_2, there is virtually no drop in pressure in the initial stages, i.e. the induction period has been reduced significantly. This observation is corroborated by Fig 3.6 (b) in which it is seen that the fuel burns much more rapidly with H_2O_2 added. It is also seen that the blend with 10% H_2O_2 doesn't show any appreciable decrease in delay over the blend with 5% H_2O_2. The reason why H_2O_2 acts as such an effective ignition promoter is that in the early stages of ignition, it rapidly decomposes via the reaction

$$H_2O_2 + M \Leftrightarrow OH + OH + M \qquad (3.12)$$

and thus serves as the major radical source (Glovitchev, 1996). Another advantage of using H_2O_2 as an additive is that it acts mainly as a gas catalyst, i.e. the mixture composition and temperature at final equilibrium remain unchanged.

Table 3.2 summarizes the numerical values of ignition delay of pure methane and the two mixtures with hydrogen peroxide. Addition of only 5% H_2O_2 reduces the ignition

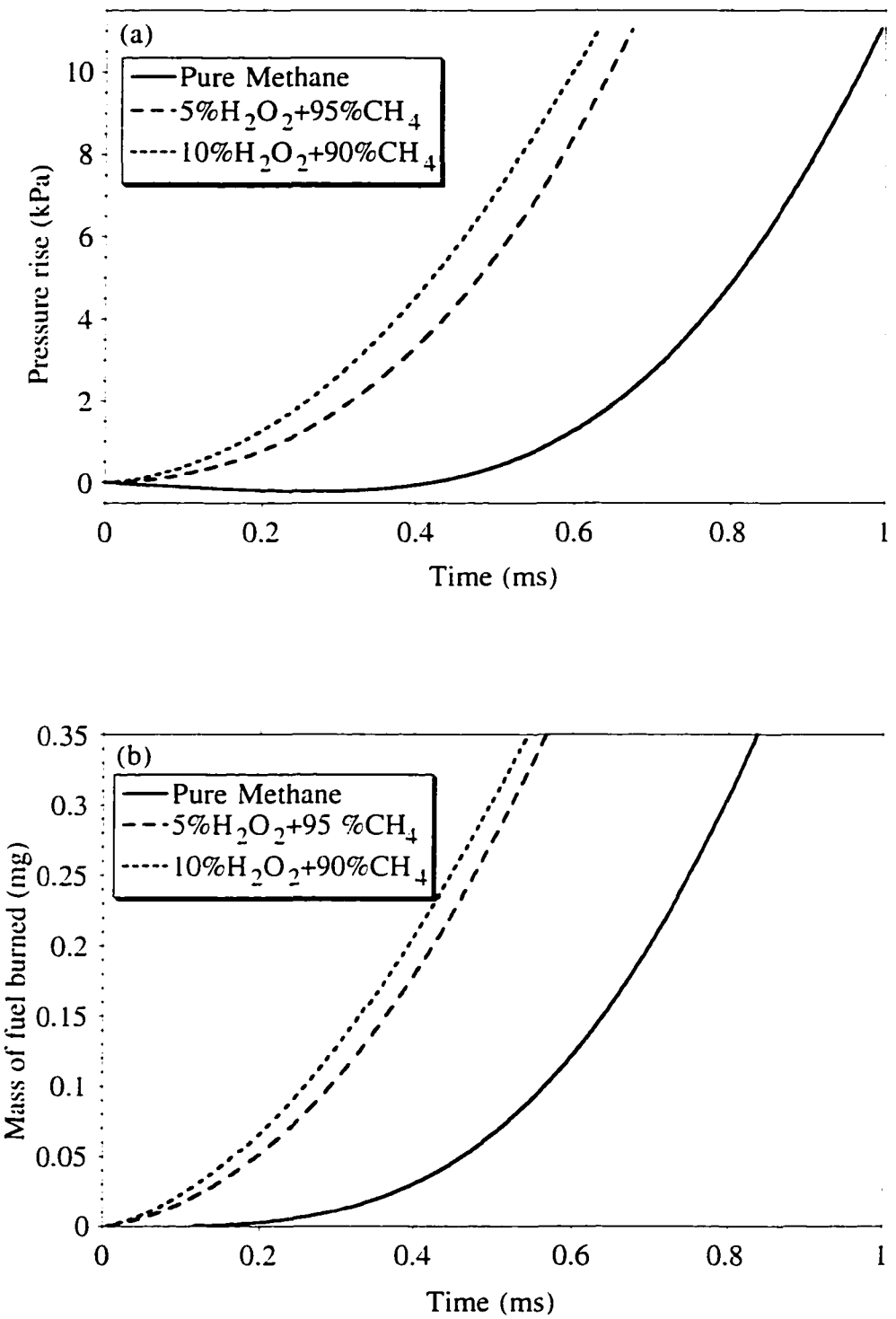

Figure 3.6: (a) Temporal variation of volume-averaged pressure rise and (b) mass of fuel burned of methane and two blends with H_2O_2 at 1250 K.

Table 3.2
Comparison of ignition delay of pure methane with two blends with hydrogen peroxide at an initial temperature of 1250 K.

Fuel	Computational pressure delay (ms)	Computational fuel burned delay (ms)
Pure Methane	0.99	0.82
95% CH_4 + 5% H_2O_2	0.67	0.55
90% CH_4 + 10% H_2O_2	0.63	0.53

delay by about 35%. Although this is not an order of magnitude reduction, as claimed by Glovitchev *et al.* (1996), it is still significant. A corresponding decrease in delay of pure methane by temperature alone would require an increase of about 150 K. This saving in ambient temperature is substantial and could be used to mitigate the high compression ratio requirement in a compression ignition natural gas engine. It should also be noted that the effect of ethane addition was much less pronounced under similar conditions (see Table 3.1).

Influence of injection rate on ignition delay and ignition location

The rate at which the fuel is added can also have a significant impact on fuel-air mixing and hence ignition delay. The fuel flow rate can be changed either by changing fuel density or the injection velocity. To isolate the thermal effects due to mixing of methane and air, the injection velocity was kept fixed at its previous value and three different fuel densities were examined that corresponded to the baseline fuel flow rate (same as experiments), five times its value and ten times its value. The injection temperature of methane was kept fixed at 400 K and the chamber was kept at an ambient temperature of 1300 K.

Figures 3.7 (a) and (b) show the variation of volume-averaged pressure rise and methane burned with time for the three mass flow rates examined, i.e., 1.2 mg/ms, 6

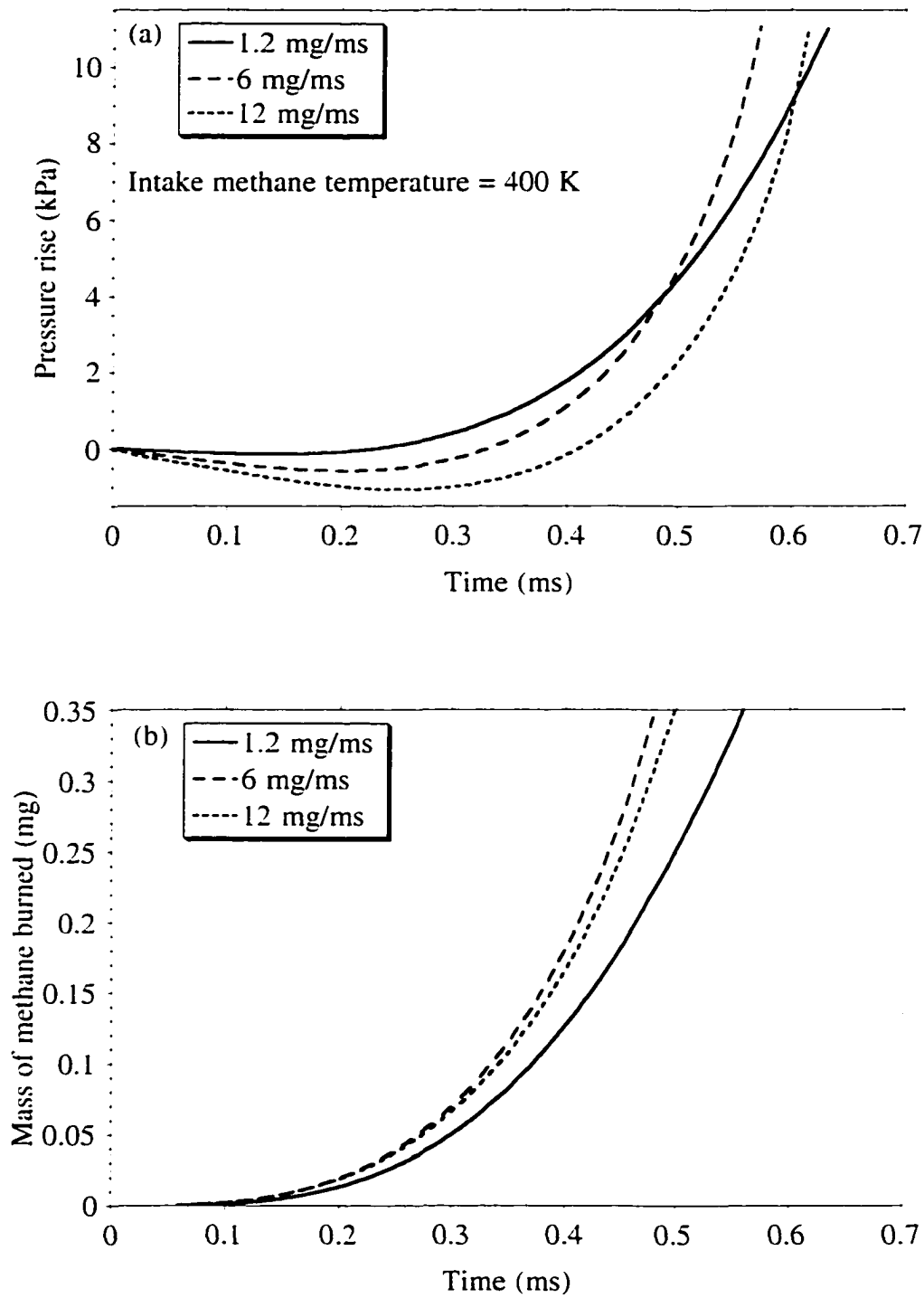

Figure 3.7: (a) Temporal variation of volume-averaged pressure rise and (b) mass of methane burned at ambient temperature of 1300 K for three injection rates.

mg/ms and 12 mg/ms. During the pre-ignition period, the chamber pressure is lowest for the maximum injection rate. This is due to the reduction in chamber temperature resulting from mixing with larger quantities of the colder injected fuel. However, the mass burning rate, which depends on the amount and temperature of flammable fuel-air mixture, is lowest for the baseline case. This is due of the fact that, for the baseline case, there is not enough fuel in the chamber to result in as vigorous a burning rate as for the two higher injection rates. The medium injection rate shows the highest burning rate, as it combines the requirement of more fuel with a lesser reduction in fuel-air mixture temperature compared to the highest injection rate. Note also that due to their higher mass burning rates, the pressure rise for the medium and highest injection rates eventually overtakes the pressure rise for the baseline injection rate. Since, over the time scale of this problem, the pressure rise and mass burned of the highest injection rate are always lower than the medium injection rate, from the point of view of ignition delay alone, an optimum injection rate can be found that balances the cooling effect of injected fuel with the requirement of adequate fuel in the chamber.

Figures 3.8 (a) and (b), shown in color, depict the temperature field in a plane that cuts through the middle of the domain. The injector is located in the center on the left side of the plane. The ambient temperature for both runs is 1300 K and the injected fuel is at 400 K. The difference between the two cases is that the mass flow rate of methane is 6 mg/ms in Fig. 3.8 (b) compared to 1.2 mg/ms in Fig. 3.8 (a), which is the baseline case. The temperature snapshot is taken at 0.47 ms from the start of injection, just after a temperature rise is detected. It can be seen that the injected fuel jet is confined to the region where the computational grid was kept very fine. The two figures show that for the baseline injection rate, ignition occurs towards the front of the injected jet, whereas for the rate that is five times higher, it occurs at the side of the jet, close to the injector. This behavior can be understood from noting the minimum values of temperature in the two figures. For the baseline case, the injection rate is very low, and the temperature of the fuel-air mixture only drops by about 60 K close to where injection occurs, whereas for the

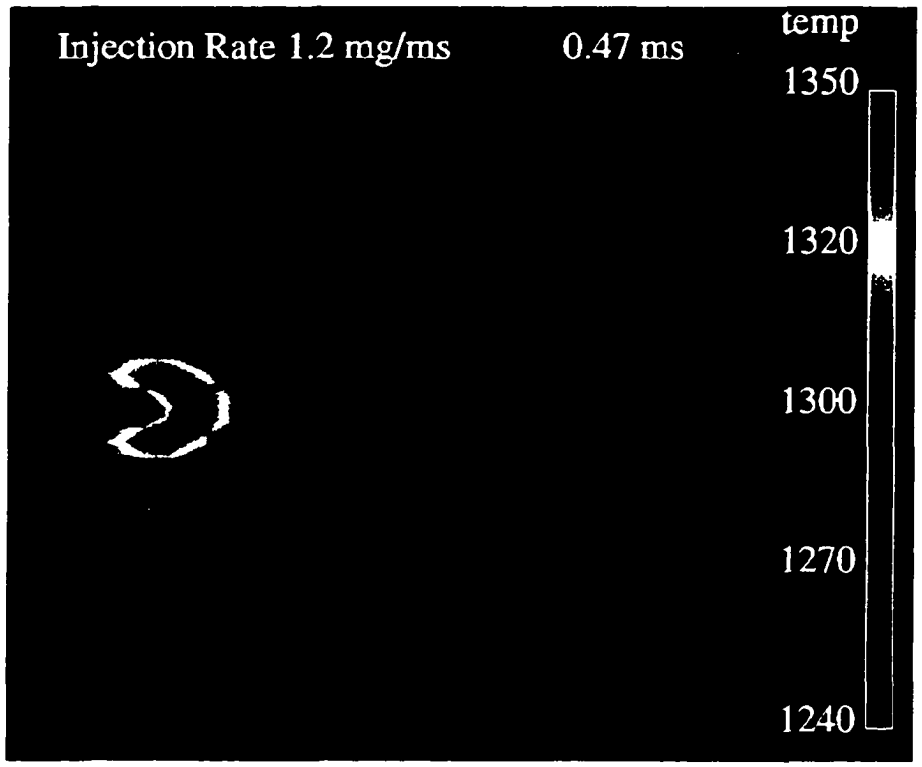

(a)

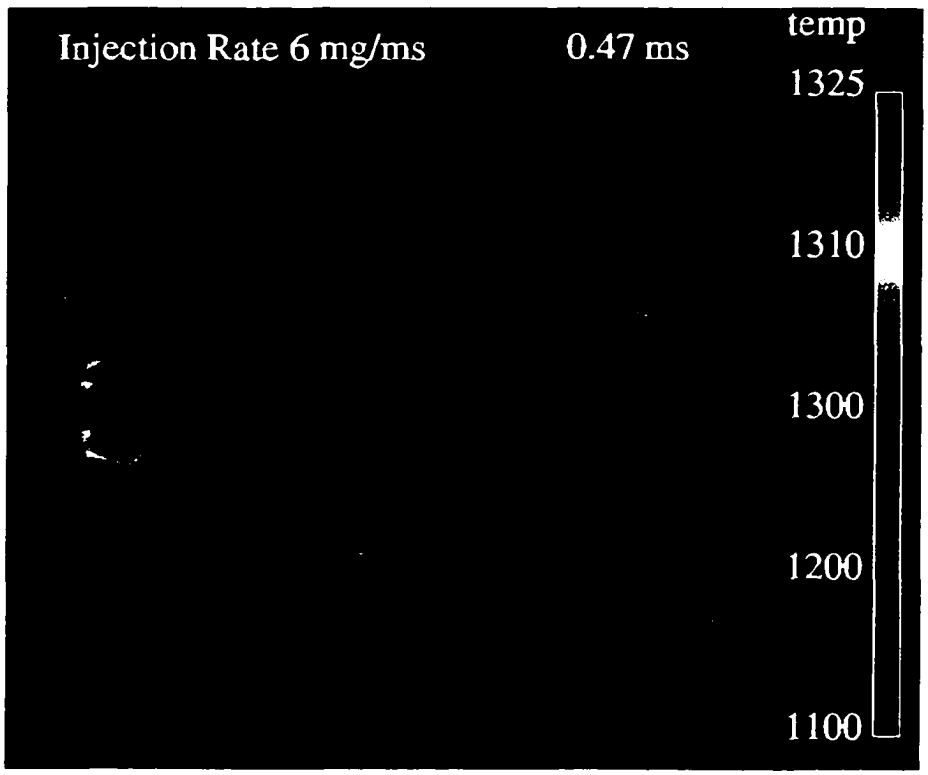

(b)

Figure 3.8: Temperature in a plane cut through the center of the domain at 0.47 ms for (a) baseline and (b) high injection rate. Fuel temperature is 400 K and ambient temperature is 1300 K.

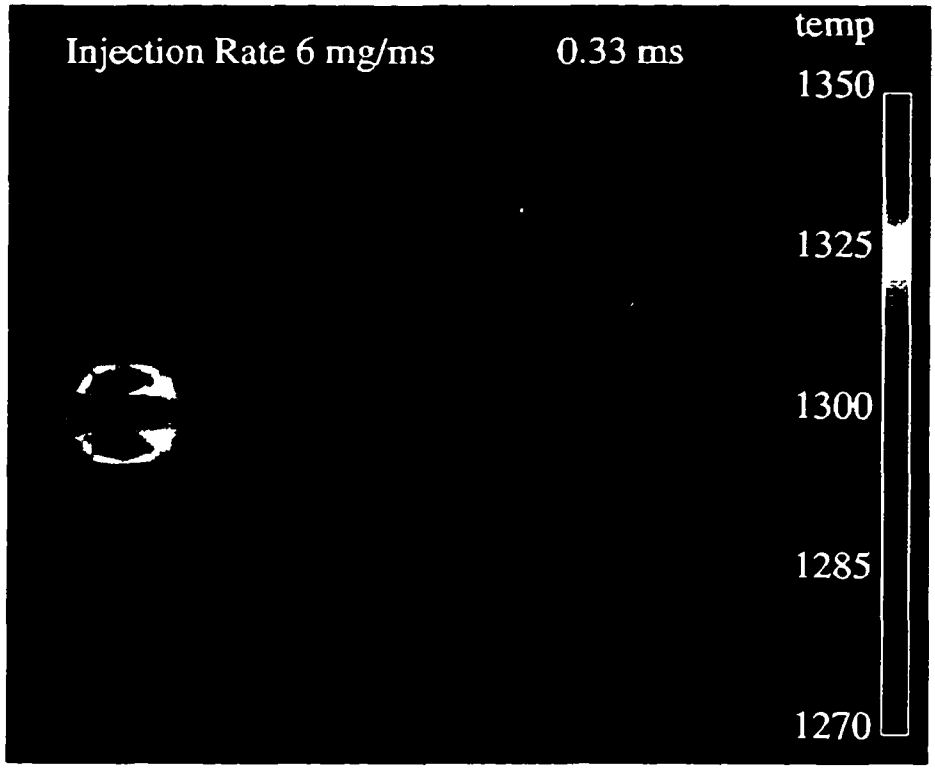

Figure 3.9: Temperature in a plane cut through the center of the domain for high fuel temperature case at 0.33 ms. Fuel and ambient temperature are 1300 K.

higher injection rate, the temperature of the mixture drops by more than 200 K in regions where appreciable mixing takes place. Also, the higher momentum of the injected gaseous jet for the second case helps in penetrating the cooling influence of the jet along its axis. Thus, ignition starts in the pockets of fuel-air mixture at the periphery of the jet close to the injector and is confined there till 0.47 ms while for the baseline case, the temperature of the fuel-air mixture is high at the periphery of the jet between the injector and the tip of the jet, so ignition is seen to occur there.

Influence of fuel temperature on ignition delay of pure methane

Since ignition is a kinetic process, very heavily dependent on fuel-air mixture temperature, the thermal energy of the incoming fuel jet can have a significant impact on the duration of reactions that lead to ignition. Figure 3.9 shows the temperature field at 0.33 ms for the case in which methane is injected at a temperature of 1300 K (same as the

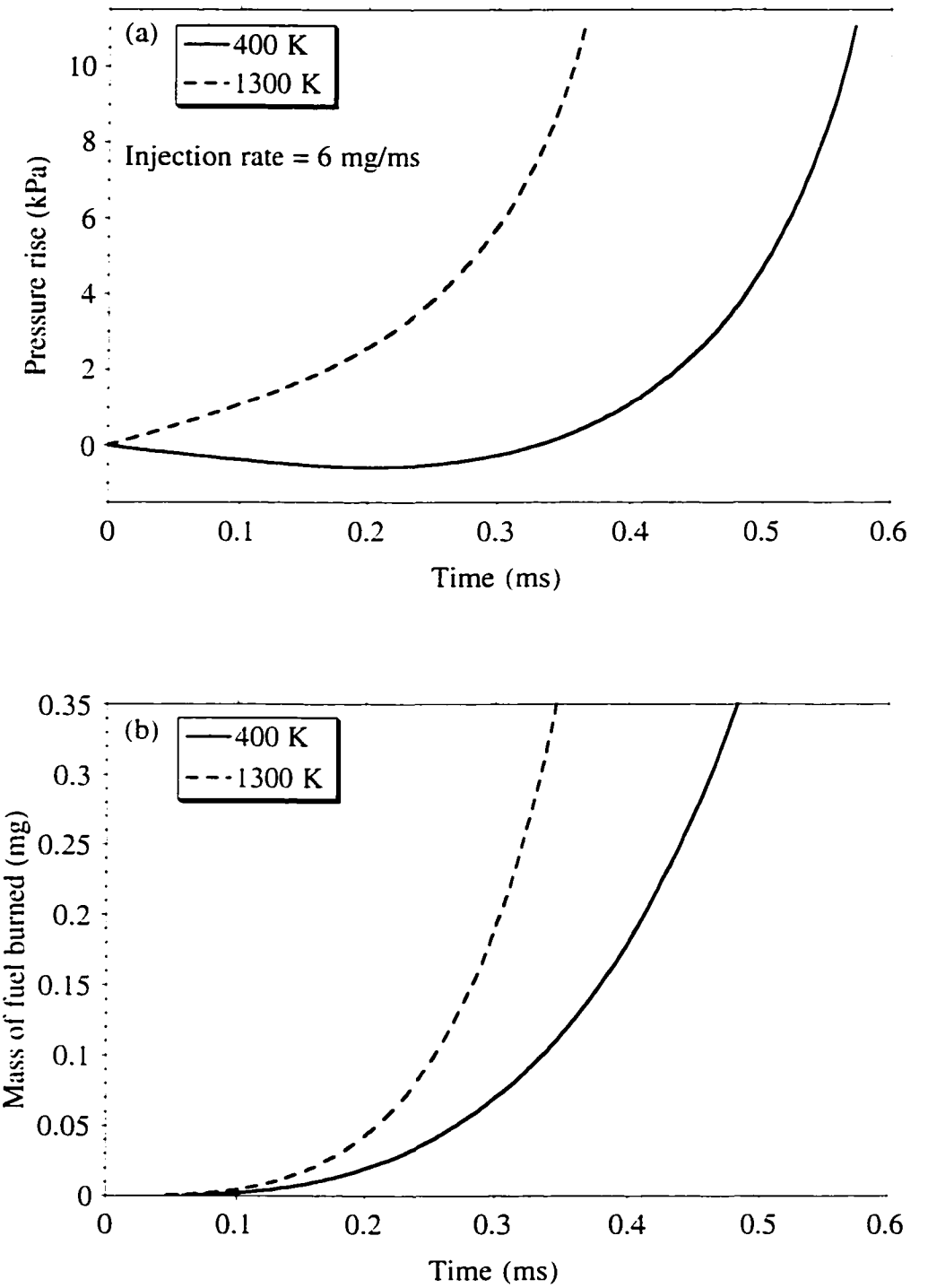

Figure 3.10: (a) Temporal variation of volume-averaged pressure rise and (b) mass of methane burned at ambient temperature of 1300 K for two intake fuel temperatures.

ambient temperature) with a rate of 6 mg/ms. Appreciable temperature rise is detected much earlier than a comparable previous case (Fig. 3.8 (b)). The minimum temperature in the domain is observed to be 1270 K and this reduction is due to the endothermic nature of pre-ignition reactions. The heat release is more vigorous and ignition is seen to occur at the side of the injected methane jet between the tip and the injector.

Figures 3.10 (a) and (b) show the temporal variation of volume-averaged pressure rise and fuel burned mass for the two intake fuel temperatures: 400 K and 1300 K at an ambient temperature of 1300 K. As pointed out in the previous paragraph, there is no decrease in pressure for the higher injection temperature. It is seen that using both the criteria, ignition delay for the higher injection temperature is reduced considerably. It should be noted that heating the incoming fuel is not without costs and additional complexities. However, an increase in fuel temperature is desirable from the point of view of ignition delay and innovative ways could be found to achieve this heating without depending on external heating sources.

Closure

A methodology for coupling the multi-dimensional flow simulation KIVA-3 with a detailed chemical kinetic mechanism consisting of 22 species and 104 elementary reactions was developed. The detailed kinetic mechanism was chosen after an extensive evaluation of its predictive capability under typical compression ignition conditions of pressure, temperature, equivalence ratio and fuel composition in a homogeneous environment (described in Chapter II). The methodology was applied to study autoignition of three different blends of natural gas, injected in a combustion bomb, under thermodynamic conditions that are typical of end of compression conditions in diesel engines.

Comparison of the predicted ignition delay with experiments yielded excellent agreement in temperature ranges from 1150 K to 1300 K. At higher ambient temperatures, it was found that the fuel consumption rate became very fast early on in the computation and the injected fuel was consumed very rapidly. The depletion of the

injected fuel resulted in a drop in the burning rate and the combustion process became mixing controlled. Closer inspection of the flow-field revealed that the maximum temperature under such conditions increased by more than 400 K compared to an increase of about 50 K at lower ambient temperatures.

Two different criteria were used to define the onset of ignition: a specified pressure rise and a specified mass of fuel burned. Although both yielded trends that were consistent with experiments, it was shown that a criterion based on specified mass of fuel burned was a more consistent choice in identifying the onset of ignition as it was a more direct measure of the ignition process rather than pressure rise which depends on the heat capacity of the mixture. Also, decrease of chamber pressure due to mixing of colder fuel with ambient air is not an issue when mass of fuel burned is used as a criterion for the length of the ignition delay period.

The influence of additives like ethane and hydrogen peroxide in reducing the ignition delay period of methane was also studied. The addition of small amounts of hydrogen peroxide (5% by volume), in particular, was found to reduce the delay substantially. The enhanced reactivity of methane in the presence of small amounts of more reactive species like hydrogen peroxide could be used in DING engines to alleviate the high temperature requirements of natural gas.

The role played by fuel injection rate and intake fuel temperature was also studied by the methodology developed here. It was found that an optimum injection rate could be found that balances the requirements of having more fuel in the chamber with the detrimental effect of mixture cooling when colder fuel is injected at a high rate. Injecting the fuel at a high temperature could help in lessening the increase in delay due to charge cooling, but could pose practical difficulties in setting up a system for heating up the fuel line.

Overall, it was shown that *both* flow and ignition modeling are needed to get accurate quantitative predictions of ignition delay under compression ignition conditions. The coupling of detailed chemistry with flow is essential if novel combustion systems are

to be studied with any degree of quantitative accuracy. Also, this approach allows one to easily study the influence of fuel flow rate, mixing rate, fuel composition and temperature on mass burning rate and location of ignition, to better optimize the design of the injector-combustion chamber system. With rapid advancements in computers and our understanding of the fundamental chemistry of higher hydrocarbons, such calculations are foreseen to increasingly become useful tools in designing better combustion systems in the near future.

CHAPTER IV

MODELING TURBULENT COMBUSTION AND POLLUTANT FORMATION

Background

Till now, our attention has been focused primarily on ignition phenomena. However, ignition is only the beginning of the story. In a reactive turbulent flow, such as in an engine, ignition and flame propagation occur at different characteristic time-scales. By assuming that the Damköhler number is small, in other words, by assuming that the characteristic time-scale of chemical reactions is much larger than a characteristic flow time-scale, we have so far been able to neglect the effect of fluctuations in temperature and species concentrations due to turbulence on the mean reaction rates. As shown below, such an assumption is justified during the ignition delay period, when the temperatures are low, and the mean quantities in the reaction rates dominate. However, neglect of the highly non-linear nature of the reaction rate can be extremely dangerous under fast chemistry conditions. This can be explained by considering a simple case of a two-component mean-reaction rate expression when it is expanded about the mean state as (Bilger, 1980):

$$-\overline{\dot{\omega}} = \overline{\rho}^2 \overline{Y}_i \overline{Y}_j A \exp\left(-\frac{E}{R\overline{T}}\right)$$
$$\left\{1 + \left(\frac{\overline{\rho'^2}}{\overline{\rho}^2}\right) + \frac{\overline{Y_i' Y_j'}}{\overline{Y}_i \overline{Y}_j} + 2\left(\frac{\overline{\rho' Y_i'}}{\overline{\rho}\,\overline{Y}_i} + \frac{\overline{\rho' Y_j'}}{\overline{\rho}\,\overline{Y}_j}\right) + \frac{E}{R\overline{T}}\left[\frac{\overline{Y_i' T'}}{\overline{Y}_i \overline{T}} + \frac{\overline{Y_j' T'}}{\overline{Y}_j \overline{T}} + \left(\frac{E}{2R\overline{T}} - 1\right)\frac{\overline{T'^2}}{\overline{T}^2}\right] + \ldots\right\} \tag{4.1}$$

where the terms are written only up to the second correlations. Although equations can be derived for the second order correlations, $\overline{Y_i'Y_j'}$, $\overline{Y_i'T'}$ etc. in terms of higher correlations, the number of variables increases and the classic "closure" problem of turbulence arises.

Under fast chemistry conditions it is known that neglect of the second and higher order correlations in Eq. 4.1 can lead to errors of several orders of magnitude. However, it is important to know whether our assumption that:

$$-\overline{\dot{\omega}} = \overline{\rho^2 Y_i Y_j A \exp\left(-\frac{E}{RT}\right)} = \overline{\rho}^2 \overline{Y}_i \overline{Y}_j A \exp\left(-\frac{E}{R\overline{T}}\right) \tag{4.2}$$

is justified or not during the ignition delay period. To do this we first note that the most important magnitude determining term in Eq. 4.1 is the one involving temperature in the exponential, $\exp(-E/R\overline{T})$. Before ignition occurs, this factor is very small and therefore results in a correspondingly small reaction rate $\overline{\dot{\omega}}$. After ignition occurs, the local temperature of the ignition sites increases dramatically and this factor starts becoming important. Also, the degree to which the second and higher order correlations affect the chemical reaction rate and heat release depends upon the relative characteristic time-scales associated with each of the individual elements in these correlations. Since, during the ignition delay period, chemical reactions take place at a rate that is much smaller than the rate of decay of turbulent fluctuations of temperature and species concentrations, the mean terms dominate and Eq. 4.2 can be assumed to be approximately true.

The foregoing simplifications do not hold forth when the chemical and flow time-scales are on the same order of magnitude and the fluid temperatures are high. In any typical turbulent reactive flow situation, the interaction of turbulence and chemical reactions occurs over a wide range of flow conditions. Weak interactions between them may simply modify the flame slightly causing wrinkles on the flame surface (Williams, 1989). Strong interactions could cause a significant modification in both the chemical reactions and the turbulence. If chemical reactions cause small density changes in the flow, then the turbulence is weakly affected by the heat release process but the turbulence

may still have a strong influence on chemical reactions (Kollmann and Chen, 1992). Since the purpose of combustion is to generate heat, one expects large density changes (of an order of magnitude) to occur, which can alter the fluid dynamics significantly. It has been seen experimentally that the entrainment process in mixing layers is significantly altered by heat release leading to different growth rates than those expected in constant density flows (Hermanson *et al.*, 1985; Dimotakis, 1989). On the other hand, strong turbulence can strain the flame to a point that chemical reactions can no longer keep up with the mixing process causing the flame to extinguish. Experiments by Masri *et al.* (1988) have shown that local flame extinction can occur prior to the flame blowout limit indicating a strong interaction between turbulence and chemistry. Excellent theoretical discussions on the interactions between turbulence and chemistry are provided by Kollmann and Chen (1992), Libby (1992), Chen and Kollmann (1994), and Ghoniem *et al.*, 1989.

To understand and quantify the complex interactions between turbulence and chemistry, it is important to identify the different length and time-scales encountered in various turbulent combustion applications. A fully developed turbulent flow can be characterized by a continuous range of length and time-scales. This range, which is called the inertial range, extends from the large energy containing eddies characterized by the integral length scale at which the turbulent kinetic energy is fed into the system, down to the smallest eddies characterized by the Kolmogorov length scale, where the energy is dissipated. Associated with the length scales are particular time-scales; a turn-over time and a particular turn-over velocity for the large-scale energy containing eddies and the small-scale Kolmogorov eddies.

Combustion reactions taking place within a turbulent flow field introduce their own time-scales. For a propagating premixed flame, the chemical reactions impose their own length and velocity scales in the form of flame thickness and flame velocity, respectively. These scales may interact with the scales of the inertial range in a very specific way, leading to different regimes in premixed turbulent combustion. These regimes are often displayed in phase-diagrams (e.g. Borghi, 1984; Bray, 1980; Williams, 1985). A

discussion of length and time-scales in premixed turbulent combustion based on Borghi's phase-diagram is provided by Peters (1989). Based on the classical theory of Kolmogorov, two characteristic length scales were derived by him for two central regimes in the phase-diagram; the regime of corrugated laminar flamelets and the regime of distributed reaction zones. These two regimes are the most important in many practical applications, particularly in engine combustion. In these two regimes there is a close interaction between turbulence and combustion, because neither of them is completely dominating.

The phase-diagram of Williams (1985), in which the Damköhler number (the ratio of flow and reaction time-scales) is plotted versus the turbulent Reynolds number over the whole range of length scales, merits further discussion. Similar to the Borghi diagram, based on the length scales of flames and turbulence, two extreme regimes are identified in this diagram. One extreme, with the flame thickness much smaller than the smallest length scale of turbulence (the Kolmogorov length scale) is identified as the flamelet regime. The other opposite extreme with flames much thicker than the Kolmogorov length scale is identified as the distributed reaction regime. It should be noted that these two extreme regimes are also identified in the Borghi phase-diagram. The nature of the intermediate regimes between these two extremes is rather complex, and is yet to be explored. Unfortunately, many practical combustion systems involve a wide range of operating conditions including the intermediate regimes.

Figure 4.1 shows the Williams phase-diagram in which the rectangle identifies combustion regimes of typical spark-ignition engine operation. This figure has been taken from the work of Abraham *et al.* (1985). It shows that spark-ignition engine combustion lies predominantly in the reaction sheet flame regime, although it cannot be conclusively said that combustion under *all* operating conditions occurs in that regime. It has been shown, with some certainty, that up to and including idle speed, combustion occurs in the reaction sheet regime (Abraham *et al.*, 1985; Heywood 1988). However, at high engine speeds, the parameters fail to satisfy the known sufficient conditions for occurrence of

either the reaction sheet regime or the distributed reaction regime, and the structure of the flame is not known.

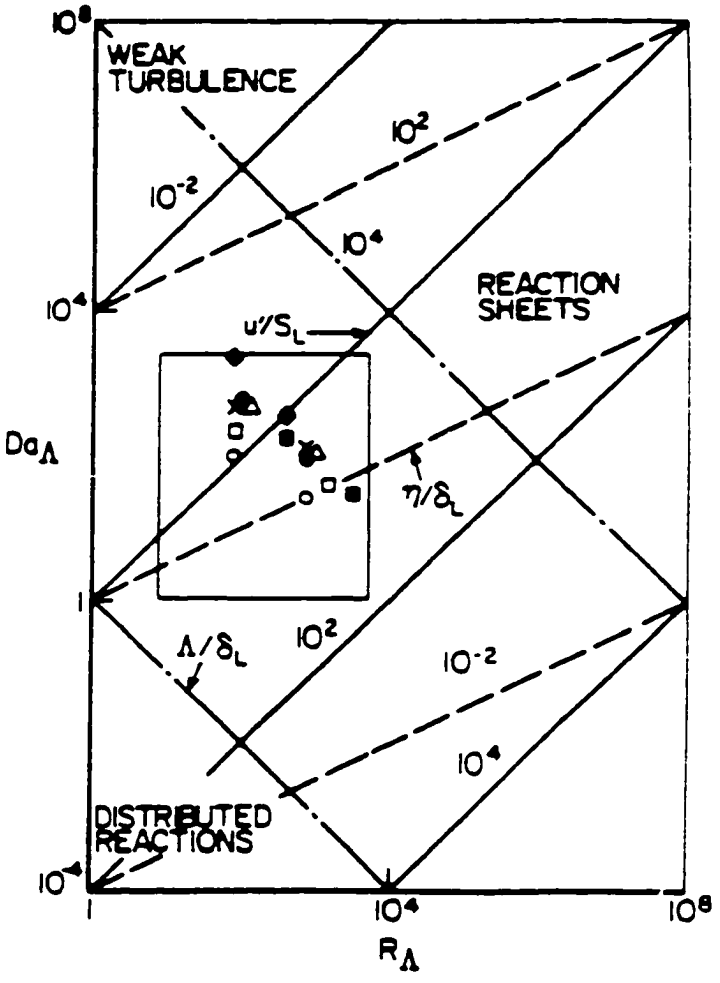

Figure 4.1: Illustration of regimes of turbulent premixed combustion. Rectangle identifies combustion regimes of spark-ignited engine operating conditions (from Abraham *et al.*, 1985).

It is clear from the foregoing discussion that turbulent combustion, in particular combustion in practical devices like engines, occurs over a wide range of regimes over which the flame structure may not be known. What implications does this have on theoretical investigations of engine combustion ? Under all but the simplest of cases, the interactions between turbulence and chemistry need to be *modeled.* Tools like direct

numerical simulations (DNS) and large eddy simulations (LES) of engine combustion are not foreseen to be practical choices for the near future, although it seems that there will soon be a shift from Reynolds average approach to the more advanced LES computations of turbulent reactive flows.

Due to the practical importance of turbulent combustion in engines and its effect on pollutant formation, the modeling of turbulence-combustion interactions has been the focus of intensive work over the years. The recent trend has been to emphasize computational methods based on physical modeling of the turbulent combustion processes. Physical modeling of turbulent combustion has evolved from initial algebraic formulations for the mean reaction rates to the more elaborate probabilistic methods of evaluation and to a variety of flamelet descriptions. However, since most of the interesting dynamics of turbulence-combustion interactions are hypothesized *a priori* in these models, solutions do not provide a better understanding of the phenomena and are limited by the modeling assumptions. So, it is extremely important to have some feeling of the range of interactions between turbulence and chemistry, before proposing/using a turbulent combustion model for a particular application.

In the present investigation, interest was in modeling turbulent combustion in direct injection natural gas engines. Apart from all the complexities of a turbulent combustion process, there are added complications in modeling the energy conversion process in direct injection engines, as it occurs over many distinctive phases, each of which requires different approximations. Fuel injected into the engine does not start burning immediately. There is a distinct delay period during which the injected fuel mixes with the air inside the combustion chamber. After the delay period is over, the fuel that has mixed with air burns rapidly in a premixed fashion. After all the premixed fuel-air mixture has been consumed, combustion continues in a non-premixed (or diffusion) manner and the rate of burning is limited by the rate of mixing of fuel and air.

Each of these processes and the transitions to and from them need to be modeled appropriately. The problem with most of the turbulent combustion models is that the

approximations inherent in them are only valid in a specific part of the fuel conversion process in direct injection engines. Nevertheless, attempts have been made in the past to propose new models or modify existing ones to describe turbulent combustion in direct injection engines. In the following sections, a few turbulent combustion models proposed in the literature are reviewed and their suitability for describing combustion in direct injection engines is investigated. Specifically, attention was focused on the following three types of models:

1. Eddy-Break-Up models (Spalding, 1971; Magnussen and Hjertager, 1976)
2. Eddy Dissipation Concept (Magnussen, 1981)
3. Flamelet models (Carrier *et al.*, 1975; Marble and Broadwell, 1977; Clavin and Williams, 1979; Spalding, 1978; Bray *et al.*, 1984; Bray, 1987, Peters, 1986, Candel *et al.*, 1991 and a number of researchers in the last decade)

Basic methods of turbulent combustion modeling are reviewed in many books (e.g. Libby and Williams, 1980; Borghi and Murthy, 1989; Williams, 1985; Kuo, 1986) and recent papers (e.g. Peters, 1986; Correa and Shy, 1987; Borghi, 1988; Pope, 1990; Bradley, 1992). These books and review papers provide a wealth of information and insight into the fascinating and often challenging field of turbulent combustion modeling.

Eddy-Break-Up Models

The Eddy-Break-Up (EBU) model was introduced by Spalding in 1971. It is based on the assumption of "fast" chemistry. Under this assumption, the chemical reactions are assumed to occur infinitely fast. Hence, the rate of reaction does not depend on the chemistry rate, but on the rate at which the fuel and oxidizer are mixed with each other. The time required to break up a turbulent eddy is taken as the characteristic mixing time-scale. This time-scale is proportional to the ratio of turbulent kinetic energy over its dissipation rate (k/ε). Based on these considerations, the mean reaction rate can be

assumed to be given in the form of an algebraic expression in terms of a typical turbulence time-scale and the local mean square fluctuation of the fuel concentration:

$$\overline{\dot{\omega}} = C_{EBU}\frac{\varepsilon}{k}\left(\overline{C'^{2}_{fuel}}\right)^{1/2} \tag{4.3}$$

C_{EBU} is assumed to be a universal constant and a value of 0.53 was suggested for it (Mason and Spalding, 1973). Further details on the development of this model can be found in Spalding (1971), Mason and Spalding (1973) and Spalding (1976). Spalding argued that the model was equally applicable to both premixed and non-premixed flames. However, Magnussen and Hjertager (1976), Pinchon (1989), and Jones and Whitelaw (1982) have questioned the applicability of this model to non-premixed flames.

Magnussen and Hjertager proposed their version of the EBU model in 1976. It was based on the same fundamental grounds as Spalding's model. For non-premixed flames, fuel and oxygen occur in separate eddies. Since chemical reactions occur very fast, the rate of combustion can be assumed to be determined by the rate of intermixing of the fuel and oxygen eddies on a molecular scale, which is given by the rate of dissipation of the eddies. Since there is a correlation between the fluctuations in the concentrations of fuel and oxygen and their respective mean values, the rate of reaction can be expressed by the mean concentrations of the reacting species. Accordingly, for non-premixed flames, depending on whether the flame is locally fuel-starving or oxygen-starving, the rate of combustion of fuel (kg/(m^3-s)) can be expressed as:

$$\overline{\dot{\omega}}_{fuel} = A\overline{C}_{fuel}\frac{\varepsilon}{k} \qquad \text{fuel-starving} \tag{4.4}$$

$$\overline{\dot{\omega}}_{fuel} = A\frac{\overline{C}_{ox}}{(O/F)_{stoic}}\frac{\varepsilon}{k} \qquad \text{oxygen-starving} \tag{4.5}$$

where A is a constant which depends on the structure of the flame and the rate of reaction between the fuel and oxygen, $\overline{C}_{fuel}$ is the local mean fuel concentration (kg/m^3), $\overline{C}_{ox}$ is the local mean oxygen concentration (kg/m^3), and $(O/F)_{stoic}$ is the stoichiometric oxygen to fuel ratio.

For premixed flames, fuel and oxygen occur in the same eddies. These eddies are separated by eddies containing hot combustion products. The rate of combustion can be assumed to be determined by the rate of spread of these hot eddies, which is given by the same mechanism as outlined above. However, an extra equation needs to be written that accounts for the dissipation of hot eddies in cases where the concentrations of hot combustion products is low. Hence, for premixed flames,

$$\overline{\dot{\omega}}_{fuel} = AB\frac{\overline{C}_{prod}}{1+(O/F)_{stoic}}\frac{\varepsilon}{k} \qquad \text{premixed} \qquad (4.6)$$

where B is a constant, and $\overline{C}_{prod}$ is the local mean concentration of the combustion products.

The three equations (4.4-4.6) are assumed to be generally applicable to both non-premixed and premixed turbulent flames. The equation that yields the minimum reaction rate is the one that determines the local rate of combustion. The main advantage of this model over Spalding's model is that it is applicable for both non-premixed and premixed flames. This makes it more suitable for combustion in applications like direct injection engines where combustion occurs in both premixed and non-premixed regimes. Also important is the fact that the combustion rate is proportional to the mean concentration of the intermittent quantities instead of the concentration fluctuations, which are much more difficult to estimate than the mean quantities.

For non-premixed flames, Magnussen and Hjertager suggested values of A=4 and B=0.5 for the model constants. Gosman and Harvey (1982) proposed values of A=20 and B=2.5 for combustion in a diesel engine. Pinchon (1989) modified these values to A=16 and B=2, while Varnavas and Assanis (1991) got best results with values of A=0.5 and B=0.5. In a recent paper, Dillies *et al.* (1997) found that they could get agreement with measurements of burned mass fraction and combustion speed in a direct injection diesel engine only by considering an arbitrarily high value of the constant B. This wide range of values for the constants shows that there is a degree of empiricism in the model, which is to be expected, as we are seeking to describe the complicated interactions

between flow and chemistry by a simplified algebraic approach. Despite the empiricism in the model, there is much theoretical and experimental evidence to support the dependence of combustion on the rate of turbulent mixing.

Implementation of the EBU model in KIVA-3

Being an algebraic formulation for the mean reaction rates, the EBU model is relatively simple to program. The formulation of Magnussen and Hjertager (Eq. 4.4-4.6) was implemented in a modified version of the KIVA-3 code. A new subroutine called *ebu* was written that calculated the fuel consumption rate at each time-step, for each computational cell, based on the minimum of Eq. 4.4-4.6. The reaction between fuel (assumed to be pure methane) and oxygen was assumed to occur through a one-step reaction:

$$CH_4 + 2O_2 \Rightarrow CO_2 + 2H_2O \tag{4.7}$$

Hence, $\overline{C}_{prod}$ was assumed to be the sum of concentrations of carbon dioxide and water. Knowing the rate of consumption of the fuel, the rate of change of the other species involved in the reaction (oxygen, carbon dioxide and water) can be found from the stoichiometry of the reaction between them (Eq. 4.7):

$$\overline{\dot{\omega}}_{CH_4} = -\min\left(\overline{\dot{\omega}}_{fuel}\right) \text{ from Eq. 4.4-4.6} \tag{4.8}$$

$$\overline{\dot{\omega}}_{O_2} = 2\,\overline{\dot{\omega}}_{CH_4}\,\frac{\overline{W}(O_2)}{\overline{W}(CH_4)} \tag{4.9}$$

$$\overline{\dot{\omega}}_{CO_2} = -\overline{\dot{\omega}}_{CH_4}\,\frac{\overline{W}(CO_2)}{\overline{W}(CH_4)} \tag{4.10}$$

$$\overline{\dot{\omega}}_{H_2O} = -2\,\overline{\dot{\omega}}_{CH_4}\,\frac{\overline{W}(H_2O)}{\overline{W}(CH_4)} \tag{4.11}$$

Here, $\overline{W}(X)$ is the molecular weight of species X and the rates of each species are in mass units. Once the rates of formation/destruction of each species are known, the heat release rate due to chemical reactions can be calculated, as before, from Eq. 3.11, the only difference being that these rates are in mass units whereas the rates in Eq. 3.11 are in mole units, so appropriate unit conversions are necessary.

To avoid any empiricism in the results due to variability of model constants, the original values proposed by Magnussen and Hjertager were used in this work. So it was assumed that A=4 and B=0.5. Since the EBU model is valid only in the limit of fast chemistry, the ignition delay period has to be modeled separately and a suitable criterion found for the transition from the ignition model to the EBU model. As noted before, during the ignition delay period, the heat release process is kinetically controlled. A detailed kinetic mechanism (DRM22) was used in conjunction with KIVA-3 in the previous chapter to simulation autoignition in a combustion bomb. This model can be used to describe the ignition delay period in a direct injection engine also. However, once the rate of heat release starts becoming high, the combustion process transitions from being kinetically controlled to being mixing controlled. A judgment has to be made for the numerical quantification of the transition point. Some popular choices are the attainment of a specified temperature due to chemical reactions or burning a specified mass fraction of the fuel. The University of Wisconsin Engine Research Center multi-dimensional modeling groups consistently use a value of 1000 K as the threshold value for transition from ignition to combustion in diesel engines (Kong *et al.*, 1995; Stephenson *et al.*, 1996; Ayoub and Reitz, 1995). Dillies *et al.* (1997) used a value of 2200 K for the transition temperature.

However, if the emphasis is on global effects of the combustion process, it is better to define the transition based on a certain mass fraction of fuel burned. After a certain mass of fuel has burned, leading to a noticeable temperature rise, one can be certain that the ignition delay period is over. This criterion is also better than specifying a certain threshold temperature *a priori*, as it is independent of the thermodynamic conditions of the fuel and oxidizer. The temperature of 1000 K, for example, would have to be raised if low heat rejection engines are to be simulated with high intake air temperatures. One might, of course, question the validity of transitioning to mixing controlled combustion, in the whole computational domain, even though burning may still be very localized after a certain amount of fuel has been consumed. In regions of the injected gas jet where the fuel

and oxidizer have still not yet mixed within flammability limits, pre-flame reactions may still be going on when the transition to mixing controlled combustion is assumed to occur. This assumption could be called into question in diesel engines in which liquid droplets are injected into the combustion chamber, which, depending on the injection pressure and air motion in the chamber, may vaporize and ignite almost anywhere in the chamber. In such a situation, it would be a better to look at a *local* criterion for the transition from ignition to combustion. However, in gaseous fuel injection, the gas jet has a coherent structure and the ignition sites are located at the periphery of the jet. Thus, using a global criterion for the transition from ignition kinetics of mixing controlled combustion is justifiable.

An important question that needs to be answered now is what the transition point should be in terms of the mass fraction of fuel burned. Should it be 2%, 4%, 6% or even 10% ? In spark-ignition engines, the ignition delay period or more appropriately, the flame development period is usually taken as the time taken to burn 10% of the fuel in the chamber, though other fractions such as 1 and 5% have also been used (Heywood, 1988). In diesel engines, Varnavas and Assanis (1991) used a value of 2% mass fraction burned for the transition. To explore this issue further, a few computations were performed in the combustion bomb geometry (see Chapter III), with pure methane injected at a rate of 12 g/s for 1 ms. The fuel temperature was assumed to be 400 K and the ambient temperature of air in the bomb to be 1300 K. The contents of the chamber were assumed to be at an ambient density of 20.4 kg/m^3. Ignition delay has already been simulated under these conditions. Figure 4.2 shows the variation of chamber pressure with time for three different transition criteria: 2%, 4% and 6% by mass of total injected fuel burned and one case in which full kinetics equations were solved throughout. Since this case is computationally very expensive, the calculation was terminated after 1 ms, whereas in the other cases it was continued till 3.5 ms. To compare the time requirements for the different runs, the full chemistry simulation for 1 ms took 89 hours of CPU time on a

SUN Ultra-2 workstation, whereas the 2%, 4%, and 6% transition cases took 21, 27, and 30.5 hours, respectively.

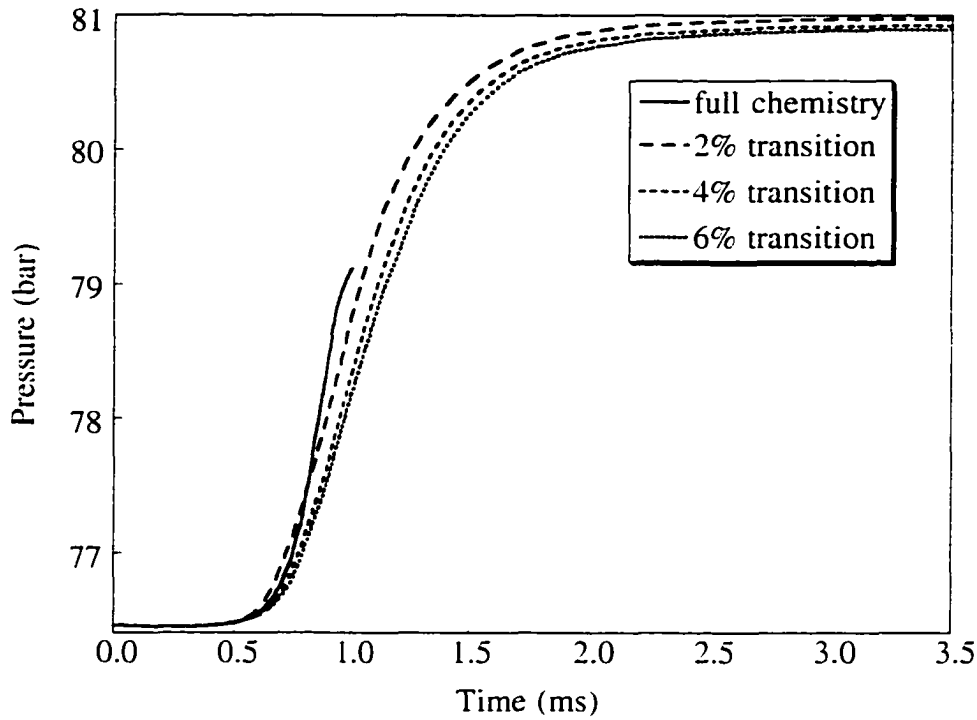

Figure 4.2: Effect of transition point on average pressure in a combustion bomb.

Figure 4.2 shows that the ignition delay period is approximately the same for all the cases considered here, although the rate of pressure rise is highest for the full chemistry case, once the delay period is over. It can also be noticed that the rate of pressure rise decreases as the transition is delayed. Since the EBU model accounts for the effect of relative magnitudes of fuel, oxygen and combustion products on the reaction rates through Eq. 4.8, the reaction rates (and hence pressure rise rates) are higher if more of the fuel and oxygen are mixed in stoichiometric proportions. Since a high injection rate was simulated for these computations in a combustion bomb, as the transition point was delayed, more of the fuel-air mixture became much richer than stoichiometric. It should be noted that fuel was injected in a quiescent chamber, and the situation would be quite different in the

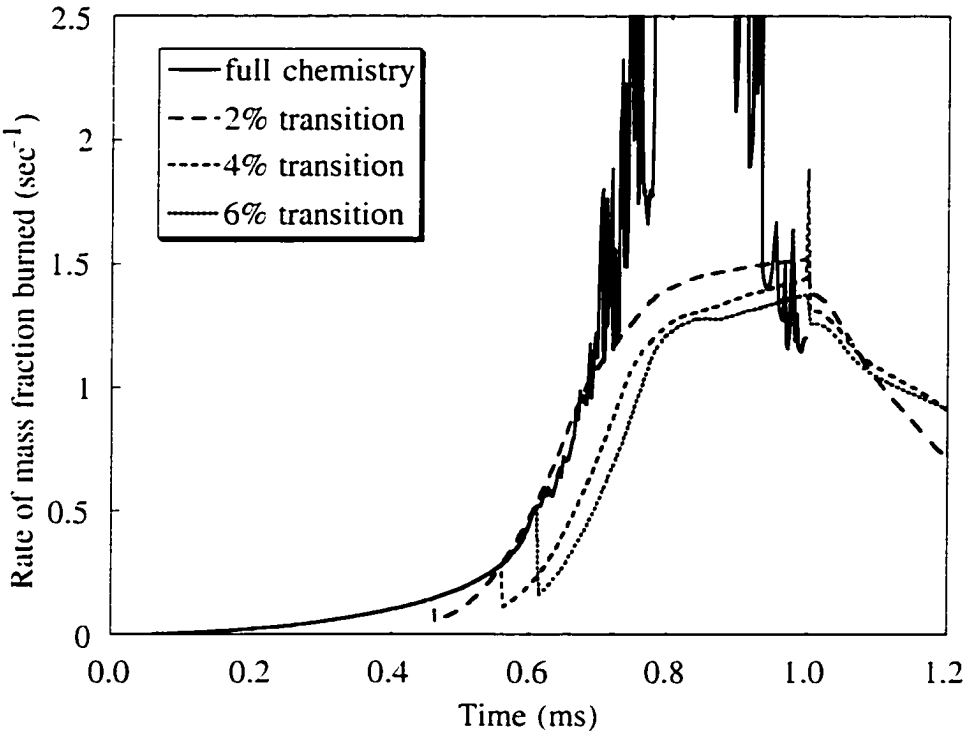

Figure 4.3: Effect of transition point on rate of mass fraction burned in a combustion bomb.

combustion chamber of an engine. Figure 4.3 shows the temporal variation of mass burning rate normalized with the total injected fuel. It can be seen that as the transition point is delayed from no transition to transition at 6% mass fraction burned, there is a greater drop in burn rate at the transition point. Continued mixing of the fuel and air increases the burn rate as injection proceeds till 1 ms, after which the burn rate begins to fall. So what is the "correct" transition point ? Definitely, the much higher mass burned rate for the case in which full kinetics are solved without any consideration for the mixing process to occur at the molecular level, is unphysical. Chemical reactions can occur only when the reactive species are mixed at the molecular level. The EBU model accounts for the rate of mixing at the molecular level through the flow time-scale, k/ε, albeit in a very simplified fashion. Since the transitions based on 4% and 6% mass fraction of fuel burned resulted in pressure traces that were almost identical, further studies were conducted by

assuming the transition to occur at 4% mass fraction of fuel burned. A few computations were done at different injection rates to verify this fact.

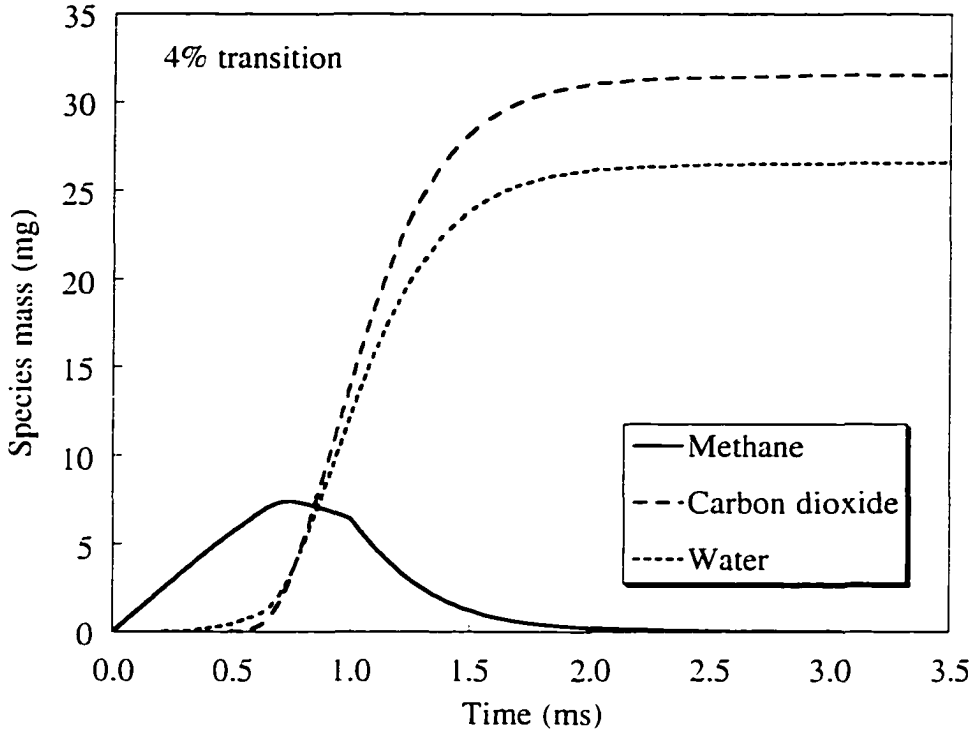

Figure 4.4: Temporal variation of species mass for the 4% transition case

Figure 4.4 shows the variation of mass of different species in the combustion chamber as a function of time. As noted before, methane is injected into the domain at a rate of 12 g/s for 1 ms. It can be seen that the mass of methane increases up to about 0.75 ms till the rate of injection is higher than the rate of burning. However, as the rate of burning continues to increase, the mass of methane starts decreasing. This rate of decrease increases after 1 ms when the fuel injection ends and eventually all the fuel in the chamber gets consumed. The variation of the mass of the combustion products (carbon dioxide and water) is also shown in Fig. 4.4. It is interesting to note that during the ignition delay period (before 0.55 ms), the mass of carbon dioxide is lower than that of water. This is due to incomplete combustion of methane to form carbon monoxide and other species and radicals, which is accounted for by the detailed chemical kinetic

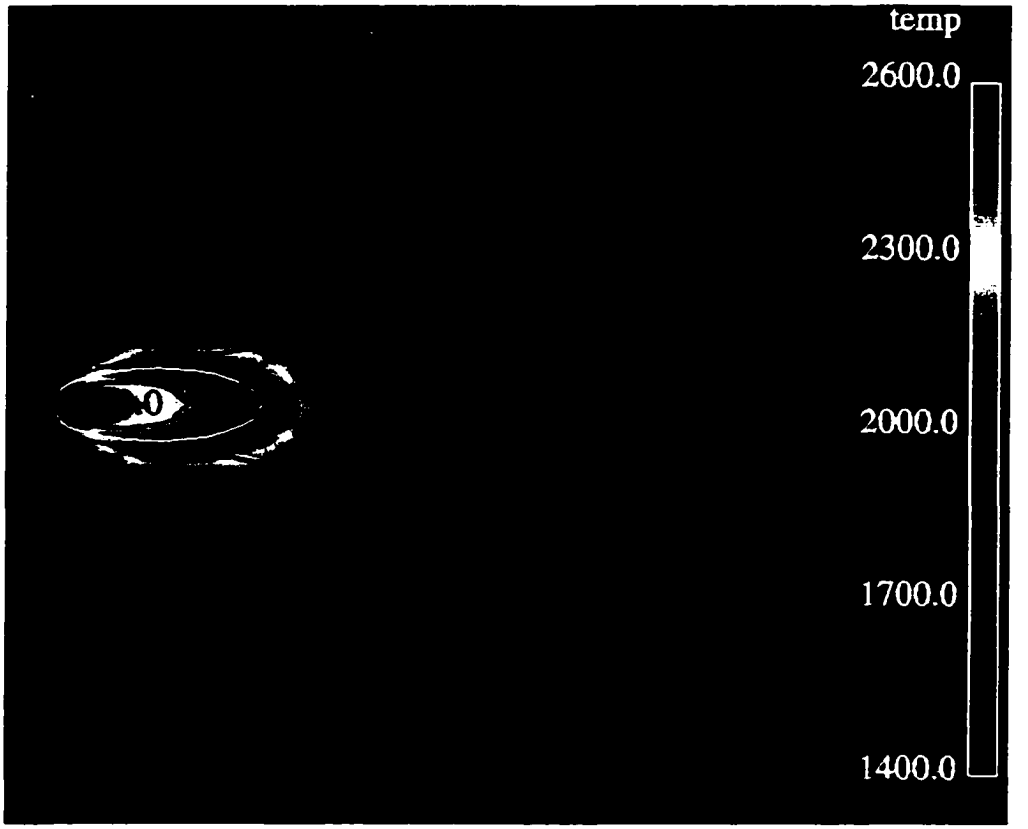

Figure 4.5: Variation of temperature in a plane cut through the center of the domain at 1 ms. Superimposed are contours of ϕ (0.5, 1.0 and 2.0).

mechanism used. However, once the EBU model is used, fuel is assumed to burn *completely* to carbon dioxide and water and so the mass of carbon dioxide becomes greater than that of water. Stoichiometry of the assumed one-step reaction between methane and oxygen (Eq. 4.7) dictates that 16 gm of methane reacts with 64 gm of oxygen to give 44 gm of carbon dioxide and 36 gm of water. Since 12 mg of methane was injected into the domain, after all the injected methane has been burned, the mass of carbon dioxide should be 33 mg and that of water should be 27 mg. At 3.5 ms, the mass of carbon dioxide in the chamber was found to be 31.55 mg and that of water is 26.56 mg.

Figure 4.5 depicts temperature in a plane cut through the center of the computational domain at 1 ms, just after fuel injection has ended. Superimposed on the temperature values are contours of the fuel-air equivalence ratio, ϕ. Three different values were chosen for ϕ: 0.5 (lean), 1.0 (stoichiometric) and 2.0 (rich). The ambient

temperature of air in the bomb was 1300 K. It can be see that due to combustion, the temperature of the flame increases up to 2600 K. The hottest regions of the flame are those that have fuel and air mixed in close to stoichiometric proportions. This is a direct consequence of the assumptions made in the EBU model. Note that on both the lean and rich sides of the diffusion flame, the temperatures are lower. There is virtually no heat release in the rich pockets of the flame (enclosed by the red $\phi = 2.0$ line).

The assumption of complete combustion is a deficiency of the EBU model as it leads to higher heat release compared to a real situation in which products of incomplete combustion are also formed. This fact can be seen by comparing Fig. 4.2 and 4.3 which show that although the rate of burning is much higher for the full kinetics case compared to any of the kinetics-EBU cases, the pressure predicted by the kinetics-EBU cases is not much less than that predicted by the full kinetics case. Also, by the nature of assumptions inherent in the EBU model, it cannot account for local flame extinction as it is valid only in the limit of fast chemistry. However, its usefulness lies in its simplicity and its ability to account for the effect of mixing on combustion so as to be able to predict global parameters like pressures, heat release rates and concentrations of major species.

Eddy Dissipation Concept (EDC)

Acknowledging the simplifications made in the EBU model by the fast chemistry assumption, Magnussen (1981) proposed a model to account for complex chemistry-turbulence interactions. Such a model could, in principle, be used to study local extinction in turbulent flows. This model is based on the Eddy Dissipation Concept (EDC) for chemical reactions in a turbulent flow field. The EDC is a reactor concept which takes into account the intermittent behavior of small scale structures of turbulence, as well as the effect of the fine structures on the chemical reactions.

In the EDC model, chemical reactions are assumed to occur in the small scale structures that characterize a turbulent flow. Chemical reactions occur when reactants are

mixed at the molecular level at sufficiently high temperatures (Magnussen, 1981). Molecular mixing determines the rate of chemical reactions in turbulent flows and the microscale processes that control it are highly intermittent i.e. they are concentrated in isolated regions that occupy a very small fraction of the volume of the fluid (Bradley, 1992). These regions are occupied by fine structures whose dimensions are small in one or two directions, but not in the third. These fine structures are believed to be vortex tubes, sheets or slabs whose characteristic dimensions are the same magnitude as the Kolmogorov microscale (Kolmogorov, 1962; Corrsin, 1962; Tennekes, 1968; Kuo and Corrsin, 1971; Kuo and Corrsin, 1972).

Since the fine structures are responsible for the dissipation of turbulence into heat and for characterizing the molecular scale processes, it can be assumed that within these structures, fuel and air will be mixed at the molecular scale. These structures can thus create the reaction space for non-uniformly distributed reactants (Byggstøyl and Magnussen, 1983). For modeling purposes, one can assume that the reactants are mixed homogeneously within the fine structures. So, the parameters needed to calculate reaction rates in the EDC model are the volume occupied by the small scale structures where reactions occur and the mass transfer rate between the fine structures and the surrounding fluid.

Based on the cascade of turbulent kinetic energy from the large scales to the dissipative fine structures, Magnussen (1981) found the characteristic length and velocity scales of the fine structures to be very closely related to the corresponding Kolmogorov scales:

$$u^* = 1.74(\nu\varepsilon)^{1/4} \tag{4.12}$$

and

$$L^* = 1.43\left(\frac{\nu^3}{\varepsilon}\right)^{1/4} \tag{4.13}$$

Here, u^* is the mass average fine structure velocity, L^* is the length scale characterizing the fine scales, ν is the kinematic viscosity of the gas mixture and ε is the rate of

dissipation of turbulent kinetic energy. Note that without the constants of proportionality, these expressions are the estimates for the Kolmogorov velocity and length scales.

Based on simple geometrical considerations, the specific mass flow rate through the fine structures can be expressed as:

$$\dot{m}^* = 2\frac{u^*}{L^*} = 2.43\left(\frac{\varepsilon}{\nu}\right)^{1/2} \tag{4.14}$$

The inverse of $\dot{m}^*$ is the hydrodynamic residence time of the fine structures and is given by:

$$\tau^* = \frac{1}{\dot{m}^*} = 0.411\left(\frac{\nu}{\varepsilon}\right)^{1/2} \tag{4.15}$$

Note that τ^*, sans the constant, is the estimate for the Kolmogorov time-scale for a turbulent flow field.

The next parameter to be determined, the mass fraction of the fine structures, γ^* depends on the assumption about the structure of the fine scales. Magnussen (1981), and Byggstøyl and Magnussen (1983) proposed an expression for γ^* based on energy transfer to the fine structures as:

$$\gamma^* = \left(\frac{u^*}{u'}\right)^3 \tag{4.16}$$

where u' is the turbulent intensity which can be calculated from the turbulent kinetic energy, k by assuming isotropic turbulence as:

$$u' = \sqrt{\frac{2}{3}k} \tag{4.17}$$

By substituting for u^* and u' from Eqs. 4.12 and 4.17 into Eq. 4.16, one obtains an estimate for the mass fraction of the fine structures as:

$$\gamma^* = \left(\frac{u^*}{u'}\right)^3 = \left[2.13\left(\frac{\nu\varepsilon}{k^2}\right)^{1/4}\right]^3 \tag{4.18}$$

Recently, Magel *et al.* (1996) argued that the expression for γ^* should be modified as:

$$\gamma^* = \left(\frac{u^*}{u'}\right)^2 = \left[2.13\left(\frac{\nu\varepsilon}{k^2}\right)^{1/4}\right]^2 \tag{4.19}$$

In their work on the simulation of detailed chemistry in a turbulent combustor flow, they preferred to use Eq. 4.19 as it has shown better agreement with experimental data. The value of γ^* is larger using Eq. 4.19 rather than Eq. 4.18 and is more realistic in situations with low turbulence levels and slow chemistry (Magel *et al.*, 1996).

A better interpretation for the expression for the mass fraction of fine structures can be obtained by viewing it as volume fraction occupied by the small scale structures in a turbulent flow field. This is a valid assumption for non-reacting turbulent flow fields which have the same density for the dissipative regions and the surroundings and can also be extended to reacting turbulent flow fields with a modification for the density change due to chemical reactions. If one views the dissipative regions as sheets with characteristic thickness on the order of the Kolmogorov microscale (η), embedded in nearly potential regions with size on the order of the integral length scale, L (volume of order L^3), their volume fraction can be estimated as (Corrsin, 1962):

$$\gamma^* = \frac{\eta L^2}{L^3 + \eta L^2} = \frac{\eta}{L + \eta} \approx \frac{\eta}{L} \tag{4.20}$$

Simple scaling relations between the integral and dissipation length and velocity scales of turbulence show that η and L are related to the corresponding velocity scales as (Tennekes and Lumley, 1983):

$$\frac{\eta}{L} = \left(\frac{u^*}{u'}\right)^3 \tag{4.21}$$

which yields the same estimate for the volume fraction of the fine scale structures as that used by Magnussen (see Eq. 4.16).

Tennekes (1968) pointed out inconsistencies in Corrsin's view of the structure of the small scales, and proposed a different model. He visualized the fine structures to be

vortex tubes of diameter η , which are being stretched by eddies of size λ , the Taylor microscale. The volume fraction occupied by the vortex tubes can then be estimated as:

$$\gamma^* = \frac{\eta^2 \lambda}{\lambda^3} = \left(\frac{\eta}{\lambda}\right)^2 \tag{4.22}$$

if one is willing to assume that the length of the vortex tubes in a volume λ^3 is proportional to λ . In isotropic turbulence, the Taylor microscale is related to the integral length scale as:

$$\frac{\lambda}{L} = \sqrt{\frac{15\nu}{u' L}} \tag{4.23}$$

By eliminating λ from Eq. 4.22 and using the scaling relations for large and small scales of turbulence, it can be shown that:

$$\gamma^* = \left(\frac{\eta}{\lambda}\right)^2 = \left[C^*\left(\frac{\nu\varepsilon}{k^2}\right)^{1/4}\right]^2 \tag{4.24}$$

Based on Magnussen's estimates for the small scale velocity and length scales (Eq. 4.12 - 4.13) and assuming isotropic turbulence (Eq. 4.17), the value of C^* can be estimated to be 0.8679. Note that Magel *et al.* (1996) also used the same form for γ^* except that their constant was different.

Since Tennekes' view for the structure of the small scales is widely held and has been the basis of a number of models for combustion at the small scales in IC engines (e.g. Tabaczysnski *et al.*, 1977; Daneshyar and Hill, 1987), the foregoing analysis provides a more solid foundation for the expression for γ^* proposed by Magel *et al.* (see Eq. 4.19). Hence, in this work, Eq. 4.19 was used instead of Eq. 4.18 originally proposed by Magnussen and his co-workers.

Assuming that only a fraction χ of the fine structures reacts, the mean density is related to the densities in the fine structures and surrounding fluid as (Magnussen, 1981):

$$\frac{1}{\bar{\rho}} = \frac{\chi\gamma^*}{\rho^*} + \frac{\left(1-\chi\gamma^*\right)}{\rho^o} \tag{4.25}$$

where the bar denotes mean quantities, the asterix denotes values in the fine structures and the circle denotes values in the surrounding fluid. When finite rate chemistry effects are included (e.g. in this work with detailed kinetics), the value of χ can be taken to be unity as it is used to account for finite rate chemistry effects when the fast chemistry assumption is used. Density weighted species mass fractions are related to the mass fractions within the fine structures and surrounding fluid as:

$$\overline{Y}_m = \chi\gamma^* Y_m^* + \left(1 - \chi\gamma^*\right) Y_m^o \tag{4.26}$$

Since mixing in the fine structures is assumed to be fast, reactions occurring in them can be modeled as a perfectly stirred reactor (PSR) that transfers mass and energy only to the surrounding fluid. Figure 4.6 schematically shows this view. This allows one to couple any detailed chemical kinetic mechanism with the EDC combustion model.

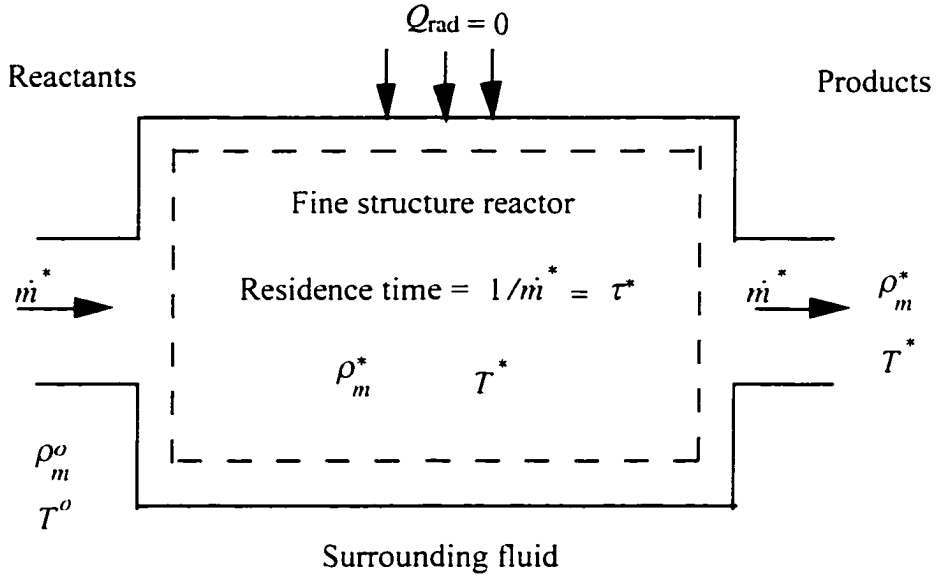

Figure 4.6: Schematic illustration of a reacting fine structure

The governing equations for mass and energy balance in the fine structures can be obtained by assuming that the rate of mixing is so intense that the temperature and composition in the reactor is the same as that which leaves the reactor volume. The mass flow rate through the reactor, $\dot{m}^*$ is assumed to be constant.

Species conservation equation for the fine structure is given by:

$$\dot{m}^*\left(Y_m^* - Y_m^o\right) = \frac{\dot{\omega}_m^* W_m}{\rho^*} \qquad m=1,\ldots,M \tag{4.27}$$

Multi-dimensional flow codes like KIVA-3 provide estimates of mean flow quantities, so the values of species mass fractions in the surroundings need to be eliminated in favor of mean values. This can be done by combining Eqs. 4.26 and 4.27, to yield species consumption rates in terms of mean, $\bar{Y}_m$ and fine structure, Y_m^* species mass fractions:

$$\frac{\dot{m}^*}{\left(1-\chi\gamma^*\right)}\left(Y_m^* - \bar{Y}_m\right) = \frac{\dot{\omega}_m^* W_m}{\rho^*} \qquad m=1,\ldots,M \tag{4.28}$$

The energy conservation equation in the PSR can be written as:

$$\frac{\dot{m}^*}{\left(1-\chi\gamma^*\right)}\sum_{m=1}^{M}\left(Y_m^* h_m^* - \bar{Y}_m \bar{h}_m\right) = \frac{\dot{Q}^*}{\rho^*} \tag{4.29}$$

Here, $\dot{Q}^*$ is the net energy rate per unit volume that is transferred between the fine structures and the surroundings by other mechanisms such as radiation and is assumed to be zero in this work. Equations 4.28 and 4.29 simulate a PSR with a residence time equal to the characteristic time-scale for mass exchange between the fine structures and the bulk fluid, which is given by:

$$\tau_r = \frac{\left(1-\chi\gamma^*\right)}{\dot{m}^*} = \left(1-\chi\gamma^*\right)\tau^* \tag{4.30}$$

Solution of the PSR equations yields the fine structure states. Once these are known, assuming that the reactions take place only in the fine structures, the net mean species reaction rate for the transport equation is given by (Magnussen, 1981; Jessee *et al.*, 1997):

$$\bar{R}_m = \frac{\bar{\rho}\chi\gamma^*\dot{m}^*}{\left(1-\chi\gamma^*\right)}\left(Y_m^* - \bar{Y}_m\right) = \frac{\bar{\rho}\chi\gamma^*}{\tau_r}\left(Y_m^* - \bar{Y}_m\right) \tag{4.31}$$

where $\bar{\rho}$ is the local mean density of the gas.

All the applications of the EDC model that can be found in the literature (Magnussen, 1981; Byggstøyl and Magnussen, 1983; Magnussen *et al.*, 1978; Magel *et*

al., 1996; Jessee *et al.*, 1997) have been for steady turbulent diffusion flames or turbulent combustor flows in which the solution was sought at steady state. However, in the present investigation, interest was in transient solutions of the turbulent reactive flow field in a direct injection engine. Hence, unsteady forms of the governing equations for species and energy conservation (Eq. 4.28 and 4.29) can be written as:

$$\frac{dY_m^*}{dt} = -\frac{1}{\tau_r}\left(Y_m^* - \bar{Y}_m\right) + \frac{\dot{\omega}_m^* W_m}{\rho^*} \qquad m = 1,\ldots,M \tag{4.32}$$

and

$$\frac{dT^*}{dt} = \frac{1}{C_p^*}\left[\frac{1}{\tau_r}\sum_{m=1}^{M}\bar{Y}_m\left(\bar{h}_m - h_m^*\right) - \sum_{m=1}^{M}\frac{h_m^*\dot{\omega}_m^* W_m}{\rho^*}\right] \tag{4.33}$$

Detailed derivation of Eq. 4.33 is given in Appendix B. Here, C_p^* is the mass average specific heat at constant pressure in the fine structure given by $C_p^* = \sum_{m=1}^{M} Y_m^* C_{p_m}^*$. Note that the term $\dot{Q}^*$ accounting for other modes of heat transfer has been eliminated from Eq. 4.33.

Equations 4.32 and 4.33 are nonlinear ordinary differential equation (ODE) initial value problems and can be solved in a manner similar to the chemical kinetic equations described in Chapters II and III. The interactions between flow and chemical reactions occur through their respective time-scales given by a residence time, τ_r and a chemical time, $\tau_{chem} = \rho^*/\dot{\omega}_m^* W_m$. The relative magnitudes of these two terms determine the rate at which species concentrations change with time. This fact is explored in the next section.

Studies using the EDC model and its implementation in KIVA-3

Before the implementation of the EDC model in KIVA-3 is described, it is instructive to investigate the behavior of this model at different flow and chemical time-scales to understand the interactions between them as described by this model. To do this, the (M+1) ODEs for species mass fractions and temperature in the fine structures

(Eqs. 4.32 and 4.33) were integrated using LSODE (Hindmarsh, 1983). The molar production rates $\dot{\omega}_m^*$, and other thermodynamic properties (enthalpy, density, specific heats etc.) were calculated using CHEMKIN-II (Kee *et al.*, 1991) and were updated each time LSODE was called for the current temperature and concentrations. The detailed chemical kinetic mechanism, DRM22 (Frenklach *et al.*, 1996) was used to describe chemistry. In this way there was no need to *a priori* fix the chemical time-scale. Since at this time, flow was not simulated, the residence time, τ_r was provided as an input to the simulation.

Figure 4.7 shows the variation of methane concentration and temperature in the fine structures as a function of time for four different residence times. The ambient temperature of both the fine structures and the surroundings is 1300 K and the ambient pressure is 50 atm. The initial values of species concentrations are specified by assuming that the fine structures contain only atmospheric air whereas the surroundings contain a stoichiometric mixture of methane and air.

The "natural" chemical time-scale of ignition for this case is approximately 0.4 ms. This is the time that will be taken for a homogeneous stoichiometric mixture of methane and air to autoignite at a temperature of 1300 K and a pressure of 50 atm. But the situation is different for a PSR case, as the residence time determines how fast the fuel diffuses to the small scales. In this way, the first term on the right hand side of Eq. 4.32 is a model for molecular diffusion fluxes. For times less than the chemical time-scale, the chemical source term in the species equation does not play a role, as the molar production rates of species are very low. The species equations (Eq. 4.32) can then be integrated analytically and used to show the dependence of fine structure mass fractions on the residence time, τ_r. In particular, the concentration of the fuel (methane) in the fine structures can be written as:

$$Y^*_{CH_4} = \overline{Y}_{CH_4}\left(1 - e^{-t/\tau_r}\right) \qquad t < \tau_{chem} \qquad (4.34)$$

where the initial mass fraction of methane in the fine structures is assumed to be zero. This equation shows the exponential dependence of methane mass fraction in the fine

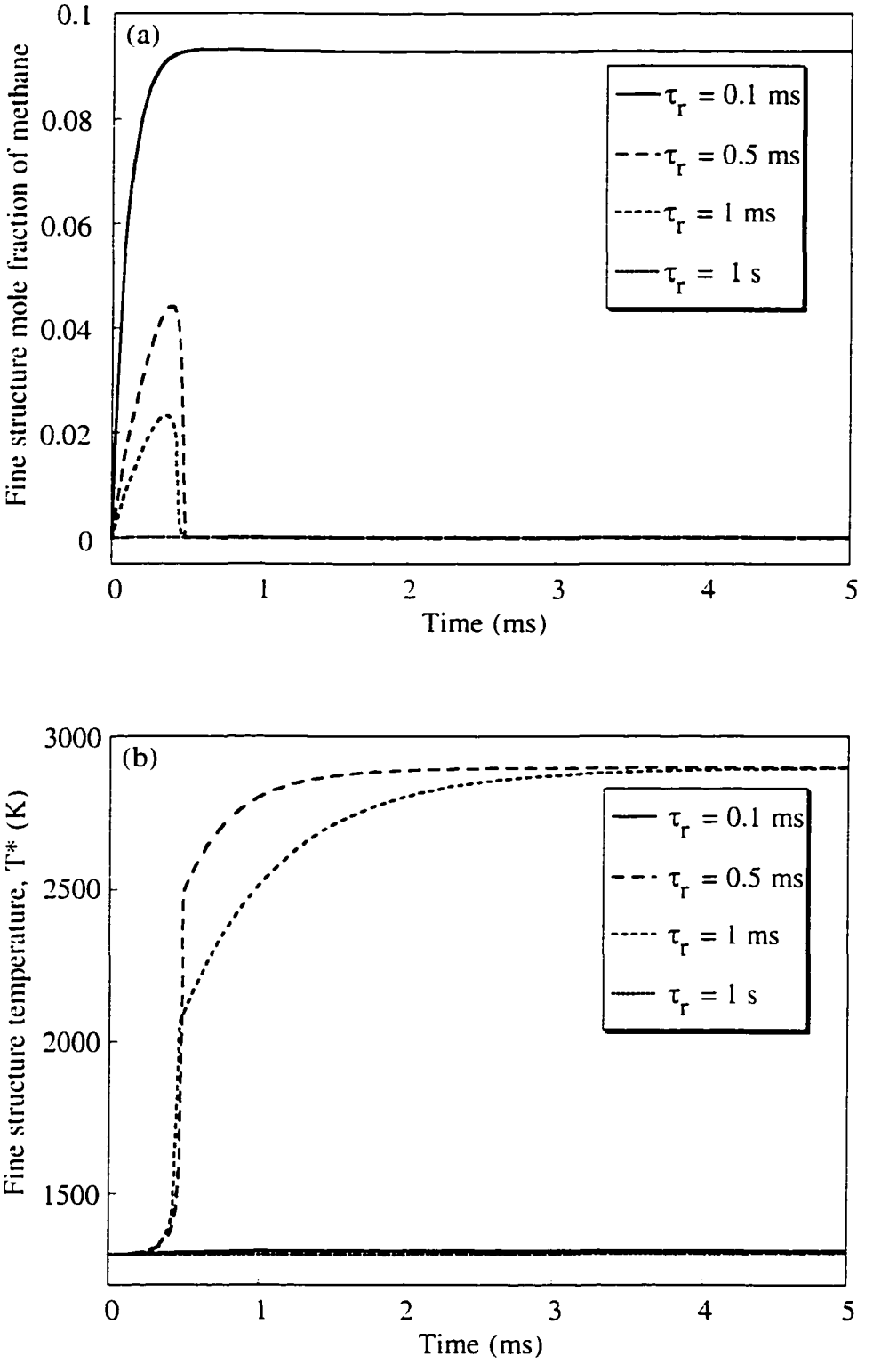

Figure 4.7: Variation of (a) fine structure fuel mole fraction and (b) fine structure temperature for different residence times.

structures on the ratio t/τ_r. When the residence time is very small, much smaller than the chemical time-scale (say for example τ_r = 0.1), the factor e^{-t/τ_r} approaches zero as time increases and the methane mass fraction quickly approaches its value in the surroundings, which is the stoichiometric value of 0.093 (see Fig. 4.7 (a)). Since the residence time in the fine structures is much smaller than the chemical time-scale, the fuel enters and leaves the fine structures before there is enough time for the pre-flame reactions to occur, so that the fuel leaves the reactor almost unreacted. The corresponding value of fine structure temperatures shows a very modest rise of 12 K (see Fig. 4.7 (b)). On the other extreme, if the residence time is very large, in fact much greater than the time of simulation (say for example, τ_r = 1 s, whereas the time of simulation is 5 ms), the factor e^{-t/τ_r} is almost unity for the duration of the simulation, and there is virtually no increase in fuel concentration in the fine structures. For this specific case, the methane mole fraction in the fine structures increases to only 8.4 x 10^{-5} at the end of 5 ms. Since there is almost no fuel in the fine structures, there is correspondingly negligible heat release, and the temperature of the fine structures increases very slightly by about 12 K from its initial value. This case could be a real situation in an IC engine in which, depending on engine speed, the fuel and air mixture has only a finite time (usually in milliseconds) to react and burn.

It is at the intermediate residence times that interesting things happen, when both flow and chemistry have a role to play. It can be easily seen from Eq. 4.34 that at time t=0, the rate of change of methane concentration in the fine structures is inversely proportional to the residence time. Hence, the smaller the value of τ_r, the faster is the rise in methane concentration in the fine structures. When τ_r is equal to 0.5 ms, the methane concentration builds up in the fine structures till 0.4 ms, the chemical time, and then starts decreasing owing to consumption due to chemical reactions. The corresponding fine reactor temperature curve shows a sudden jump from about 1500 K to 2500 K when the chemical time is reached. After that, the temperature increases at a decreasing rate as the fuel concentration in the reactor is continuously decreasing.

Equilibrium is reached when all the fuel is consumed and then the temperature remains constant at its equilibrium value. The same process occurs when τ_r is 1 ms, albeit sooner. Since the residence time is larger, fuel builds up at a slower rate. So, by the time the chemical time is reached, less fuel has accumulated in the fine structure reactor (see Fig. 4.7 (a)). Correspondingly, there is a lower jump in temperature at this time, after which the temperature continues to rise as the fuel is being consumed, till the equilibrium state is reached. The same equilibrium temperature is reached as compared to the residence time of 0.5 ms, although the state of equilibrium is reached much later. This is due to the relative differences in the magnitudes of the flow and chemical time-scales.

From the foregoing discussion, it can be seen that the relative magnitudes of the chemical and flow time-scales have significant impact on the chemical reactions in the fine structures. In principle, this model should be able to account for local extinction effects which occur when the local rate of strain is so high that the heat release rate is not able to keep pace with it and extinction occurs. This is the same situation as a case in which the residence time is much smaller than the chemical time-scale. It was shown above that in such a situation, the temperature in the fine structures would not increase from its initial value and local extinction could be assumed to occur.

Before the implementation of the EDC model in KIVA-3 is described, it would be prudent to ponder the applicability of the EDC model to typical engine situations. Are the Kolmogorov time-scales in IC engines of the same order as the chemical time-scales ? For a premixed spark-ignition engine, the typical integral length scale is on the order of 2-3 mm and the turbulence intensity, u' is approximately 1 m/s towards the end of compression when the spark is fired and most of the intake generated turbulence has been dissipated (Tabaczynski, 1983). This yields an integral time-scale or eddy turn-over-time of about 2-3 ms. Various estimates of the Reynolds number close to top-dead-center (TDC) of compression provide a value on the order of 100 (Abraham *et al.*, 1985). Since the Kolmogorov time-scale (τ^*) is related to the integral time-scale (t') as (Tennekes and Lumley, 1983):

$$\frac{\tau^*}{t} = Re^{-1/2} \tag{4.35}$$

the value of the τ^* can be estimated to be on the order of 0.2-0.3 ms. This is the same range as the chemical time-scale in engines, as the ignition delay period is usually less than 2 ms (Heywood, 1988). So, provided correct estimates of the Kolmogorov time-scale are available, the EDC model could be used to describe the turbulent combustion process in IC engines, at least the premixed configuration. As we shall see later, however, the situation is quite different in direct injection engines.

The EDC model was implemented in KIVA-3V (Amsden, 1997), the latest version of the KIVA family of codes. The procedure to calculate the source terms in the energy and species equations was the same as that used for detailed kinetics, described in detail in Chapter II. For each computational cell, at each time-step, Eqs. 4.32 and 4.33 were integrated to get the fine structure state. The residence time was calculated from Eq. 4.30 assuming that χ was unity. The values of τ^* and γ^* were obtained from their respective definitions given in Eqs. 4.15 and 4.19 by using the local values of turbulence kinetic energy, its dissipation rate and the kinematic viscosity of air, calculated at the fine structure temperature. KIVA-3V uses a Sutherland formula to calculate the value of dynamic viscosity of pure air as a function of temperature. The standard k-ε model of turbulence, as implemented in KIVA-3V, was used to calculate values of the turbulence parameters.

Once the fine structure species concentrations and temperature were known, the mean reaction rates were determined from Eq. 4.31. The chemical source term in the mean energy equation was determined by multiplying the heat released in the fine structures by their mass fraction, γ^*.

It is obvious from the above formulation, that it is absolutely imperative for the numerical scheme to yield correct values for the residence time, which depends on the estimates for turbulence parameters. An incorrect value for the residence time would make the EDC model completely ineffective. The chemical time-scale is predicted by the

detailed chemical kinetic scheme DRM22, which has been tested under a variety of conditions before and has yielded correct estimates of the chemical time-scale. However, the ability of the k-ε turbulence model to predict correct values of the turbulence parameters is not unquestionable.

Initial calculations using the EDC model in KIVA-3V were done on a medium size engine whose dimensions and other details are provided in the next chapter. The engine was run at 1500 RPM. Fuel (pure methane) was injected at 25° before top-dead-center (BTDC) and fuel injection was terminated at 5° BTDC. The calculation was started at bottom-dead-center (BDC) of compression and terminated at BDC of expansion. No chemical activity was seen to occur under these conditions. This is not surprising when one looks at the dramatic increase in in-cylinder turbulence due to the gaseous fuel injection process. The variation of mass averaged turbulence intensity (u') and mass averaged turbulent kinetic energy dissipation rate (ε) is shown in Fig. 4.8 (a) and (b) as a function of crank angle. It can be clearly seen that u' increases by a factor of two due to the fuel injection process compared to a simple motoring case, which is more representative of conditions in a spark-ignition engine. The increase in ε is even more dramatic. It increases by more than two orders of magnitude right after fuel injection starts. This has direct consequences on the predicted value of the Kolmogorov time-scale, given by Eq. 4.15. A two order increase in ε, decreases τ^* by a factor of 10. Note that it is the *average* value that increases so dramatically. Since most of the turbulent activity is associated with the injected gas jet which occupies only a small fraction of the combustion chamber during the injection process, the increase in turbulence in regions where fuel is present is much higher. These processes conspire to make the EDC model ineffective as it is in effect simulating extinction like conditions in the regions containing fuel.

To test the model further, the value of residence time was artificially multiplied by 500 so that an estimate of the residence time comparable to the chemical time-scale could

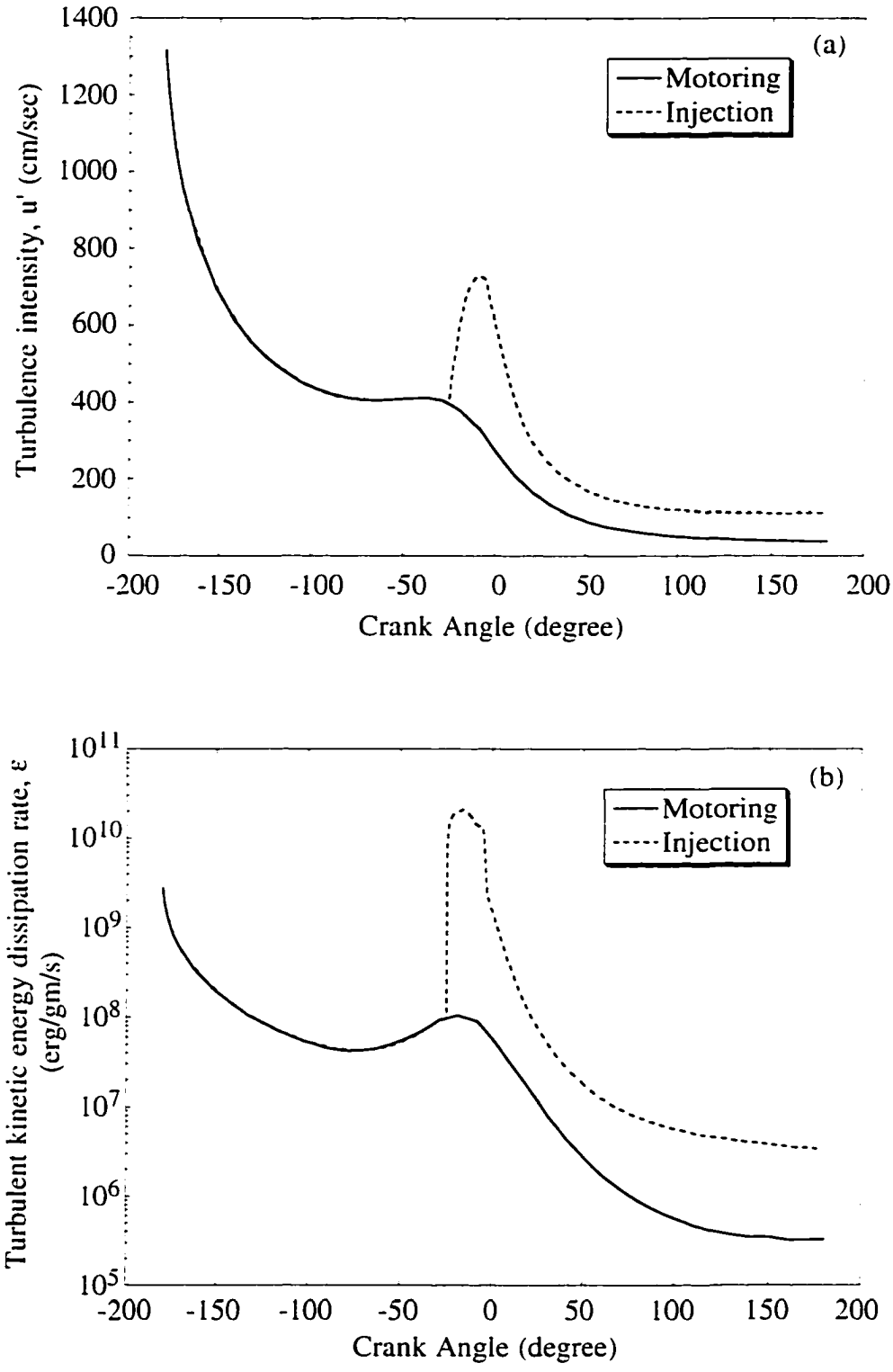

Figure 4.8: Variation of (a) turbulence intensity and (b) turbulent kinetic energy dissipation rate as a function of crank angle for motoring and fuel injection.

be achieved. In this case, a rise in mean temperature was observed during the expansion stroke, however the simulation crashed at about 45° into the expansion stroke. It should be pointed out here that the EDC model is very susceptible to convergence failure as the ODE solver, LSODE has to deal with a wide variety of residence times at each time-step in the different computational cells. Another problem with the use of the EDC model in an engine is the huge penalty in terms of computational time, as the full kinetics equations have to be solved throughout the computation.

To summarize, although the EDC model seeks to improve upon some of the simplifications in the EBU models by trying to describe the interactions between flow and chemistry based on the small scale structure of turbulence, it is not appropriate for direct injection combustion studies in engines in its present format. As pointed out before, all the studies reported using this model have been for steady state applications. If the calculation is carried on for a long time, eventually all the fuel will diffuse to the fine structures, and the results will be less sensitive to the values of residence times. In transient calculations, it is imperative to have the right values of turbulence parameters right from start so that accurate time-resolved results may be obtained.

Coherent Flamelet Models of Turbulent Combustion

The third and last category of models considered for describing the turbulent combustion process in direct injection engines are the so called flamelet models that are valid in the limit of fast chemistry. When chemistry is fast compared to the characteristic time-scales of turbulence, combustion occurs in thin layers called flamelets. The flamelet concept views the instantaneous turbulent flame as an ensemble of thin laminar flamelets, whose structure is locally laminar and essentially one-dimensional. These flamelets are transported by the flow, wrinkled and distorted by the turbulent eddies, but retain their laminar structure locally. The coherent flamelet description of turbulent combustion was

first proposed by Marble and Broadwell (1977) for non-premixed cases and has since then been modified by a number of researchers.

The biggest advantage of the flamelet concept is that it allows for the decoupling of complex chemistry from the analysis of the turbulent flow field. Since the flame is locally laminar, its properties can be calculated in advance and stored in libraries that can be called for the local conditions of the flow field. This provides a great reduction in computational costs as compared to models like the EDC. The flamelet libraries can be constructed based on simple algebraic relationships to provide local rates of consumption of fuel per unit flame area (Marble and Broadwell, 1977) or could be more elaborate formulations that account for parameters that affect turbulent reactive mixtures and could also contain information about ignition and extinction conditions (see for example, Clavin and Joulin, 1989, who constructed a flamelet library for premixed turbulent wrinkled flames by considering parameters such as the gas expansion parameter, the Markstein number (describing stretch and curvature effects on the local combustion rate) and the Froude number (when gravity effects are important)). However, as will be shown later, the creation of flamelet libraries for direct injection engine combustion is a non-trivial task.

As was pointed out in the introduction to this chapter, there is evidence to support the fact that at least under some operating conditions, engine combustion occurs in the regime of flamelets, where the flame thickness is much smaller than the smallest length scales in the turbulent flow-field and the Damköhler number is large. Such a regime also exists in other practical situations like continuous flow aircraft combustors, ramjets, rocket motors and industrial furnaces (Candel *et al.*, 1994).

It is noteworthy that flamelet descriptions are not unique. Different researchers, primarily in France (Poinsot, Candel, Darabiha, Veynante, Lacas), England (Bray and his co-workers), Germany (Rogg, Peters and his co-workers) and the United States (Pope, Cheng) have evolved their own formulations of the flamelet models. However, all of them share the following ingredients:

- A description of the turbulent flow consisting of Favre averaged equations describing the mean flow variables and the main species concentrations and relevant closure equations.
- A laminar flamelet submodel (or submodels) that provides the local structure and properties of the flamelets.
- A set of rules that couple the flamelet submodel to the turbulent flow description.
- Additional models accounting for chemical reactions that take place outside the flamelets.

A major portion of flamelet models are based on probabilistic methods. They use a probability density function (pdf) approach to couple the local analysis to the flow description. Peters (1984a, 1986), Liew and Bray (1981), and Liew *et al.* (1984) have been the main protagonists of this approach for non-premixed combustion. The individual flamelets are assumed to belong to a family and are described in terms of a conserved scalar, the reactant composition (the mixture fraction, Z) and the strain rate (or the scalar dissipation rate, χ) that is imposed on the flame sheet by the flow field. It is then assumed that there is a unique relationship between a scalar quantity ϕ and the normalized conserved scalar, ξ: $\phi = \phi(\xi, \chi_{st})$ where χ_{st} is the scalar dissipation rate at the stoichiometric point. The couple (ξ, χ_{st}) may be treated as a random variable having a joint pdf and this function may be presumed or calculated. Since flame stretch increases the scalar dissipation rate in a turbulent flow field, Peters (1986) pointed out that if the magnitude of χ exceeded a critical value χ_q, the diffusion flamelet will extinguish. For non-premixed combustion it was concluded by Peters that the outer mixing field dominates the flamelet behavior by imposing the scalar dissipation rate because the flamelet is attached to the surface of stoichiometric mixture.

The flamelet model for non-premixed combustion was also extended to partially premixed cases by Peters (1984b) and Rogg *et al.* (1986). The degree of partial premixing of the reactants could also have an effect on the turbulent flame structure. Partial

premixing is important in practical applications like engines where fuel and air mix with each other during the ignition delay period. Also, species could mix at the molecular level after local flamelet extinction has occurred in a turbulent flame. If conditions in the turbulent flame are favorable after molecular mixing, the mixed reactants could ignite and burn in a premixed fashion. In these cases, the turbulent non-premixed flame may be treated as an ensemble of laminar, partially premixed diffusion flamelets (Rogg *et al.*, 1986).

Based on the conserved scalar approach and the experimentally observed fact that the dissipation of essentially all the instantaneous scalar energy occurs in locally one-dimensional layer-like structures, Dahm and his co-workers (Dahm and Bish, 1995; Bish and Dahm, 1995) have proposed an improved type of flamelet model. These dissipation layers are a direct consequence of the dynamics of scalar mixing in turbulent flows and are independent of the extent of chemical non-equilibrium in the flow. The presence of these layer-like scalar dissipation structures in turn indicates a locally one-dimensional structure in the underlying chemical species fields. Unlike the classical flamelet model, this strained dissipation and reaction layer (SDRL) model does not require thin reaction zones, and can produce broad (distributed) concentration fields and reaction zones, as well as thin (flamelet-like) species concentration and reaction rate fields, depending on the local stoichiometry and the degree of chemical nonequilibrium. This model was used to study a turbulent jet diffusion flame and was found to show significant improvements over the classical flamelet model.

The problem with all the proposed flamelet formulations briefly reviewed so far is that they are either impractical for studying engine combustion or require major modifications to make them suitable for the engine configuration. In direct injection engines, for example, the turbulent combustion model has to be suitably modified to describe the ignition delay period and the two distinct phases of burning - the premixed and the non-premixed burn. Each of these phases has to be numerically quantified and the

transitions to and from it adequately described. The problem with the pdf approaches is that they are not very practical especially when complex chemistry is to be considered.

The type of flamelet models that are amenable to engine applications are based on a balance equation for the flame surface density (Musculus and Rutland, 1995; Dillies *et al.*, 1993; Cheng and Diringer, 1991). This equation describes the transport of the mean reactive surface by the turbulent flow field and accounts for the physical mechanisms that produce and destroy the flame area. The coherent flamelet model, as proposed initially by Marble and his co-workers (Carrier *et al.*, 1975; Marble and Broadwell, 1977) identifies the dominant physical mechanisms of turbulent combustion such as production of flame area through stretching and its annihilation by reactant consumption. Considering a non-premixed flame involving a global reaction $F + sO \rightarrow P$ between the two main species F and O, the balance of flame surface may be written as (Candel *et al.*, 1994):

$$\frac{\partial \Sigma_f}{\partial t} + v_k \frac{\partial \Sigma_f}{\partial x_k} = \frac{\partial}{\partial x_k}\left[D_t \frac{\partial \Sigma_f}{\partial x_k} \right] + \alpha \varepsilon_s \Sigma_f - \beta \left(\frac{V_{DF}}{X_F} + \frac{V_{DO}}{X_O} \right) \Sigma_F^2 \qquad (4.36)$$

where Σ_f is the flame surface density (flame surface area per unit volume), D_t is the turbulent diffusivity, V_{DO} and V_{DF} are the volume rates of consumption of oxidizer and fuel per unit flame area (to be calculated from analytical expressions or provided by a flamelet library), and X_O and X_F are the oxidizer and fuel mole fractions. The effect of the turbulent flow field and combustion on the flame surface density is modeled by the last two terms. The second term on the right hand side is a production term and describes the increase of flame area due to the local strain rate $\varepsilon_s = \varepsilon / k$. The last term on the right hand side accounts for flame shortening mechanisms due to mutual interaction of adjacent flame elements. α and β are two modeling parameters whose values were assumed to be 20 and 5, respectively by Musculus and Rutland (1996).

Once the flame surface density is known, the local chemical source term, $\dot{W}_i$ can be found from the following expression:

$$\dot{W}_i = \rho V_{Di} \Sigma_f \tag{4.37}$$

where ρ is the local average mass density and V_{Di} is the local consumption/production rate of species i per unit flame area (in m^3/s per m^2, which corresponds to a speed unit, m/s).

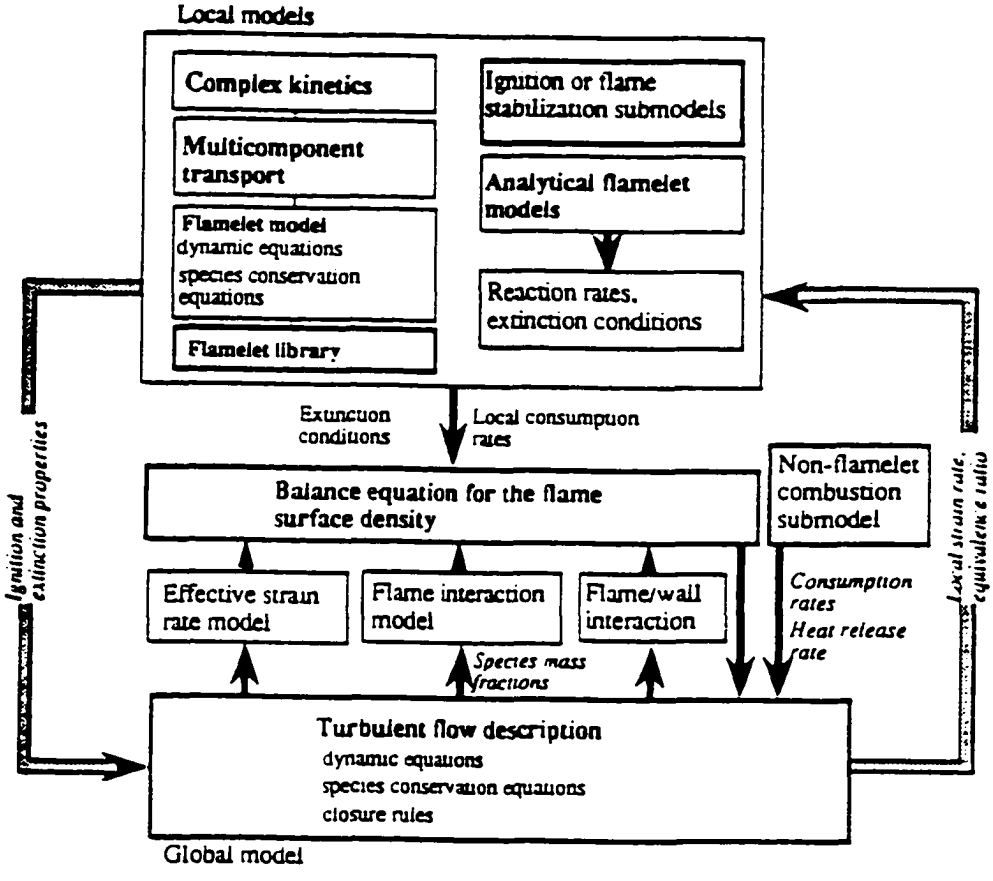

Figure 4.9: General organization of the flame surface density model. (From Candel *et al.*, 1994)

Figure 4.9 shows the general organization of the flame surface density model. It shows the interaction between local models, in the form of a flamelet library or analytical expressions, that provide local flame properties and a global model that provides the turbulent flow description. Specific submodels can be used to describe ignition and flame stabilization. Other submodels can be used to provide the effective strain rate, the mean

strain rate production term, the destruction of the flame surface and combustion outside the flamelets.

As pointed out before, to extend this model to direct injection engine combustion, two characteristics need to be incorporated. These are the ignition delay of the injected fuel and the premixed and non-premixed (or diffusion) burns. The ignition delay period can be described using the coupled detailed chemistry and multi-dimensional flow methodology described in the previous chapter. To model the premixed and non-premixed burns, Dillies *et al.* (1993), introduced two flame surface densities into the calculation, one for the premixed burn and the other for the non-premixed burn. A third surface density was also introduced as a contact surface between the fuel and oxidizer, with the pure reactants diffusing through this surface to form premixed reactants before ignition. This three surface density model was based on the ideas of Veynante *et al.* (1989) who proposed a flamelet model combining premixed and non-premixed flames.

Dillies *et al.* viewed combustion in a diesel engine as a five step process. These five steps are:

1. Contact between reactants just after injection and the establishment of a passive contact surface separating them.
2. Mixing between reactants across the contact surface to form pockets of premixed gases.
3. Auto-ignition under diesel conditions to form a transient premixed flame.
4. Premixed combustion to consume premixed fuel-air mixture and the formation of a non-premixed surface.
5. Non-premixed burn with the establishment of a non-premixed flame having fuel and burnt gases on one side and oxidizer and burnt gases on the other side.

Musculus and Rutland (1995) reported problems with the implementation of the coherent flamelet model of Dillies *et al.* In particular they reported difficulties with the coupling terms between transport equations for the contact surface and the non-premixed

burn surface. They also reported problems with the contact surface when there was no reaction.

Musculus and Rutland viewed the diesel combustion process as a sequence of the following five phases:

1. Low temperature ignition kinetics that can be described by a multi-step kinetic mechanism for fuel oxidation. The model used by them was only applicable for low temperature regimes.
2. Transition to high temperature ignition kinetics, which occurs wherever the local temperature exceeds 1050 K. The transition also uses a ramp function to keep the heat release predicted by the ignition model close to the heat release predicted by the high temperature premixed burn model. The ignition model heat release is scaled down if it exceeds a critical multiple (chosen to be 3.5) of the high temperature premixed burn rate.
3. High temperature premixed burn is modeled using a simple one step global Arrhenius reaction that has been tuned for high temperature kinetics. The premixed burn was assumed to occur only on the oxidizer side of the diffusion flame, so it was necessary to differentiate between fuel which is premixed and located on the oxidizer side of the flame and fuel which is not mixed with oxygen and is located on the fuel side of the diffusion flame. A new transport equation was added to account for the premixed fuel.
4. Transition to non-premixed burn was based on a critical Damköhler number criterion. Once the local Damköhler number, defined as the ratio of the k-ε model large scale turbulence time-scale to the Arrhenius chemical time-scale, exceeded 50, a transition to non-premixed burn was assumed to occur and a diffusion flame was initiated. The flame area was also initialized during the transition by assuming the droplet area as the initial flame area. Once the transition occurred, both premixed and non-premixed burns could occur in a computational cell.

5. Non-premixed burn was simulated by solving a transport equation for global surface area density (Eq. 4.36), although different forms of the production and destruction terms were used. Analytical expressions for local volume consumption rates of the fuel were used to calculate the global reaction rate from Eq. 4.37. Modifications were required to account for facets of diesel combustion that are not accounted for by the classical coherent flame model for non-premixed combustion. It is necessary to define the relative position of the flame to determine the species concentrations on either side of the non-premixed flame to calculate the local consumption rates. Also, the volume fraction of the oxidizer side of the flame is needed so that bulk species densities used in the transport equation for the premixed fuel can be converted to local species densities which are used in the determination of the reaction rates.

It is clear from the above discussion that the application of the coherent flamelet model to diesel or direct injection engine combustion is non-trivial. A lot of approximations are needed to suitably describe the myriad phases of combustion from the moment the fuel is injected to the time a non-premixed flame is established. Also, so far, only analytical expressions have been used to calculate local consumption rates. In this work, interest was in kinetic modeling of the combustion process so that estimates of pollutants could also be obtained, but the creation of a flamelet library for direct injection engine combustion is computationally very intensive. Assuming the library would be used only for the non-premixed combustion phase, it has to account for parameters like temperature, pressure, mixture fraction and scalar dissipation rate (or strain rate) at the least. Local consumption rates would depend on interpolation for values of these parameters in this four-dimensional space. Another major problem in generating flamelet libraries is the specification of accurate boundary conditions for the flamelet calculations. It is impossible to get the right boundary conditions for each flamelet embedded in the turbulent flow field. So, the values used will always be in error and incorporation of a number of boundary conditions would make the flamelet libraries even more unmanageable in terms of storage space and retrieval time of the desired local values.

The generation of the flamelet libraries themselves is also a non-trivial task. Calculations need to be performed for laminar, planar or cylindrical, strained non-premixed and premixed flames using detailed chemistry. Although such a study could be a Ph. D. dissertation topic in itself, codes are available nowadays that can do these calculations readily. One such code is the Universal Laminar Flame and Flamelet Computer Code RUN-1DL (Rogg, 1993; Rogg, 1994) that is distributed free of cost to universities by Prof. B. Rogg and Dr. W. Wang of the Ruhr-Universität Bochum in Germany (email: run-1dl@LStM.Ruhr-Uni-Bochum.De). This code has been developed to simulate steady or unsteady, laminar, one-dimensional and quasi one-dimensional, chemically reacting flows, such as strained premixed, non-premixed, or partially premixed diffusion flames. It can also be readily used in conjunction with CHEMKIN-II to study detailed chemical kinetic mechanisms.

So, although the generation of flamelet libraries themselves was not a major issue, their size and the number of approximations made in modifying the coherent flamelet model for direct injection combustion, were thought to be major drawbacks of this approach. The flowfield and combustion process in an engine are themselves so complex, that if a model having a number of approximations is used, it would be very difficult to explain whether the predictions were obtained due to model approximations or some parameters in the engine. Lack of experimental data on DING engines to verify the validity of some of these approximations was also a deterrent. Hence, it was decided to use a simpler turbulent combustion model, which though would not be as rigorous as the models that describe the interactions between chemistry and flow in detail, would give reasonable estimates of the turbulent combustion process in direct injection engines. The EBU model, described in detail earlier in this chapter, is one such model. Initial simulations using it showed that it was capable of accounting for the large scale mixing process on chemical reactions. This model was used in conjunction with detailed chemistry (for the ignition delay period) to describe combustion in direct injection natural gas engines. These studies are described in the next chapter.

Modeling Pollutant Formation

Although combustion releases heat which is converted into useful work in applications like IC engines, in the process, many harmful pollutants are formed. A day may come, soon one hopes, when more efficient and environmentally friendly ways will be found to convert chemical energy of the fuel into heat. Till then, one has to deal with the fact that a combustion process will produce pollutants that harm human health and deteriorate the quality of the environment we live in. However, not all combustion processes produce the same amount of pollutants per unit work done. Research is continuing into finding better ways to design combustion systems to minimize pollutants while maximizing the heat/work generated, and modeling has and will continue to play a major role in this effort.

Although the major types of combustion-generated pollutants include particulate matter, unburned hydrocarbons, carbon monoxide, oxides of nitrogen, sulfur dioxide and greenhouse gases, in diesel engines, the major pollutants are nitrogen oxides (NOx), hydrocarbon emissions and particulate matter (primarily soot). Direct injection engines are not a significant source of carbon monoxide (Heywood, 1988). Since, natural gas is composed primarily of methane and other lower hydrocarbon fuels, particulate matter emissions in these engines are almost non-existent.

Pollutant formation rates in combustion processes are slow and are determined by detailed kinetics. In general, concentrations of pollutants in IC engine exhaust differ from values calculated using chemical equilibrium at the exhaust temperature (Heywood, 1988). In this work, emphasis was placed on modeling of nitric oxide (NO) formation in DING engines under various operating conditions of speed and load. Oxides of nitrogen impact the environment in several ways: as a reactant in the production of photochemical smog, as a reactant that affects concentrations of stratospheric ozone, and as a contributor to acid rain and the greenhouse effect (Bowman, 1992). These factors have mandated stringent regulations on the production of nitrogen oxides. Further details on the harmful

effects of various pollutants and the modeling of their properties and production rates can be found in the review by Faeth (1996).

The oxides of nitrogen that are lumped together in the commonly used term NOx are nitric oxide (NO), nitrous oxide (N_2O) and nitrogen dioxide (NO_2). Recent studies suggest that combustion processes are not a major source of N_2O (Faeth, 1996). Chemical equilibrium considerations show that for burned gases at typical temperatures, the ratio NO_2/ NO should be negligibly small (Heywood, 1988). Experimental data have shown that this is true for spark-ignition engines, however in diesel engines, NO_2 can be 10 to 30% of the total exhaust NOx emissions. The percentage of NO_2 in the exhaust is highest at low loads and decreases with increasing engine speed. Since NO is the primary constituent in NOx emissions, the modeling of its formation was the focus of this study.

NO forms both in the flame front (described as "prompt" NO by Fenimore who first observed it in 1970) and in the post-flame gases. In engines, however, combustion occurs at high pressures so the flame reaction zone is extremely thin (~ 0.1 mm) and the residence time of different species in the flame front is very short. Also, since the cylinder pressure rises during most of the combustion process, the burned gases produced early in the combustion process are compressed to a higher temperature than they reached immediately after combustion. Thus, NO formation in post-flame gases almost always dominates any flame-front-produced NO (Heywood, 1988).

The NO produced in post-flame gases is also called thermal NO and the mechanism for its formation was first proposed by Zeldovich *et al.* in 1947. In recent years, the mechanism proposed by Zeldovich *et al.* was modified by the addition of one more reaction and termed the extended Zeldovich mechanism (Heywood, 1988). This reaction consists of three reversible reactions and seven species. Due to the importance of NOx as an environmental pollutant, a number of studies can be found in the literature that propose mechanisms for modeling its formation. Some of these studies that are relevant for natural gas flames and for practical combustion applications are due to Miller and Bowman (1989), Takeno, (1995), Correa (1992), Breen *et al.* (1993), Pourkashanian *et al.*

(1993), Al-Fawaz *et al.* (1994), Brown and Heywood (1986), Glarborg *et al.* (1992), Sick *et al.* (1998) and Josefsson *et al.* (1998).

The extended Zeldovich mechanism for thermal NO production, with rate constants as given in Heywood (1988), was used to study NO formation in DING engines. This mechanism consists of the following three reversible reactions which describe the oxidation of atmospheric (molecular) nitrogen to produce NO:

$$O + N_2 \Leftrightarrow NO + N \tag{4.38}$$

$$N + O_2 \Leftrightarrow NO + O \tag{4.39}$$

$$N + OH \Leftrightarrow NO + H \tag{4.40}$$

These reactions mainly proceed in the high temperature, fuel-lean, post-flame regions of combustion processes where the required pools of O and N radicals are available (Faeth, 1996). The forward rate constant for reaction (4.38) and the reverse rate constants for reactions (4.39) and (4.40) have large activation energies which result in a strong temperature dependence of NO formation rates and to a lesser extent on burned gas oxygen concentrations and pressure (Bowman, 1992).

A few calculations were performed to understand the dependence of NO formation rates on temperature and radical concentrations. These calculations were done at three different input temperatures for atmospheric air with different initial concentrations of O and N radicals. The ambient pressure was assumed to be 70 atmospheres. The governing ODEs for species concentrations (Eq. 2.3) and energy (Eq. 2.2) were integrated using LSODE, and CHEMKIN-II was used to calculate the molar production rates for each of the seven species at each time-step.

For the calculations, the reactants were assumed to be atmospheric air in the proportion of 79% N_2 and 21% O_2 by volume. When only pure air was used, no NO was formed, even at extremely high temperatures. This is a direct consequence of the extended Zeldovich mechanism (Eq. 4.38 - 4.40). It can be clearly seen that none of the rates of production of any species will be non-zero if only the concentrations of molecular nitrogen and oxygen are initially non-zero. Radicals, specifically O and N, have to be

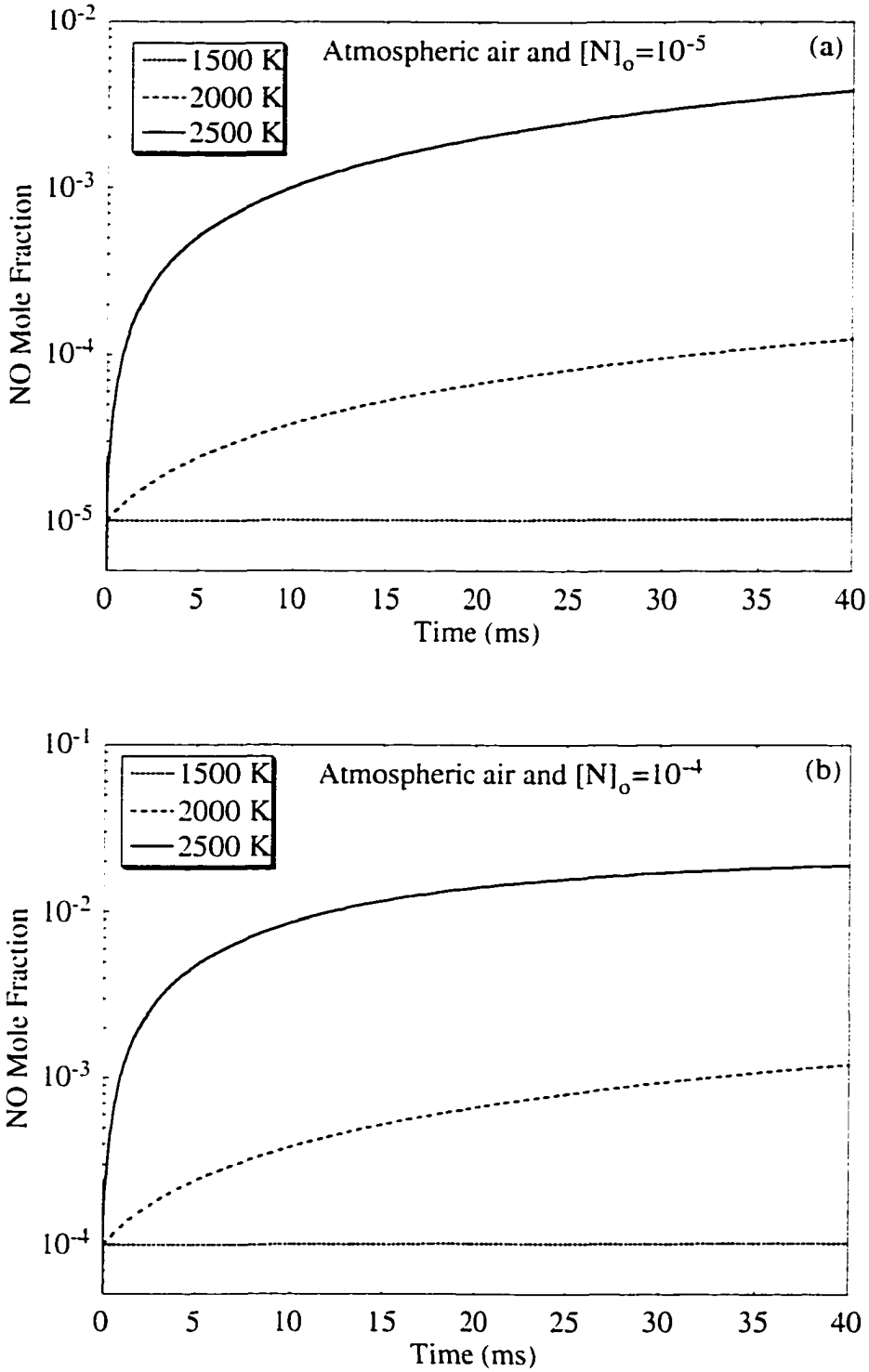

Figure 4.10: Variation of NO mole fraction with time at three initial temperatures for atmospheric air with different initial N atom mole fractions:
(a) $[N]_o = 10^{-5}$ and (b) $[N]_o = 10^{-4}$

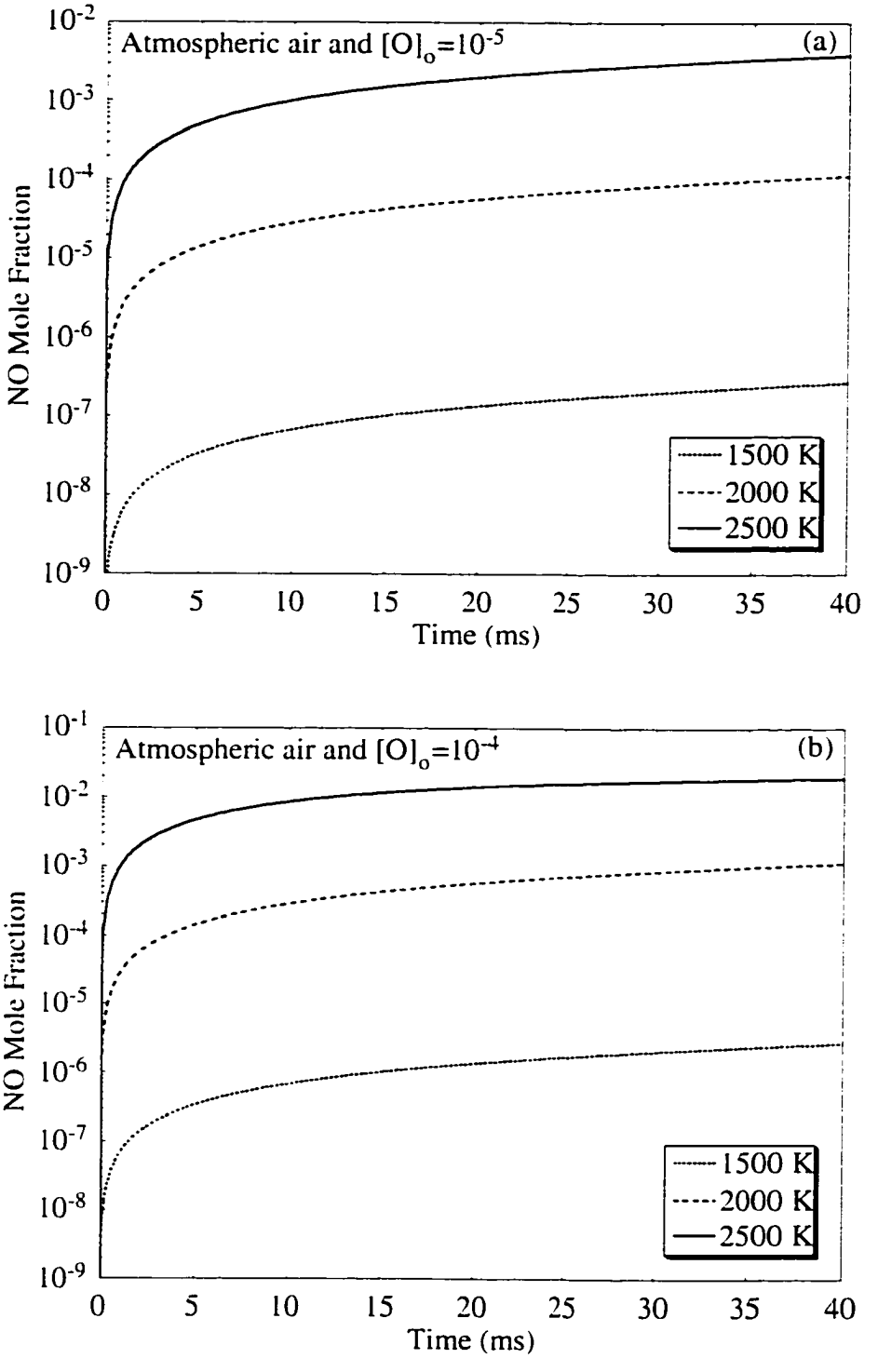

Figure 4.11: Variation of NO mole fraction with time at three initial temperatures for atmospheric air with different initial O atom mole fractions:
(a) $[O]_o = 10^{-5}$ and (b) $[O]_o = 10^{-4}$

present in non-zero concentrations for NO to be formed. Figures 4.10 (a) and (b) show NO mole fractions as a function of time at three different temperatures for initial mole fractions of N radicals of 10^{-5} and 10^{-4}, respectively. Figures 4.11 (a) and (b) show NO mole fractions for three different temperatures when the initial mole fractions of O radicals are 10^{-5} and 10^{-4}, respectively. The other non-zero species are oxygen and nitrogen molecules in atmospheric proportions. For Fig. 4.10, it can be seen that in all cases the NO mole fraction jumps from zero to the initial N radical mole fraction value (10^{-5} for 4.10 (a) and 10^{-4} for 4.10 (b)) almost immediately. After the initial increase, at the lowest temperature there is virtually no increase in NO concentration, whereas for the higher temperatures NO concentration continuously increases throughout the calculation, which is terminated at 40 ms. This has important consequences for NO concentration in engines, as depending on engine speed, the high temperature pockets of burned products would be compressed to even higher temperatures for different times. Note that a temperature difference of 500 K from 2500 K to 2000 K results in more than an order of magnitude difference in NO mole fractions. This shows how sensitive NO formation is to temperature. Investigation of other minor species (OH and H) mole fractions revealed that both of them achieved their equilibrium values almost immediately. In fact their concentrations did not change after the first time-step of the calculation which was taken to be 40 μs. For the cases shown in Figs. 4.10 and 4.11, the equilibrium values of these species were less than 10^{-15} showing that their concentrations were insignificant. O and N radicals also achieved their equilibrium values almost immediately, although their values were higher than OH and H. O radicals always attained the initial mole fraction value, be it that of O or N. N radical concentrations were dependent on the temperature of the simulation and the initial N or O radical mole fraction and attained values ranging from 10^{-14} at 1500 K to 10^{-10} at 2500 K for cases shown in Figs. 4.10 (a) and 4.11 (a) and values ranging from 10^{-14} at 1500 K to 10^{-9} at 2500 K for cases shown in Figs. 4.10 (b) and 4.11 (b). It was also found that NO formation is endothermic, though it leads to a

very slight decrease in temperature. The temperature drop was almost negligible up to 2000 K and it decreased by about 50 K for 2500 K.

Figures 4.10 and 4.11 also show that NO formation is not only dependent on temperature but also on the concentration of radicals like N and O. An order of magnitude increase in initial N concentration leads to a corresponding order of magnitude increase in NO concentrations at all the temperatures considered. However, when the O radical concentration is changed (see Fig. 4.11), the change is not so linear. In fact, the variation of NO is quite different when O radical concentration is specified to that when N radical concentration is specified (see Fig. 4.10). In Fig. 4.11, even at the lowest temperature, the NO concentration increases with time, although the values it attains are orders of magnitude lower than for the same initial concentration of N radicals. But at higher temperatures the values for both cases are on the same order of magnitude. This shows the interesting interactions between temperature and radical concentrations on NO formation.

Implementation of the extended Zeldovich mechanism in KIVA-3V

The extended Zeldovich mechanism as defined by Eq. 4.38 to 4.40 can be implemented in KIVA-3V in a manner similar to the natural gas oxidation mechanism, DRM22 whose implementation was described in the previous chapter. However, it was found that CHEMKIN-II was not able to handle two different kinetic mechanisms in the same calculation. The link file created by CHEMKIN-II, containing all the information about Zeldovich kinetics, could not be coupled with KIVA-3V along with the link file for DRM22. Hence, the species production rates for each of the seven species in the extended Zeldovich mechanism were coded manually into KIVA-3V. A new subroutine named *nox* was written that was called at each time-step and was used to calculate the updated densities of each of the species taking part in the extended Zeldovich mechanism, namely O_2, N_2, O, N, OH, H and NO. The species production rates were calculated using the law of mass action and Arrhenius form of the rate constants and were integrated using

LSODE. An updated temperature, obtained after accounting for chemical heat release (from DRM22 during the ignition delay period and from the EBU model during the turbulent combustion phase), was used in subroutine *nox* for the NO calculations. The NO sub-model itself did not participate in the heat release process as it was shown earlier that NO formation is only weakly endothermic. Hence NO chemistry itself does not have a direct influence on the fuel oxidation process, although it is intimately linked with it as the temperature and the reactions that produce the species needed for NO formation take place in an environment created by the combustion reactions.

As pointed out earlier, radicals such as N and O are needed for the production of NO. Since these could not be obtained from the fuel oxidation reactions, it was assumed that they were in equilibrium with their respective molecular states at the local temperature and pressure. This is a valid assumption as it was shown before that during the NO formation process, the radical concentrations achieve their equilibrium values very quickly. The equilibrium assumption for the minor species is routinely used with the Zeldovich kinetics (Heywood, 1988; Josefsson *et al.*, 1998). However, it should be pointed out that if the equilibrium assumption for NO itself is used, it could lead to over-prediction of NO concentrations during the initial stages (compression stroke in an engine), as the rate of NO formation is kinetically controlled and not much NO forms in the initial stages even though temperatures are high, and under-prediction during the later stages (expansion stroke), when NO concentrations actually freeze as temperatures drop.

The equilibrium concentrations for the species used in the extended Zeldovich mechanism were obtained from solution of the simultaneous equilibria of the following six reactions important in hydrocarbon oxidation:

$$N_2 \Leftrightarrow 2N \tag{4.41}$$

$$O_2 \Leftrightarrow 2O \tag{4.42}$$

$$2CO_2 \Leftrightarrow 2CO + O_2 \tag{4.43}$$

$$H_2 \Leftrightarrow 2H \tag{4.44}$$

$$2OH \Leftrightarrow O_2 + H_2 \tag{4.45}$$

$$2H_2O \Leftrightarrow 2H_2 + O_2 \tag{4.46}$$

The equilibrium concentrations of each of the ten species involved in the above six reactions can be obtained from additional four equations of element conservation of carbon, hydrogen, oxygen and nitrogen. The ten equations can then be reduced to an algebraic system which can be solved using the Newton-Raphson iteration method. An algorithm for the solution of simultaneous equilibria given by Eq. 4.41 to 4.46 was devised by Meintjes and Morgan (1987) and is already implemented in KIVA-3V in the subroutine *chmqgm*. It should be noted that due to the manner in which the equations are solved, it is always necessary to have at least trace amounts of carbon present in each computational cell. Since the equilibrium concentrations were post-processed based on local cell temperatures and species concentrations and were to be used only for the NO calculations, it was assumed that they did not contribute to the chemical heat release process.

Closure

In this chapter, it was shown that accounting for the interactions between chemistry and flow is extremely important to describe the combustion process occurring in a turbulent medium like an IC engine. Both flow and chemistry interact with each other over a wide range and in many cases, the structure of the flame in these regimes is not clear. This is especially true for practical combustion devices like engines. So, a judgment has to be made about the kind of interactions that would occur over most of the operating regime and suitable ways have to be found to describe those interactions.

Due to the classical closure problem of describing the higher moments accurately when turbulence and chemistry interact, the problem reduces to one of modeling. Different turbulent combustion models have been proposed over the years and some of these were reviewed in this chapter. These range from the algebraic, "mixed-is-burned"

models like the Eddy-Break-Up model to the more sophisticated models like the Eddy Dissipation Concept and various forms of the Coherent Flamelet model that describe the influence of flow on chemistry in greater detail. However, a detailed examination of the latter models revealed that they were unsuitable for direct injection engine applications in their present format and required major modifications. Due to lack of experimental data on DING engines to verify the validity of some of these modifications, it was felt that using a model that did not require a number of constants and modeling approximations, but still contained some physics of the turbulent combustion process, would be more appropriate to understand the effect of various operating parameters like load and speed on direct injection natural gas engine performance and emissions. Hence, the EBU model was implemented in KIVA-3V and used in conjunction with a detailed kinetic mechanism for natural gas oxidation (DRM22) to simulate ignition and combustion of natural gas. An appropriate criterion for the transition from chemistry controlled heat release to mixing controlled combustion was found to be the specification of a certain mass fraction of total injected fuel burned.

Pollutant formation is an evil that accompanies the heat release process in a combusting mixture. Since NO is the main pollutant in DING engines, along with unburned hydrocarbon emissions, its production was simulated by using the extended Zeldovich mechanism. The effect of temperature and radical concentrations on NO formation rates was explored to gain a better understanding of their influence on NO concentrations. It was found that NO formation is slow and kinetically controlled and is very sensitive to mixture temperature and concentration of radicals like N and O.

In the next chapter, all the models described so far to simulate ignition, combustion and pollutant formation are combined to study these processes in a typical medium-size direct injection engine.

CHAPTER V

MODELING IGNITION, COMBUSTION AND POLLUTANT FORMATION IN DIRECT INJECTION NATURAL GAS ENGINES

Background

In the previous chapters, different methods to model natural gas ignition, combustion and pollutant formation were described and their applicability to direct injection natural gas engines assessed. It was decided to use a detailed multi-step chemical kinetic mechanism for natural gas oxidation to predict ignition delay in DING engines. Correct predictions of the ignition delay period, at different loads and speeds, are essential as the delay has a significant impact on the subsequent combustion process, and thus engine performance and emissions. After the ignition delay period is over, it was decided to use a mixing controlled combustion model that describes the conversion of fuel to products of complete combustion through a one-step chemical reaction. Such a model was shown to be able to give reasonable predictions of thermodynamic parameters like pressure and temperature and also the concentrations of major species like carbon dioxide and water. A kinetic mechanism for nitric oxide formation was also coupled with the ignition/combustion models and used to predict NO formation. This mechanism used the equilibrium values of concentrations of radicals and the temperatures and pressures predicted by the combustion models. It did not participate in the heat release process itself.

The last major endeavor in this work was to study the ignition, combustion and pollutant formation processes in DING engines. The focus was on assessing the effect of engine operating parameters (speed and load) on performance and emissions. The engine

boost levels and injection timing were also changed to investigate their effect on engine output. In the next section, details of the engine simulations in terms of the geometry and other input parameters are described.

Details of Engine Simulations

The engine geometry chosen for the simulations was based on a medium heavy-duty diesel engine typical of engines used for urban bus and Class 4 through 7 truck applications. Such an engine geometry was used earlier in injection and mixing studies by Jennings and Jeske (1994a and 1994b) and Papageorgakis (1997). The choice of a medium heavy-duty engine was based on the fact that if the DING technology proves to be successful, engines in this category would prove to be the mainstream application. Details of the simulated engine configuration along with injection data, baseline operating conditions and modeling choices made in this study are shown in Table 5.1.

The engine simulations were done using KIVA-3V (Amsden, 1997), the latest version in the KIVA family of codes. A 45° sector mesh was used for the calculations, assuming symmetry for an eight hole injector. This greatly reduced the computational costs, as only 1/8th of the cylinder had to be simulated. Periodic boundary conditions were assumed for the front and back faces of the sector mesh, which consisted of 42 × 3 × 25 cells in the three dimensions. Although grid-independence tests were not done, the grid used in these calculations was finer than that used by Papageorgakis (1997) for a similar engine geometry. Since a "Mexican-Hat" shape for the piston bowl was assumed, care was taken to ensure that the compression ratio was 16:1. The height of the cylinder head was adjusted till the desired compression ratio was obtained. The values shown for engine geometry in Table 5.1 were obtained after all the desired adjustments in cylinder head height were done.

The temperature of the fuel (pure methane) was assumed to be 400 K, the same value as in the combustion bomb calculations of Chapter III. At this temperature,

Table 5.1

Details of the simulated engine geometry, injection data, baseline operating conditions and modeling choices made in this study.

Engine Geometry	
Bore	12.45 cm
Stroke	15.5 cm
TDC Clearance Height	0.37 cm
Connecting Rod Length	31.0 cm
Piston Bowl Shape	Mexican-Hat
Compression Ratio	16.01:1
Displaced Volume/cylinder	1.86 *l*
Injection Data	
Fuel Temperature	400 K
Injection Velocity	508.5 m/s
Injection Timing	25° BTDC / 10° BTDC
Injection Duration	20° CA
Injection Profile	Slug
Injection Angle	45° with respect to horizontal
Baseline Operating Conditions	
Speed	1500 RPM
Overall Equivalence Ratio (ϕ)	0.6
Injection Timing	25° BTDC
Intake Pressure	3 bar
Modeling Choices	
Duration Of Simulations	180° BTDC - 180° ATDC
Intake Air Temperature	675 K
Intake Pressure	3 bar / 4 bar
Initial Turbulent Intensity	1.7 × Mean Piston Speed
Initial Swirl Ratio	1.0
Exhaust Gas Recirculation (EGR)	10%
Turbulence Model	RNG Based k-ε
Cylinder Wall Heat Flux	Nil (Adiabatic)

assuming the flow is choked, the sonic velocity is 508.5 m/s. This value was assumed for the injection velocity. The fuel was injected at an angle of 45° with respect to the horizontal. A few preliminary calculations showed that this injection angle gave better mixing than if the fuel was injected more horizontally. The injection duration was assumed to be 20° and the fuel was injected in a slug profile. Assuming that the fuel was injected in the middle of the computational domain, which spanned 45°, the three components of velocity could be calculated in a manner shown in Fig. 5.1.

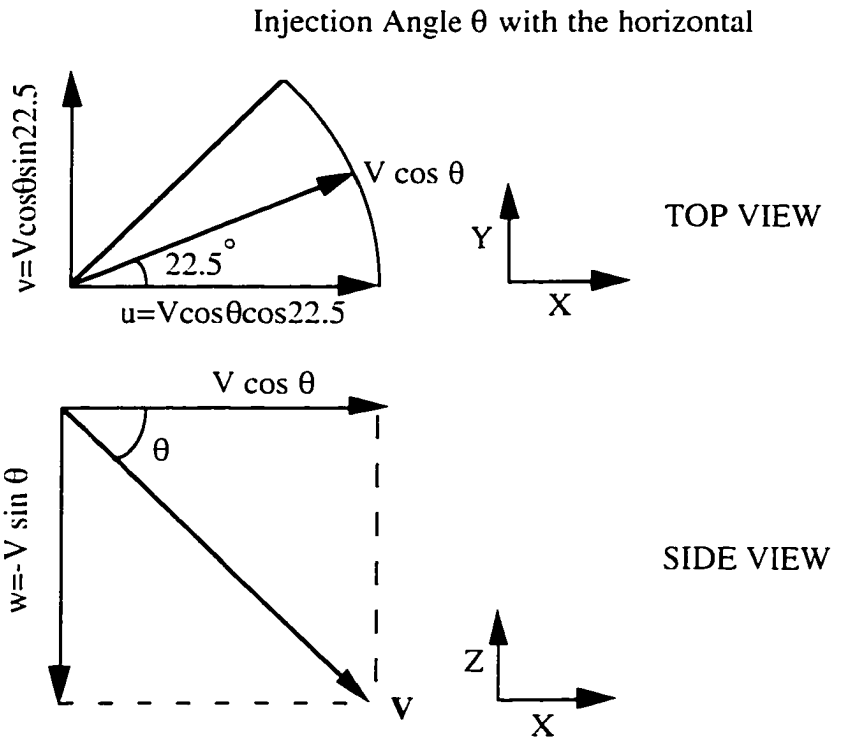

Figure 5.1: Determination of injection velocity components.

For the engine simulations, it is important to make reasonable choices for different engine parameters, otherwise the results may be meaningless. Since it has already been shown that autoignition of methane requires much higher temperatures than diesel fuel, either very high intake air temperatures or very high compression ratios are needed to achieve these temperatures at the time of fuel injection. A compromise between both of these parameters was obtained by using a compression ratio of 16:1 (a reasonable value

for medium size heavy-duty diesel engines) and an intake air temperature of 675 K (402 °C). This choice of the intake air temperature ensured that the fuel was injected at air temperatures close to 1200 K. Although the value of 402 °C is quite high for intake air temperature, a few assumptions were made that would make it possible to achieve this value. These are summarized as follows:

1. It was assumed that the walls of the combustion chamber were adiabatic. Low heat rejection engines result in higher exhaust temperatures and thus hotter residual temperatures, which mix with fresh intake air to increase the temperature of the air inside the cylinder. Since the walls of adiabatic engines are hotter, the intake air also gets heated during the intake process, thereby further increasing its temperature.
2. To make the intake air even hotter, it was assumed that the engine was running with an Exhaust Gas Recirculation (EGR) of 10%. So the intake mixture consisted of 10% exhaust (by mass), re-cycled from the previous engine cycle. Using EGR is an effective way to reduce NO emissions, as the intake air is diluted. For modeling purposes, it was assumed that the exhaust consisted of products of complete combustion (carbon dioxide and water). Assuming stoichiometric combustion of methane and pure air, the mass fractions of CO_2 and H_2O can be readily calculated. Hence, the initial mass-fractions of different species could be specified in the following manner:

$$Y_i = 0.9\ (\text{Fresh Air}) + 0.1\ (\text{EGR})$$
$$= 0.9\ (0.23\ O_2 + 0.77\ N_2) + 0.1\ (0.1514\ CO_2 + 0.1239\ H_2O + 0.7247\ N_2)$$
$$= 0.207\ O_2 + 0.7655\ N_2 + 0.0151\ CO_2 + 0.0124\ H_2O$$

3. The third factor which could be used to increase the intake air temperature is turbo-charged operation. Diesel engines for heavy-duty applications are usually turbo-charged. If the intake air is compressed, but not cooled, its temperature will rise. Typical boosts at full load are about 2.5 or less for diesel engines, but in this work it was assumed that the boost was at least 3. Choice of a high boost is also important in terms of volumetric efficiency. A higher than normal charge temperature results in

insufficient mass inside the chamber at atmospheric pressures. So a hot engine needs to be run turbo-charged to get enough mass of charge inside the chamber.

The combination of each of the above factors could provide high intake air temperatures and make the calculations more realistic. Although KIVA-3V has the capability of simulating moving valves, the calculations shown here were done in the closed part of the cycle, from 180° before top dead center (BTDC) to 180° after top dead center (ATDC). This was due to the fact that only 1/8th of the cylinder volume was being simulated and if the valves were to be included, at least 180° sector mesh would have to be used, assuming four symmetrically placed valves. Even if the closed part of the cycle in being simulated, it is important to prescribe the correct values for turbulence parameters like intensity, as it is the intake process that generates most of the turbulent kinetic energy in the chamber. Since turbulence intensity has a major influence on large-scale mixing, it was felt that correct specification of its initial values is important. Experiments in engines have shown that the intake generated flow velocity is proportional to the engine speed (Heywood, 1988). Based on the normalized values of turbulent intensity with mean piston speed, it can be assumed that at 180° BTDC, the following relationship exists between turbulence intensity (u') and mean piston speed ($\bar{S}_p$):

$$u' = 1.7\bar{S}_p \tag{5.1}$$

where the mean piston speed is defined as $\bar{S}_p = 2LN$ where L is the stroke and N is the engine crankshaft speed. The constant 1.7 was also confirmed by running a quasi-dimensional diesel engine simulation (Assanis and Heywood, 1986) at different engine speeds. An RNG based k-ε model, as implemented in KIVA-3V, was used to describe turbulence.

Since most direct injection engines have some intake generated swirl, it was assumed that the swirl ratio (R_s) was unity. Swirl ratio is defined as the angular velocity of a solid-body rotating flow ω_s, which has equal angular momentum to the actual flow, divided by the crankshaft angular rotational speed:

$$R_s = \frac{\omega_s}{2\pi N} \tag{5.2}$$

As noted before, in this work the emphasis was on investigating the effect of engine operating conditions of speed and load on engine performance and emissions. These were coupled with engine boost levels and injection timing to study how they affected the engine output. The baseline operating conditions against which the results of other cases were compared were shown in Table 5.1. Parametric studies were conducted by varying each of these conditions systematically. The values chosen for each of the parametric studies are shown in Table 5.2. The baseline values are highlighted in bold. The speeds chosen span the range of typical diesel engine operation. The overall equivalence ratio of 0.6 corresponds to high load operation and that of 0.2 to low load operation. The boost of 4 bar was chosen to see if it could have a significant effect on engine performance compared to 3 bar. Since injection timing usually varies with load and speed in modern engines to keep the emissions low, it was decided to investigate two timings: early, with fuel injection from 25° BTDC to 5° BTDC and late, with fuel injection from 10° BTDC to 10° ATDC. As shown later, injection timing can have dramatic influence on NO and unburned hydrocarbon levels in the exhaust.

Table 5.2
Conditions for parametric studies done in this work.

Speed (RPM)	Overall Equivalence Ratio	Injection Timing (Crank Angle)	Intake Pressure (bar)
800	0.2	**25° BTDC**	**3**
1500	**0.6**	10° BTDC	4
2200			

Considering all the possible combinations results in twenty-four studies. However, the results of all the computations will not be described. Parameters will be changed one by one from the baseline case and their effect on the engine investigated. Before the parametric studies are described, the baseline case results are explored in detail.

Baseline Engine Calculation Results

Figure 5.2 depicts the variation of volume-averaged pressure with crank angle and cylinder volume, for motoring and firing cases at 1500 RPM. It can be seen that for the motoring case, the cylinder pressure is symmetrical about the top-dead-center (TDC) position. This is due to the assumption of adiabatic conditions for the cylinder walls. If the wall boundary conditions were prescribed differently, e.g. isothermal, the temperature would drop during the expansion stroke and the pressures would be slightly lower. The P-V plot is a line in Fig. 5.2 (b) for the motoring case due to this assumption.

Figure 5.2 also shows that after fuel injection begins, at 25° BTDC, there is no discernible rise in cylinder pressure for about 10° crank angles (CA) compared to the motoring case. This is due to the ignition delay period when the fuel and air are mixing with each other and pre-combustion reactions are occurring. The numerical value of ignition delay, defined as the time taken to burn 4% of the total injected fuel, is 8.2° CA for this early injection case. The combination of early injection and an overall equivalence ratio of 0.6 results in very high peak cylinder pressures for the firing case. The peak firing pressure occurs at about 4° ATDC. Due to combustion, the gas temperatures are much higher in the expansion stroke than the motoring case, so the pressures are correspondingly higher. It is the higher expansion pressure that delivers the useful work that an engine produces. The area under the P-V curve for the firing case in Fig. 5.2 (b) indicates the gross indicated work (GIW), which is defined as the difference of expansion work and compression work. Since the pumping loop is not simulated, for brevity, the gross indicated work is referred to as indicated work. The ratio of indicated work to displaced volume is called the indicated mean effective pressure (IMEP). IMEP is a useful measure of an engine's performance. The higher the value, at a given engine speed, the more the power delivered to the crank-shaft. Table 5.3 shows the values of IMEP and typical DING emissions like NO, unburned hydrocarbons (UHC) and CO_2 at 150° ATDC when the exhaust valve in typical direct injection engines opens. It should be

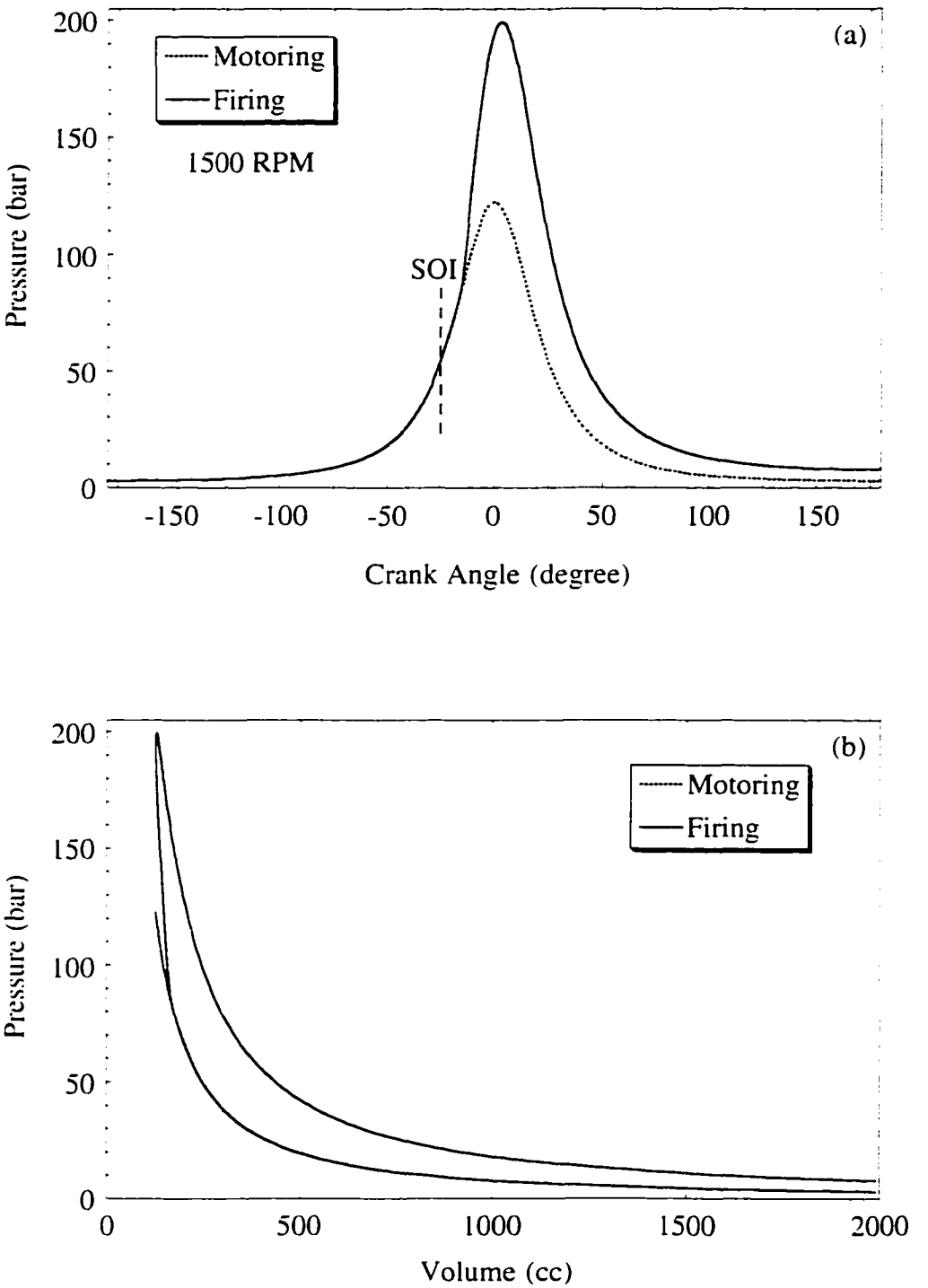

Figure 5.2: Variation of volume-averaged cylinder pressure with (a) crank angle and (b) cylinder volume for motoring and firing at the baseline case.

noted that UHC values were simply based on the mass of methane left in the combustion chamber at 150° ATDC. No specific model, like blowby based on a crevice flow model or absorption/desorption of fuel in the oil film, was used to predict UHC. Thus, the levels of UHC shown in this work are due to the inability of the combustion process to consume the fuel by 150° into the expansion stroke.

Table 5.3
Engine performance and emissions for the baseline case.

IMEP (bar)	NO (ppm)	UHC (ppm)	CO_2 (ppm)
15.83	3382	1692	65222

Although the predictions of exhaust emissions cannot be taken as accurate numerical values at these conditions due to the simplifications made in the modeling approach, the values so obtained lie in the general range of these emissions for diesel engines (Heywood, 1988; Bosch Automotive Handbook, 1993). Interest is primarily in their relative values as engine operating parameters are changed.

Figure 5.3 shows the variation of mass-averaged temperature with crank angle for the baseline case. It can be seen that there is a slight drop in temperature during the ignition delay period when colder fuel is being injected in the cylinder, but chemical heat release has not yet started taking place. After the delay period is over, the average temperature in the cylinder increases rapidly to around 2350 K and then decreases during the expansion stroke when the piston starts moving downwards. It can also be seen from Fig. 5.3 that at the time of fuel injection (25° BTDC), the average fuel temperature in the cylinder is about 1200 K.

Figure 5.4 shows the variation of fuel-air equivalence ratio in a plane that has been cut through the center of the sector mesh, for pure injection (non firing) and the baseline firing case at 10° ATDC. The non-firing case shows that the fuel moves along the surface of the piston bowl while the piston is moving up, and then rolls upwards as the piston starts its descent. The light blue, green and yellow portions in Fig. 5.4 (a) are those that

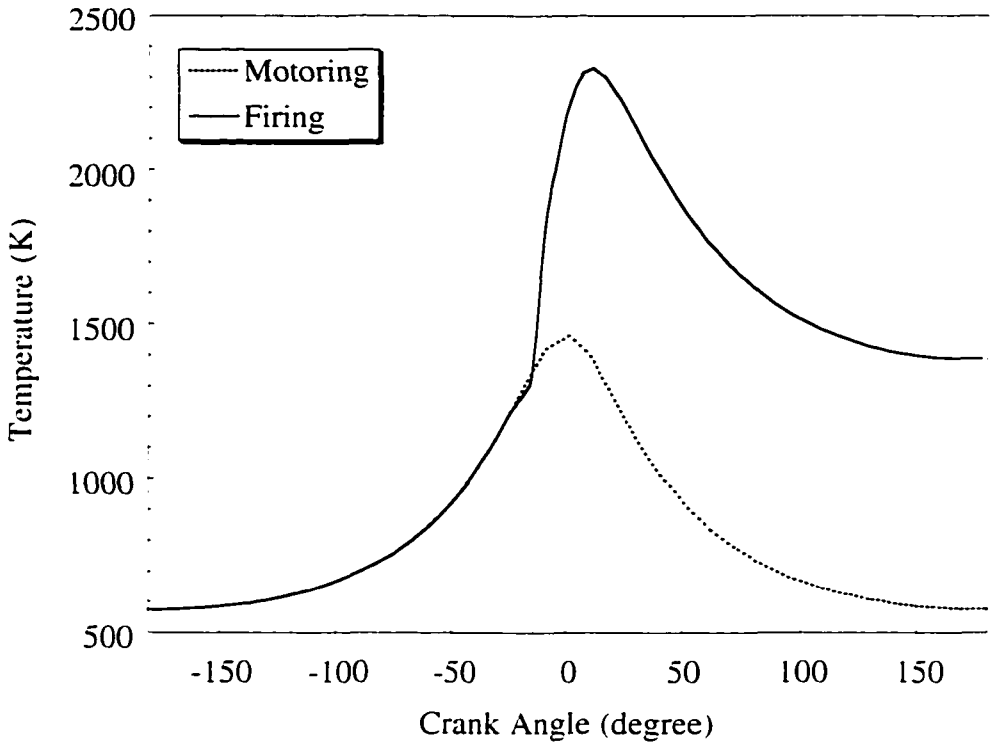

Figure 5.3: Variation of mass-averaged temperature with crank angle for the baseline case.

are conducive for combustion as the fuel and air are mixed within reasonable proportions. By the nature of the EBU model of combustion, the local rate of burning is highest in regions that have low turbulence time-scale, k/ε and fuel-air mixtures that are in close to stoichiometric proportions. The shape of the piston bowl plays a very significant role in aiding the mixing of injected fuel with air. This fact was explored in greater detail in an independent study by Papageorgakis (1997). The firing case shows that the regions where the fuel has been consumed are indeed the regions in the non-firing case where the equivalence ratios ranges from 0.3 to stoichiometric. Two distinct pockets of rich fuel-air mixture can still be seen by 10° ATDC in the firing case. As shown later, by this time, more than 75% of the injected fuel has been consumed. The pocket on the left, on top of the piston bowl is due to the accumulation of the fuel as it hits the piston top directly from the injector. The pocket on the right, on the side of the piston bowl, is due to the slow rolling of the fuel along the side of the piston. Fig. 5.4 clearly shows the importance

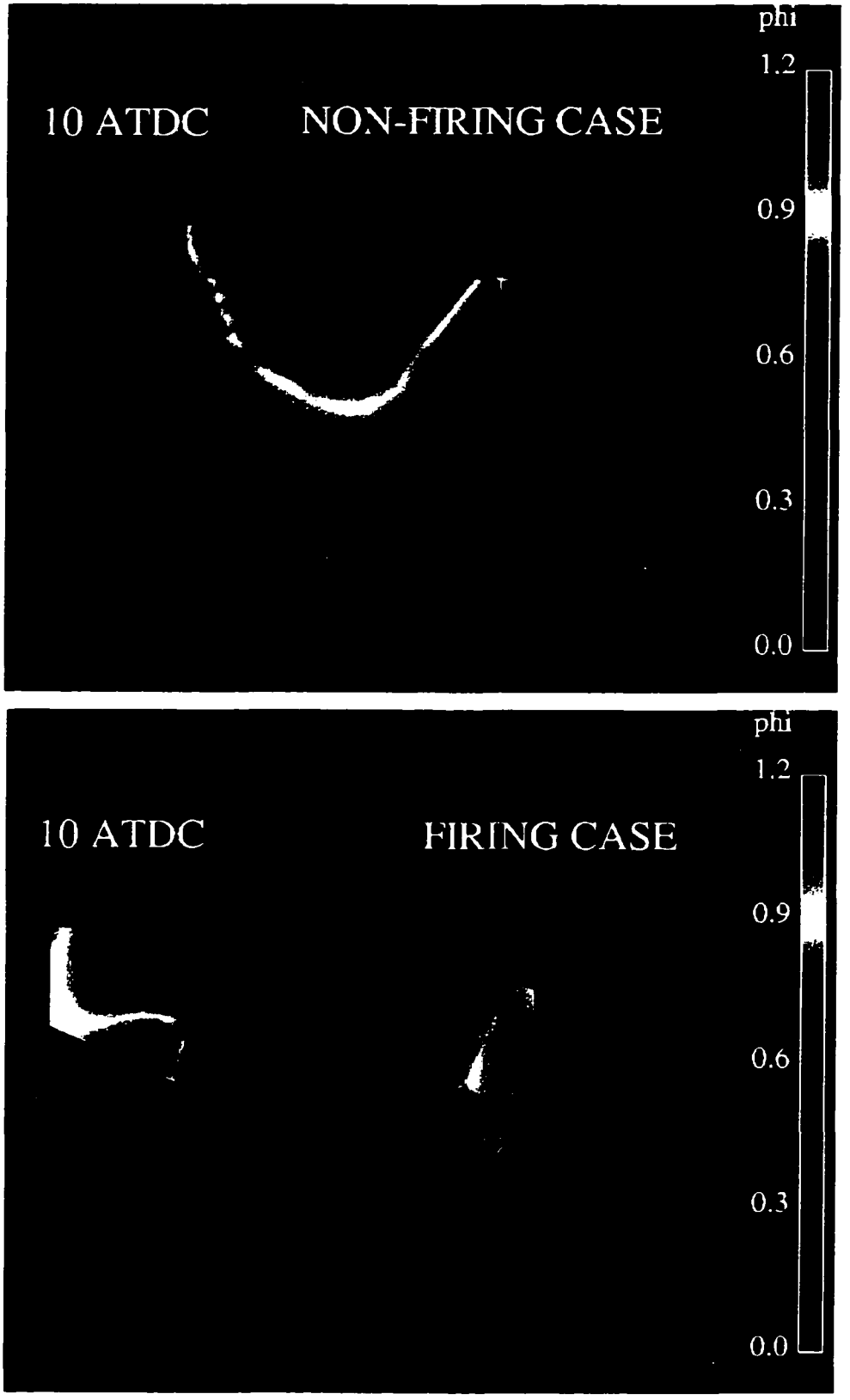

Figure 5.4: ϕ values in the cylinder at 10° ATDC for (a) non-firing and (b) firing cases.

of fuel-air mixing in determining how soon the injected fuel would be consumed.

Figure 5.5 (a) shows the variation of different species masses in the combustion chamber as a function of crank angle. It can be seen that methane is injected in a linear profile from 25° BTDC to 5° BTDC. The unburned methane mass is the same as the injected methane mass till the ignition delay period is over. After that there is a rapid consumption of methane that has mixed with air during the delay period, leading to the premixed burning phase. The unburned methane mass correspondingly shows a decline. There is a slight increase in unburned methane mass after the initial decline due to a reduction in the rate of burning after the initial premixed burn peak. After fuel injection ends at 5° BTDC, the unburned methane mass continuously decreases due to consumption. The mass of CO_2 in the chamber is initially constant at a value of 54.2 mg, which is the mass of CO_2 in the intake air due to an assumption of 10% EGR. After combustion starts, CO_2 concentration starts increasing and continues to increase till the end of the calculation as fuel is being continuously burned . It should be noted that CO_2 is locally assumed to be in equilibrium with CO. This was done to predict species needed for the NO calculations. Due to this assumption, the rate of increase of CO_2 mass decreases slightly at 10° ATDC when the temperatures in the chamber are locally at their highest values (see Fig. 5.3). However, the equilibrium assumption does not have an impact on the values of CO_2 concentrations shown in Table 5.3 because by 150° ATDC, the cylinder temperature falls down considerably and it is seen that the CO ppm values are lower than CO_2 ppm values by more than two orders of magnitude.

Figure 5.5 (b) shows the variation of NO concentration with crank angle in parts per million (ppm). It is seen that NO formation is slow and peaks around 15° ATDC, when cylinder temperatures are very high. The critical time period for NO formation has been shown to be when the burned gas temperatures are at a maximum, i.e., between the start of combustion and shortly after peak cylinder pressure has occurred (Heywood, 1988). Mixture that burns early in the combustion process is especially important as it is

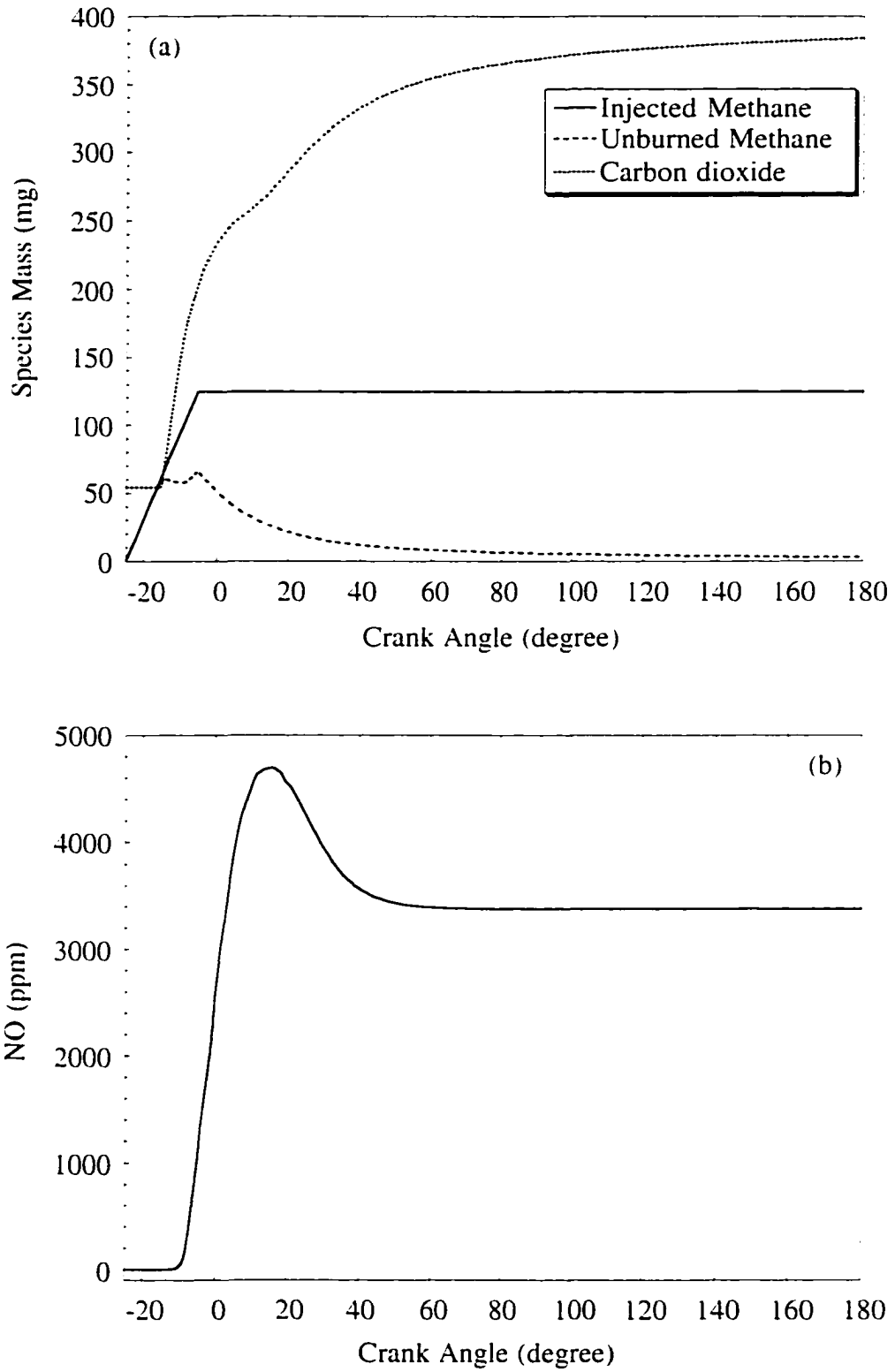

Figure 5.5: Variation of (a) species mass and (b) NO with crank angle for the baseline case.

compressed to a higher temperature, increasing the NO formation rate, as combustion proceeds and cylinder pressure increases. During the expansion stroke, the burned gas temperatures decrease as the cylinder gases expand. This, coupled with the mixing of high-temperature gas with air or cooler burned gas, freezes the NO chemistry and its concentration remains essentially constant during the late expansion process. At very high temperatures, some NO dissociates into N and O and its concentration decreases. It can be seen from Fig. 5.5 (b) that all the NO forms in the 25° CA period from the start of combustion (about 15° BTDC). Both freezing of NO values and decrease in its concentration from the peak value, have been observed experimentally (Heywood, 1988). This shows the extended Zeldovich mechanism is capable of predicting the NO formation process correctly.

Figure 5.6 shows values of temperature and NO density in a plane cut through the center of the sector mesh at 5° BTDC. This is the time by which all the fuel has been injected and combustion has started in earnest. The fuel is injected at an angle of 45° with respect to the horizontal, but due to the flow-field created by the upward motion of the Mexican-hat shaped piston bowl, it is forced to strike the piston bowl very close to the axis of the cylinder. The fuel then spreads along the surface of the piston. This results in fuel rich mixtures along the surface of the piston and leaner mixtures towards the cylinder head. This fact can be seen in Fig. 5.6 (b) which shows contours of equivalence ratios. The red, yellow, green, light blue and dark blue lines denote ϕ of 5.0, 2.0, 1.0, 0.5 and 0.1, respectively. As already discussed before, the reaction rates, and consequentially, the temperatures are highest for close to stoichiometric mixtures. Due to heat release, the temperature of the outer edges of the gas jet increases to around 2700 K. NO starts forming at around 8° BTDC (see Fig. 5.5 (b)) and it is interesting to note that the regions in which NO initially forms, not only are the temperatures high, but the fuel-air mixture is slightly lean of stoichiometric. In a recent study, Dec and Canaan (1998) found experimentally using PLIF imaging of NO formation in diesel engines, that no

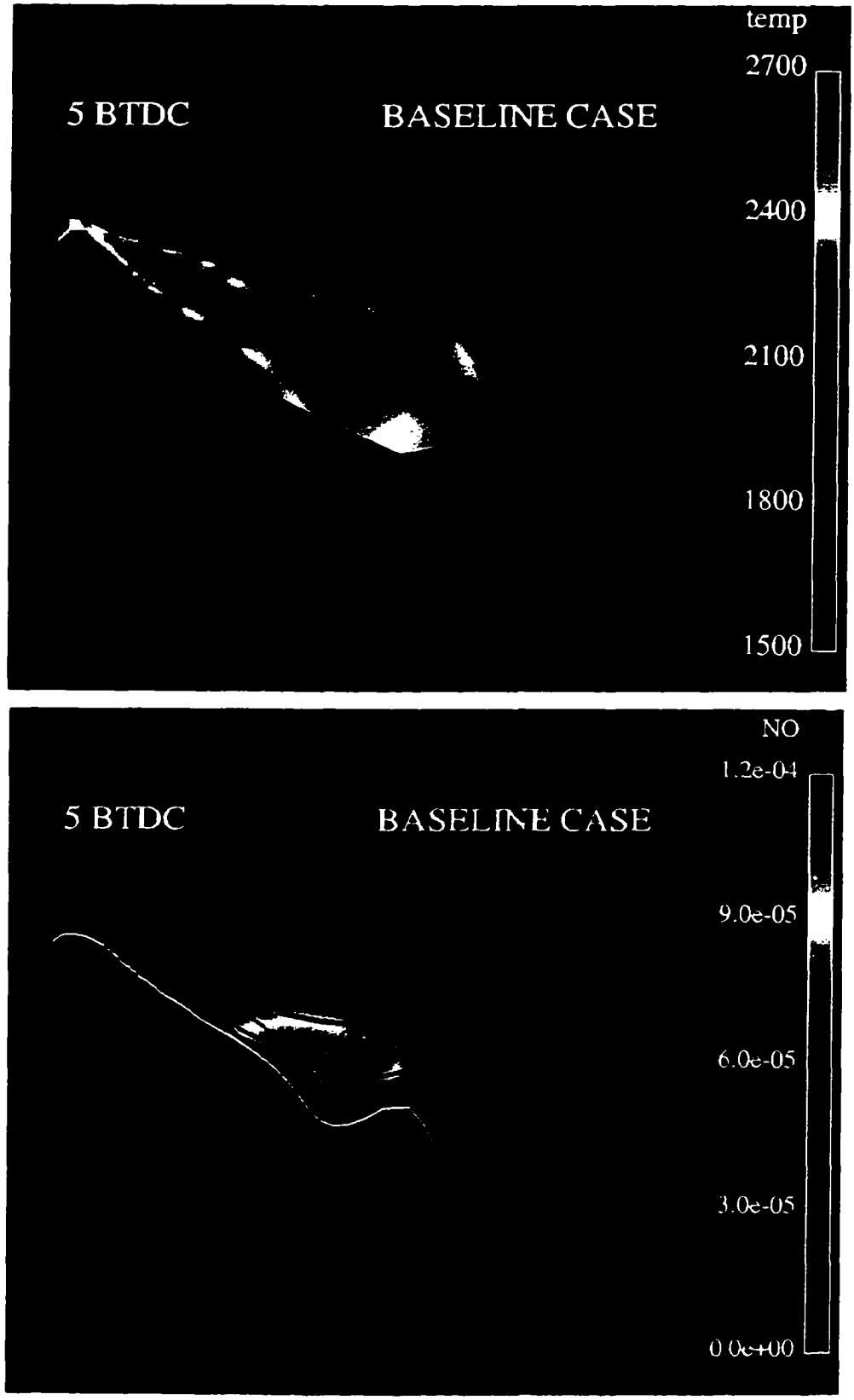

Figure 5.6: (a) Temperature (K) and (b) NO density (gm/cc) with superimposed ϕ contours, at 5° BTDC.

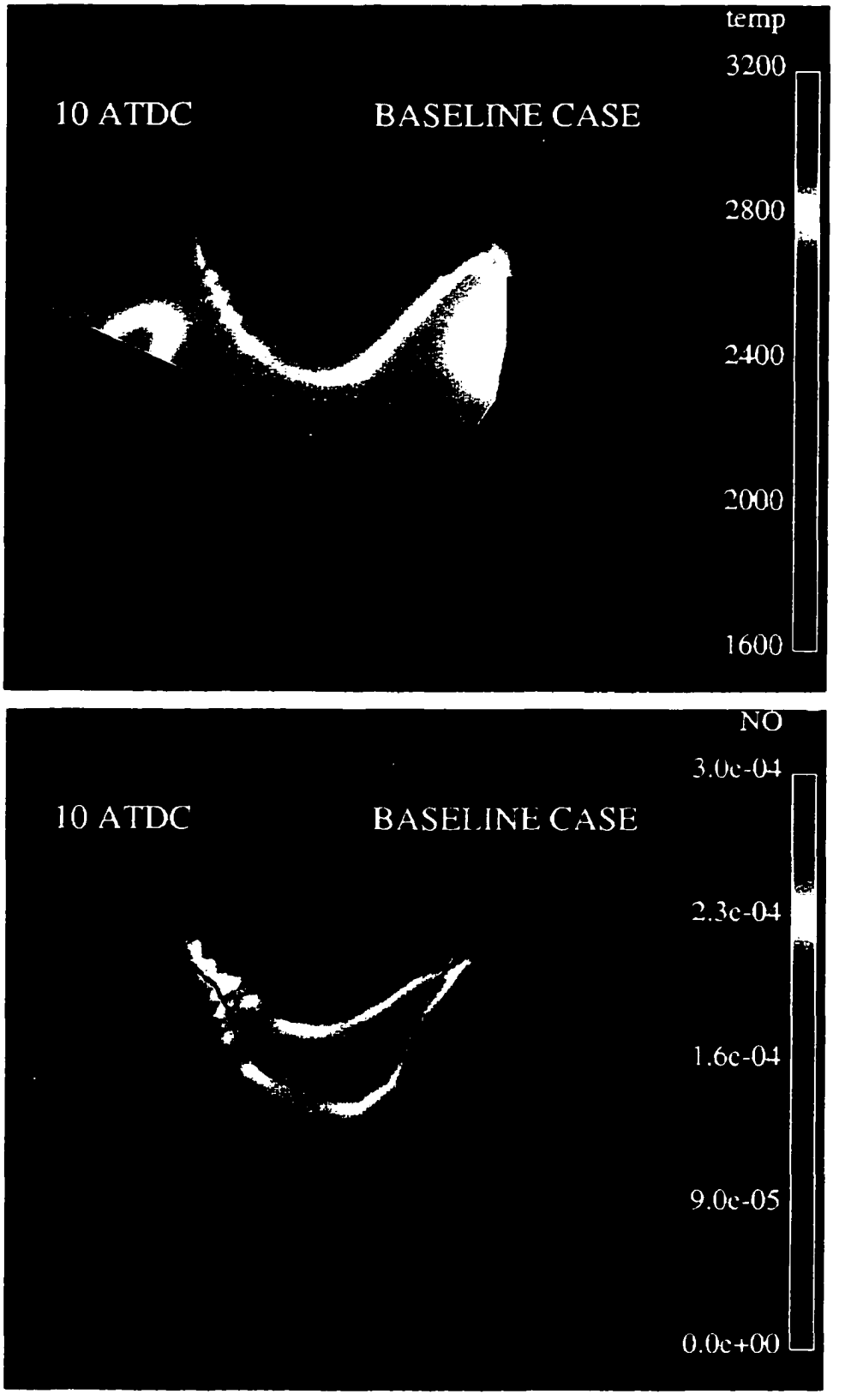

Figure 5.7: (a) Temperature (K) and (b) NO density (gm/cc) with superimposed ϕ contours, at 10° ATDC.

measurable NO was formed during the initial premixed burn and the first NO appeared in a thin layer around the fuel jet periphery just after the diffusion flame was established. In this work too, it is seen that the first NO is formed in the outer edges of the injected methane jet where the fuel-air mixture is slightly lean of stoichiometric.

Figure 5.7 shows temperature and NO densities at 10° ATDC when NO concentrations are at their peak. Fuel injection was stopped at 5° BTDC, so the intake generated jet structure has disappeared by now. Burned gas temperatures show values of 3200 K in the regions near the injector where some fuel may still be present. It can be seen that most of the combustion chamber, except the squish region on the outer edges, has been engulfed by the flame. Since most of the injected fuel has been consumed, only the dark blue ϕ contour line corresponding to a value of 0.1 can be seen across the combustion chamber. There are still pockets of richer fuel air mixtures present in the cylinder though (see Fig. 5.4 (b) also). Peak NO concentrations occur in regions that have temperatures in the range of 2500 K-3000 K. NO concentrations do not peak in the highest temperature regions, but in the regions where post-flame gases reside. This is due to the slow chemistry of NO formation. Dec and Canaan (1998) found that as much as 1/3 of all NO produced is formed in the hot post-combustion gases after combustion ends. They also found that NO is found throughout the portion of the combustion chamber where the reacting fuel jet had traveled. This picture is also seen in Fig. 5.7 (b).

Figure 5.8 shows the variation of methane mass fraction burned and its rate of burning, with crank angle. As described before, under the baseline operating conditions, it takes about 8° CA before the ignition delay is over. Till then the injected fuel and air have time to mix and by the time the ignition delay period is over, the rate of burning becomes quite high. The first peak in Fig. 5.8 (b) is reached when the transition from full kinetics to the EBU model occurs. After the transition, the burning rate drops slightly, but then continues to rise as the fuel injection process enhances turbulence and hence the rate of mixing. However, as the injection process continues, the in-cylinder turbulence is not able

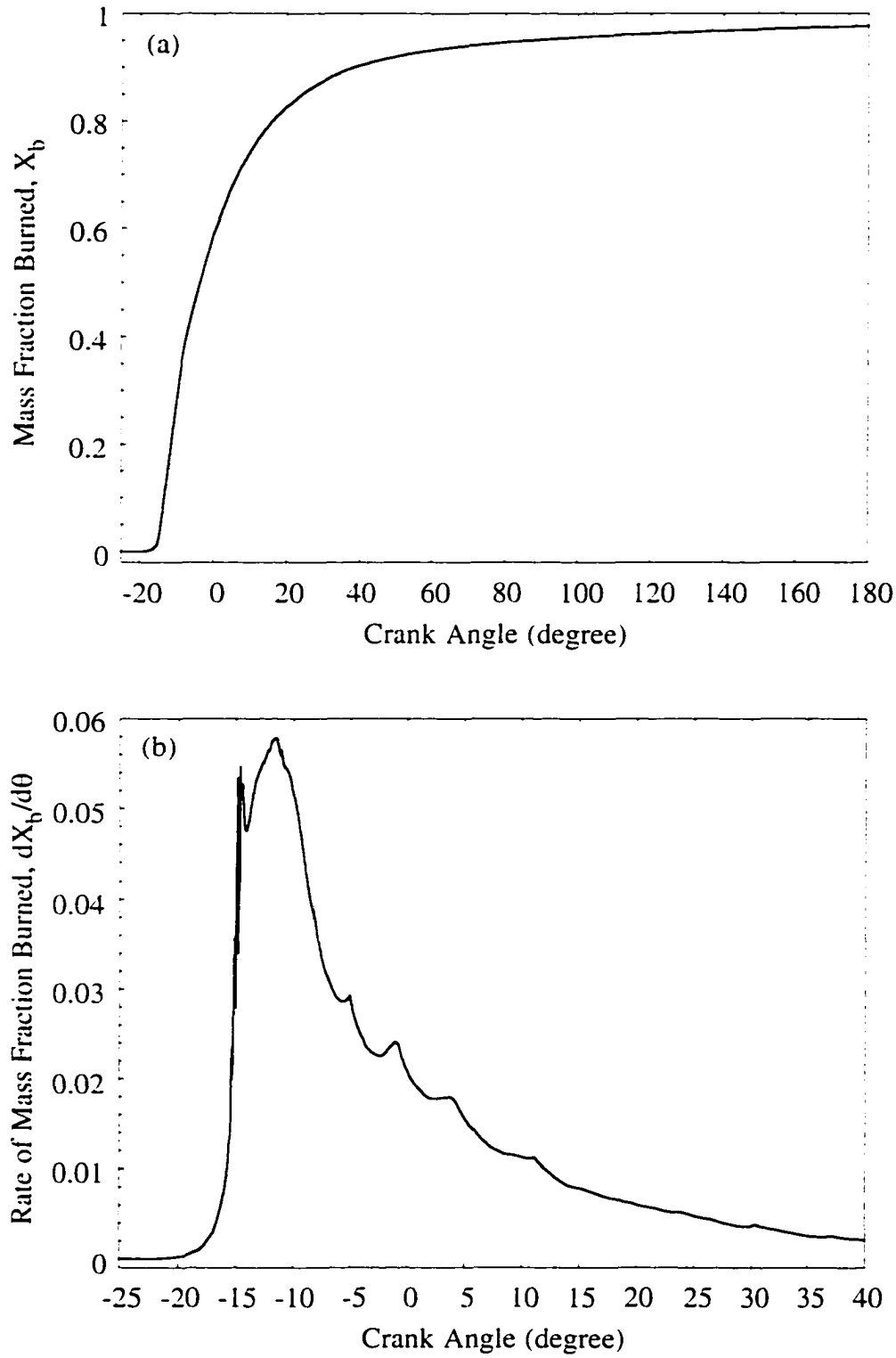

Figure 5.8: Variation of (a) methane mass fraction burned and (b) rate of mass fraction burned with crank angle for the baseline case.

to mix the fuel with air and so the burning rate starts falling. This trend continues after fuel injection ends at 5° BTDC. The mass fraction burned curve shown in Fig. 5.8 (a), shows the classical S shaped profile that is so characteristic of combustion in both diesel and spark-ignition engines. It can be seen that not all the injected fuel has burned by the time the calculation was terminated at 180° ATDC. One reason for the incomplete burning of the fuel is that the constants in the EBU model probably need to be increased during expansion when cylinder densities fall. More about this is said later. The unburned fuel is considered as unburned hydrocarbon emissions and is undesirable as methane is a greenhouse gas and along with CO_2 has been linked to global warming.

Results of the baseline case have shown that the ignition-combustion-pollutant formation prediction methodology used in this work provides physically meaningful results. In the next few sections, various engine operating parameters will be changed one by one and the results compared to the baseline case.

Effect of Engine Speed

The speed with which the crank shaft rotates can have a significant impact on engine performance and emissions. As the crank shaft spins faster, the ignition delay period changes as more crank angles are traversed in the same time. The changed delay period affects combustion and hence pressure rise and pollutant formation. Also, as the engine runs faster, in-cylinder turbulence increases since the flow past the intake valve scales with engine speed. At higher RPM, there is less time for heat transfer from the burned gases to the cylinder walls, resulting in higher exhaust temperatures. Since wall heat transfer was assumed to be zero in the present study, this factor does not affect the computational results. Figure 5.9 shows the variation of volume-averaged pressure with crank angles and cylinder volume, at three engine speeds. The medium speed corresponds to the baseline case and was discussed in the previous section. The injection timing was kept fixed for all the speeds at the baseline value of 25° BTDC (early injection). Full load

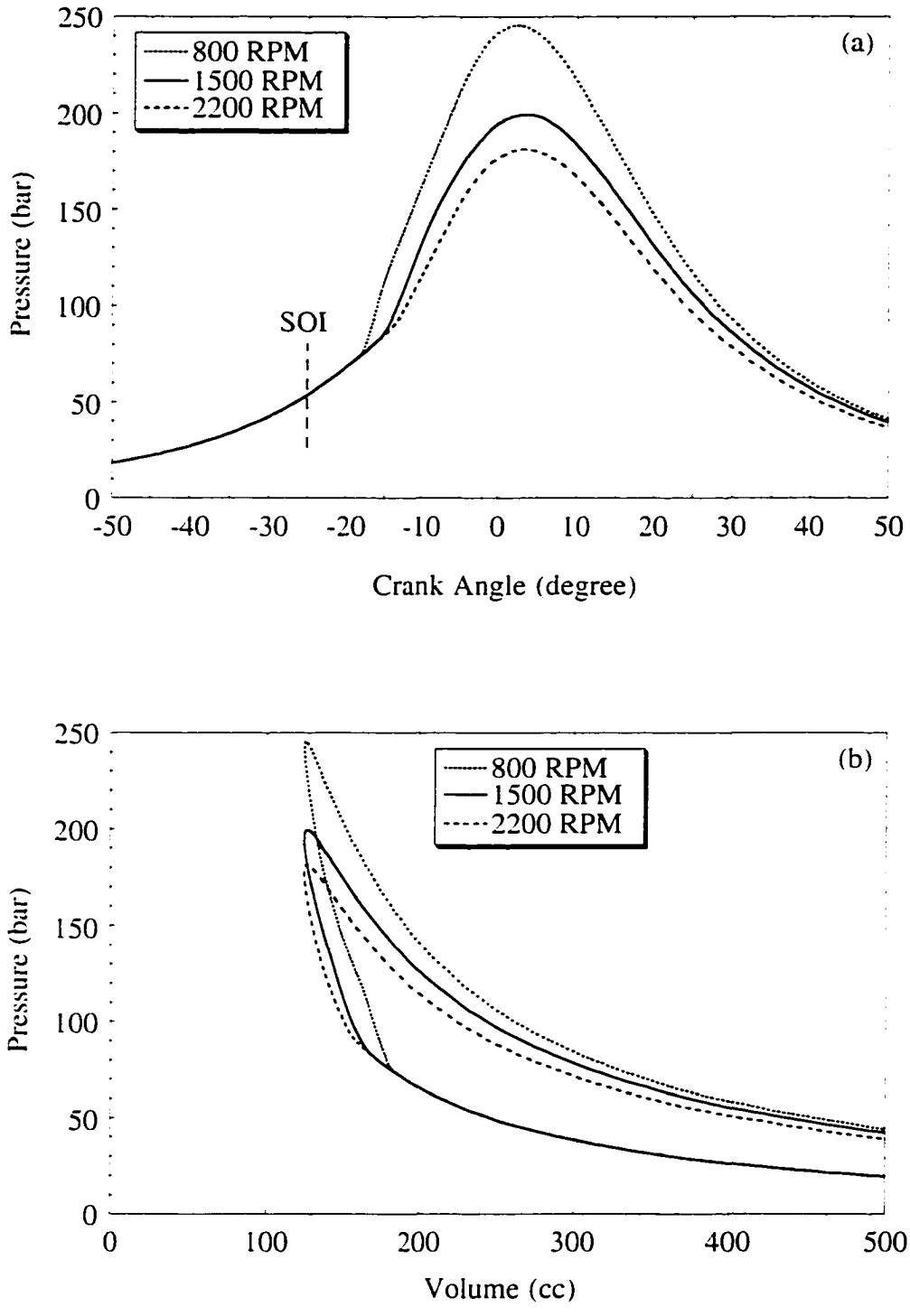

Figure 5.9: Variation of volume-averaged cylinder pressure with (a) crank angle and (b) cylinder volume at three different engine speeds.

engine operation was assumed with an intake pressure of 3 bar. It is seen that the pressure starts rising earlier for the slowest speed, followed by the medium and fastest speeds. Figure 5.9 (a) clearly shows that the ignition delay period is longest for the highest speed. However, the delay measured in seconds actually decreases with speed. This is because the piston moves up more per unit time with increasing speed, leading to an increase in pressure and temperature of air inside the cylinder, both of which decrease ignition delay. Table 5.4 shows the values of ignition delay measured both in crank angles and time for the three engine speeds examined.

Table 5.4
Variation of ignition delay with engine speed.

	Ignition Delay	
Speed (RPM)	Crank Angles (degree)	Time (ms)
800	7.3	1.521
1500	10.4	1.150
2200	12.3	0.934

As the ignition delay in crank angles increases, it takes longer for the fuel-air mixture to start burning, and consequentially the pressure rise is lower. The earlier the fuel-air mixture starts burning during the compression stroke, the higher the cylinder pressure gets as the heat release only aids the increase in pressure due to compression. Although this increases the compression work significantly (see Fig. 5.9 (b)) for the lower speed, the peak pressure is much higher than the other cases, so the expansion work is also higher. The net result is that the IMEP for the lowest speed is the highest. Table 5.5 shows the values of IMEP and typical pollutants concentrations at 150° ATDC.

Figure 5.9 (b) also confirms that the IMEP for the slowest speed is the highest. However, NO concentrations are also the highest for the slowest speed. Is high performance at low speeds really needed with so much penalty in terms of NO emissions ? Probably not ! Engines idle at low speeds when there is hardly any load on them. This

points out to the need of retarding fuel injection timing at lower speeds. More about the effect of speed on emissions is said later. The peak pressure trends observed here using multi-dimensional modeling were also confirmed using a quasi-dimensional diesel engine simulation (Assanis and Heywood, 1986).

Table 5.5
Effect of speed on engine performance and exhaust emissions.

Speed (RPM)	IMEP (bar)	NO (ppm)	UHC (ppm)	CO_2 (ppm)
800	17.22	4789	1.88×10^{-4}	66780
1500	15.83	3382	1692	65222
2200	13.76	2144	6942	59799

Figures 5.10 (a) and (b) show the variation of mass fraction of fuel burned and its rate of burning, respectively with crank angle. As discussed before, for the slowest speed, the ignition delay period gets over sooner and aided by the turbulence generated by the fuel injection process (which is terminated at 5° BTDC for all three speeds), almost all the injected fuel gets burned by 20° ATDC. But for the higher speeds, burning continues late into expansion as not much time is available to consume the fuel by the end of the calculation (180° ATDC). It is seen that, as the speed increases, the fraction of unburned fuel also increases leading to increasing UHC emissions shown in Table 5.5.

Measured in crank angles, the rate of burning is the highest for the slowest speed during the kinetics controlled phase (the first peak Fig. 5.10 (b)). This is not surprising if one looks at the relationship between the rate of burning expressed in crank angles with the rate of burning expressed in time:

$$\frac{dX_b}{d\theta} = \frac{dX_b}{dt}\frac{dt}{d\theta} = \frac{dX_b}{dt}\frac{1}{6N} \tag{5.3}$$

where N is the engine speed measured in rpm. As shown in Fig. 5.11 (b), the value of dX_b/dt is relatively independent of engine speed during the "premixed burn" phase.

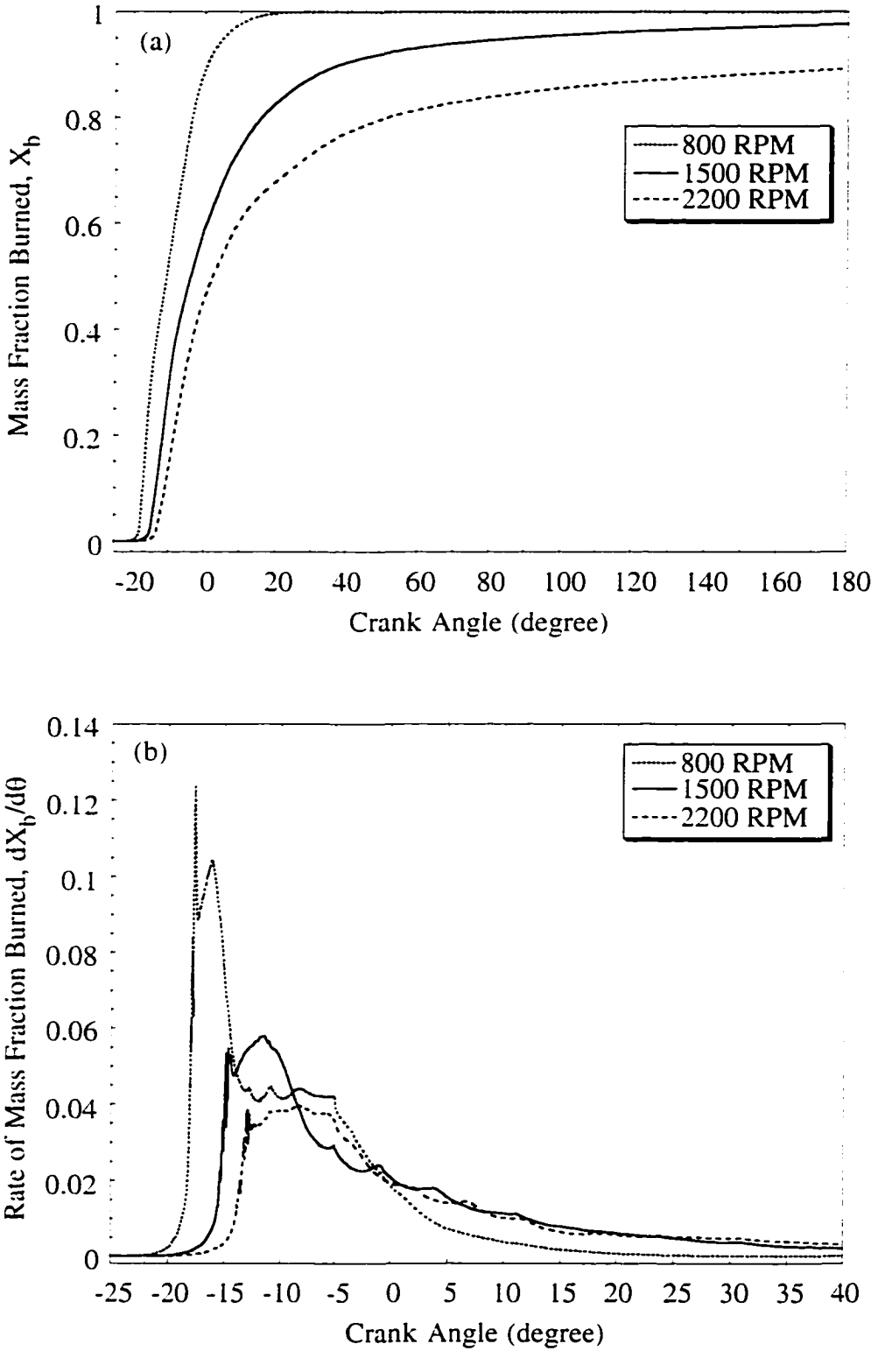

Figure 5.10: Variation of (a) mass fraction of fuel burned and (b) rate of mass fraction of fuel burned with crank angle at three different engine speeds.

Thus, $dX_b/d\theta$ is inversely proportional to engine speed, leading to the highest value for the slowest speed.

Figures 5.11 (a) and (b) show the temporal variation of mass fraction of fuel burned and its rate of burning (expressed in time units), respectively. It is seen that as the engine speed increases, the delay period decreases, and initially the rate of burning is highest for the highest speed. However, during the latter stages of the burning process, the mass fraction burned profiles switch positions and the burning rate of the lowest speed attains the maximum value. These apparent contradictions can be explained by looking at the piston position for each of the three speeds as a function of time, as shown in Table 5.6.

Table 5.6
Piston position (in crank angle degrees) as a function of time for different engine speeds. (TDC position is referenced to as 0° CA)

Speed (RPM)	1 ms	2 ms	3 ms	4 ms	5 ms
800	-20.2	-15.4	-10.6	-5.8	-1.0
1500	-16.0	-7.0	2.0	11.1	20.0
2200	-11.8	1.5	14.5	28.0	41.0

By 1 ms into the injection process, the piston only moves up to 20.2° BTDC at 800 RPM. The ignition delay period is yet not over and so the rate of burning is very small (see Fig. 5.11 (b)). However, at 2200 RPM, the piston moves up to 11.8° BTDC in 1 ms. This is the time just after the delay period is over, and the rate of burning attains its first peak. By 2 ms, the piston has moved up to 15.4° BTDC at 800 RPM. This is the time at which the second peak in the mass fraction burned plot is seen at this speed. As discussed in the previous section, the second peak is due to the increased turbulence due to fuel injection. However, at 2200 RPM, fuel injection has already ended by 2 ms as the piston has moved up to 1.5° ATDC. The mass burning rate is correspondingly lower than the two lower speeds, where mixing rates due to injection generated turbulence are still high. By 5 ms, the piston has only moved up to 1° BTDC at 800 RPM, whereas it

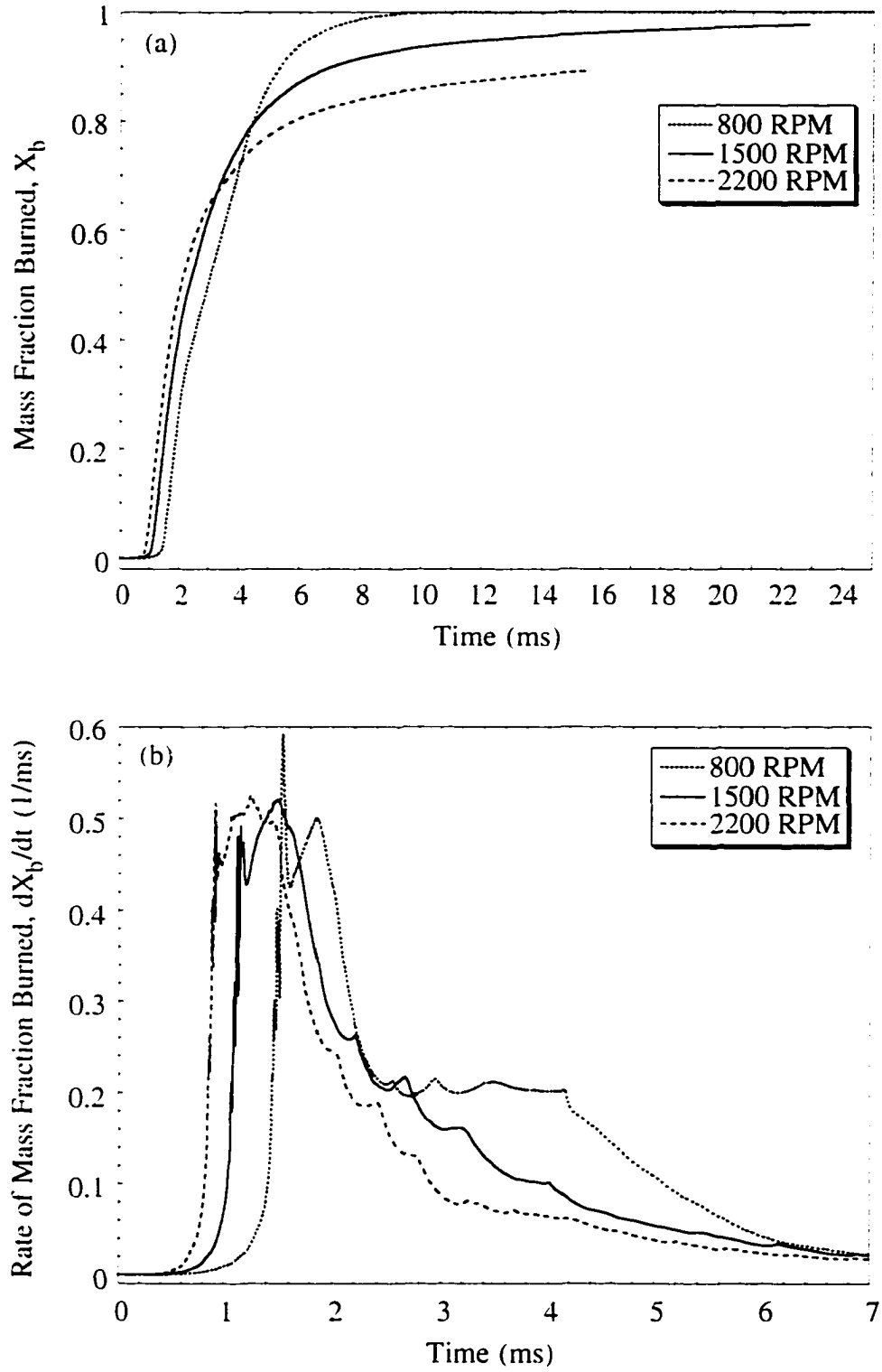

Figure 5.11: Variation of (a) mass fraction of fuel burned and (b) rate of mass fraction of fuel burned with time at three different engine speeds.

has moved down to 41° ATDC at 2200 RPM. Since the burning rates are higher for the slowest speed from 2 ms to 5 ms, the mass fraction burned profiles show a crossing-over with the fuel getting consumed almost completely at the lowest speed by about 10 ms.

The effect of speed on engine turbulence can be seen more clearly in Figs. 5.12 (a) and (b). These figures show the variation of mass-averaged turbulence intensity (u') with crank angle and time, respectively. The initial turbulence intensity is highest at 2200 RPM as the turbulence levels at the start of the calculation were scaled with engine speed. During the compression stroke, turbulence decays due to viscous dissipation. When fuel injection starts at 25° BTDC, there is a rapid increase in u' at all the three speeds. The turbulence intensity continues to increase till the duration of fuel injection, and then starts decaying after fuel injection ends. It is interesting to observe that the peak value of u' at 800 RPM is almost the same as the peak value of u' at 1500 RPM, although u' at the time of fuel injection at 800 RPM is much lower (see Fig. 5.12 (a)). This can be explained by looking at Fig. 5.12 (b). At lower engine speeds, the fuel injection duration in real time is actually longer since the injection duration in crank angles was kept fixed for the calculations. This leads to a greater increase in turbulence levels, as the injection velocity was kept fixed while changing the fuel density to modify the injection rates.

During the injection process, a kink in the turbulence values is observed in both figures. This is due to a change in turbulence values due to combustion. Since these calculations were done in the closed part of the cycle, by prescribing uniform turbulence intensity through out the cylinder, the effect of intake generated turbulence structures was not taken into account. If the intake process is also modeled, it has been shown that the turbulence does not decay as rapidly as it does when the intake process is not modeled (Kong and Hong, 1997). However, in DING engines, this may not be a major issue as it is the injected fuel jet that generates its own turbulence and plays a major role in affecting the fuel-air mixing process.

Figure 5.13 (a) shows the variation of mass-averaged temperature with crank angle. As expected, the temperature at the slowest speed attains the highest value. This is

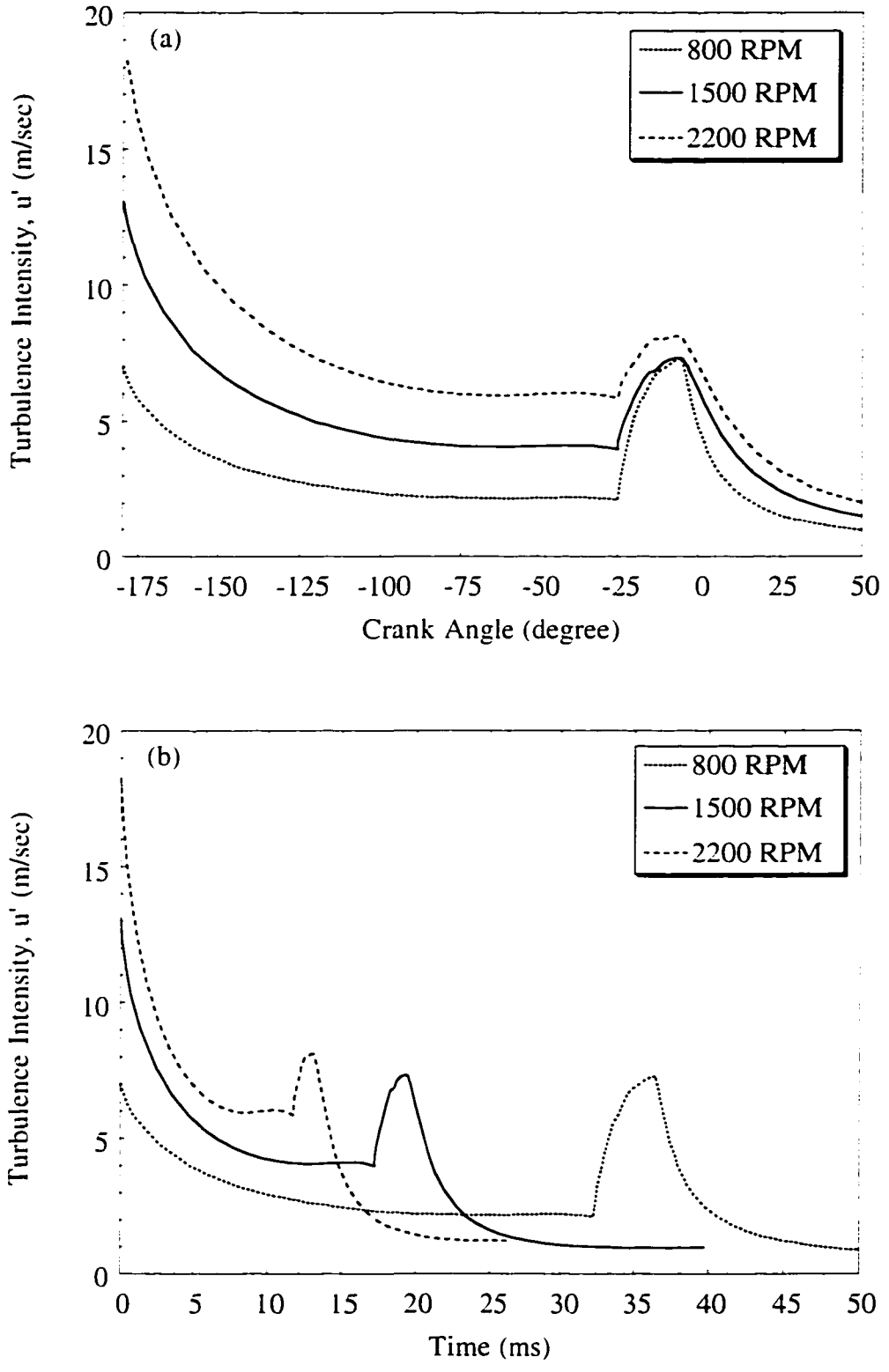

Figure 5.12: Variation of mass-averaged turbulence intensity with (a) crank angle and (b) time at three different engine speeds.

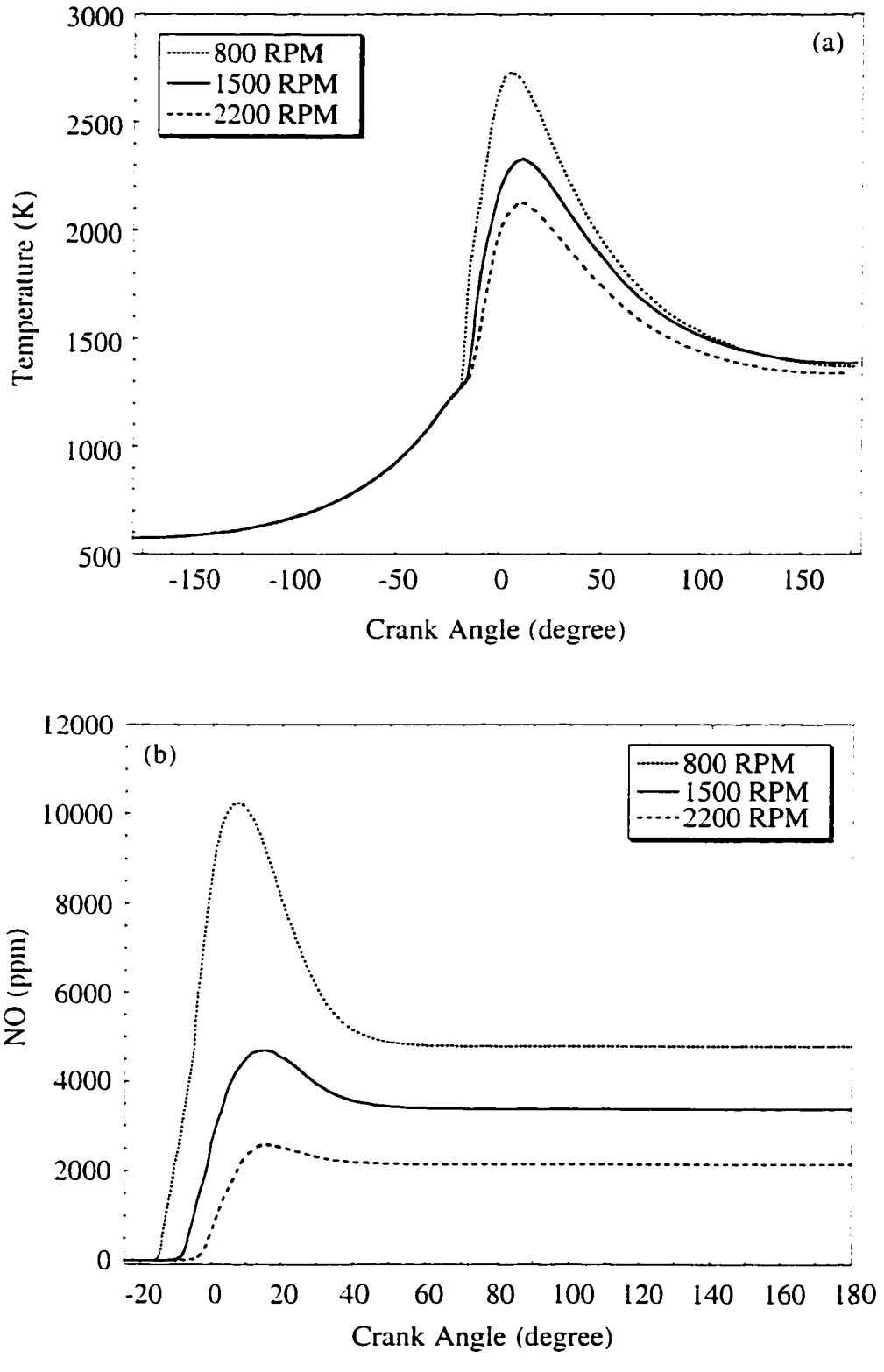

Figure 5.13: Variation of (a) mass-averaged temperature and (b) NO with crank angle at three different engine speeds.

because the fuel-air mixture starts burning earlier and is compressed to even greater temperatures towards the end of the compression stroke. It should be kept in mind that if heat transfer from the hot gases to the cylinder walls was also modeled, the temperature profiles would be different since more time is available at low speeds for heat transfer to occur. Late into expansion, the average temperature at 800 RPM falls below that of 1500 RPM, as all the fuel in the cylinder was consumed much earlier at the slower speed, leading to a steady drop in temperature during expansion and concurrent mixing with cooler ambient air. However, burning continues late into expansion at the higher speeds, so the temperatures are correspondingly high.

Figure 5.13 (b) shows the variation of NO in ppm as a function of crank angle at the three speeds examined here. Due to early burning, more compression and resulting higher temperatures, NO concentrations peak at a much higher value at 800 RPM than the higher engine speeds. Another factor that aids more NO formation at lower speeds is the ample availability of time for the slow NO formation process. It can be seen that peak NO forms between 10 and 15° ATDC when the cylinder temperatures are also at their highest values (see Fig. 5.13 (a)). There is much more decomposition of NO at 800 RPM compared to the higher speeds, as the temperatures are much higher for this case. The excessively high values of NO are a pointer to the fact that early injection at low speeds is probably not a good idea. Heywood (1988) has observed that engine speed does not affect the shape of the NO vs. crank angle curve, as seen here.

Figures 5.14 (a) and (b) show the variation of NO density (gm/cc) at 800 and 2200 RPM, respectively at a crank angle of 10° ATDC in a plane cut through the center of the computational domain. The values of fuel-air equivalence ratio are also superimposed on these plots. The coloring scheme for the ϕ countours is the same as before: red (5.0), yellow (2.0), green (1.0), light blue (0.5), and dark blue (0.1). For 1500 RPM, the reader is referred to Fig. 5.7 (b). The huge difference in NO ppm shown in Fig. 5.13 (b) at different speeds can be easily explained by looking at its distribution in the combustion chamber. At 800 RPM, the burned gases are at a relatively high temperature for a longer

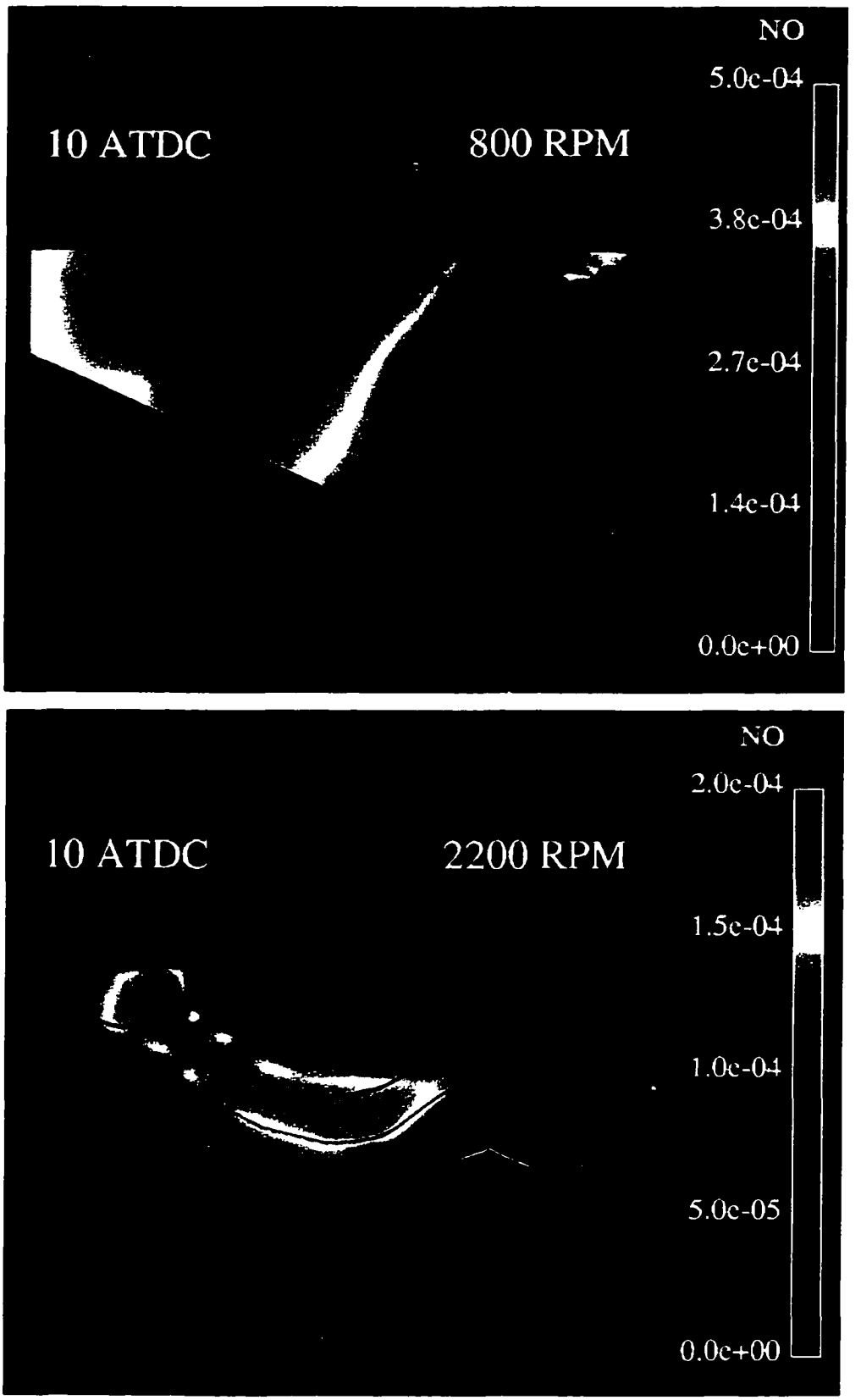

Figure 5.14: NO density (gm/cc) with superimposed ϕ contours at 10° ATDC at (a) 800 RPM and (b) 2200 RPM.

duration. Also, most of the cylinder is filled with hot burned gases as the injected fuel has already burned by this time. Both these factors lead to high NO concentrations that are spread in most of the cylinder. The appearance of only one dark blue contour of ϕ in Fig. 5.14 (a) testifies to the fact the there is virtually no unburned fuel left in the cylinder by 10° ATDC.

Looking at Fig. 5.14 (b), it can be seen that not only are peak NO concentrations confined to the center of the domain, but their values are also much lower than 800 RPM. Both these factors lead to lower NO ppm at 2200 RPM. The values at 1500 RPM are in-between those at 800 and 2200 RPM, as can be seen by comparing Fig. 5.14 with Fig. 5.7 (b). The appearance of yellow contours of ϕ in Fig. 5.14 (b) show that there are still fuel-rich pockets in the cylinder. Similar to the 1500 RPM case, peak NO occurs in fuel-air mixtures that are leaner than stoichiometric, confirming previous theoretical and experimental investigations (Heywood, 1988; Dec and Canaan, 1998).

Effect of Engine Load

Load in direct-injection engines is controlled by the amount of fuel injected into the combustion chamber. The maximum amount of fuel that can be injected in diesel engines is limited by smoke production and is usually less than an overall fuel-air equivalence ratio of 0.7. In this study, two different values of overall ϕ were chosen: 0.6, corresponding to high load operation, and 0.2, corresponding to low load operation. The engine speed was kept fixed at 1500 RPM and the fuel was injected at 25° BTDC. The high load operation corresponds to the baseline case discussed earlier. Overall ϕ is based on the total amount of fuel injected and the amount of air inside the cylinder at the start of the calculation. It should be pointed out that the mass of injected fuel was changed by changing the density of the fuel (pure methane), while keeping the injection duration constant at 20° CA. In actual diesel engine operation, the mass of injected fuel is changed

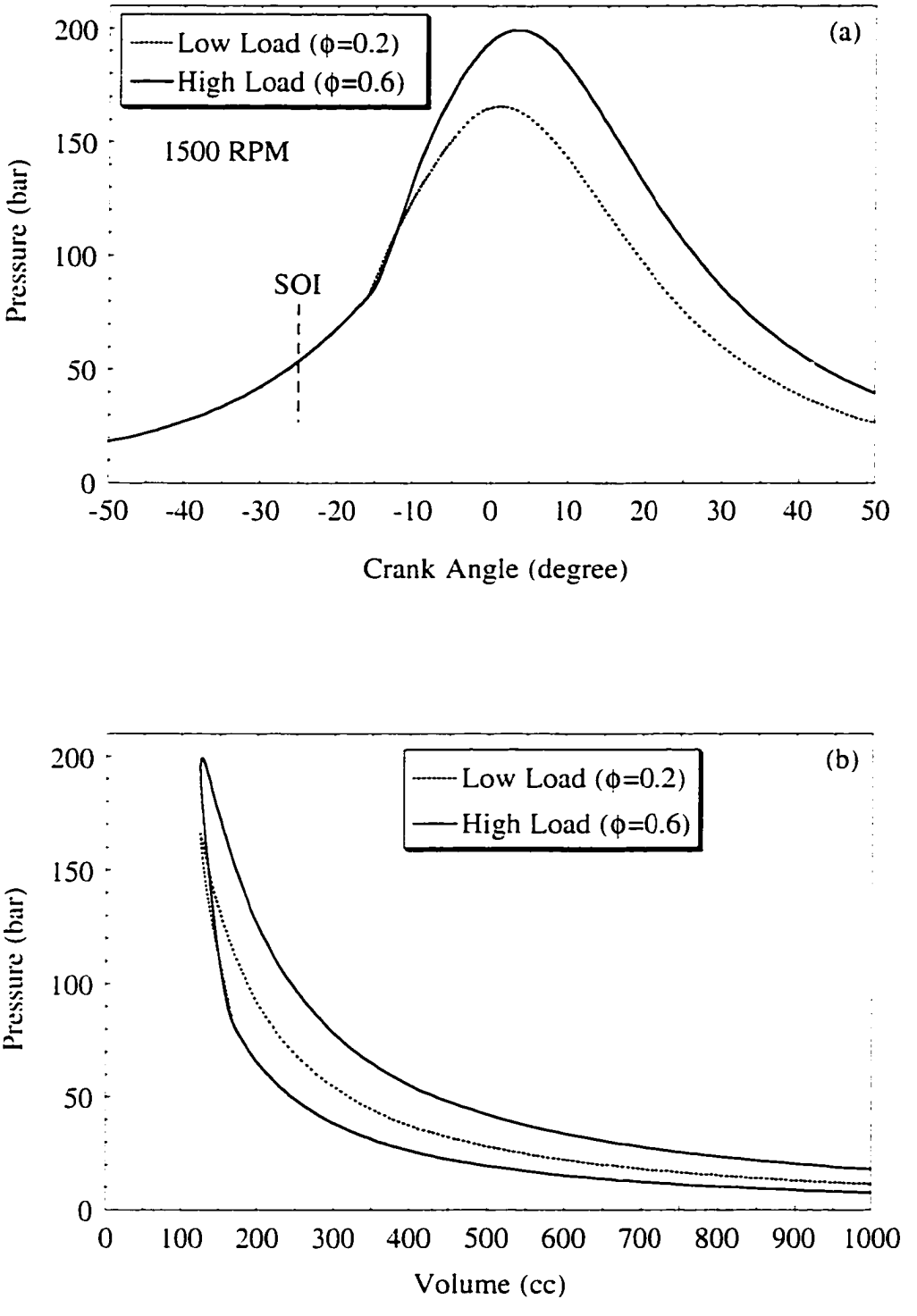

Figure 5.15: Variation of volume-averaged cylinder pressure with (a) crank angle and (b) cylinder volume for two loads.

by changing the *duration* of injection, so injection timing is usually advanced as load increases.

Figures 5.15 (a) and (b) show the variation of volume-averaged pressure with crank angle and cylinder volume, respectively at 1500 RPM for the two loads examined here. The compression pressure is the same for both cases, as the level of boost pressure was kept the same at 3 bar. At low load, the peak cylinder pressure increases above the motoring value of 122 bar (see Fig. 5.2 (a)), by 43 bars. At high load, it increases by 77 bars. The reasons why the peak pressure does not scale with the amount of injected fuel are two fold: firstly, the delay period increases slightly as more fuel is injected (10.4° CA compared to 9.2° CA for the low load case), owing to cooling of fuel-air mixture as more colder fuel is injected into the cylinder, and secondly, not all the injected fuel at high load is consumed due to reasons explained for the baseline case. It should be noted that ignition delay in a diesel engine also increases with load during engine starting conditions, but it decreases for an engine running at steady state as the residual gas temperature and wall temperature increase with load. This results in higher charge temperature at the time of injection, leading to a shortening of the ignition delay period (Heywood, 1988). In these calculations everything else was kept fixed at the baseline values, except for load, hence the effect of actual steady state conditions is not seen.

Although the peak pressures for the high load case are not three-fold compared to the low load case, cylinder pressures during expansion for the high load case are much higher, leading to a much higher IMEP. Table 5.7 summarizes the performance and emissions of the DI engine as the load is changed.

Table 5.7
Effect of load on engine performance and exhaust emissions.

Load (ϕ)	IMEP (bar)	NO (ppm)	UHC (ppm)	CO_2 (ppm)
0.2	6.046	3110	33.1	29576
0.6	15.83	3382	1692	65222

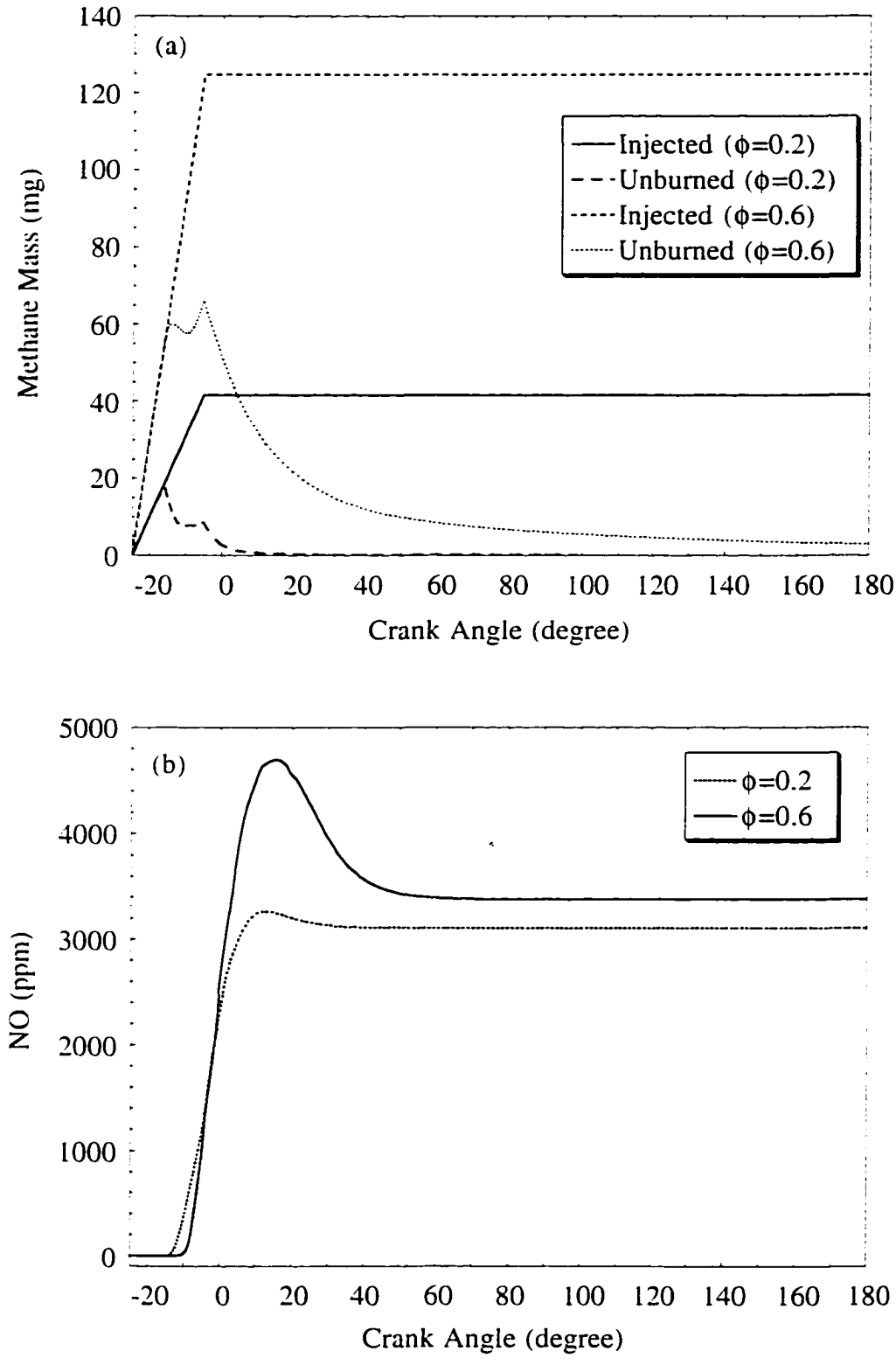

Figure 5.16: Variation of (a) injected and unburned methane mass in the cylinder and (b) NO with crank angle at two different engine loads.

Exhaust emissions show interesting trends with increasing load. NO increases only slightly, UHC emissions increase dramatically and CO_2 values increase by slightly more than two times. Figure 5.16 (a) shows the variation of mass of injected and unburned methane in the cylinder as a function of crank angle. The injected methane profiles show that the amount of fuel injected at high load is three times that of the low load case. The injected methane starts getting consumed earlier for the low load case, as evidenced by the departure of the unburned methane plot from the injected fuel line. Also, for the low load case, the fuel gets consumed almost entirely by about 20° ATDC, whereas for the high load case some unburned fuel remains at 150° ATDC, leading to an increase in the UHC concentrations shown in Table 5.7.

The amount of CO_2 produced is directly proportional to the amount of fuel burned due to the single-step mixing controlled combustion model used in the present study. This leads to its value being around 2.2 times for the high load case as compared to the low load case.

Figure 5.16 (b) shows the variation of NO concentration with crank angle for the two loads examined. It can be seen that due to non-uniform fuel distribution in a direct injection engine, even low load cases can produce significant NO. Since burning starts earlier at low load, initial NO concentrations are higher, but soon the high load NO values surpass those of low load, but not by much. High load NO concentrations eventually freeze out at values that are about 9% higher than the low load case. This is very different from NO formation in spark-ignition engines where its values fall much more rapidly with decreasing equivalence ratio (Heywood, 1988).

Effect of Injection Timing

As pointed out while discussing the effects of engine speed, injection timing needs to be changed with engine operating conditions. Modern engines are designed to achieve the best possible brake specific fuel consumption (bsfc) while keeping emissions low

enough to satisfy the constraints put by emission standards. Changing injection timing is an effective method to regulate IMEP and pollutant concentrations.

To study the effect of injection timing on performance and emissions, the baseline case was compared to a case in which everything else was kept fixed at the baseline values except the injection timing, which was retarded to 10° BTDC. Hence, injection was assumed to occur from 10° BTDC to 10° ATDC. Figures 5.17 (a) and (b) show the variation of volume-averaged pressure with crank angle and cylinder volume, respectively for the two injection timings studied here. It can be seen that peak pressure for retarded timing is much lower, as is to be expected. Although the ignition delay period for retarded timing is much smaller than that for early injection timing (3.12° CA compared to 10.4° CA for early injection), most of the burning occurs after TDC, and hence cylinder pressures are much lower. The ignition delay decreases as injection timing is retarded due to an increase in cylinder pressure and temperature as the piston moves closer to TDC. The work during compression is much lower for retarded timing (see Fig. 5.17 (b)), but the expansion work is also lower as expansion pressures are much lower. This leads to a lower IMEP for the retarded injection timing case. Table 5.8 summarizes the performance and emission characteristics as the injection timing is changed.

Table 5.8
Effect of injection timing on engine performance and exhaust emissions.

Injection Timing (° BTDC)	IMEP (bar)	NO (ppm)	UHC (ppm)	CO_2 (ppm)
25	15.83	3382	1692	65222
10	9.418	829	21816	45397

As can be seen from Table 5.8, retarding injection timing can be a very effective method to reduce NO emissions. However, the UHC emissions increase as a significant portion of the fuel remains unburned. This is seen in Fig. 5.18 which shows the variation of mass fraction of fuel burned with crank angle. When fuel is injected late, only 60% of

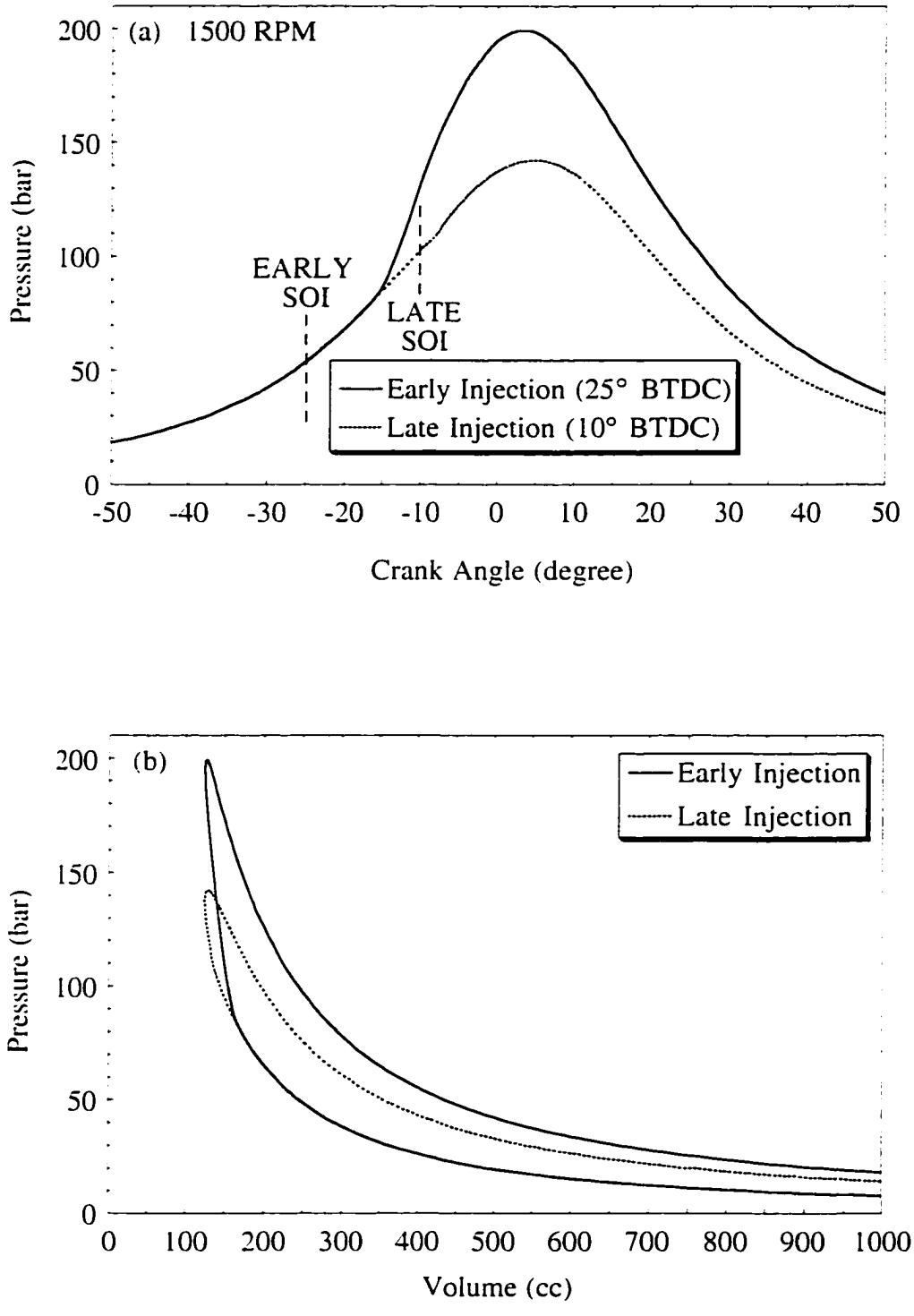

Figure 5.17: Variation of volume-averaged cylinder pressure with (a) crank angle and (b) cylinder volume for two injection timings.

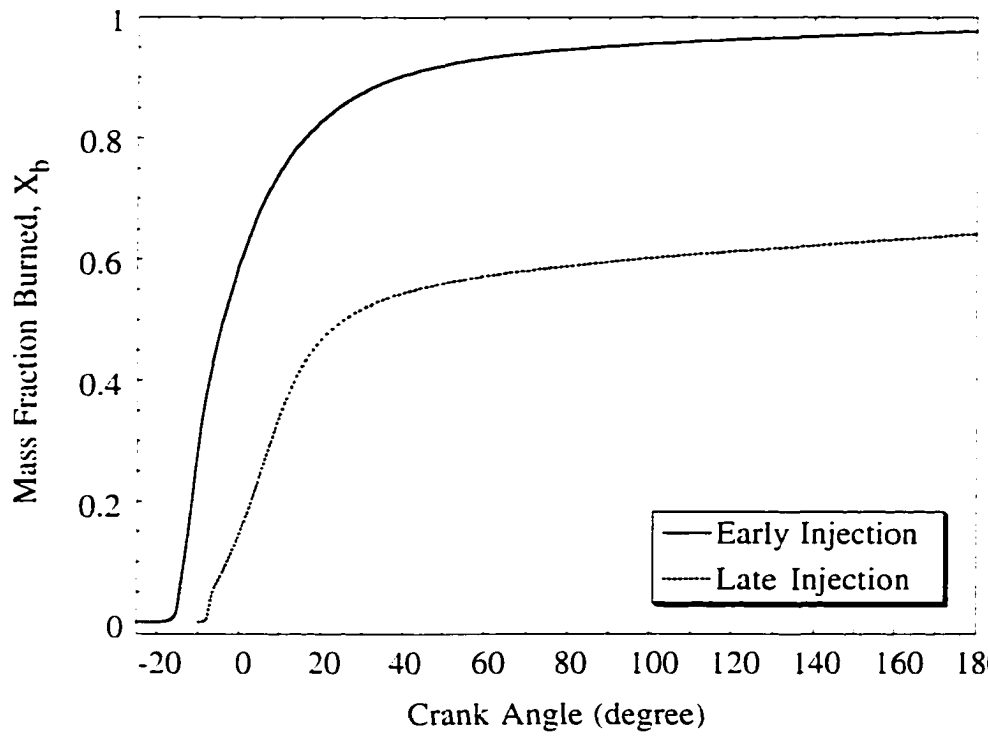

Figure 5.18: Variation of mass fraction of fuel burned with crank angle for two different injection timings.

it is burned by the end of the calculation. This is not only due to decreased turbulence levels during the expansion stroke when most of the burning takes place, but also due to a feature of the EBU model itself.

In the EBU model of mixing controlled combustion, it is assumed that the rate of burning of the fuel is proportional to the local mean concentration of the fuel, oxidizer or combustion products, expressed in mass units (see Eqs. 4.4-4.6). During expansion, the local mean densities of the reactants and products decrease as the cylinder volume increases. This directly decreases the rate of burning. Both reduced turbulence levels and reduced species densities lead to a decrease in mass of fuel burned for the late injection case. Figure 5.18 clearly shows that for the late injection case, the rate of burning becomes almost insignificant after 30° CA. Experimental data are needed to confirm whether the EBU model constants need to be changed for the late injection case.

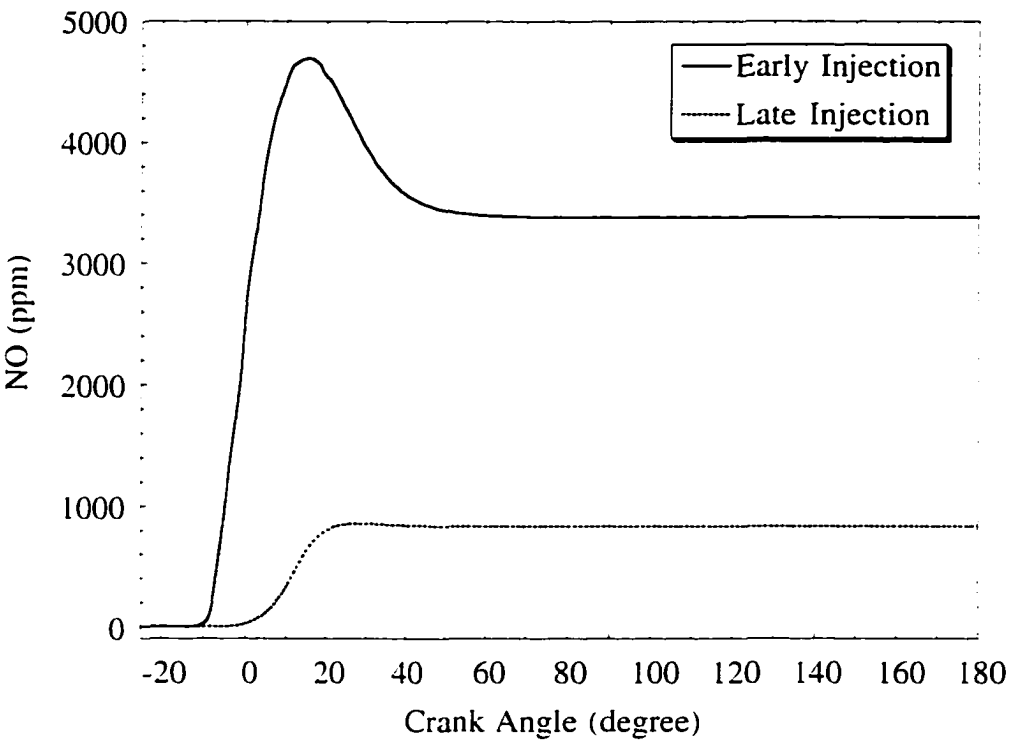

Figure 5.19: Variation of NO with crank angle for two different injection timings.

Figure 5.19 shows the variation of NO concentration with crank angle for early and late injection timings. It is apparent that as the fuel is injected later (timing is retarded), the peak temperatures and pressures are lower, so much less NO forms. There is virtually no dissociation of NO as the temperature of the burned gases is not high enough. As noted before, retarded injection is commonly used to help control NO emissions. The penalty in terms of IMEP is pretty modest compared to the substantial reductions in NO levels.

Figure 5.20 shows the variation of NO density (in gm/cc) at 20° ATDC, in a plane cut through the center of the computational domain. NO concentrations peak at around this time for the late injection case (see Fig. 5.19). It can be seen that the values of maximum local NO densities are five times lower than those of the baseline case (see Fig. 5.7 (b)). As seen previously, NO peaks in regions lean of stoichiometric. The ϕ contours have the same coloring scheme and values as before. Most of the NO is concentrated in

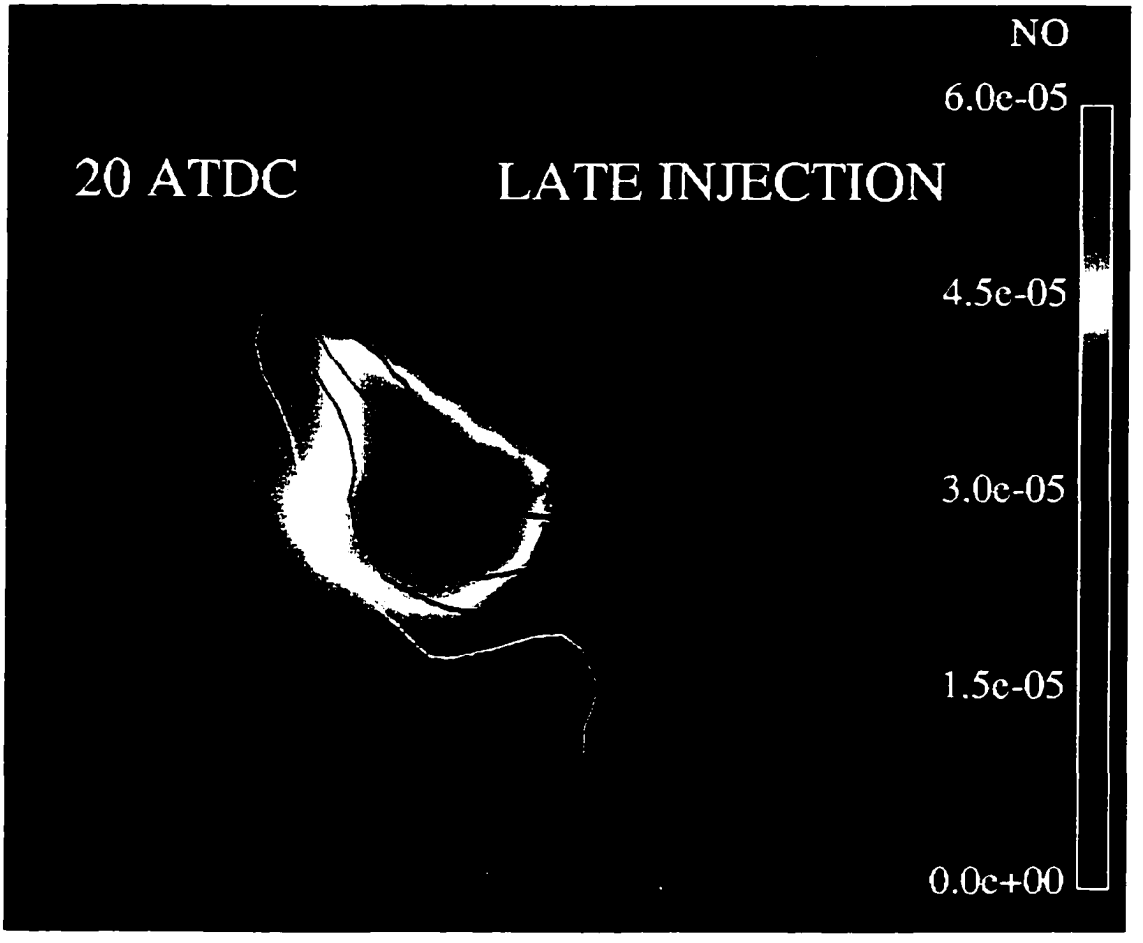

Figure 5.20: Variation of NO density (gm/cc) at 20° ATDC for the late injection case, with superimposed ϕ contours .

the outer edges of the flame. The blue regions in Fig. 5.20 correspond to fresh charge that has still not mixed with the injected fuel. This shows that significant portions of the combustion chamber have yet to burn, even 30° after fuel injection started.

Effect of the Level of Boost

Turbocharged engine operation is an effective method to increase engine power output. In fact most medium heavy-duty diesel engines are turbocharged. As the intake air pressure is raised, unless engine design and operating conditions are changed, maximum pressures and thermal loading increase almost in proportion (Heywood, 1988). So the

level of boost is limited by stress levels in critical mechanical components, as they limit the maximum cylinder pressure that can be tolerated under continuous engine operation.

The effect of intake air pressure on engine performance and emissions was studied by increasing the boost from 3 bar (baseline value) to 4 bar. The mass flow rate of the fuel was correspondingly changed to keep an overall equivalence ratio of 0.6. The engine speed was kept fixed at 1500 RPM. Figures 5.21 (a) and (b) show the variation of volume-averaged pressure with crank angle and cylinder volume, respectively at two different levels of boost. The ignition delay decreases slightly for 4 bar boost (9.5° CA compared to 10.4° CA for 3 bar boost), as the pressure increases during compression due to higher value of intake air pressure. The peak pressure reached for 4 bar boost (266 bar) is 4/3 times that of the peak pressure of the 3 bar boost (199 bar). This shows that peak pressures vary proportionally with the level of boost, if engine operating parameters are not changed. The increased boost obviously results in a higher IMEP. This can be clearly seen by comparing the area under the P-V diagram in Fig. 5.21 (b). Table 5.9 shows the values of IMEP and exhaust emissions (at 150° ATDC) with changing level of boost.

Table 5.9
Effect of level of boost on engine performance and exhaust emissions.

Intake Pressure (bar)	IMEP (bar)	NO (ppm)	UHC (ppm)	CO_2 (ppm)
3	15.83	3382	1692	65222
4	21.04	3463	1670	65335

The ratio of IMEP for 4 bar intake pressure to 3 bar intake pressure is 1.329, almost the same as the ratio of the intake pressures themselves. This is to be expected as the peak pressures are in the same ratio and more importantly, they occur at almost the same crank angle position (3.5° ATDC). It should be noted that even a small change in the crank angle position of peak pressure can have a significant impact on IMEP, as it changes the relative position of the peak pressure on the P-V diagram. Combining these

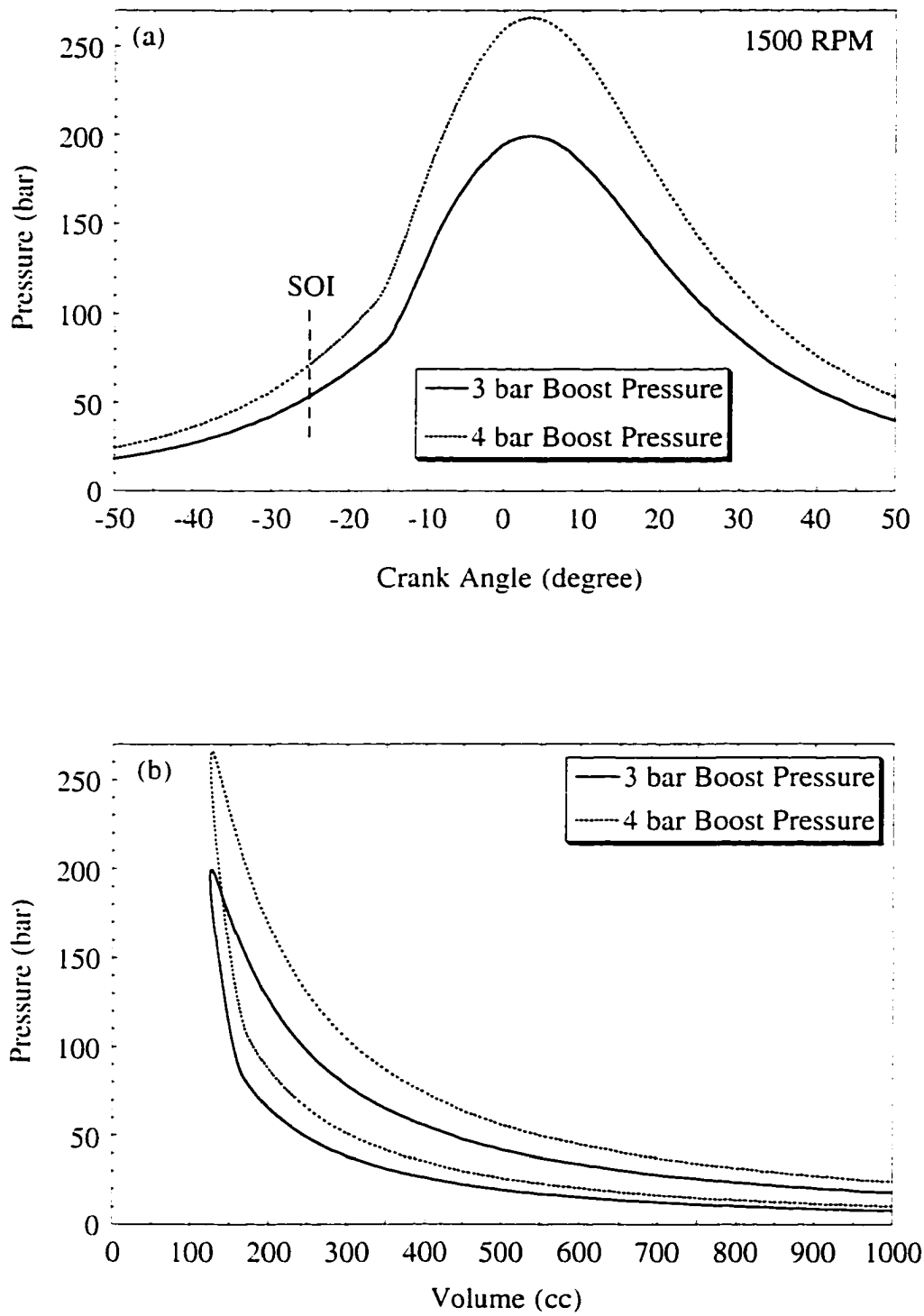

Figure 5.21: Variation of volume-averaged cylinder pressure with (a) crank angle and (b) cylinder volume for two levels of boost.

observations with those of the previous section, it can be seen that using increased boost with retarded timing can be an effective method to reduce NO emissions, while keeping desired levels of performance.

Table 5.9 also shows that normalized engine emissions (in ppm) are hardly affected by the level of boost, if the operating parameters are not changed. This is not surprising as the UHC and CO_2 emissions primarily depend on the amount of fuel burned, which is proportionally the same in both cases (compared to the mass of charge), as nothing has changed to alter the character of the combustion process. NO emission levels also show similar values although they are not so much a function of the total amount of fuel burned as of the burned gas temperatures and the duration for which the hot products reside in the chamber. This is explained by looking at Fig. 5.22 which shows the variation of mass-averaged cylinder temperature with crank angle. Since the intake air temperature was kept fixed at 575 K for both cases (to isolate the effect of intake pressure on the results), and since ignition delay and the subsequent combustion process were similar in character, the average temperatures are almost the same for both the cases. This results in almost the same levels of NO, as seen in Fig. 5.23.

Closure

The models developed in the previous chapters to simulate ignition, combustion and pollutant formation were coupled together to simulate these processes in a direct injection natural gas engine. Details of the engine geometry chosen for the calculations were given along with an explanation for the modeling choices made. It was pointed out that assuming reasonable input conditions for the simulations is important if meaningful interpretations of the results are to be made.

A baseline operating regime was taken as medium speed (1500 RPM), high load (ϕ=0.6), medium boost (3 bar) and early injection timing (25° BTDC). Results obtained for the baseline case were examined in detail and it was found that they were qualitatively

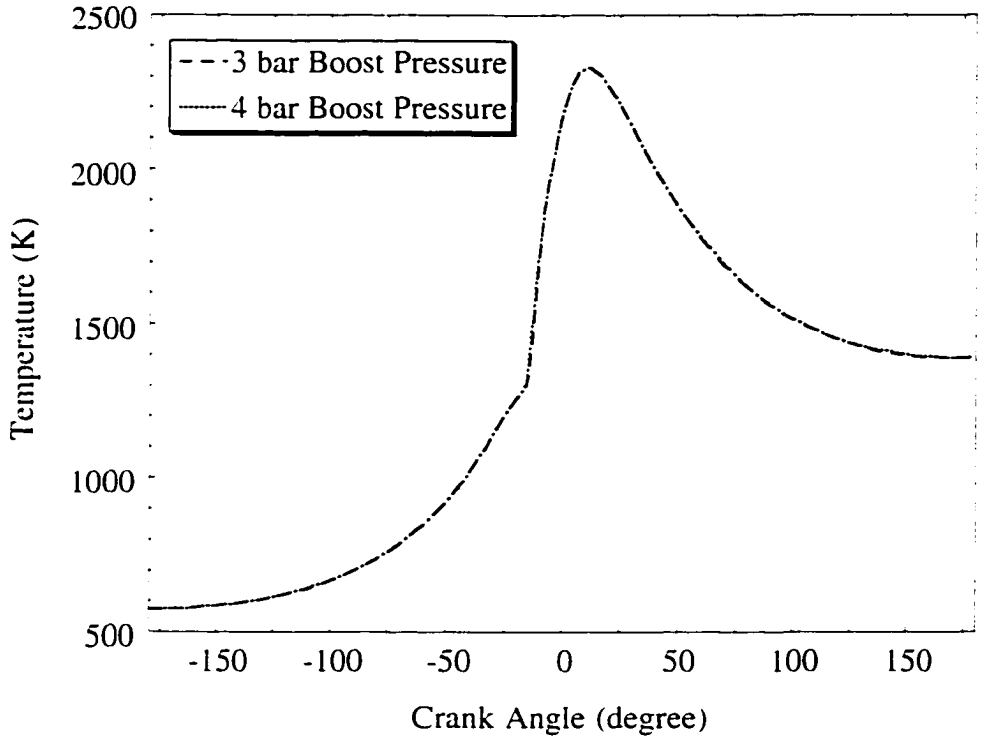

Figure 5.22: Variation of mass-averaged temperature with crank angle for two levels of boost.

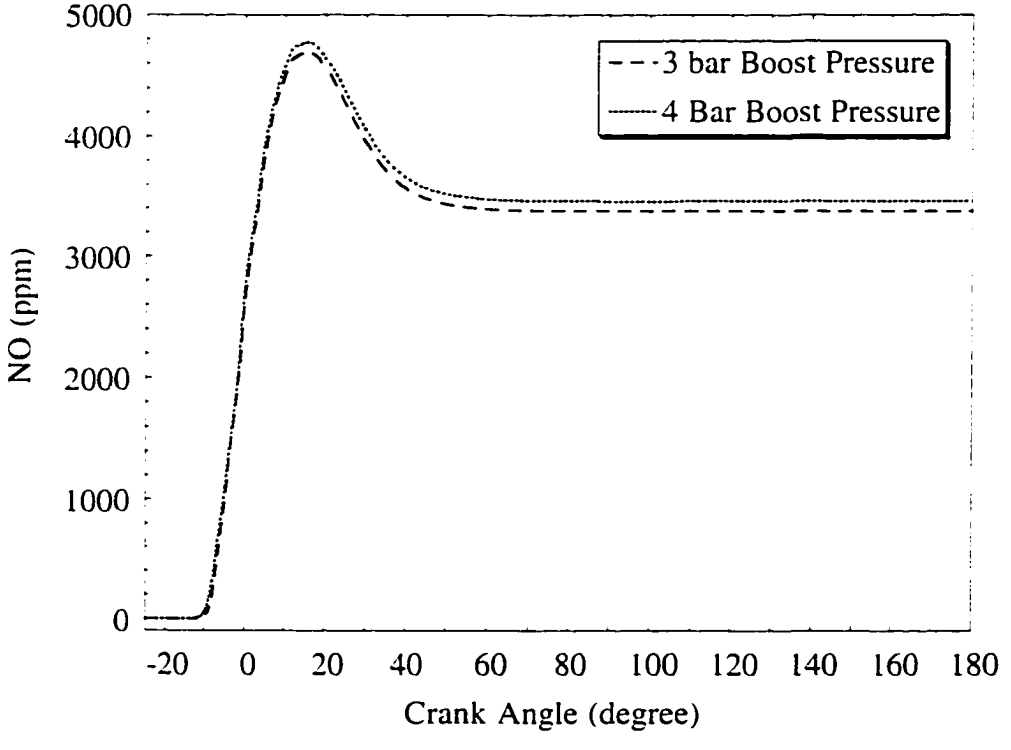

Figure 5.23: Variation of NO with crank angle for two levels of boost.

reasonable and could be explained in a rational manner.

The effect of different operating parameters like speed and load, and also different strategies like injection timing and level of boost, was examined by changing them one-by-one from the baseline case. Engine speed was found to significantly affect the ignition delay period and the subsequent combustion process. It was shown that as the engine speed changes, variation of engine parameters with *both* crank angle and time must be used to gain a better understanding of the processes occurring in engines. It was also pointed out that at lower speeds, injection timing must be retarded, so that the fuel does not start burning too early, leading to an undesirable increase in NO emissions.

Engine load was shown to increase engine performance as well as CO_2 and UHC emissions. NO emissions increased only slightly with increasing load. Since most of the NO is formed in pockets of burned mixtures that are formed early in the combustion process, due to the non-homogeneous nature of combustion in DING engines, even low load cases can produce significant NO.

Changing injection timing can be an effective strategy to control the advent of combustion, and thus peak pressures and temperatures and hence emissions. It was shown that retarding fuel injection, at medium speeds, can dramatically reduce NO in the exhaust, without too much of a sacrifice in engine performance.

Increase in the level of boost increases peak pressures and IMEP in the same proportion, if the engine operating parameters are not changed. Thus, increased boost with retarded timing could be effective methods to reduce NO when high performance from the engine is desired.

This chapter concludes the formal description of the studies associated with this dissertation. In the next chapter, a summary of the work done is provided along with recommendations for future work.

CHAPTER VI

CONCLUDING REMARKS AND RECOMMENDATIONS FOR FUTURE WORK

Concluding Remarks and Key Contributions

This work was concerned with the modeling of ignition, combustion and pollutant formation processes in direct injection engines. Throughout the study, emphasis was on gaining a better fundamental understanding of each of these processes. The work was divided into several phases that dealt with different aspects of the problem separately. Although the main conclusions of each phase were summarized at the end of each chapter, the salient features and key contributions of this work are noted below:

1. Ignition of mixtures of methane and ethane was simulated using a detailed chemical kinetic mechanism that was found after a systematic study of its predictive capabilities under typical end-of-compression conditions in direct injection engines. The evaluation process revealed that the choice of a suitable detailed mechanism is essential to account for all the thermodynamic and fuel composition related parameters that fuel injected in a direct injection engine encounters.
2. A methodology to couple detailed chemistry with multi-dimensional flow simulation was developed in this work and was used to study the autoignition of different natural gas mixtures injected in a combustion bomb at high temperatures and pressures. The coupled approach showed excellent agreement with measurements of ignition delay in a combustion bomb. This agreement, in a relatively simple geometry, is heartening as it shows that the different pieces of the complicated problem of natural gas ignition in direct injection applications were reasonably well approximated by the modeling approach used. The ignition delay process is primarily controlled by chemistry and

the calculations provide some level of confidence in the detailed chemical kinetic mechanism used. These computations also provided confidence in the assumption that the fluctuations in temperature and species concentrations do not have an impact on reaction rates during the ignition delay period. Thus, use of mean values of these quantities in calculating reaction rates and heat release is justified.

3. Computational costs associated with the coupling of detailed chemistry with multi-dimensional flow simulation were not found to be a major issue for natural gas. The longest calculation reported in this study took less than a week of CPU time on a SUN Ultra2 workstation. With rapid advancements in computational speed and memory with each passing year, coupled with better understanding of the chemistry of higher hydrocarbons fuels, this approach should be feasible to describe their autoignition in the near future.
4. A key contribution of the ignition work was the establishment of a suitable criterion for the onset of ignition. Using intuitive arguments supported by calculations, it was shown that, compared to a specified pressure rise, a delay based on a specified mass of fuel burned is a more consistent criterion when comparing ignition delay of different fuels over a range of thermodynamic conditions. The coupled flow-chemistry approach also allows one to investigate the effect of injection parameters and fuel composition related factors like additives, fuel injection rate, fuel temperature and velocity on ignition delay and location of ignition. These studies are not possible by the purely kinetics based approaches that are usually used with detailed chemistry.
5. Once the rate of heat release becomes high, the influence of flow turbulence on reaction rates can no longer be ignored. The description of ignition and combustion processes has to be completely different as these processes occur over very different chemical time-scales. Keeping this in mind, the interactions between flow and chemistry were explored in detail with a view to find a coherent description of the turbulent reactive process as applied to a direct injection engine. The different

regimes of combustion in engines on typical phase-diagrams were identified. Three different turbulent combustion models, the Eddy-Break-Up model, the Eddy Dissipation Concept, and the Coherent Flamelet model were investigated in detail to not only study their applicability in direct injection engines, but also to investigate the feasibility of their implementation in a reactive flow code. It was found that though the latter two models described the molecular mixing of reactants in a more sophisticated manner, it is the simpler EBU model that was most conducive to direct injection engine combustion studies. Since combustion in DI engines does not occur in one single phase or regime, a myriad of approximations are needed in the more detailed models to make them suitable for engine combustion. Due to lack of experimental data to verify the validity of some of these assumptions, it was decided to use the simple "mixed-is-burned" approach to describe combustion after the ignition delay period was over. Such an approach made the interpretation of the modeling results easier, although it did sacrifice some important physics of the combustion process like local flame extinction, effect of flow-field strain rate on chemical reactions, non-equilibrium effects on reaction rates, etc.

6. Pollutant formation modeling in this work was restricted to nitric oxide formation. A detailed examination of the extended Zeldovich mechanism for thermal NO formation revealed that the NO formation rates were very sensitive to temperature and concentrations of O and N radicals. The extended Zeldovich mechanism was implemented in KIVA-3V and the minor species were assumed to be in equilibrium concentrations at the local temperature. The qualitative predictions of NO formation matched very well with recent experimental observations using PLIF.
7. Finally, calculations in a medium size heavy-duty direct injection engine showed that the modeling approach developed in this work was able to capture the effect of operating conditions, coupled with different strategies for injection timing and level of boost, on engine performance and exhaust emissions. Detailed examination of the baseline operating case showed that the combined ignition-combustion-pollutant

formation models developed in this work were able to give a very realistic picture of these processes in a DING engine. It was also found that changing injection strategies with load and speed could be a good way to control emissions, while maintaining desired engine performance.

Now that this work is over, and a reasonably comprehensive description of the ignition and combustion processes in DING engines has been developed, it is worthwhile to look at some future directions. Some recommendations for future work that could follow from this dissertation are described in the next section.

Recommendations for Future Work

1. The detailed chemical kinetic mechanism used in this work consisted of 22 species and 105 reactions. Although this mechanism has itself been reduced from a more detailed kinetic mechanism, efforts could be made to eliminate reactions and species that are not important in the high pressure and temperature conditions that are typically prevalent in direct injection engines. The computational costs involved in using a detailed kinetic mechanism scale approximately as $(M+1)^2$, where M is the maximum number of species in a kinetic mechanism. A reduction in the number of species can therefore have a significant effect on lowering the computational time and memory requirements. Caution must, however, be exercised during the reduction procedure. Often times, the reduced mechanisms are valid in only a very specific set of circumstances. This makes them practically useless for a more general study. So a judgment must be made based on the available computational resources about the degree of reduction sought.
2. This work primarily focused on autoignition and combustion of natural gas injected in air. However, most DING engines operate with some ignition assist as the high intake air temperature requirement for autoignition comes with a cost penalty in terms of lower volumetric efficiency. The more commonly used approaches are pilot fuel

injection and glow-plug assisted ignition. Future studies could concentrate on either of these methods to simulate more "real" DING engines. Studies using pilot fuel injection would be limited by the chemistry of the pilot fuel, typically diesel. Although reduced mechanisms for higher hydrocarbons have been proposed, their ability to simulate ignition delay will have to be examined. To simulate glow-plug assisted ignition, attention will have to be focused on transient boundary layer heat transfer from a hot surface, which is still an area of active research. Also, adequate grid resolution will have to be provided next to the glow-plug surface to resolve the boundary layer.

3. In the EBU model of combustion, it was assumed that the fuel and air burned in stoichiometric proportions to products of complete combustion. This is a very idealized approach. Improvements could be made to make the EBU model more realistic. Considerations for the local stoichiometry of the fuel-air mixture could be used to predict formation of products of incomplete combustion like H_2 and CO. Also, values of local strain rate could be compared with experimentally measured values of strain rates that cause flame extinction to account for local flame extinction effects.
4. In these simulations only the closed part of the engine cycle was simulated. Although effort was made to prescribe correct initial turbulence intensities at the start of the calculation, as pointed out in Chapter V, it has been shown that intake generated flow structures are preserved late into compression. The presence of these structures leads to a lower dissipation of turbulent kinetic energy compared to a calculation in which a uniform value is assumed without simulating the intake process. The difference in turbulence levels could have an impact on subsequent mixing of injected fuel with air. Although the fuel injection process itself creates its own turbulence, it would be interesting to observe the effect of simulation of the intake process on the DI ignition and combustion processes.

5. Lack of experimental data from DING engines was a major handicap in this work. Spatially and temporally resolved measurements are needed to corroborate/contradict the modeling results shown in this study. Apart from global parameters like cycle-resolved cylinder pressure data, spatial distributions of temperature and certain combustion species using laser diagnostic techniques must be made available to improve the modeling assumptions. However, at this point it is worthwhile to point out that experiments of complex physical systems like engines are also subject to difficulties similar to those experienced by the modeler. Like models, experimental diagnostics are generally calibrated in simple controllable configurations before being applied to realistic problems. So, in making comparisons between model and measurement in complex systems like engines, the exercise should be more appropriately viewed as one of *reconciliation* between model and measurement rather than as one of *validation* of a model.

To conclude, this study and many more like this, are attempts to simulate complex physical phenomena by making reasonable choices at each step along the way. Sometimes reason has to be tempered with computational expediency, and in the end the problem boils down to judicious choices based on constraints an individual researcher may face. Before implementing any complex model into a simulation, attempts should be made to isolate it as much as possible from varying inputs so that its own behavior may be understood properly. In this work, both the EDC turbulent combustion model and the extended Zeldovich thermal NO formation kinetics model were first studied in isolation and a much better appreciation of their behavior achieved. Another thing to keep in mind while doing numerical simulations is to avoid getting drowned in numbers. Sometimes it is easy to take a computational output as the absolute truth without questioning it. After all, the output is only as good as the input, the model and the solution procedure used. It is important to have a good feeling of each of these before even trying to explain the results.

Prudence should be exercised while doing the numerical calculations. Since for the privileged ones among us, computations don't cost real money, there is a tendency to run as many cases as possible by postponing the thinking process to the end. However, if the thinking is done before hand, a lot of effort can be saved by avoiding sifting through megabytes and megabytes of output, not to mention the savings in computer time and storage. Of course, this may not be true for a completely new problem about which almost no understanding exists, but most of us are fortunate enough to have some feel of the problem being studied.

The comments made above were from the personal experience of the author. However, for the computational neophyte who wants to learn more about the art and science of numerical reactive flow simulation, there is an excellent book by Oran and Boris (1987) that talks about similar issues, but from the perspective of two very experienced researchers. The third chapter in particular is a must read for anybody wanting to know how to develop and use simulation methods correctly. In the end, it is worth pointing out that no study can really be complete if the investigator does not have an enthusiasm for the work being done. A half-hearted effort can only lead to a mediocre output. To quote Wilson (1952), "Scientific research, not being a routine process but requiring originality and creative thought, is very sensitive to the psychological state of the scientist. An uninterested worker is unlikely to produce the new ideas necessary for progress. One famous scientist has expressed this idea by saying that the problem should be important in the larger picture of one's view of the world." That is really the essence. Enthusiasm and interest in one's work and a feeling that what is being done is important and useful.

APPENDICES

APPENDIX A

DERIVATION OF THE GOVERNING ENERGY EQUATION FOR A CONSTANT VOLUME SYSTEM (Eq. 2.2)

For an adiabatic, constant volume system, the first law states that the internal energy of the mixture (u) is a constant. This can be written in rate form as:

$$\frac{du}{dt} = 0 \tag{A.1}$$

or,

$$\frac{d(\sum Y_m u_m)}{dt} = 0 \tag{A.2}$$

where, the mixture internal energy is given by $u = \sum Y_m u_m$ and the summation is over all the species in the chamber. Expanding Eq. A.2:

$$\sum\left(Y_m \frac{du_m}{dt} + u_m \frac{dY_m}{dt} \right) = 0 \tag{A.3}$$

Rewriting, Eq. A.3 as:

$$\sum Y_m \frac{du_m}{dt} = -\sum u_m \frac{dY_m}{dt} = -\sum \frac{u_m \dot{\omega}_m W_m}{\rho} \tag{A.4}$$

where, Eq. 2.3 from the text has been used to replace the rate of change of species mass fractions. From the definition of specific heat at constant volume:

$$\frac{du_m}{dt} = C_{v_m} \frac{dT}{dt} \tag{A.5}$$

and the definition of mean specific heat of a mixture at constant volume, $\overline{C}_v = \sum Y_m C_{v_m}$, Eq. A.4 can be re-written as:

$$\overline{C}_v \frac{dT}{dt} = -\frac{1}{\rho} \sum u_m \dot{\omega}_m W_m \tag{A.6}$$

which is the same as Eq. 2.2 used in the text.

APPENDIX B

DERIVATION OF THE TRANSIENT FORM OF THE GOVERNING ENERGY EQUATION FOR A PERFECTLY STIRRED REACTOR (PSR) (Eq. 4.33)

By neglecting the energy transfer due to other mechanisms such as radiation, the transient form of the energy equation in the PSR (Eq. 4.29) can be written as:

$$\frac{dh^*}{dt} = -\frac{1}{\tau_r}\sum\left(Y_m^* h_m^* - \overline{Y}_m \overline{h}_m\right) \tag{B.1}$$

From the definition of h^* and C_p^* :

$$h^* = \sum Y_m^* h_m^* \tag{B.2}$$

and,

$$C_p^* = \sum Y_m^* C_{p_m}^* \tag{B.3}$$

Taking the derivative of Eq. B.2 with respect to time and substituting in Eq. B.1:

$$C_p^* \frac{dT^*}{dt} + \sum h_m^* \frac{dY_m^*}{dt} = -\frac{1}{\tau_r}\sum\left(Y_m^* h_m^* - \overline{Y}_m \overline{h}_m\right) \tag{B.4}$$

where Eq. B.3 has been used along with the definition of specific heat at constant pressure. The rate of change of species mass fraction, $\frac{dY_m^*}{dt}$ can be replaced by its by Eq. 4.32 from the text. Expanding all the terms in Eq. B.4 after the substitution yields:

$$C_p^* \frac{dT^*}{dt} = \frac{1}{\tau_r}\sum h_m^*\left(Y_m^* - \overline{Y}_m\right) - \sum \frac{h_m^* \dot{\omega}_m^* W_m}{\rho^*} - \frac{1}{\tau_r}\sum\left(Y_m^* h_m^* - \overline{Y}_m \overline{h}_m\right) \tag{B.5}$$

Eliminating common terms in Eq. B.5 and rearranging leads to:

$$C_p^* \frac{dT^*}{dt} = \frac{1}{\tau_r}\sum \overline{Y}_m\left(\overline{h}_m - h_m^*\right) - \sum \frac{h_m^* \dot{\omega}_m^* W_m}{\rho^*} \tag{B.6}$$

which is the same as Eq. 4.33 used in the text.

BIBLIOGRAPHY

BIBLIOGRAPHY

Abraham, J., Williams, F. A., and Bracco, F. V., "A Discussion of Turbulent Flame Structure in Premixed Charges," SAE Paper 850345, 1985.

Aesoy, V., *Hot Surface Assisted Compression Ignition in a Direct Injection Natural Gas Engine*, Dr. Ing. Thesis, Dept. of Marine Engineering, Norwegian Institute of Technology, University of Trondheim-NTH, Norway, 1996.

Agarwal, A. and Assanis, D. N., "Modeling the Effect of Natural Gas Composition on Ignition Delay under Compression Ignition Conditions," SAE Paper 971711, 1997.

Al-Fawaz, A. D., Dearden, L. M., Hedley, J. T., Missaghi, M., Pourkashanian, M., Williams, A., and Yap, L. T., "NOx Formation in Geometrically Scaled Gas-Fired Industrial Burners," poster presented at the Twenty-fifth Symposium (International) on Combustion, The University of California, Irvine, CA, 1994.

Amsden, A. A., "KIVA-3: A KIVA Program with Block-Structured Mesh for Complex Geometries," Los Alamos National Laboratory Report LA-12503-MS, 1993

Amsden, A. A., "KIVA-3V: A Block Structured KIVA Program for Engines with Vertical or Canted Valves," Los Alamos National Laboratory Report LA-13313-MS, 1997.

Assanis, D. N. and Heywood, J. B., "Development and Use of a Computer Simulation of the Turbocompounded Diesel System for Engine Performance and Component Heat Transfer Studies," SAE Paper 860329, 1986.

Ayoub, N. S. and Reitz, R. D., "Multidimensional Computation of Multicomponent Spray Vaporization and Combustion," SAE Paper 950285, 1995.

Bilger, R. W., "Turbulent Flows with Non-premixed Reactants," in *Turbulent Reacting Flows* (P. A. Libby and F. A. Williams, Eds.), Topics in Applied Physics, Vol. 44, p. 65, Springer-Verlag, Berlin, 1980.

Bilger, R. W., Stårner, S. H., and Kee, R. J., "On Reduced Mechanisms for Methane-Air Combustion in Nonpremixed Flames," *Combustion and Flame*, Vol. 80, p. 135, 1990.

Bish, E. S. and Dahm, W. J. A., "Strained Dissipation and Reaction Layer Analyses of Nonequilibrium Chemistry in Turbulent Reacting Flows," *Combustion and Flame*, Vol. 100, p. 457, 1995.

Borghi, R. and Murthy, S. N. B. (Eds.), *Turbulent Reactive Flows*, Lecture Notes in Engineering, Vol. 40, Springer-Verlag, New York, 1989.

Borghi, R., "On the Structure of Turbulent Premixed Flames," in *Recent Advances in Aeronautical Sciences* (C. Bruno and C. Casci, Eds.), Pergamon, 1984.

Borghi, R., "Turbulent Combustion Modeling," *Progress in Energy and Combustion Science*, Vol. 14, p. 245, 1988.

Bosh GmbH, *Automotive Handbook*, 3rd Edition, Stuttgart, Germany, 1983.

Bowman, C. T., "Control of Combustion-Generated Nitrogen Oxide Emissions: Technology Driven by Regulation," *Twenty-fourth Symposium (International) on Combustion*, p. 859, The Combustion Institute, Pittsburgh, 1992.

Bradley, D., "How Fast Can We Burn ?," *Twenty-fourth Symposium (International) on Combustion*, p. 247, The Combustion Institute, Pittsburgh, 1992.

Bray, K. N. C., "Methods of Including Realistic Chemical Reaction Mechanisms in Turbulent Combustion Model," in *Complex Chemical Reactions* (J. Warnatz and W. Jager, Eds.), Springer-Verlag, Heidelberg, 1987.

Bray, K. N. C., "Turbulent Flows with Premixed Reactants," in *Turbulent Reacting Flows* (P. A. Libby and F. A. Williams, Eds.), Topics in Applied Physics, Vol. 44, Springer-Verlag, Berlin, 1980.

Bray, K. N. C., Libby, P. A., and Moss, J. B., "Flamelet Crossing Frequencies and Mean Reaction Rates in Premixed Turbulent Combustion," *Combustion Science and Technology*, Vol. 41, p. 143, 1984.

Breen, B. P., Urich, J. A., Spalding, D. B., Smith, B. L., and Kramer, E. D., "Development of a Computer Model for Evaluation of NOx Control Alternatives," FACT-Vol. 17, *Combustion Modeling, Cofiring and NOx Control*, p. 109, ASME, 1993.

Brown, A. J. and Heywood, J. B., "A Fundamentally-Based Stochastic Mixing Model Method for Predicting NO and Soot Emissions from Direct-Injection Diesel Engines," in *Calculations of Turbulent Reactive Flows* (R. M. C. So, J. H. Whitelaw and H. C. Mongia, Eds.), AMD-Vol. 81, p. 293, ASME, 1986.

Burcat, A., Scheller, K., and Lifshitz, A., "Shock-Tube Investigation of Comparative Ignition Delay Times for C1-C5 Alkanes," *Combustion and Flame*, Vol. 16, p. 29, 1971.

Byggstøyl, S. and Magnussen, B. F., "A Model for Flame Extinction in Turbulent Flow," *Turbulent Shear Flows*, Vol. 4, p. 381, Springer-Verlag, Berlin, 1983.

Candel, S., Veynante, D., Lacas, F., Darabiha, N., and Rolon, C., "Current Progress and Future Trends in Turbulent Combustion," *Combustion Science and Technology*, Vol. 98, p. 245, 1994.

Candel, S., Veynante, D., Lacas, F., Maistret, E., Darabiha, N., and Poinsot, T., "Coherent Flame Model: Applications and Recent Extensions," in *Advances in Combustion Modelling* (B. Larrouturou, Ed.), p. 19, World Scientific, Singapore, 1991.

Carrier, G. F., Fendell, F. E., and Marble, F. E., "The Effect of Strain Rate on Diffusion Flames," *SIAM Journal of Applied Mathematics*, Vol. 28, p. 463, 1975.

Champion, M., Deshaies, B., Joulin, G., and Kinoshita, K., "Spherical Flame Initiation: Theory versus Experiments for Lean Propane-Air Mixtures," *Combustion and Flame*, Vol. 65, p. 319, 1986.

Chen, J. -Y. and Kollmann, W., "Comparison of Prediction and Measurement in Non-premixed Turbulent Flames," in *Turbulent Reacting Flows* (P. A. Libby and F. A. Williams, Eds.), Topics in Applied Physics, Vol. 44, p. 211, Academic Press, New York, 1994.

Cheng, W. K. and Diringer, J. A., "Numerical Modeling of SI Engine Combustion with a Flame Sheet Model," SAE Paper 910268, 1991.

Choi, M. Y., Dryer, F. L., and Haggard, J. B., "Observations on a Slow Burning Regime for Hydrocarbon Droplets: n-Heptane/Air Results," *Twenty-third Symposium (International) on Combustion*, p. 1597, The Combustion Institute, Pittsburgh, 1991.

Clavin, P. and Joulin, G., "Flamelet Library for Turbulent Wrinkled Flames," in *Turbulent Reactive Flows* (R. Borghi and S.N.B. Murthy, Eds.), Lecture Notes in Engineering, Vol. 40, p. 213, Springer-Verlag, New York, 1989.

Clavin, P. and Williams, F. A., "Theory of Premixed-Flame Propagation in Large Scale Turbulence," *Journal of Fluid Mechanics*, Vol. 56, p. 81, 1979.

Correa, S. M. and Shyy, W., "Computational Models and Methods for Continuous Gaseous Turbulent Combustion," *Progress in Energy and Combustion Science*, Vol. 13, p. 249, 1987.

Correa, S. M., "A Review of NOx Formation Under Gas-Turbine Combustion Conditions," *Combustion Science and Technology*, Vol. 87, p. 329, 1992.

Corrsin, S., "Turbulent Dissipation Fluctuations," *The Physics of Fluids*, Vol. 5, p. 1301, 1962.

Dahm, W. J. A. and Bish, E. S., "Molecular Mixing and Chemical Reactions in Turbulent Flows," Fall Eastern States Section Meeting of the Combustion Institute, Worcester Polytechnic University, Worcester, MA, 1996.

Daneshyar, H. and Hill, P. G., "The Structure of Small-Scale Turbulence and its Effect on Combustion in Spark Ignition Engines," *Progress in Energy and Combustion Science*, Vol. 13, p. 47, 1987.

Dec, J. E. and Canaan, R. E., "PLIF Imaging of NO Formation in a DI Diesel Engine," SAE Paper 980147, 1998.

di Blasi, C., Continillo, G., Crescitelli, S., Russo, G., and Tufano, V., "Numerical Simulation of Induced Ignition of Methane-Oxygen Mixtures," *International Chemical Engineering*, Vol. 31, No. 1, p. 94, 1991.

Dillies, B., Ducamin, A., Lebrere, L., and Neveu, F., "Direct Injection Diesel Engine Simulation: A Combined Numerical and Experimental Approach from Aerodynamics to Combustion," SAE Paper 970880, 1997.

Dillies, B., Marx, K., Dec, J., and Espey, C., "Diesel Engine Combustion Modeling Using the Coherent Flame Model in KIVA-II," SAE Paper 930074, 1993.

Dimotakis, P. E., "Turbulent Free Shear Layer Mixing," AIAA Paper 89-0262, 1989.

Faeth, G. M., "Pollutant Emissions for Combustion Processes of Mobile Power and Propulsion Systems," in *Modern Developments in Propulsion and Combustion* (G. D. Roy, Ed.), 1996.

Fenimore, C. P., "Formation of Nitric Oxide in Premixed Hydrocarbon Flames," *Thirteenth Symposium (International) on Combustion*, p. 373, The Combustion Institute, Pittsburgh, 1970.

Fleming, R. D. and Bechtold, R. L., "Natural Gas (Methane), Synthetic Natural Gas and Liquefied Petroleum Gases as Fuels for Transportation," SAE Paper 820959, 1982.

Fraser, R. A., Siebers, D. L., and Edwards, C. F., "Autoignition of Methane and Natural Gas in a Simulated Diesel Environment," SAE Paper 910227, 1991.

Frendi, A. and Sibulkin, M., "Dependence of Minimum Ignition Energy on Ignition Parameters," *Combustion Science and Technology*, Vol. 73, p. 395, 1990.

Frenklach, M. and Bornside, D. E., "Shock-Initiated Ignition in Methane-Propane Mixtures," *Combustion and Flame*, Vol. 56, p. 1, 1984.

Frenklach, M., Wang H., Goldenberg, M., Bowman, C. T., Hanson, R. K., Smith, G. P., Golden, D. M., Gardiner, W. C., and Lissianski, V., Gas Research Institute Topical Report: "GRI-Mech - An Optimized Detailed Chemical Reaction Mechanism for Methane Combustion," Report No. GRI-95/0058, 1995.

Frenklach, M., Wang H., Yu C,-L., Goldenberg, M., Bowman, C. T., Hanson, R. K., Davidson, D. F., Chang, E. J., Smith, G. P., Golden, D. M., Gardiner, W. C., and Lissianski, V., *http://www.me.berkeleyedu/gri_mech/*, 1995.

Glarborg, P., Lilleheie, N. I., Byggstøyl, S., Magnussen, B. F., Kilpinen, P., and Hupa, M., "A Reduced Mechanism for Nitrogen Chemistry in Methane Combustion," *Twenty-fourth Symposium (International) on Combustion*, p. 889, The Combustion Institute, Pittsburgh, 1992.

Gebert, K., Beck, N. J., Barkhimer, R. L., Wong H.-C., and Wells, A. D., "Development of Pilot Fuel Injection System for CNG Engine," SAE Paper 961100, 1996.

Ghoniem, A. F., Heidarinejad, G., and Krishnan, A., "Turbulence-Combustion Interactions in a Reacting Shear Layer," in *Turbulent Reactive Flows* (R. Borghi and S.N.B. Murthy, Eds.), Lecture Notes in Engineering, Vol. 40, p. 639, Springer-Verlag, New York, 1989.

Glovitchev, V. I., Pilia, M. L., and Bruno, C., "Autoignition of Methane Mixtures: The Effect of Hydrogen Peroxide," *Journal of Propulsion and Power*, Vol. 12, No. 4, p. 699, 1996.

Gosman, A. D. and Harvey, P. S., "Computer Analysis of Fuel-Air Mixing and Combustion in an Axisymmetric D. I. Diesel Engine," SAE Paper 820036, 1982.

Hermanson, J. C., Mungal, M. G., and Dimotakis, P. E., "Heat Release Effects on Shear Layer Growth and Entrainment," AIAA Paper 85-0142, 1985.

Heywood, J. B., *Internal Combustion Engine Fundamentals*, McGraw-Hill, Inc., 1988.

Hindmarsh, A. C., "ODEPACK, A Systematized Collection of ODE Solvers," in *Scientific Computing* (R. S. Stepleman *et al.*, Eds.), Vol. 1, p. 55, *IMACS Trans. on Scientific Computation* (North-Holland, Amsterdam), 1983.

Hunter, T. B., Wang, H., Litzinger, T. A., and Frenklach, M., "The Oxidation of Methane at Elevated Pressures: Experiments and Modeling," *Combustion and Flame*, Vol. 97, p. 201, 1994.

Hupperich, P. and Dürnholz, M., "Exhaust Emissions of Diesel, Gasoline and Natural Gas Fueled Vehicles," SAE Paper 960857, 1996.

Jennings, M. J. and Jeske, F. R., "Analysis of the Injection Process in Direct Injected Natural Gas Engines: Part I-Study of Unconfined and In-Cylinder Plume Behavior," *Journal of Engineering for Gas Turbines and Power*, Vol. 116, p. 799, 1994a.

Jennings, M. J. and Jeske, F. R., "Analysis of the Injection Process in Direct Injected Natural Gas Engines: Part II-Effects of Injector and Combustion Chamber Design," *Journal of Engineering for Gas Turbines and Power*, Vol. 116, p. 806, 1994b.

Jessee, J. P., Gansman, R. F., and Fiveland, W. A., "Multi-Dimensional Analysis of Turbulent Natural Gas Flames Using Detailed Chemical Kinetics," *to be published.*

Jones, W. P. and Whitelaw, J. H., "Calculation Methods for Reacting Turbulent Flows: A Review, *Combustion and Flame*, Vol. 48, p. 1, 1982.

Josefsson, G., Magnussen, I., Hildenbrand, F., Schulz, C., and Sick, V., "Multidimensional Laser Diagnostic and Numerical Analysis of NO Formation in a Gasoline Engine," submitted to the Twenty-seventh Symposium (International) on Combustion, The University of Colorado, Boulder, CO, 1998.

Karim, G. A. and Wierzba, I., "Safety Measures Associated with the Operation of Engines on Various Alternative Fuels," *Reliability Engineering and System Safety*, Vol. 37, p. 93, 1992.

Karim, G. A., Ito, K., Abraham, M., and Jensen, L., "An Examination of the Role of Formaldehyde in the Ignition Processes of a Dual Fuel Engine," SAE Paper 912367, 1991.

Kazakov, A. and Frenklach, M., *http://diesel.fsc.psu.edu/~gri_mech/drm/home_drm.html*, 1996.

Kee, R. J., Rupley, F. M., and Miller, J. A., "CHEMKIN-II: A Fortran Chemical Kinetics Package for the Analysis of Gas-Phase Chemical Kinetics," Sandia National Labs Report SAND89-8009B, 1991.

Kim, S. S., Kim, C. G., Chang, U. K., Pang, H. S., Han, J. O., and Cho, Y. S., "A Study on Efficiency and Emission Enhancements in a 4-Stroke Natural Gas Lean Burn Engine," SAE Paper 960849, 1996.

King, S. R., "The Impact of Natural Gas Composition on Fuel Metering and Engine Operational Characteristics," SAE Paper 920593, 1992.

Kollmann, W. and Chen, J. -Y, "The Interaction of Turbulence and Chemical Kinetics," in *Major Research Topics in Combustion* (M. Y. Hussaini, A. Kumar and R. G. Voigt, Eds.), p. 359, Springer-Verlag, New York, 1992.

Kolmogorov, A. N., "A Refinement of Previous Hypotheses Concerning the Local Structure of Turbulence in a Viscous Incompressible Fluid at High Reynolds Number," *Journal of Fluid Mechanics*, Vol. 13, p. 82, 1962.

Kong, S-C, Han, Z., and Reitz, R. D., "The Development and Application of a Diesel Ignition and Combustion Model for Multidimensional Engine Simulation," SAE Paper 950278, 1995.

Kong, S-C, Hong, C-W, "Multidimensional Intake Flow Modeling of a Four-Stroke Engine with Comparisons to Flow Velocity Measurements," SAE Paper 970883, 1997.

Kuo, A. Y-S and Corrsin, S., "Experiments on Internal Intermittency and Fine-Structure Distribution Functions in Fully Turbulent Fluid," *Journal of Fluid Mechanics*, Vol. 50, p. 285, 1971.

Kuo, A. Y-S and Corrsin, S., "Experiments on the Geometry of the Fine-Structure Regions in Fully Turbulent Fluid," *Journal of Fluid Mechanics*, Vol. 56, p. 447, 1972.

Kuo, K. K., *Principles of Combustion*, John Wiley & Sons, 1986.

Libby, P. A. and Williams, F. A., *Turbulent Reacting Flows*, Topics in Applied Physics, Vol. 44, Springer-Verlag, Berlin, 1980.

Libby, P. A., "Comments on the Interaction of Turbulence and Chemical Kinetics," in *Major Research Topics in Combustion* (M. Y. Hussaini, A. Kumar and R. G. Voigt, Eds.), p.423, Springer-Verlag, New York, 1992.

Liew, S. K. and Bray, K. N. C., "A Flamelet Model of Turbulent Non Premixed Combustion," *Combustion Science and Technology*, Vol. 27, p. 69, 1981.

Liew, S. K., Bray, K. N. C., and Moss, J. B., "A Stretch Laminar Flamelet Model of Turbulent Nonpremixed Combustion," *Combustion and Flame*, Vol. 56, p. 199, 1984.

Magel, H. C., Schnell, U. and Hein, K. R. G., "Simulation of Detailed Chemistry in a Turbulent Combustor Flow," *Twenty-sixth Symposium (International) on Combustion*, p. 67, The Combustion Institute, Pittsburgh, 1996.

Magnussen, B. F. and Hjertager, B. H., "On Mathematical Modeling of Turbulent Combustion with Special Emphasis on Soot Formation and Combustion," *Sixteenth Symposium (International) on Combustion*, p. 719, The Combustion Institute, Pittsburgh, 1976.

Magnussen, B. F., "On the Structure of Turbulence and a Generalized Eddy Dissipation Concept for Chemical Reaction in Turbulent Flow," 19th AIAA Science Meeting, St. Louis, MO, 1981.

Magnussen, B. F., Hjertager, B. H., Olsen, J. G., and Bhaduri, D., "Effects of Turbulent Structure and Local Concentrations on Soot Formation and Combustion in C_2H_2 Diffusion Flames," *Seventeenth Symposium (International) on Combustion*, p. 1383, The Combustion Institute, Pittsburgh, 1978.

Marble, F. E. and Broadwell, J. E., "The Coherent Flame Model for Turbulent Chemical Reactions," Report No. TRW-9-PU, Project Squid Headquarters, Chaffee Hall, Purdue University, IN, 1977.

Mason, H. B. and Spalding, D. B., "Prediction of Reaction Rates in Turbulent Premixed Boundary-Layer Flows," Combustion Institute European Symposium, p. 601, 1973.

Masri, A. M., Bilger, R. W., and Dibble, R. W., "Turbulent Non-premixed Flames of Methane Near Extinction: Mean Structure from Raman Measurements", *Combustion and Flame*, Vol. 71, p. 245, 1988.

Meintjes, K. and Morgan, A. P., "Element Variables and the Solution of Complex Chemical Equilibrium Problems," General Motors Research Publication GMR-5827, 1987.

Miller, J. A. and Bowman, C. T., "Mechanism and Modeling of Nitrogen Chemistry in Combustion," *Progress in Energy and Combustion Science*, Vol. 15, p. 287, 1989.

Mulholland, J. A., Sarofim, A. F., and Beer, J. M., "On the Derivation of Global Ignition Kinetics from a Detailed Mechanism for Simple Hydrocarbon Oxidation," *Combustion Science and Technology*, Vol. 87, p. 139, 1992.

Mullins, B. P., *Spontaneous Ignition of Liquid Fuels*, Butterworths Scientific Publications, London, 1955.

Musculus, M. P. and Rutland, C. J., "An Application of the Coherent Flamelet Model to Diesel Engine Combustion," SAE Paper 950281, 1995.

Naber, J. D., Siebers, D. L., Caton, J. A., Westbrook, C. K., and Di Julio, S. S., "Natural Gas Autoignition Under Diesel Conditions: Experiments and Chemical Kinetic Modeling," SAE Paper 942034, 1994.

Nichols, R. J., "The Challenges of Change in the Auto Industry: Why Alternative Fuels?", *ASME Trans., Journal of Engineering for Gas Turbines and Power*, Vol. 116, p. 727, 1994.

Nicol, D. G. and Malte, P. C., "Development of Global and Reduced Chemical Kinetic Mechanisms for Methane-Air Combustion," poster presented at the Twenty-fifth Symposium (International) on Combustion, The University of California, Irvine, CA, 1994.

O'Conner, L, "Building Natural Gas Locomotives," in *Mechanical Engineering*, p. 82, ASME, April 1994.

Oran, E. S. and Boris, J. P., *Numerical Simulation of Reactive Flow*, Elsevier, New York, 1987.

Papageorgakis, G., *Turbulence Modeling of Gaseous Injection and Mixing in DI Engines*, Ph.D. Thesis, Dept. of Mechanical Engineering and Applied Mechanics, The University of Michigan, Ann Arbor, 1997.

Peters, N. and Kee, R. J., "The Computation of Stretched Laminar Methane-Air Diffusion Flames Using a Reduced Four-Step Mechanism," *Combustion and Flame*, Vol. 68, p. 17, 1987.

Peters, N., "Laminar Diffusion Flamelet Models in Non-Premixed Turbulent Combustion," *Progress in Energy and Combustion Science*, Vol. 10, p. 319, 1984a.

Peters, N., "Laminar Flamelet Concepts in Turbulent Combustion," *Twenty-first Symposium (International) on Combustion*, p. 1231, The Combustion Institute, Pittsburgh, 1986.

Peters, N., "Length and Time Scales in Turbulent Combustion," in *Turbulent Reactive Flows* (R. Borghi and S.N.B. Murthy, Eds.), Lecture Notes in Engineering, Vol. 40, p. 242, Springer-Verlag, New York, 1989.

Peters, N., "Partially Premixed Diffusion Flamelets in Non-Premixed Turbulent Combustion," *Twentieth Symposium (International) on Combustion*, p. 353, The Combustion Institute, Pittsburgh, 1984b.

Pinchon, P., "Three Dimensional Modeling of Combustion in Prechamber Diesel Engine," SAE Paper 890666, 1989.

Pope, S. B., "Computations of Turbulent Combustion: Progress and Challenges," *Twenty-third Symposium (International) on Combustion*, p. 591, The Combustion Institute, Pittsburgh, 1990.

Pourkashanian, M. P., Missaghi, M., and Yap, T. L., "Reduction of NOx Emissions Using CFD as a Design Tool," FACT-Vol. 17, *Combustion Modeling, Cofiring and NOx Control*, p. 95, ASME, 1993.

Raine, R. R., Zhang, G., and Pflug, A., "Comparison of Emissions from Natural Gas and Gasoline Fueled Engines - Total Hydrocarbon and Methane Emissions and Exhaust Gas Recirculation Effects," SAE Paper 970743, 1997.

Rogg, B., "RUN-1DL: The Cambridge Universal Laminar Flamelet Computer Code," in *Reduced Kinetic Mechanisms for Applications in Combustion Systems* (N. Peters and B. Rogg, Eds.), Lecture Notes in Physics, Vol. m15, , Appendix C, p. 350, Springer-Verlag, Berlin-Heidelberg, 1993.

Rogg, B., "RUN-1DL: The Universal Laminar Flame and Flamelet Computer Code," User Manual, 1994.

Rogg, B., Behrendt, F., and Warnatz, J., "Turbulent Non-Premixed Combustion in Partially Premixed Diffusion Flamelets With Detailed Chemistry," *Twenty-first Symposium (International) on Combustion*, p. 1533, The Combustion Institute, Pittsburgh, 1986.

Rose, J. W. and Cooper, J. R., *Technical Data on Fuel*, Seventh Edition, John Wiley & Sons, New York, 1977.

Rubas, P. J., *An Experimental Investigation of the Injection Process in a Direct-Injected Natural Gas Engine Using PLIF and CARS*, Ph. D. Thesis, Dept. of Mechanical and Industrial Engineering, University of Illinois at Urbana-Champaign, 1997.

Shnidman, L., Ed., *Gaseous Fuels*, Second Edition, American Gas Association, New York, 1954.

Sick, V., Hildenbrand, F., and Lindstedt, P., "Quantitative Laser-Based Measurements and Detailed Chemical Kinetic Modelling of Nitric Oxide Concentrations in Methane/Air Counterflow Diffusion Flames," submitted to The Twenty-seventh Symposium (International) on Combustion, The University of Colorado, Boulder, CO, 1998.

Sloane, T. M. and Ronney, P. D., "A Comparison of Ignition Phenomena Modelled with Detailed and Simplified Kinetics," *Combustion Science and Technology*, Vol. 88, p. 1, 1992.

Smooke, M. D. (Ed.), "Reduced Kinetic Mechanisms and Asymptotic Approximations for Methane-Air Flames : A Topical Volume," *Lecture Notes in Physics*, Vol. 384, Springer-Verlag, New York, 1991.

Spalding, D. B., "Development of the Eddy-Break-Up Model of Turbulent Combustion," *Sixteenth Symposium (International) on Combustion*, p. 1657, The Combustion Institute, Pittsburgh, 1976.

Spalding, D. B., "Mixing and Chemical Reactions in Steady Confined Turbulent Flames," *Thirteenth Symposium (International) on Combustion*, p. 649, The Combustion Institute, Pittsburgh, 1971.

Spalding, D. B., "The Influence of Laminar Transport and Chemical Kinetics on the Time Mean Reaction Rate in a Turbulent Flame," *Seventeenth Symposium (International) on Combustion*, p. 431, The Combustion Institute, Pittsburgh, 1978.

Stephenson, P. W., Claybaker, P. J., and Rutland, C. J., "Modeling the Effects of Intake Generated Turbulence and Resolved Flow Structures on Combustion in DI Diesel Engines," SAE Paper 960634, 1996.

Tabaczynski, R. J., "Turbulence Measurements and Modelling in Reciprocating Engines-an Overview," Paper No. C51/83, Inst. Mech. Engg. Proceedings, 1983.

Tabaczynski, R. J., Ferguson, C. R., and Radhakrishnan, K., " A Turbulent Entrainment Model for Spark-Ignition Engine Combustion," SAE Paper 770647, *SAE Transactions*, Vol. 86, 1977.

Takeno, T., "NO Emission Characteristics and Formation Mechanisms of Methane Air Flames," in *Transport Phenomena in Combustion* (S. H. Chan, Ed.), Vol. 1, p. 101, Taylor & Francis, Washington, D.C., 1995.

Tan, Y., Dagaut, P., Cathonnet, M., Boettner, J. C., Bachman, J. S., and Carlier, P., "Natural Gas and Blends Oxidation and Ignition : Experiments and Modeling," *Twenty-fifth Symposium (International) on Combustion*, The Combustion Institute, Pittsburgh, 1994.

Tang, Z. J., Dwyer, H. A., and Fernandez, G., "A Study of the Low Mach Number Flow Model with Time-Dependent Rapid Chemistry," *Twenty-Third Symposium (International) on Combustion*, p. 795, The Combustion Institute, Pittsburgh, 1991.

Tennekes, H. and Lumley, J. L., *A First Course in Turbulence*, The MIT Press, Cambridge, Massachusetts, 1983.

Tennekes, H., "Simple Model for the Small-Scale Structure of Turbulence," *The Physics of Fluids*, Vol. 11, p. 669, 1968.

Tromans, P. S. and Furzeland, R. M., "An Analysis of Lewis Number and Flow Effects on the Ignition of Premixed Gases," *Twenty-first Symposium (International) on Combustion*, p. 1891, The Combustion Institute, Pittsburgh, 1988.

Varnavas, C. A. and Assanis, D. N., "Combustion Studies in a Diesel Engine Using a Multi-dimensional Engine Simulation," Energy-Sources Technology Conference and Exhibition, New Orleans, LA, 91-ICE-2, ASME, 1991.

Veynante, D., Lacas, F., and Candel, S. M., "A New Flamelet Combustion Model Combining Premixed and Non-Premixed Turbulent Flames," AIAA Paper 89-0487, 1989.

Warnatz, J., *Combustion Chemistry*, (Ed. W. C. Gardiner, Jr.), p. 197, Springer-Verlag, 1984.

Warnatz, J., Maas, U., and Dibble, R. W., *Combustion-Physical and Chemical Fundamentals, Modelling and Simulation, Experiments, Pollutant Formation*, Springer-Verlag, Berlin, 1996.

Weaver, C. S., "Natural Gas Vehicles-A Review of the State of the Art," SAE Paper 892133, 1989.

Westbrook, C. K. and Dryer, F. L., "Simplified Reaction Mechanisms for the Oxidation of Hydrocarbon Fuels in Flames," *Combustion Science and Technology*, Vol. 27, p. 31, 1981.

Westbrook, C. K. and Pitz, W. J., "High Pressure Autoignition of Natural Gas/Air Mixtures and the Problem of Engine Knock," GRI Topical Report, GRI-87/0264, 1987.

Westbrook, C. K., "An Analytical Study of Shock Tube Ignition of Mixtures of Methane and Ethane," *Combustion Science and Technology*, Vol. 20, p. 5, 1979.

Willi, M. L. and Richards, B. G., "Design and Development of a Direct Injected, Glow Plug Ignition Assisted, Natural Gas Engine," ICE-Vol. 22, Heavy Duty Engines: A Look at the Future, ASME, p. 31, 1994.

Williams, F. A., "Structure of Flamelets in Turbulent Reacting Flow and Influence of Combustion on Turbulence Fields," in *Turbulent Reactive Flows* (R. Borghi and S.N.B. Murthy, Eds.), Lecture Notes in Engineering, Vol. 40, p. 195, Springer-Verlag, New York, 1989.

Williams, F. A., *Combustion Theory*, 2nd Edition, Addison-Wesley Publishing Company, Redwood City, CA, 1985.

Wilson, Jr., E. B., *An Introduction to Scientific Research*, McGraw-Hill Book Company, Inc., New York, 1952.

Wong, Y. K. and Karim, G. A., "An Analytical Examination of the Effects of Exhaust Gas Recirculation on the Compression Ignition Process of Engines Fueled with Gaseous Fuels," SAE Paper 961936, 1996.

Yossefi, D., Ashcroft, S. J., Hacohen, J., Belmont, M. R., and Thorpe, I., "Combustion of Methane and Ethane with CO_2 Replacing N_2 as a Diluent: Modelling of Combined Effects of Detailed Chemical Kinetics and Thermal Properties on the Early Stages of Combustion," *Fuel*, Vol. 74, No. 7, p. 1061, 1995.

Zabetakis, M G., *Flammability Characteristics of Combustible Gases and Vapors*, US Bureau of Mines Bulletin 627, 1965.

Zamansky, V. M. and Borisov, A. A., "Promotion of High-Temperature Self-Ignition," *Progress in Energy and Combustion Science*, Vol. 18, p. 297, 1992.

Zeldovich, Y. B., Sadovnikov, P. Y., and Frank-Kamenetskii, D. A., *Oxidation of Nitrogen in Combustion*, Academy of Sciences of USSR, Moscow, 1947.

Zhou, G. and Karim, G. A., "An Analytical Examination of Various Criteria for Defining Autoignition Within Heated Methane-Air Homogeneous Mixtures," *Journal of Energy Resources Technology*, Vol. 116, p. 175, 1994.

IMAGE EVALUATION TEST TARGET (QA-3)

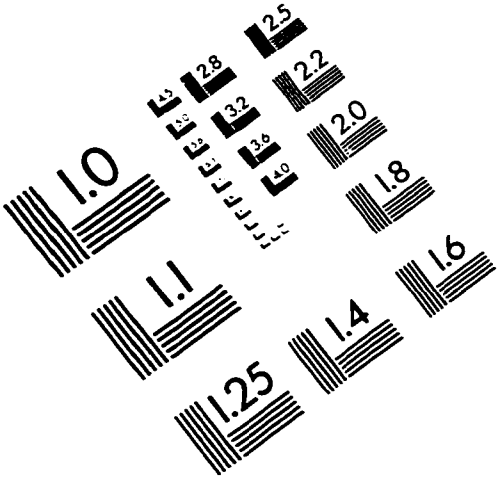

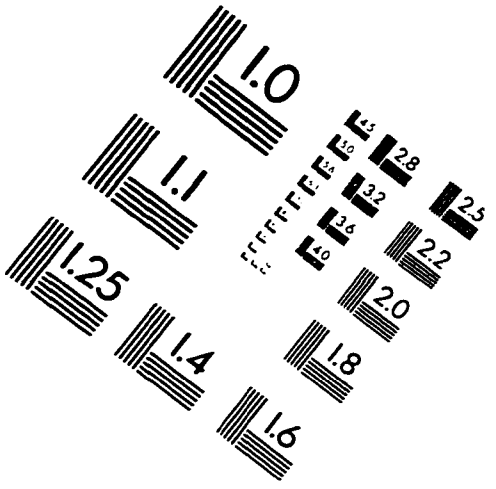

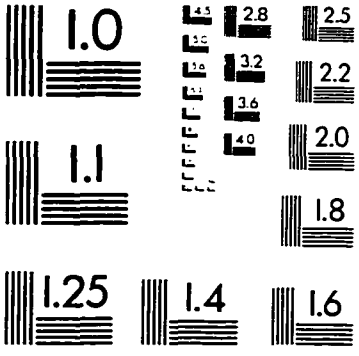

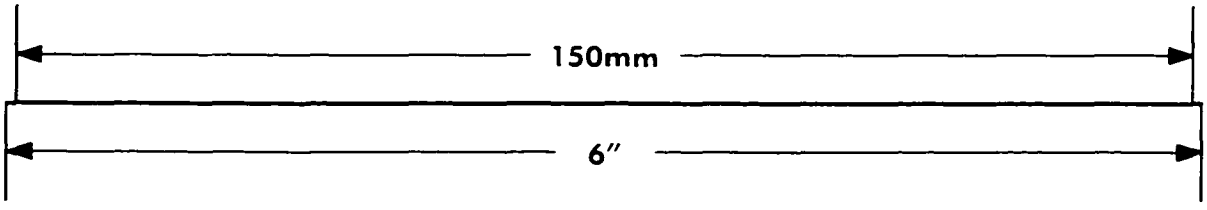

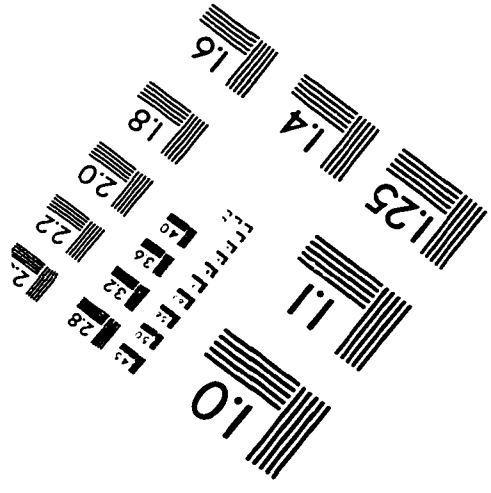

APPLIED IMAGE, Inc
1653 East Main Street
Rochester, NY 14609 USA
Phone: 716/482-0300
Fax: 716/288-5989